Assessing the immunomodulatory and haemostatic role of platelets in the type 2 inflammatory response to *Schistosoma mansoni*

Joanna Greenman

Doctor of Philosophy (PhD)

University of York

Biology

September 2023

Abstract

Beyond their role in haemostasis, platelets have been shown to be strongly immunomodulatory, particularly in type 1 inflammatory responses to bacteria and viruses. However, the role of platelets in type 2 inflammation, that characterises helminth infection and allergy is poorly understood. More than 200 million people globally are chronically infected with schistosome parasites which has a massive burden of >3 million disability adjusted life years. Despite large (~1cm long) worms residing in the vasculature for 5-10 years, they do not induce severe inflammation or coagulation. However, infected individuals display a plethora of debilitating symptoms including hepatosplenomegaly and intestinal haemorrhaging due to thousands of schistosome eggs transiting through and lodging within host tissues. This thesis aims to assess the haemostatic alterations and functional consequences of platelet-immune cell cross-talk in schistosomiasis.

We used a murine model of chronic *Schistosoma mansoni* infection to examine specific platelet-leukocyte interactions and the effect these have on inflammation. Chronic schistosome infection induces thrombocytopenia (~500x10^3/mm^3) that persists after drug-mediated worm clearance. *In vivo* platelet tracking revealed accelerated hepatic and splenic platelet clearance in schistosome infection, and this occurred in an FcγR-independent manner. Furthermore, there was a significant increase in platelets aggregating with specific hepatic macrophage subsets (Ly6C^{lo}MHCII^{lo}RELMα^{hi}). Live cell imaging *in vitro* experiments revealed that platelets enhanced the phagocytic ability of M2 macrophages without altering MHCII or RELMα expression. Surprisingly, platelets from schistosome-infected mice spontaneously aggregated in the absence of exogenous agonists despite not having an activated platelet phenotype, yet show prolonged clotting time. We used multiple experimental strategies to deplete or increase platelet numbers in schistosome infection, and this highlighted the challenges of separating the haemostatic and immunological roles of platelets *in vivo.* Work in this thesis demonstrates how schistosome infection disrupts platelet lifespan and functionality, whilst promoting enhanced interactions with immune cells.

Table of Contents

Table of Figures

Table of Tables

Acknowledgements

The entirety of my PhD would not have been possible without the support which has come in many different forms from so many different people.

Firstly, I would like to thank my two supervisors James Hewitson and Ian Hitchcock, they have shared so much knowledge and wisdom with me and have given me the opportunity to learn an incredible array of skills. James, from throwing me in the deep-end from day one has helped me grow in confidence and has pushed me to achieve my absolute best. Thank you for the patience with animal handling training and for carrying out so many other procedures for me too. Thank you for helping me become a better, rigorous scientist – who also loves flow! Ian, thank you for continual encouragement and reassurance, I always left our meetings feeling like finishing my PhD was possible. I would also like to express my gratitude to my TAP members Paul Kaye and Dimitris Lagos for their time and invaluable input into the progress of my project, I always learnt so much from these meetings.

I am immensely grateful to all the technology facility staff, with particular thanks to Karen Hogg, Graeme Park and Grant Calder. I am so appreciative of their expertise and extreme patience with my many questions and problems over the past 4 years, they have always been met with a smile. I would also like to thank all the BSF staff for their continual support both practically and emotionally. I have found the animal work really hard, particularly at the start so without their patience, particularly from Chris Turnbull, there is no way I would have managed to achieve what I have done.

My time in York and in the lab would not have been half as fun without all the people past and present on Q1 and Q2. I have loved being part of both groups and have appreciated the readiness to help from so many people. I would particularly like to thank Shinjini Chakraborty for her friendship, thoughtfulness and support with multiple harvests. Thank you to Katie West and Magnus Gywnn for their friendship and willingness to help on big experiment days. Thank you to Lucie Moss for being a wonderful human being, without her moral support, organisation and sense of humour the platelet modulation

experiments would not have been possible and the coagulometer may have been smashed!

Thank you to all my friends and family for their unwavering love, prayers and encouragement. Particularly thank you to my parents for their company on video calls during late night experiments, their help to keep everything in perspective and their unconditional love. Thank you to Dad for being the best “technician” on the other end of a phone I could have ever hoped for, his wisdom, experience, time and support has been invaluable. Finally, I would like to thank Jon who’s love, and friendship has picked me up when I have needed it most. He has been so understanding and over the last 4 years has been willing to plan visits around infections, plan our wedding around my PhD timescale and plan our honeymoon around an international conference! He has shared in the highs and lows of my PhD experience and has always been a listening ear at the end of the day - I cannot thank him enough.

Thank you to you all.

Joanna

Author's declaration

I declare that this thesis is a presentation of original work and I am the sole author. This work has not previously been presented for a degree or other qualification at this University or elsewhere. All sources are acknowledged as references.

1. Introduction

1.1 Schistosomiasis

1.1.1 Epidemiology

Schistosomiasis, also known as bilharzia, is a chronic parasitic disease that is caused by infection with the platyhelminth parasite *Schistosoma* (1). In 2019, the WHO estimated there were over 250 million people infected with the parasite and requiring treatment, with at least 90% of those being in Africa (2). Transmission has been identified in more than 78 countries and after malaria, schistosomiasis is one of the major causes of morbidity and mortality throughout many African countries (3). The poor and rural communities, reliant on the agricultural and fishing trades are predominantly affected as a result of inadequate hygiene and recurrent exposure to infested water (4). The morbidity of this disease is a major problem, with over 3.3 million disability-adjusted life years being attributed to schistosome infections annually (3).

There are two main forms of schistosomiasis, caused by three major schistosome species; intestinal schistosomiasis associated with *Schistosoma mansoni* (*S. mansoni*) and *Schistosoma japonicum* (*S. japonicum*), and urogenital schistosomiasis associated with *Schistosoma haematobium* (*S. haematobium*). *S. haematobium* and *S. mansoni* both occur in Africa and the Middle East, with *S. mansoni* also present in the Americas, whereas *S. japonicum* is primarily localised to Asia (5).

1.1.2 Parasite lifecycle

The disease is transmitted through exposure to water containing the infective parasite. Individuals can become infected when cercariae are released by schistosome species-specific freshwater snails. *S. mansoni* and *S. haematobium* require freshwater *Biomphalaria* and *Bulinus* snail hosts respectively, with *S. japonicum* using the amphibious freshwater *Oncomelania* species (5). Released cercariae are capable of penetrating human skin, and at the point of entering the body they shed their tails and become schistosomula. Once within the human host, the parasites migrate around the body in the venous circulation, passing through the heart and lungs, before eventually residing and maturing in the liver. On average, schistosomes are

able to survive in the circulation for 5-10 years and can directly take up nutrients across their body surface as well as by ingestion of blood into the gut, lysing erythrocytes as they pass down the parasite's specialised oesophagus (6). As schistosomes lack an anus, potentially toxic degradation products, such as haem, are expelled via regurgitation. Mature male and female worms copulate, and as paired adult schistosomes, they migrate within the portal system, against the blood flow, towards the mesenteric veins of the gut (7). *S. haematobium* is an exception to this, finally colonising the vessels of the bladder wall instead of the gut mesentery (5). However, in both cases, upon maturation and pairing the schistosomes start laying fertilised eggs. In the case of *S. mansoni* and *S. japonicum* (mesentery colonising schistosomes), eggs transit from the blood, across intestinal tissue, to reach the lumen of the intestine and are excreted. However, many eggs become lodged in the host liver resulting in granulomatous inflammation (8). Within an egg a miracidium develops and is released upon contact of the egg with fresh water. Released miracidium swim in search of a specific snail which acts as an intermediate host. Within the snail the miracidium transforms into a sporocyst, which undergoes asexual reproduction, ultimately releasing infective cercariae (9) (**Figure 1.1**).

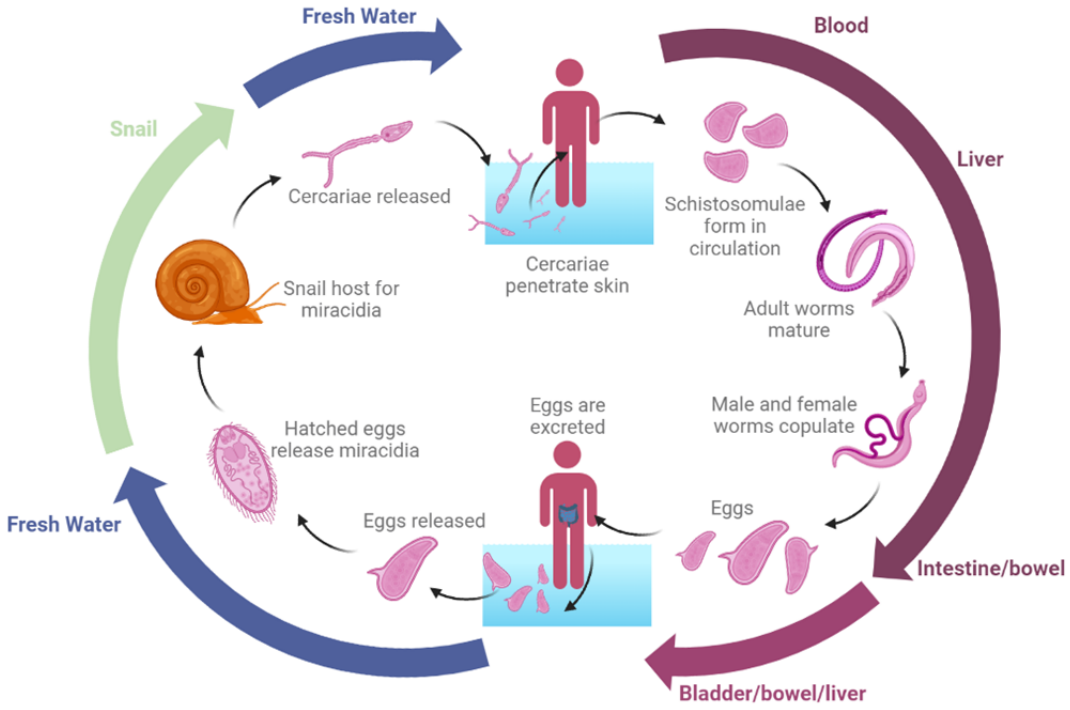

Figure 1.1 Schistosoma mansoni lifecycle
Illustration of the multiple *S. mansoni* lifecycle stages including the fresh water and intermediate host stage, as well as within a human-host. Based on (10).

1.1.3 Pathology/immunology of infection

Initial penetration and circulation of the schistosomula stimulates an early acute response in the host, primarily against specific cell surface antigens and/or worm secretions in the first 3-5 weeks, characterised by a mixed T helper 1 (Th1) and Th2-like response. Inflammatory cytokines such as IL-1, IL-6 and tumour necrosis factor (TNF)α, associated with Katayama Fever, are elevated (11). Individuals living in endemic regions rarely display signs of febrile illness, potentially as a result of *in utero* sensitisation, thereby reducing the development of a strong pro-inflammatory Th1 response (12). However, following the start of parasite egg laying, around 5-6 weeks post-infection, the Th1 response recedes and is replaced by a dominant Th2-like response (raised levels of IL-4, IL-5 and IL-13) (11). The presence of schistosomes and their eggs induces the differentiation of Th2 cells which promotes B cell class switching, favouring IgE production. Schistosome eggs are highly immunogenic and also release a multitude of immunomodulatory secretory products (13,14). Alpha-1 (α1) is a 38-40kDa dimeric glycoprotein, secreted by schistosome eggs, which has subsequently been named IL-4 inducing principle of *S. mansoni* eggs (IPSE). Schramm *et al.* (2007) demonstrated that IPSE is vital for IL-4 production by basophils in the liver, and that IPSE/α-1-depleted egg antigen did not result in cytokine production (14). Human eosinophils express both FcεRI and II (murine eosinophils only express FcεRI) that binds IgE, promoting their activation and degranulation upon antigen binding (15). In the absence of IL-4, and the associated Th2 response to dampen the pro-inflammatory response, schistosome infection in mice is lethal by 9 weeks post-infection (16–18). This mortality is associated with over-expression of pro-inflammatory mediators such as IFNγ, TNFα and inducible nitric oxide synthase (iNOS).

The Th2 response leads to formation of granulomas containing large numbers of alternatively activated macrophages and eosinophils around eggs that have become trapped within the liver and intestine (*S. mansoni*, *S. japonicum*) or in the bladder and urogenital system (*S. haematobium*) (19–22). As adult worms are long-lived in the vasculature, female worms continue producing hundreds of eggs per day resulting in the chronic state of infection (11). Despite the

requirement for a Th2 response in modulating infection progression, it is a double-edged sword as this mechanism is responsible for hepatic fibrosis and portal hypertension causing chronic morbidity and can itself be life threatening. Interestingly, between 8 and 20 weeks of infection, hepatic granulomas reduce in size which suggests a degree of hypo-responsiveness develops during chronic infection (23). The formation of granulomas around parasite eggs has beneficial effects for both the host and parasite as intestinal granulomas facilitate egg translocation to the lumen but as a consequence the gut wall becomes perforated which increases bacterial entry into host circulation (24–26). However, this mechanism remains controversial as some studies have not seen any increase in endotoxin levels of schistosome-infected individuals (27). Nevertheless, by trapping eggs within granulomas, host tissue is protected from exposure to highly antigenic eggs and hepatotoxic inflammatory egg components e.g. omega 1, which supports host survival and in turn parasite survival as well (23).

1.1.4 Treatment

Praziquantel (PZQ), developed in the 1970s by Bayer, has been the anthelminthic drug of choice, delivered by mass drug administration for the past 10 years (28,29). PZQ is effective against all forms of schistosomiasis, however it is less effective at killing parasites in their juvenile life-cycle stage compared with mature adult worms (29). Despite being used to treat millions of people, the mode of action is poorly understood, but studies of PZQ-resistant worms are providing crucial information about the mechanism of action (30,31). There are three, non-mutually exclusive, proposed mechanisms, i.e. inhibition of calcium influx into the worm, blocked muscle contraction and tegumental surface modifications (32–41). Ultimately, PZQ treatment results in death of adult worms, which stops schistosome egg production and limits infection progression. However, PZQ does not affect the existing immunogenic eggs that are lodged within tissues or directly reverse existing pathology and it also does not offer high levels of resistance against re-infection (42,43). Although, there are studies that suggest PZQ treatment does offer a low level of immunity by driving the switching of host immunoglobulin (Ig) production from IgA to a predominantly IgG1 response

(44,45). Unfortunately, over recent years the efficacy of PZQ has diminished with “hotspots” emerging where mass drug administration is not working, most notably in endemic areas within Africa, including Egypt, Senegal, Uganda, Ivory Coast and Kenya (46–48). This may be as a result of intense infection transmission and the development of drug resistance (29,49). The limited prevention of re-infection is problematic given people living in endemic rural areas often cannot avoid contact with infected water, either due to poor sanitation or necessity for their livelihood (1). People travelling to endemic areas are not given PZQ as a prophylactic due to its lack of effectiveness against juvenile schistosomula and its short half-life (1). The anti-malarial drug artemisinin has been shown to be effective against juvenile schistosomula and therefore could be used as a prophylactic treatment for both travellers and high-risk groups such as fishermen and flood relief workers (50). Oxaminiquine, is a pro-drug that is enzymatically activated by schistosome parasites and has also been used as a treatment, primarily in Brazil, but it is only effective against *S. mansoni* (51). For both PZQ and oxaminiquine to be effective, the infected individual must have a functioning immune system (52–54).

There is currently no vaccine publicly available for protection against any of the *Schistosoma spp*. Over the past decade more than a hundred potential vaccine candidates have been explored and shown promising results *in vivo,* however relatively few have progressed to human clinical trials (55). Many studies have shown older children and adults living in endemic areas to develop a degree of schistosome resistance to re-infection during their lifetime and this has been mimicked in mouse models. Mice treated with irradiated cercariae conferred up to an 80% protection against infection (42,56,57). However, the mechanism of this protection is poorly understood and therefore difficult to elicit through immunisation. One of the difficulties of vaccine development is the inherent ability of schistosomes to evade the host immune system and remain in the circulation for years. One potential vaccine target has been parasitic intestinal enzymes. These have had limited prior exposure to the immune system, and therefore infected individuals are unlikely to have pre-existing antibodies against these proteins. It is proposed that a vaccine

based on these intestinal enzymes will stimulate neutralising antibody production, meaning when the parasite feeds on the blood, antibodies will also be ingested and hopefully interfere with parasite digestion resulting in their death (58). An alternative approach has been to target the excretory/secretory (ES) products which are crucial for modifying the environment, enabling immune cell evasion (59). However, the high degree of redundancy in parasitic ES products means a combination of multiple factors may be required to drive sufficient immunity (58). The newest approach has been to target extracellular vesicles (EV) which are released in the ES products. These lipid-bound vesicles contain both proteins and small RNAs and have significant immunomodulatory effects (60). Despite vaccination with EV isolated from helminth ES products showing promise in murine models, it is not currently feasible to scale up the bioprocessing derivation of specific ES-containing EV. Therefore, focus is now on identifying specific EV antigens which can be produced and incorporated into a vaccine and elicit the same response as isolated EV.

The only three vaccine candidates currently in clinical trials are against *S. haematobium* 28-kDa glutathione S-transferase (rSh28GST), *S. mansoni* 14-kDa fatty acid-bind protein (Sm14) and *S. mansoni* tetraspanin, 9-kDa surface antigen (Sm-TSP-2)(61). The constant advancement of genetic and proteomic screening is being utilised to examine large numbers of surface tegument proteins of parasites at different stages of their lifecycle that are functionally important but also accessible as potential targets (62). A promising candidate that has been the focus of much research for 22 years is Sm-p80, this is the large subunit of a schistosome calcium-activated neutral protease calpain (63). Next generation RNA-sequencing and transcriptomic analysis has allowed the identification of immune signatures from different vaccine strategies with Sm-p80 as the target and helps build up a big picture about the mechanism of action (63).

1.1.5 Specific immune cell response to type 2 inflammation

Eosinophils: In healthy mice, eosinophils contribute less than 5% of all blood leukocyte populations and are relatively short-lived in the circulation (~18hr) before migrating to, and residing in the thymus, gastrointestinal tract, lung,

mammary glands or adipose tissue (~6 days) (64,65). However, following a helminth infection or allergic inflammation, numbers dramatically increase both in circulation and within tissues (66). IL-5 and the eotaxin chemokines (CCL11, CCL24, CCL26) activate eosinophils, promoting their differentiation and survival in the peripheral tissues, promoting eosinophilia. Furthermore, thymic stromal lymphopoietin (TSLP), which is expressed by many leukocytes (including dendritic cells (DC), T cells and B cells), as well as IL-25, which can be produced by Th2 cells and epithelial cells, also promote eosinophilia through the induction of IL-5 (67). IFNγ and eotaxins are just some of the signals that can also stimulate eosinophil degranulation and the release of a multitude of cationic proteins, cytokines, chemokines, growth factors and enzymes into the surrounding tissues (68). Cross-talk between eosinophils and different immune cells has been demonstrated in many different contexts. In adipose tissue eosinophils are the major source of IL-4 which maintains alternatively activated macrophage survival and maintenance of glucose homeostasis (69). Furthermore, in the context of allergic lung inflammation, alternatively activated macrophages enhance eosinophil recruitment to the tissue through the release of Ym1 (70). In the case of granulomatous inflammation, following schistosome egg injections, eosinophils contribute over 25% of the immune cells present in the granulomas (71). However, depleting eosinophils by treating mice with neutralising IL-5 monoclonal antibodies or using eosinophil lineage depleted mice (ΔdblGATA) does not reduce schistosome egg excretion in the faeces, liver granuloma size or fibrosis (72,73). In humans, ongoing clinical trials are being performed to test the efficacy and safety of drugs such as Benralizumab which is an IL-5Rα–directed cytolytic monoclonal antibody, in the treatment of uncontrolled asthma with eosinophil inflammation (74). So far, these eosinophil-depletion treatments appear to be well tolerated and effective with no apparent association with increased infections or malignancies (74).

T cells: Granulomatous inflammation in schistosome infection is reliant on a strong $CD4^+$ T cell response. $CD4^+$ T cells become activated following recognition of specific schistosome egg antigen (SEA) peptides presented on MHCII molecules of professional antigen presenting cells (75). As mentioned

previously, during the initial phase of infection, prior to egg deposition there is a mixed Th1/Th2 response. Egg deposition drives a strong Th2 response which gradually is dampened as the immune response is modulated in the chronic stages of infection, during which anti-inflammatory cytokines, such as IL-10 are elevated (11). $CD4^+$ T cells isolated within days of an initial infection express high levels of IFNγ, whereas those isolated from hepatic granulomas 8 weeks post-infection express high levels of IL-4, IL-13 and IL-5, and very little IFNγ (76). The depletion of $CD4^+$ T cells and the infection of T cell deficient mice both significantly reduce schistosome egg excretion, demonstrating the importance of T cells in granulomatous inflammation (17,54). Moreover, co-infection of individuals with *S. mansoni* and human immunodeficiency virus (HIV) show the same trend of fewer $CD4^+$ T cells and lower faecal egg counts (77). In both mice and humans, other subsets of T cells, such as regulatory T cells (Tregs) also expand during chronic infection. Tregs suppress DC activity and inhibit granuloma development and fibrosis (78–84). In this thesis we examine the interaction of immune cells and platelets in schistosome infection, in this regard the interactions between platelets and T cells are poorly understood. *In vitro* studies show T cell-platelet interactions can occur through contact-dependent and -independent mechanisms and these interactions can inhibit $CD4^+$ T cell proliferation (85,86). However, even in healthy individuals the effects of platelets on T cell differentiation and cytokine production is less clear, with the studies on human blood showing platelets can either enhance or inhibit IFNγ and TNFα production (85–87), which may reflect differences in starting cell populations, e.g. peripheral blood mononuclear cells or isolated $CD4^+$ T cells. Moreover, the complexity of T cell-platelet interactions is further complicated by the inflammatory context/disease state. For example, in patients with immune thrombocytopenia, platelets express auto-antigen driving enhanced production of IFNγ and IL-2 by $CD4^+$ T cells (88). The interaction of platelets and T cells in murine models is also complex and context specific. One example of this is murine cerebral malaria where platelets enhance $CD8^+$ T cell cytokine production and survival, whereas in murine polymicrobial sepsis platelets have the opposite effect (89).

B cells: The role of B cells in the regulation of schistosome infection is not fully clear as Hernandez *et al.* (1997) showed B cells are essential for Th2 polarisation (but not granuloma formation), whereas Jankovic *et al.* (1998) showed B cell deficient mice do not have any significant changes in T cell proliferation or differentiation (90,91). In mice the hepatic B cell population expands over the course of schistosome infection, particularly from 10 weeks post-infection (92). This correlates with a contraction of B cells in the mesenteric lymph nodes. The expansion of B cells in infection is polyclonal, resulting in increased antigen-specific and non-specific antibody production (93,94). SEA-specific antibody production is initiated following schistosome egg deposition and persists throughout infection, with IgM levels peaking at 12-16 weeks and IgG at 20 weeks post-infection (95). Studies culturing peripheral blood mononuclear cells from active schistosome-infected patients with serum from chronically infected patients or with immune-complexes with SEA resulted in reduced granuloma formation *in vitro*, suggestive of a protective and immunosuppressive effect on granulomatous inflammation (96).

Macrophages/monocytes: Mills *et al.* (2000) defined two distinct activation phenotypes of macrophages that develop in response to cytokine stimulation or pathogen molecules (97). These are commonly referred to as M1 (classically activated) and M2 (alternatively activated) macrophages. However, it is also well appreciated that *in vivo* the spectrum of macrophage activation is complex and additional activation states exist (98,99).

Understanding the mechanisms and stimuli required for macrophage polarisation *in vivo* has led to the development of more realistic and biologically relevant *in vitro* models. Polarisation to M1 macrophages requires two steps: firstly a “priming” step, then a ligand-toll-like receptor (TLR) interaction. IFNγ is thought to be the best primer of macrophages and is usually produced, and maintained at high levels by the activation of natural killer (NK), innate lymphoid cell (ILC)-1 and Th1 cells (100). The second step of ligand-TLR interactions usually occur in the presence of microbial organisms expressing pattern associated molecular patterns (PAMP). *In vitro*, the polarisation of murine macrophages to an M1-like phenotype is usually achieved by the

overnight culture of macrophages with a combination of lipopolysaccharide (LPS) and IFNγ (100). As M1 macrophages express iNOS to metabolise arginine to citrulline and nitric oxide, iNOS is commonly used as a marker of classical activation (98). In contrast, M2 macrophages develop in response to Th2-associated cytokines, IL-4 and IL-13 (101,102). In murine macrophages, this causes activation of STAT6 and upregulates the transcription of genes including: arginase 1 (*Arg1*), resistin-like molecule alpha (RELMα) (*Retlna*) and chitinase-like protein Ym1 (*Chil3*) (103–105). Of note, there are no human homologues of *Retlna* and *Chil3,* and *Arg1* is not produced in human macrophages in response to IL-4/IL-13. Instead, dual staining of transglutaminase 2 and mannose receptor C type 1 (CD206) are commonly used for identification of M2-like macrophages in humans (106).

Hepatic macrophages in both mice and humans originate from the yolk sac during embryonic development and also from blood monocytes. The majority of tissue resident macrophages (Kupffer cells) are produced from early embryonic progenitors in the yolk sac before definitive haematopoiesis from haematopoietic stem cells (HSC) in the bone marrow (BM) takes over (107). Lineage tracking experiments in mice have shown that macrophages produced as early as E8.5 persist into adulthood (108). Under steady-state conditions Kupffer cells undergo self-renewal (107). Kupffer cells are primarily located along sinusoids and act as the first line of defence for the liver; removing blood-borne pathogens (109). Moreover Kupffer cells are vitally important for the removal of desialylated, aged platelets through the macrophage galactose lectin (110).

As haematopoiesis shifts from the foetal liver to the BM during development, macrophages arise from HSC along the differentiation hierarchy (107). Following Kupffer cell depletion, it appears that recruited monocyte derived-macrophages are able to differentiate and become fully functional Kupffer cells (109). However, the liver microenvironment has a massive effect on the differentiation process of monocyte derived macrophages (111). There are two main murine populations of monocytes: Ly6C^{hi} (classical) and Ly6C^{lo} (non-classical or patrolling). Different pathogens induce specific cytokine and inflammatory mediators that drive distinct differentiation and maturation of BM

derived monocytes (112,113). Schistosome infection gives rise to a Th2 response and results in elevated monopoiesis in the BM and the release of classical monocytes, also called inflammatory monocytes (Ly6C^{hi}, CX$_3$CR1^{lo}, CCR2^{+}), and non-classical or patrolling monocytes (Ly6C^{lo}, CX$_3$CR1^{hi}, CCR2^{lo}) into the circulation (114). Schistosome eggs activate classical monocytes and CCL2 mediates recruitment of inflammatory monocytes into tissues, such as the liver, during schistosome infection. The microenvironment within granulomas gives rise to macrophage alternative activation through the upregulation of many genes including *Chi3l3*, *Pdl2*, *Arg1* and *Retlna* which trigger transforming growth factor (TGF)-β production and the deposition of collagen (114). Moreover, the M2 differentiation and IL-10 production has been shown to suppress M1-like activation (114).

Girgis *et al.* (2014) showed by adoptive transfer of Ly6C^{lo} and Ly6C^{hi} monocytes, that Ly6C^{hi} monocytes are precursors for M2 macrophages that predominate in schistosome infection (115). Furthermore, Gundra *et al.* (2014) showed that monocyte-derived macrophages are the primary contributors to M2 macrophages within *S. mansoni* egg granulomas (103). It has since been shown that monocyte recruitment to liver is IL-4Rα independent and that resident Kupffer cells are almost completely lost by 8 weeks of infection (116).

1.2 Platelets and haemostasis

1.2.1 Megakaryopoiesis and Thrombopoiesis

Platelets are small, disc-shaped cell fragments produced from megakaryocytes (MK) with a lifespan of 8-10 days in humans and ~5 days in mice (117). In 1906, James Homer Wright proposed that “blood plates are detached portions of the cytoplasm of those giant cells of the BM and spleen” which Howell named “megakaryocytes” (118,119). The process of megakaryopoiesis and thrombopoiesis has since been extensively studied.

Platelet membrane glycoproteins are coated with terminal sialic acids, which protect against clearance and destruction. As platelets age they become desialylated by sialidases, which are produced endogenously, as well as

exogenously by many bacteria and viruses. These cleave terminal sialic acid residues exposing β-galactose sugars which are recognised by the Ashwell-Morrell receptor (AMR) on hepatocytes, resulting in platelet clearance (120).

MK are large (30-100μm – human, 20-30μm – murine diameter) cells that are rare (~0.01-0.05%) compared with other haematopoietic populations in human BM (121–123). For decades, it was believed that MK arise from the sequential differentiation and lineage restriction along the myeloid arm from HSC. HSC give rise to multipotent progenitors (MPP) and the MPP2 population preferentially differentiates towards the common myeloid progenitors (CMP) that can produce either the granulocyte/monocyte progenitors (GMP) or the megakaryocyte/erythroid progenitors (MEP). There are two major drivers of CMP differentiation in mice and humans, PU.1 (SPI1) which favours GMP development and GATA-1 which regulates MEP (124). Both MK and erythrocytes can arise from the shared MEP population, with Cannabinoid receptor interacting protein (CNRIP1), Krüppel-like factor (KLF1), and Lymphoid enhancer-binding factor 1 (LEF1) becoming upregulated in erythro-biased cells and CD41, CD61, CD42, nuclear factor 1B (NF1B), and von Willebrand factor (vWF) increasing in MK-destined cells (125–127). However, a new dogma is emerging, recently reviewed by Leila *et al.* (2019), that identifies a population of long-term HSC and MPP2 that are capable of directly differentiating into MK (121,128,129). Sanjuan-Pla *et al.* (2013) identified that vWF^+ HSC were strongly biased (~60%) towards the production of MK and platelets, and were in fact above vWF- HSC in the tree of haematopoietic differentiation (129). It was then shown that these murine HSC could differentiate directly into CMP-, MEP- or MK-biased HSC whilst retaining self-renewal capacity (129,130).

As MK mature, they become polyploid (up to 128N) by undergoing endomitosis. Endomitosis was believed to be characteristic of late anaphase failure (131,132). However, it is now thought that endomitosis is due to a failure in cytokinesis and the formation of the contractile ring and spindle elongation (133). Once mature, MK extend pseudopodia-like projections, known as proplatelets. These processes extend from the BM into the vasculature where thousands of platelets bud-off and enter the circulation

(134–136). The complete mechanism behind proplatelet and mature platelet formation is not yet fully understood, however it is believed that the MK cytoskeleton and associated machinery drives platelet production (137). The contents of MK, including the organelles and granules are also transported to the proplatelet tips and are included during platelet budding (138). Recent studies using live cell imaging and super resolution microscopy of primary mouse MK have shown how MK differentially sort and package the contents of α-granules into the platelets produced (139).

There are many cytokines involved in MK maturation and platelet production, with thrombopoietin (TPO) regarded as being the most important. In 1994, TPO and its receptor c-MPL were discovered, leading to a dramatic increase in the number of groups investigating their role in megakaryopoiesis and thrombopoiesis (139–145). TPO is primarily produced by hepatocytes in the liver and secreted into circulation (145,147). In healthy individuals, TPO binds to MPL on circulating platelets and is sequestered (148). This sponge theory of TPO ensures that when platelet numbers are low more TPO becomes available to bind to MPL on MK (149,150). This results in receptor-ligand complex internalisation and the intracellular signalling cascade involving Janus kinase (JAK)2 and signal transducer and activator of transcription (STAT)3/5, ultimately causing the upregulation of MK specific genes (151). In both mice and humans, TPO has been identified as a critical regulator of platelet production through its role in supporting MK survival, proliferation and differentiation from progenitors (152).

Traditionally, the BM has been identified as the major site of platelet production, however there have been several studies exploring pulmonary platelet production (153–155). Aschoff (1893) was the first to show MK in lung blood vessels and a greater number of platelets in the blood exiting the lung compared with that entering (154,156). The controversy surrounding the theories of platelet production occurring in the lung, is primarily due to the lack of direct evidence of lung MK being functionally able to produce platelets (157). However, in the last decade, Lefrancais *et al.* (2017) performed intravital microscopy and showed large numbers of MK circulating through the lung and producing ~10 million platelets per hour (~50% total platelets) into the

circulation (158). Moreover, recent single-cell RNA sequencing studies have also shown lung MK to express more immune-associated molecules than BM MK, suggesting not only do lung MK contribute to platelet production but also contribute in the response to pathogenic challenge (159).

Extramedullary haematopoiesis may occur in response to infections, myeloproliferative neoplasms and some leukaemias (160). Severe BM stress can result in progenitor and precursor cells localising to peripheral organs, such as the liver and spleen (161–163). For example, in sepsis megakaryocyte-erythroid progenitors traffic from the BM to the spleen where they differentiate to platelet-producing MK with immune-protective roles in the acute inflammatory state (164). As megakaryopoiesis and thrombopoiesis rely on specific cues from the extracellular matrix, such as type I collagen promoting MK differentiation but inhibiting proplatelet formation, it is still not clear whether all extramedullary MK are functional in producing platelets (165). Therefore, in response to some infections like *S. mansoni* where there is a lot of fibrosis and collagen deposition, MK functionality may be impacted (161).

1.2.2 Haemostasis

Historically, the majority of platelet research has focussed on their involvement in haemostasis and their ability to bind rapidly and aggregate at sites of vascular injury, ultimately forming an insoluble thrombus and reducing the risk of excessive bleeding (166). There are two main stages to the formation of the stable thrombus; primary and secondary haemostasis. Primary haemostasis is the process of vasoconstriction, platelet rolling, aggregation and plug formation on exposed sub-endothelial tissue (167). Secondary haemostasis is the process that results in the deposition and crosslinking of fibrin, ultimately stabilising the platelet plug and forming an insoluble thrombus (167). It can be broken down into 2 converging pathways, the intrinsic and extrinsic pathways which culminate in the production of activated factor X (Xa) (168). The intrinsic pathway can be stimulated by the presence of negatively charged surfaces or molecules, and the extrinsic pathway is triggered by the exposure of platelets to tissue factor (TF) following vascular damage (169,170). In addition, platelets also interact with exposed collagen and extracellular matrix proteins which causes platelet activation, the expression

of numerous surface molecules including active conformation integrin αIIb/β3 (also known as GPIIbIIIa or CD41/CD61) and P-selectin (CD62P), as well as the degranulation and release of soluble factors e.g. adenosine diphosphate (ADP), thromboxane A2 and serotonin (**Figure 1.2**). These pathways were first described as a waterfall of clotting factors sequentially converted to enzymatically active forms (**Figure 1.2**).

In combination, these activation responses drive platelet-platelet and platelet-fibrinogen interactions aiding platelet plug formation and stimulating secondary haemostasis and the coagulation cascade (117,171–173). All these pathways are tightly regulated, closely connected and critical in converting mechanical information, in the form of vascular damage, into biochemical signals that allow the rapid plugging of the damaged site through a stable fibrin thrombus (174).

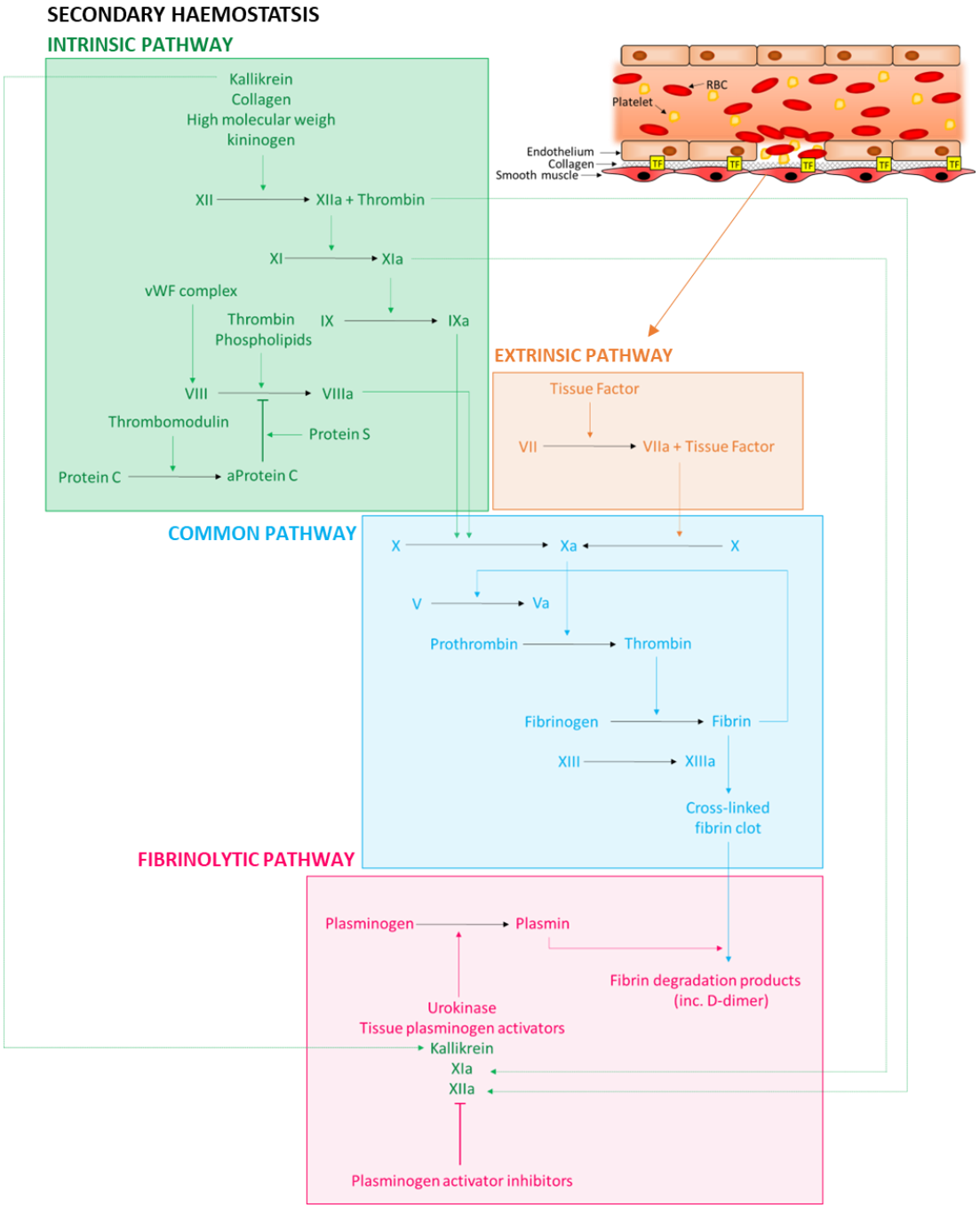

Figure 1.2 Coagulation cascade

Summary of the blood coagulation cascade, highlighting the converging intrinsic (green) and extrinsic (orange) pathways which result in the activation of Factor X and the common pathway (blue). Activation of the common pathway gives rise to the formation of a stable fibrin clot. Under steady-state conditions a fibrin clot is degraded by the process of fibrinolysis (pink). Blunt arrow (⊢) represents inhibition, sharp arrow (←) represents activation.

1.2.3 Thrombocytopenia and ITP

In humans, immune thrombocytopenia (ITP) is defined as reduced platelet number (<100 x10^9/L, whereas normal range 150-450 x10^9/L). Primary ITP is idiopathic, whereas secondary ITP arises as a result of underlying conditions/treatments, such as systemic autoimmune disorders, drug-mediated, or infectious diseases (175). Despite significantly depleted platelet numbers, patients with platelet counts >30x10^9/L rarely display severe bleeding phenotypes, which only occurs with platelets <10x10^9/L (176). The reduction in platelets can be caused by accelerated platelet clearance, reduced platelet production or a combination of both of these factors.

Studies in the 1950s by Harrington *et al.* identified the mechanism of antibody-mediated platelet destruction through the transfusion of plasma from ITP patients resulting in thrombocytopenia in healthy individuals (177). The majority of auto-antibodies are IgG (particularly IgG1), however IgM class antibodies have also been detected and appear to be responsible for fixing complement and facilitating platelet clearance (178,179).

Macrophages are the major phagocytes responsible for steady-state splenic platelet clearance, and in response to inflammatory cytokines activated macrophages drive clearance of auto-antibody-opsonised platelets. Activated macrophages may also increase expression of major histocompatibility complex (MHC)-II to enhance auto-antigen presentation, contributing to a persistent “feed-forward” loop (180). Auto-antibodies against platelet GPIIb/IIIa are the most common (~70%), but auto-antibodies against the GPIb-IX-V complex, GPIa-IIa and GPVI are also found (181). A recent study demonstrated that the more antibodies patients had against different antigenic targets on the platelets, the more severe the thrombocytopenia (182). Through clinical studies and murine models, the best understood mechanism of platelet destruction is via the recognition of fragment crystallisable (Fc) regions on auto-antibody-opsonised platelets by FcγRI, FcγRIIa (human only) and FcγRIIIa on tissue resident macrophages in the spleen (183–185).

As the platelet-producing pre-cursors, MK also express on their surface many of the same glycoproteins as platelets, auto-antibodies bind MK as well as

platelets thereby inhibiting MK production and maturation (186). MK autophagy is also suppressed resulting in impaired MK formation and differentiation, which gives rise to larger, but fewer platelets (187–189).

In ITP patients without auto-antibodies, increased levels of cytotoxic $CD8^+$ T cells have been detected. These cytotoxic $CD8^+$ T cells directly lyse platelets, induce platelet apoptosis and inhibit thrombopoiesis by MK (190,191). In addition, cytotoxic T cells can also drive platelet desialylation resulting in accelerated platelet clearance by hepatocytes (192).

1.2.4 Thrombocytopenia in liver disease

Thrombocytopenia is seen in ~60-80% of chronic liver disease (CLD) patients (193). Unlike ITP, CLD often causes a reduction in TPO secretion into the circulation as hepatocytes are the primary producers of this factor, and low circulating TPO prevents the stimulation of MK to produce more platelets (149,150). Furthermore, platelet production can be inhibited as a result of BM progenitor cell suppression, which can be caused by viruses, excess alcohol and iron overload which is a result of red blood cell lysis and reduced hepcidin, also produced by the liver (194).

Splenomegaly often accompanies CLD due to portal hypertension, and this redirection of blood circulation causes platelet sequestration within the spleen (195). As the platelets are still present, they are still able to “sponge” circulating TPO, thereby preventing MK stimulation and the production of more platelets into the circulation.

Thrombocytopenia in CLD can also occur due to platelet destruction caused by increased shear stresses, immunological mechanisms, increased fibrinolysis, bacterial translocation and infection (194). Shear stress enhances platelet aggregation through the conformational change of ultra-large von Willebrand factor to an extended chain form (196). Finally, auto-antibodies against both platelets and MK can arise as a result of autoimmune- and chronic-hepatitis (194,197). In many CLD patients there is also an enhanced production of clotting factors as well as reduction of inhibitory factors which leads to accelerated intravascular coagulation and fibrinolysis, and ultimately enhanced platelet consumption (198). Liver cirrhosis can cause endotoxemia

which can enhance pro-inflammatory cytokine production which reduces MK differentiation. This can also promote B cell production of auto-antibodies which drives platelet opsonisation and clearance, contributing to enhanced platelet-monocyte aggregates (199–202).

1.3 Platelets and immunomodulation

More recently, platelet function has been shown to extend beyond their classical role in haemostasis and they are now known to function as immune cells during inflammation and infection (203–205). In this regard, platelets express cytokine and chemokine receptors, TLR and many other adhesion molecules (206) (**Figure 1.3**).

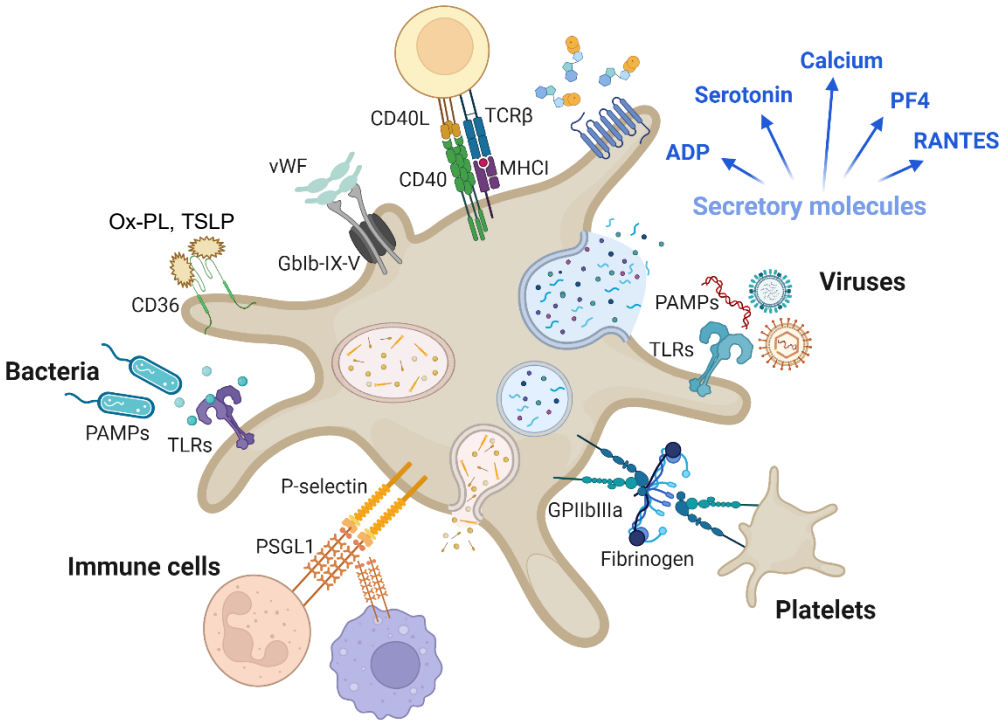

Figure 1.3 Immunological features of murine platelets
Simplified illustration of some of the receptors, molecules and secreted compounds that contribute towards the immune-modulatory role of platelets. PSGL1 - P-selectin glycoprotein ligand-1, TLR – Toll-like receptors, PAMPS - pathogen-associated molecular patterns, TSP-1 – thrombospondin-1, oxPL – oxidised phospholipids, vWF – vonWillebrand Factor, MHCI – major histocompatibility complex, TCR – T cell receptor, ADP - Adenosine diphosphate, PF4 – platelet factor 4, RANTES - Regulated upon Activation, Normal T Cell Expressed and presumably Secreted. Based on (207)

1.3.1 Platelets in non-infectious disease

Cancer: Cancer development is typically associated with cellular immortality, evasion of the immune system, cell death signals and growth suppressors. Moreover, cancer cells have sustained proliferative signals and are able to reprogramme energy metabolism as well as induce angiogenesis to support survival (208). Platelets can become activated in response to both the pro-inflammatory tumour environment as well as activation molecules like ADP released directly from tumour cells. Furthermore, C-type lectin-like immune receptor 2 (CLEC-2) and TLR4 on platelets can directly interact with podoplanin which is expressed at the invasive front of many tumours and the high-mobility group box 1 (HMGB1) released from dying tumour cells respectively (209). Together the activated platelets release a multitude of growth factors (e.g. VEGF, PDGF and TGF-β) which in turn cause an upregulation of IL-8, CCL2 and CXCL12 by the tumour cells. These cytokines drive tumour proliferation, angiogenesis and chemoresistance.

Tumours also induce platelet aggregation which provides a physical, protective barrier around the tumour cells, thereby protecting them from shear stress as well as shielding them from immune surveillance by NK cells (209). Ultimately, tumour cell-induced platelet aggregation aids metastatic spreading and tumour growth. The tumour associated platelet aggregates also contribute to the risk of cancer-related thrombosis and associated conditions like strokes and pulmonary embolisms (210). Therefore, inhibiting these aggregates is a potentially important therapeutic intervention for cancer patients (**Figure 1.4**).

Despite the pro-tumour roles of platelets, the close interactions associated with platelets and tumour cells can be harnessed for drug delivery and immune cell re-programming to reduce tumour growth and tumour relapse after surgical treatment. Recently, mouse models have been used to genetically engineer MK to produce platelets that express programmed cell death (PD)-1 and are loaded with the chemotherapeutic drug cyclophosphamide (211). These modified platelets can be transplanted into tumour-induced mice post-tumour removal and naturally migrate to the site of surgery due to the very nature of platelets patrolling the vasculature. Platelet PD-1 will bind any remaining

tumour PD-L1, driving the release of cyclophosphamide from the platelets. Cyclophosphamide activates $CD8^+$ cytotoxic T cells by killing Treg cells thereby removing their inhibitory signals. This allows CD8-mediated killing of any remaining tumour cells not excised during surgery and ultimately reducing the risk of relapse. In this study, mice treated with cyclophosphamide-loaded, PD-L1-expressing platelets showed significantly supressed tumour growth and improved survival (211).

Atherosclerosis: Atherosclerotic lesions occur from the repeated exposure to injurious stimuli which damage the vessel wall and result in complex cellular interactions and signalling. Sustained elevations in plasma low-density lipoproteins (LDL) molecules results in accumulation in the sub-endothelium, where they aggregate and undergo a variety of modifications (e.g. oxidation, enzymatic cleavage) (212). As a consequence of chemotactic secretions and adhesion receptor expression, leukocytes and monocytes are recruited (213). These recruited immune cells form plaques which perpetuate the inflammatory response and drive vascular remodelling and thrombus formation. Hypercholesterolemia induces platelet activity, thereby driving circulating platelet-monocyte aggregates (214). Platelets also drive the recruitment of monocytes into atherosclerotic plaques, resulting in enhanced platelet-macrophage aggregates (215,216). Furthermore, platelets skew plaque macrophages to a pro-inflammatory phenotype through the upregulation of suppression of cytokine signalling 3 (SOCS3). As a consequence of the platelet interactions the macrophages are less able to perform efferocytosis, which drives lesion growth (**Figure 1.4**) (217).

Allergy: It has been known for more than 50 years that allergic individuals display platelet abnormalities (218,219). Platelets are activated in allergy, resulting in platelet degranulation and release of platelet-specific products such as platelet factor (PF4) and β-thromboglobulin (220). The mechanism of platelet activation in allergy has been linked to pro-inflammatory/stimulatory molecules (e.g. platelet activating factor and thromboxane A2), IgE and direct activation by allergens (220). Both experimental animal models and patient samples have shown the involvement of platelets in leukocyte recruitment to allergen exposed tissues. Eosinophil recruitment to the airways requires their

activation and this has been positively associated with platelets due to the interaction of platelet P-selectin and eosinophil PSGL-1 (206,221). Activated airway eosinophils release inflammatory mediators which cause mucus overproduction, airway remodelling and broncho-restriction (220). In multiple different animal models, platelet depletion using anti-platelet antibodies causes a significant reduction in eosinophil infiltration and decreased hyperresponsiveness after allergen exposure (**Figure 1.4**) (206,222).

Whilst targeting platelet-eosinophil interactions for pharmacological benefits using existing anti-platelet drugs has not been extensively studied, some studies have shown that treatment with P2Y12 antagonists have only limited effect on pulmonary leukocyte recruitment. This suggests that the response of platelets to inflammatory stimuli in the process of host defence may be different from that associated with platelet aggregation following vessel damage (223).

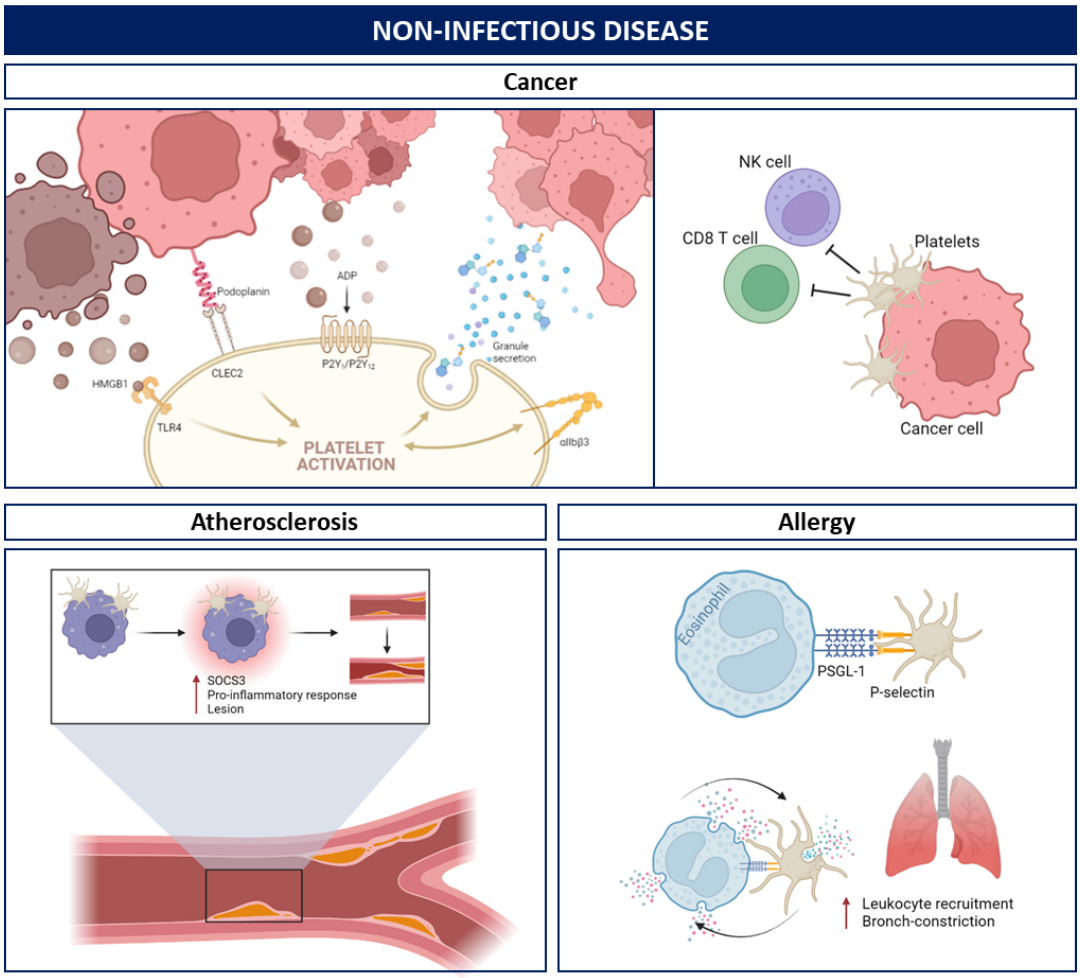

Figure 1.4 Summary of the immunological role of platelets in non-infectious diseases
Platelets play an important role in many non-infectious diseases. In cancer platelets have been shown to become activated following the release of molecules such as HMGB1 and ADP as well as direct contact e.g. through CLEC-2 – podoplanin interactions. Platelet activation results in degranulation and the release of a plethora of signalling molecules which can drive tumour proliferation and angiogenesis. Moreover, platelets can coat tumour cells thereby shielding them from immune cell recognition and killing. In atherosclerosis, hypercholesterolemia drives platelet activation and recruitment of macrophages/monocytes which perpetuates inflammation. Platelets also skew monocytes towards a pro-inflammatory phenotype through the upregulation of SOCS3 which exacerbates plaque formation. In allergy platelets are activated and interact with immune cells such as eosinophils through P-selectin – PSGL-1 dependent interactions. This drives a feedforward activation loop and exacerbates the inflammation. In addition, platelets drive leukocyte recruitment to the inflamed tissue such as the lung in allergic asthma. TLR – Toll-like receptor, HMGB - High mobility group box, CLEC - C-type lectin-like type, ADP – Adenosine diphosphate, NK – Natural killer, SOCS - Suppressor Of Cytokine Signalling, PSGL – p-selectin glycoprotein ligand.

1.3.2 Platelets in infectious disease

Bacterial infections: Platelets have a plethora of roles in bacterial infections from directly interacting with the invading bacterial pathogen, orchestrating the inflammatory response, and forming thrombi in response to activation and endothelium damage (224). There are multiple platelet surface receptors such as GPIIb/IIIa and FcγRIIa, which facilitate platelet-bacterium interactions. As a result of these interactions, platelets directly internalise bacterium as well as enhance their destruction by other components of the immune system including complement (225).

Platelets are also important in the recruitment and polarisation of specific immune subsets at different stages of infection. For example, Rossaint *et al.* (2021) demonstrated in a *Klebsiella pneumonia* infection, that platelets drive the recruitment of neutrophils into the lungs to stimulate bacterial killing. During the resolution phase of infection, platelets form platelet-Treg aggregates, enhancing the production of IL-10 and TGFβ, which re-program macrophages to an anti-inflammatory, wound-healing phenotype that is essential for inflammatory resolution (226). Interestingly, the platelet response to infection appears context-specific as Carestia *et al.* (2019) showed in an *in vivo* model of sepsis that platelets actually promote a pro-inflammatory macrophage phenotype which enhances bacterial clearance and increases infection survival (227). In both these murine infection models, platelet counts negatively correlated with disease severity, with low platelet levels being associated with reduced host survival.

Bacterial infections typically induce endothelium damage and increase the exposure of TF on endothelial cells as well as circulating monocytes and neutrophils (228). Moreover, bacterial infection drives platelet and coagulation factor activation as well as activated factor cleavage, together these haemostatic changes cause disseminated intravascular coagulation (DIC), where fibrin clots are deposited in the microvasculature (229). This impairs oxygen delivery to vital organs and can be fatal (**Figure 1.5**).

Viral infections: During the SARS-CoV2 pandemic, extensive research uncovered the complex two-sided relationship between platelets and viruses

during infection. It had previously been shown that platelets can endocytose viruses such as enteroviruses, influenza A and HIV type-1, through the interaction of viruses with dendritic cell-specific intercellular adhesion molecule-3-grabbing nonintegrin (DC-SIGN) and CLEC-2 on the surface of platelets (215,230). Conversely, despite their lack of nucleus and their ability to directly kill viruses, other studies have shown platelets serve as hosts for viral replication (231). This can favour viral survival and dissemination as they are protected from immune detection.

As well as direct antimicrobial effects, activated platelet-leukocyte interactions and platelet secretions can be beneficial for viral clearance, highlighting the complex double-edged sword associated with platelet-virus interactions (**Figure 1.5**) (215,232). For example, viral activation of platelets stimulates the release of monocyte chemoattractant protein 1 and granulocyte-macrophage colony stimulating factor, both of which are important for leukocyte recruitment and viral targeting (215). Activated platelets also release pro-thrombotic molecules such as serotonin, which drives a hypercoagulable pathological state and DIC (216,233,234). Elevated platelet-leukocyte aggregates and thrombi also contribute to thrombocytopenia seen in response to severe infection which correlates with poorest infection prognosis and haemorrhaging risk (215,216).

Protozoal infections: Similar to bacterial and viral infections described above, platelets can both directly kill some protozoa (e.g. *Plasmodium spp*.) but also contribute to disease progression through the development of microvascular occlusions and thrombocytopenia (235). In a *P. falciparum* infection, platelets directly bind to infected erythrocytes which can both mediate erythroid clumping and microvascular occlusion but also allow platelet factor 4-mediated killing of the parasites (236). Interestingly, TPO levels are significantly elevated in patients with severe *P. falciparum* malarial infections but reduced in people with visceral leishmaniasis (VL) (237). VL induces a strong type 1 inflammatory response with abundant IFNγ, IL-12 and TNF. A complex array of haematological and immune perturbations are found in the clinic and mouse models, including anaemia and thrombocytopenia (238). Interestingly, in one murine model, Rani *et al.* (2021) demonstrated that

despite no change in MK number, morphology was altered and maturation was reduced by infection (238). Moreover, the expansion of highly active, pro-inflammatory splenic macrophages was shown to contribute to elevated platelet clearance. Despite the many differences in these two protozoal infections (malaria and leishmaniasis), in both cases mAb platelet depletion did not significantly affect parasite burden (**Figure 1.5**) (239).

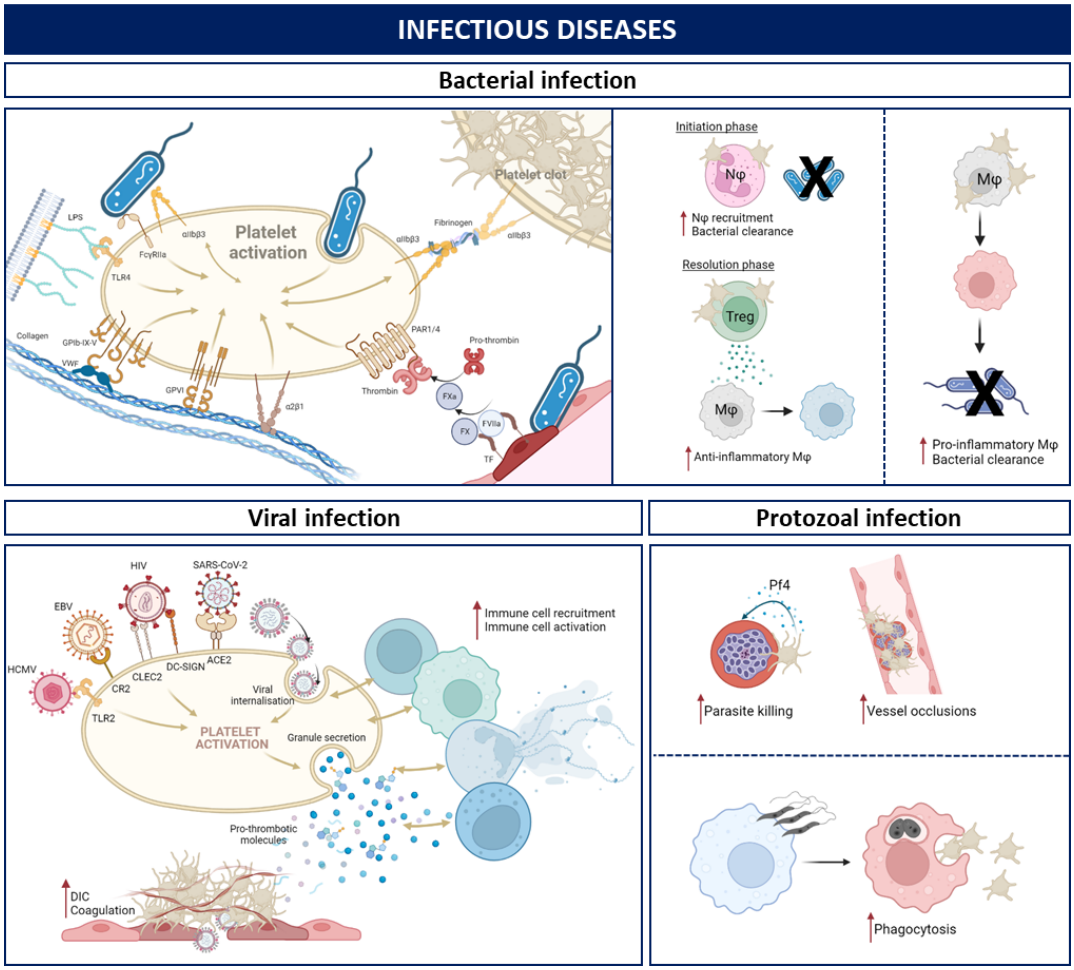

Figure 1.5 Summary of the immunological roles of platelets in infectious diseases
Platelets have many different effects in a range of infectious diseases. In bacterial infections platelets have a range of responses from directly interacting with the invading bacterial pathogen, orchestrating the inflammatory response, and forming thrombi in response to activation and endothelium damage. The platelet response appears to be context specific with platelets having differing roles throughout the progression of a *K. pneumonia* infection which differs from the pro-inflammatory response in an *E. coli* model of sepsis. In viral infections platelets can directly interact with invading viruses via a range of receptors, resulting in their internalisation and platelet activation. Platelet activation and degranulation drives immune cell recruitment and activation which in turn drives platelet activation and release of pro-thrombotic molecules which give rise to thrombus formation in the vasculature. Again, in protozoal infections such as malaria and leishmaniasis the role/impact on platelets is context specific. With platelets driving the aggregation and clearance of infected erythrocytes in a *P. falciparum* infection or platelets being cleared more rapidly in an *L. donovani* infection. LPS – Lipopolysaccharide, TLR – Toll-like receptor, PAR - Protease-activated receptors, vWF –

Von Willebrand factor, HCMV – Human cytomegalovirus, EBV – Epstein–Barr virus, HIV - Human immunodeficiency virus, SARS-CoV2 - Severe acute respiratory syndrome coronavirus 2, CLEC - C-type lectin-like type, ACE - Angiotensin-converting enzyme, DIC – Disseminated intravascular coagulation, PF4 – platelet factor 4.

1.3.3 Platelets involvement in schistosome infection

Human studies: Over the past 50 years there has been a growing interest in platelet number and functionality in *S. mansoni* infection (240–247). In all human studies examining blood parameters during infection, a degree of thrombocytopenia has been observed in a subset of patients, with some studies reporting thrombocytopenia (platelet count < 100 x 10^9/L) in as many as 95% of individuals with hepatosplenic schistosomiasis (241). Impaired coagulation and haemostatic functions were also observed alongside the reduced platelet counts. International normalised ratio (INR), partial thromboplastin time (PTT), D-dimer levels and fibrin degradation products are all elevated in *S. mansoni* infected individuals (240,242,246). This indicates impaired thrombus formation, consistent with internal bleeding pathologies being associated with schistosome infection (21). Due to the prevalence of thrombocytopenia and loss of haemostatic equilibrium in schistosome infections, it was investigated whether platelet levels are predictive of disease pathology. Most studies have shown there to be a negative correlation between platelet number and faecal egg count, as well as platelet number and spleen size (240,242,244,246). The haemostatic changes that occur in schistosome infection are summarised in **Table 1**.

Table 1: Haemostatic changes in human schistosome infection

Haemostatic changes *S. mansoni* infection	Range	Fold change (mean ± 2SD)	References
Thrombocytopenia (Significant reduction compared with controls)	Plt count (x10^3/µl) Healthy: 229.6 - 277 *Sm*: 55.9 – 244	1.26 (0.79)	(240–246, 248–250)
Normal platelet range	150-450 (x10^3/µl)	-	(251)
Circulating TPO unaffected			(244,245, 252)
Reduced serum TPO			(253)
Spleen size negatively correlates with platelet count			(236–238, 240,243, 248,249)
Spleen size does NOT correlate with platelet count			(241)
Increased clotting time	PT (s) Healthy: 11.9 – 13.9 *Sm*: 13.8 – 17.1 aPTT (s) Healthy: 23.4 – 31.2 *Sm*: 34.3 – 37.9	PT 1.15 (0.18) aPTT 1.31 (0.54)	(240,242, 246,248)
Reduced MPV	Healthy: 8.69 – 9.7 *Sm:* 6.05 – 8.39 (µm^3)	1.32 (0.80)	(248,250)

Plt – platelet, TPO – Thrombopoietin, PT – prothrombin time, aPTT – activated partial thromboplastin time, MPV – Mean platelet volume

Platelet production/destruction: It is not well understood how schistosome infection leads to thrombocytopenia. Serum TPO levels do not correlate with platelet numbers in human studies, and therefore the focus has shifted towards enhanced clearance of platelets in the periphery instead of deficient platelet production (244,245). In 2003, Stanley *et al.* proposed schistosomiasis leads to immune-dependent thrombocytopenia. Infection of athymic, T cell depleted, mice did not lead to significant reductions in platelet number (256). The authors suggested that schistosomes and platelets share cross-reactive antigens, and so infection leads to auto-antibodies against platelets. In support of this, non-infected rabbits immunised with human or mouse platelets produce cross-reactive antibodies capable of recognising schistosome molecules (256). However, this does not prove antibodies elicited by *S. mansoni* infection cross-react with platelet antigens and induce

their clearance from circulation. More recently, it has been shown that human platelets display a more activated phenotype in *S. mansoni* infection, with increased expression of surface P-selectin negatively correlating with platelet number (257). In a murine model of essential thrombocythaemia they demonstrated that activated platelets are cleared by monocytes and neutrophils in both a P-selectin dependent and independent manner. This ultimately results in fewer platelets in circulation and the accumulation of activated platelets in the spleen (258). Whether this is occurring in schistosome infection, is yet to be examined.

Effects on haemostasis: One of the main mysteries concerning platelets in *S. mansoni* infection is that despite the presence of the large worm pair (~1cm long and 1mm in diameter) in the vasculature, they can survive in the circulation for decades without inducing coagulation (259). This evasion of the coagulation cascade is surprising given that schistosomes induce both stasis and endothelial activation, two of the three factors of Virchow's triad that stimulate thrombosis (9,259). As such, several groups have investigated components of schistosomes that may prevent haemostasis (259).

Three phosphatases have been uncovered that provide a degree of anti-thrombotic activity. *S. mansoni* ectonucleotide pyrophosphatase-phosphodiesterase (NPP) 5 is a tegument phosphatase, most highly expressed by adult worms (260). SmNPP5 inhibits platelet aggregation in response to ADP agonists and to a lesser extent with collagen, by promoting ADP hydrolysis so preventing platelet activation and the coagulation cascade (261). The same group also showed another *S.mansoni* tegument phosphatase, alkaline phosphatase (AP), highly expressed by adult worms, can cleave adenosine monophosphate (AMP) to adenosine (262,263). As adenosine is an immunosuppressant, SmAP supports parasite survival and evasion of the immune system as well as inhibiting thrombus formation (263). SmAP has also been shown to cleave polyphosphate (PolyP) (262), which is released by immune cells and activated platelets leading to inflammation and pro-thrombotic pathways (264). Therefore, SmAP cleavage of PolyP, inhibits inflammation and thrombosis (262).

Finally, *S. mansoni* ATP-diphosphohydrolase (SmATPDase), expressed by both larval and adult worms, is the primary phosphatase responsible for ATP and ADP hydrolysis (6,265,266). Together, these studies show the worm surface contains at least three phosphatases with overlapping functionality which can reduce platelet activation and coagulation, as well as promoting immune evasion.

Direct platelet-schistosome interactions: Platelets can directly interact with different schistosome lifecycle stages, and this can have both pro- and anti-parasite consequences. Platelets can bind directly to parasite eggs and this has been shown to promote both faecal egg excretion and enhance the attachment of eggs to vascular surfaces (267–270). As described above, platelets do not often associate with live intact worms due to the different tegumental phosphatases, however platelets do directly interact with damaged or dead adult worms as well as schistosome eggs (268). *In vitro* experiments with purified platelets from healthy people cultured with isolated *S. mansoni* eggs, cercariae, schistosomula and adult stages demonstrate that platelets adhere to schistosome eggs. It appears that platelet-egg interactions are required for egg excretion as mice treated with rabbit anti-mouse platelet serum have a significant reduction in faecal egg excretion. Interestingly, the later this was given in schistosome infection i.e. 42 compared with 32 days post-infection, the greater the reduction in egg excretion but also the increase in mortality (269). Moreover, the injection of schistosome eggs alone induced acute thrombocytopenia *in vivo* (269). These data suggest that platelet adherence to schistosome eggs is favourable in protecting them from the immune system (as described in bacterial and viral infections) but also in aiding the adherence and migration across the endothelium (267). However, in a similar way to the tegument phosphatases, eggs possess many proteins which prevent the full coagulation cascade. Doenhoff *et al*. (2003) showed that schistosome egg proteins possess fibrinolytic activity, in a similar manner to plasmin, thereby preventing the formation of stable, potentially life-threatening, fibrin thrombi (271).

There is a small collection of papers from ~30 years ago that have shown platelets are directly responsible for schistosome killing and clearance (272–

275). The transfer of platelets from infected rats into naive recipients resulted in reduced worm burdens (275). From *in vitro* cytotoxicity assays with rat and mouse platelets, the killing of *S. mansoni* schistosomula is enhanced in the presence of platelets which has been linked to IgE mediated killing, and platelet activation with C-reactive protein and TNF (273–275).

Together these studies reveal that platelet counts are lower both in schistosome-infected individuals in endemic areas as well as in murine models of infection. Due to the intravascular localisation of adult worms it is clear that they have had to evolve ways in which to evade the immune system and thrombus formation through a specialised tegument which contains tegumental phosphatases capable of inhibiting the coagulation cascade. Given the liver is the primary site of pathology in *S. mansoni* infection, and the importance of this organ in the production of haematopoietic growth factors, coagulation factors and steady-state platelet clearance, highlights multiple ways in which platelets and their production, clearance and functionality may be impacted during an infection. However, it is unclear as to how a schistosome infection is affecting platelets or what role, if any, platelets are specifically performing in fighting infection.

1.4 Hypothesis and Aims

The central hypothesis of this thesis is that schistosome infection promotes platelet-leukocyte interactions which drives thrombocytopenia. Moreover, these platelet-leukocyte interactions lead to cross-talk that regulates immune cell phenotypes.

In this thesis I aim to:

1) Assess the impact of schistosome-induced type 2 inflammatory immune responses on platelet production and immune cell interactions
2) Assess the haemostatic consequences of schistosome infection
3) Assess the immunomodulatory capacity of platelets on macrophages
4) Assess the role of platelets in schistosome infection using *in vivo* models where platelet numbers have been increased or depleted

2. Materials and Methods

2.1 Ethics statement

Ethical approval for the study was obtained from the Animal Welfare and Ethical Review Board of the Department of Biology, University of York. All procedures were performed under the authority of United Kingdom Home Office Project Licenses PFB579996, PP5712003 and P49487014.

2.2 Infection of mice with *S. mansoni*

C57BL/6, MPL$^{-/-}$ and FcRγ$^{-/-}$ mice 6 to 12 weeks of age, bred and maintained at the Biological Services Facility, University of York, were used for all experiments. The mice were housed in individually ventilated cages under specific pathogen-free conditions and provided with food and water *ad libitum*. Mice (7-12 weeks old at start of experiment) were infected with *S. mansoni* cercariae (25-100) for 30min under anaesthesia via percutaneous penetration of the shaved abdomen. Cercariae were freshly shed from *Biomphalaria glabrata* snails exposed to a light source. Mice were weighed before the start of the experiments and regularly after infection (weekly for 6 weeks and then three times per week) to monitor for infection-induced weight loss. No animal was allowed to lose 20% starting body weight. As discussed in the results, mice were sacrificed at different time points following infection and tissues harvested.

2.3 *In vivo* platelet tracking

C57BL/6 mice were injected intravenously (IV) with 0.05µg/g of body weight of anti-GPIb-V-IX conjugated DyLight 649 or 488 (Emfret X649 or X488) in 200µl phosphate buffered saline (PBS). Saphenous bleeds or tail bleeds were taken at 1, 24, 48, 72 and 96hr after injection and 5µl of blood was collected into 50µl acid-citrate-dextrose (ACD) buffer (13.2g/L sodium citrate dihydrate, 4.8g/L anhydrous sodium citrate, 14.7g D-Glucose, pH 7.4). Blood samples were co-stained with 0.2µg CD41-phycoerythrin (PE) (BioLegend 133906) for 30min and diluted in sterile-filtered 1x PBS before acquiring on a BD-LSRFortessa X-20 flow cytometer.

2.4 ITP

To assess acute ITP mice were injected intraperitoneally (IP) with anti-mouse CD41 (MwReg30, Biolegend 133901) or IgG1κ (Biolegend, 400402) at 0.2mg/kg of mouse in PBS and harvested 12-24hr later. To assess the effects of sustained ITP in infection, at 6 weeks post *S. mansoni* infection mice were injected with α-CD41/IgG1 three times a week for 1 week and then 0.4mg/kg for a further 1 week.

2.5 Tissue preparation

Single cell suspensions of spleen were produced by passing them through a 70μm cell strainer in FACS buffer (PBS with 0.5% $BSA_{(w/v)}$ and 0.05% $azide_{(v/v)}$) before being centrifuged at 450 xg, 4°C for 5min. Livers and lungs were finely chopped in Hank's balanced salt solution (HBSS) (HyClone SH30030-02) and incubated at 37°C for 45min with 160U/ml DNase and 0.8U/ml Liberase TL (Roche Diagnostics 492430). Digestion was stopped by adding final concentration 10mM Ethylenediaminetetraacetic acid (EDTA) and diluted with Dulbecco's Modified Eagle Medium (DMEM) (Gibco 21969-035) supplemented with 10%$_{(v/v)}$ foetal calf serum (FCS), 2mM L-glutamine, 100U/ml penicillin G, and 100μg/ml streptomycin (cDMEM). Samples were passed through a 100μm cell strainer, and centrifuged twice at 450 xg, 4°C for 5min. Pellets were re-suspended in 8ml of 33% isotonic percoll (GE Healthcare 17-0891-01) / PBS and centrifuged at 700 xg, room temperature for 12min without brake or acceleration. Blood was collected in FACS buffer supplemented with 10mM EDTA and was centrifuged at 450 xg, 4°C for 5min. Red blood cells were lysed in single cell suspensions using Ammonium-Chloride-Potassium (ACK) (BioWhittaker 10-548E) red cell lysis buffer (5min at room temperature) and counted using a haemocytometer with trypan blue exclusion to identify live cells before resuspension. $2x10^6$ cells per sample were subsequently stained for flow cytometric analysis.

2.6 Intracellular cytokine stimulation

Liver cells ($1\text{-}4x10^6$ /well) were stimulated in 96 well plates with 100ng/ml LPS (Sigma L2880) and 10μg/ml Brefeldin A (Sigma B7651) and incubated at 37°C for 3hr. Non-adherent cells were collected before recovering adherent cells

by incubating with macrophage detachment buffer (3mM EDTA, 10mM glucose in PBS, 37°C for 10min). Collected cells were stained for flow cytometry. To assess T cell cytokine production, 1-4x10^6 cells/well were stimulated with 1µg/ml Ionomycin (Sigma I0634), 0.5µg/ml Phorbol 12-myristate 13-acetate (PMA) (Sigma P8139) and 10µg/ml Brefeldin A (Sigma B7651) and incubated at 37°C for 4hr. Cells were collected and stained for flow cytometry.

2.7 CD64 enrichment and cell sorting

Liver single cell suspensions were prepared as in **Section 2.5** and blocked with 0.5µg anti-CD16/32 (Clone 93, Biolegend, 101301) for 10min at 4°C. Cells were stained with 1.5µg anti-CD64-biotin (Clone X54-5/7.1, Biolegend, 139318) for 10min at 4°C before being washed in 10ml of MACS buffer (PBS + 0.5% BSA) and centrifuged at 450 xg, 5min at 4°C. The cell pellet was re-suspended in 30µl anti-biotin MicroBeads (Miltenyi Biotec, 130-090-485) in 70µl MACS buffer and incubated at 4°C for 15min. Samples were thoroughly washed in 10ml MACS buffer and re-suspend in 1ml MACS buffer. LS columns (Miltenyi Biotec, 130-042-401) were prepared by washing with 3ml MACS buffer before adding all the labelled liver samples to the column. The flow-through was collected for quality control. A further 3ml MACS buffer was added to the column before removing the column from the magnet. The column was transferred to a fresh tube and flushed with 5ml MACS buffer to collect the enriched fraction. Both the flow-through and enriched fractions were passed over fresh columns to improve enrichment and yield. Both the flow-through and enriched samples were counted using trypan blue exclusion on a haemocytometer. Samples were stained for sorting.

2.8 Flow cytometry

For flow cytometry staining, cells were washed with 1x PBS and stained with live-dead Zombie Aqua (Biolegend 423101). Subsequently, Fc receptors were blocked with 3µl rat IgG (2mg/ml stock, Sigma). Samples were stained with fluorescently conjugated antibodies for flow cytometric analysis (**Table 2**). Cells were first stained for surface markers before fixation. Cells stained with surface markers alone were fixed with 4% formaldehyde (PFA)/PBS (Fisher

bioreagents BP531), 20min on ice. The combination of surface markers used for immune cell population identification is displayed in **Table 3** and an example of the gating strategy employed on both liver and spleen tissue is shown in **Figure 2.1**. All axes are displayed as biexponential apart from FSC-A which is shown on a linear scale. For intracellular staining, cells were either treated with Foxp3 Transcription Factor Fixation/ permeabilisation buffer (eBiosciences 00-5223-56, 00-5123-43, for RELMα, iNOS and Ym-1 expression) or IC Fixation/permeabilisation buffer (BD 554722, for intracellular cytokines). Intracellular markers were stained following permeabilisation with 1x Permeabilisation wash buffer (eBiosciences 00-8333-56 or BD 554723) (**Table 4**). Samples were acquired on a BD-LSRFortessa X-20 flow cytometer and analysed using FlowJo V10.6.1.

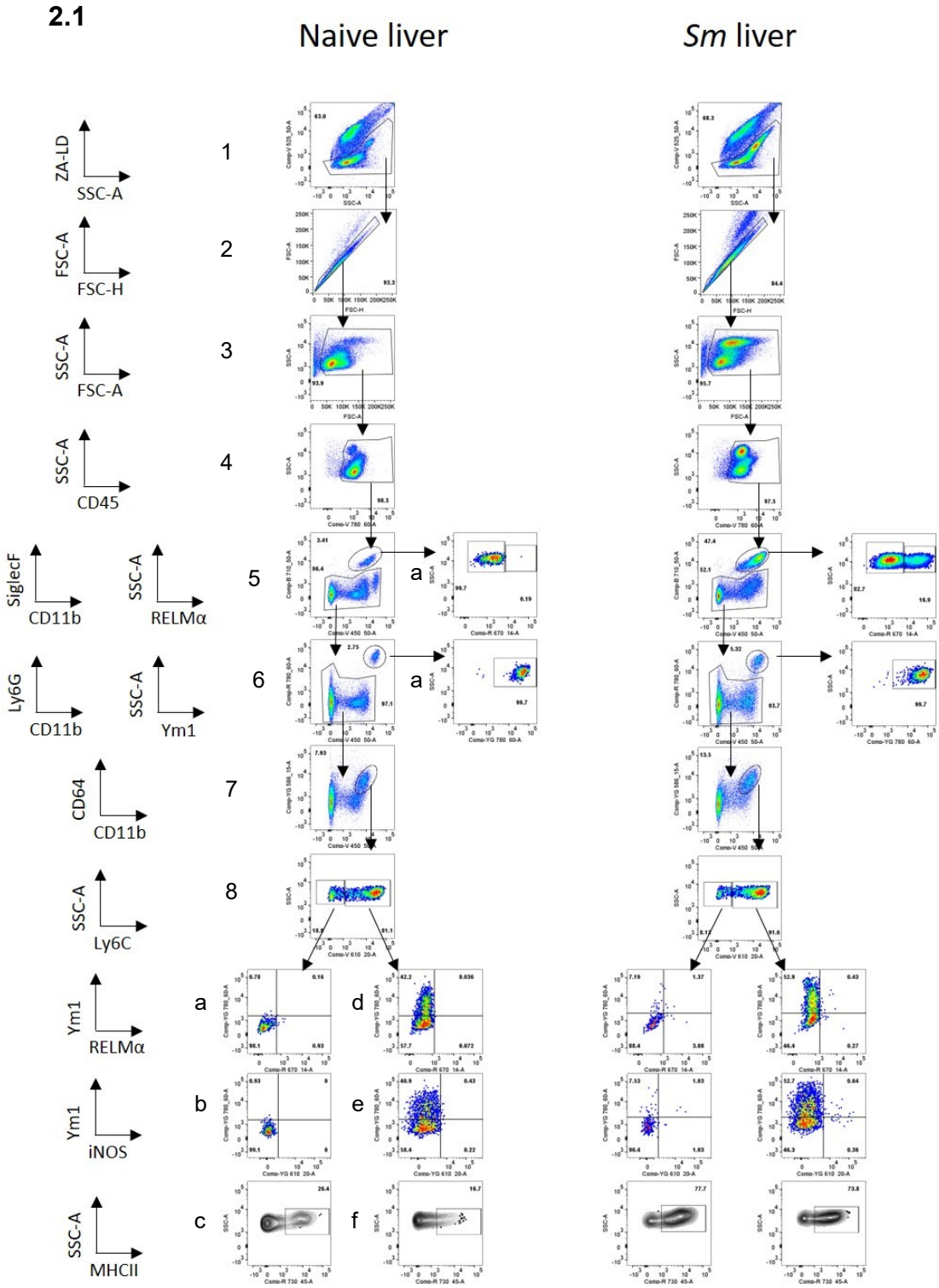

Figure 2.1 Gating strategy used to identify the immune populations

Example gating is shown in the liver, but the same gating strategy was also applied to spleen tissue. The axes are presented as biexponential apart from FSC-A. Each step allows identification of distinct populations 1) live cells, 2) singlets, 3) intact cells, 4) CD45⁺ leukocytes, 5) eosinophils, 5a) RELMα⁺ eosinophils, 6) neutrophils, 6a) Ym1⁺ neutrophils, 7) CD64⁺ myeloid cells, 8) macrophages and monocytes. Macrophages (Ly6C⁻) were then classified based on a) Ym1 RELMα, b) Ym1 iNOS and c) MHCII. Monocytes (Ly6C⁺) could also be classified based on d) Ym1 RELMα, e) Ym1 iNOS and f) MHCII.

Table 2 Extracellular flow cytometry antibodies

Extracellular marker	Clone	Fluorochromes	Supplier	Dilution
CD11b	M1/70	PB, PerCP-Cy5.5	Biolegend	**1:500**
F4/80	BM8	FITC	Biolegend	**1:500**
CD64	X54-5/7.1	PE, PE-Cy7	Biolegend	**1:500**
CD41	MWReg30	FITC, PE, APC, A700	Biolegend	**1:500**
CD61	2C9.G2	PE	Biolegend	**1:500**
SiglecF	1RNM44N	PerCP-e710	eBioscience	**1:500**
Ly6G	1A8	APC-Cy7, FITC	Biolegend	**1:500**
Ly6C	HK1.4	BV605	Biolegend	**1:1000**
CD115	AFS98	PE-dazzle	Biolegend	**1:1000**
CD4	RM4-5	PerCP-Cy5.5, BV650	Biolegend	**1:500**
CD8α	53-6.7	APC	Biolegend	**1:500**
TCRβ	H57-597	PE-Cy7	Biolegend	**1:500**
CD19	6D5	APC-Cy7	Biolegend	**1:500**
CD45.2	104	BV785	Biolegend	**1:500**
NK1.1	PK136	FITC	Biolegend	**1:500**
MHCII	M5/114.15.2	A700, BV650	Biolegend	**1:500**
CD45	30-F11	PE, APC, BV785	Biolegend	**1:200**
EPCR	1560	PE	StemCell	**1:100**
Sca1	D7	APC	Biolegend	**1:100**
CD48	HM48-1	PE-Cy7	Biolegend	**1:100**
CD150	TC15-12F12.2	BV605	Biolegend	**1:100**
CD44	IM7	FITC	Biolegend	**1:500**
CD62L	MEL-14	PE	Biolegend	**1:500**
JON/A	JON/A	PE	Emfret	**1:250**
CD62P	RMP-1	PE-Cy7	Biolegend	**1:250**
CD29	HMβ1-1	A488	Biolegend	**1:250**
CD42d	1C2	AP\c	Biolegend	**1:250**
CD49b	HMα2	A488	Biolegend	**1:250**
CD140a	APA5	PE-Cy7	eBiosciences	**1:250**
CD154	MR1	PE	Biolegend	**1:250**
CD88	20/70	PE-Cy7	Biolegend	**1:250**

Table 3: Surface marker identification of immune cell subsets for different experiments

Figure(s)	Tissue	Population	Markers
3.1C-D 3.18C-D 3.26B 6.2D	Blood	Eosinophils	**CD11b^{+}SiglecF^{+}SSC-A^{hi}**
		Neutrophils	**CD11b^{+}SiglecF^{-}Ly6G^{+}**
		Classical monocytes	**CD11b^{+}SiglecF^{-}Ly6G^{-} CD115^{+}Ly6C^{+}**
		Non-classical monocytes	**CD11b^{+}SiglecF^{-}Ly6G^{-} CD115^{+}Ly6C^{-}**
		B cells	**CD11b^{-}SiglecF^{-}Ly6G^{-}TCRβ^{-} CD19^{+}**
		CD4 T cells	**CD11b^{-}SiglecF^{-}Ly6G^{-}CD19^{-} TCRβ^{+}CD4^{+}**
		CD8 T cells	**CD11b^{-}SiglecF^{-}Ly6G^{-}CD19^{-} TCRβ^{+}CD4^{-}**
3.3B-C 3.5A-D 3.19A-C 3.20A-C 3.26D-F 6.2E-F 6.7D-G 6.12D-G 6.20A-D 6.25A-D	Liver Spleen	Eosinophils	**CD11b^{+}SiglecF^{+}**
		Neutrophils	**CD11b^{+}SiglecF^{-}Ly6G^{+}**
		Monocytes	**CD11b^{+}SiglecF^{-}Ly6G^{-} CD64^{+}Ly6C^{+}**
		Macrophages	**CD11b^{+}SiglecF^{-}Ly6G^{-}CD64^{-} Ly6C^{-}**
		B cells	**CD11b^{-}SiglecF^{-}Ly6G^{-}TCRβ^{-} CD19^{+}**
		CD4 T cells	**CD11b^{-}SiglecF^{-}Ly6G^{-}CD19^{-} TCRβ^{+}CD4^{+}**
		CD8 T cells	**CD11b^{-}SiglecF^{-}Ly6G^{-}CD19^{-} TCRβ^{+}CD4^{-}**
3.16A-B	Liver Spleen	Eosinophils	**CD11b^{+}SiglecF^{+}**
		Neutrophils	**CD11b^{+}SiglecF^{-}Ly6G^{+}**
		Monocytes	**CD11b^{+}SiglecF^{-}Ly6G^{-} F4/80^{+}Ly6C^{+}**
		Macrophages	**CD11b^{+}SiglecF^{-}Ly6G^{-}F4/80^{-} Ly6C^{-}**
		B cells	**CD11b^{-}SiglecF^{-}Ly6G^{-}TCRβ^{-} CD19^{+}**
		T cells	**CD11b^{-}SiglecF^{-}Ly6G^{-}CD19^{-} TCRβ^{+}CD4^{+}**

Table 4: Intracellular flow cytometry antibodies and conjugates

Intracellular antibodies	Clone	Fluorochrome	Supplier	Dilution
IL-10	JE55-16E3	PE	Biolegend	**1:250**
IL-4	11B11	PE-dazzle, APPC	Biolegend	**1:250**
IFNγ	XMG1.2	FITC, e450	Biolegend	**1:250**
IL-13	W17010B	PE	Biolegend	**1:250**
TNFα	MP6-XT22	BV421	Biolegend	**1:250**
iNOS	CxNF7	e610	Biolegend	**1:1000**
Ym1	BAF2446	Biotinylated	R&D Biosystems	**1:125**
RELMα	Peprotech	Unconjugated	H1717	**1:200**

Secondary/ conjugate	Species	Fluorochrome	Supplier	Dilution
Anti-rabbit IgG	Polyclonal goat	A647	Invitrogen	**1:400**
Streptavidin	NA	PE-Cy7	Biolegend	**1:400**

2.9 Confocal microscopy

Liver and spleen samples were frozen in optimal cutting temperature (OCT) compound (CellPath Ltd. KMA-0100-00A) in a dry ice/ethanol slurry and stored at -80^{o}C. Femurs were fixed overnight in 4% PFA/PBS$_{(v/v)}$, decalcified in 10% EDTA/PBS$_{(w/v)}$ for 2 days, and cryopreserved in 20% sucrose/PBS$_{(w/v)}$ for 1 day, with all incubations carried out at 4^{o}C. Bones were then frozen as the livers were in OCT. Tissue cryosections (8-10µm) were made with a Leica CM 3050S cryostat, transferred to SuperFrost PlusTM slides, air-dried and stored at -20^{o}C. For staining, slides were fixed in ice-cold acetone (5min), washed in wash buffer (0.5% BSA/PBS$_{(w/v)}$), and blocked in wash buffer + 5% rat serum (30min). Samples were avidin-biotin blocked (Lab Vision™ Avidin biotin Blocking Solution, ThermoFisher, TA-0150BB), washed x3 in wash buffer before incubating with primary antibodies for 1hr at room temperature (**Table 5**). Unbound primary antibody was washed twice prior to samples being incubated for 45min with secondary antibodies (**Table 5**) and/or streptavidin conjugated fluorophores. Unbound secondary antibody was washed twice. Finally, samples were stained with 4′,6-diamidino-2-phenylindole (DAPI) (1µg/ml, 5min, Sigma) and coverslips were mounted with ProLong^{TM} Gold (ThermoFisher P10144). Tissues were imaged on a Zeiss LSM780 confocal microscope and analysed using Zen software and Fiji ImageJ.

For imaging cultured/single cell suspensions, cells were centrifuged at 450 xg, 5min at 4^{o}C and Fc receptors were blocked as described previously (**Section 2.8**) using 3µl Rat IgG (2mg/ml stock). Samples were stained with antibodies for surface markers for 30min on ice then washed and stained with the appropriate secondary antibodies/streptavidin for a further 30min on ice. Samples were washed and re-suspended in 200µl 4% PFA/PBS$_{(v/v)}$ for 10-15min on ice. Following fixation and permeabilisation cells were washed and nuclei stained in 100µl DAPI (1µg/ml)/PBS for 5min on ice. Cells were washed and re-suspended at ~2x10^{4}–1x10^{6} /200µl in wash buffer. The cell suspension was loaded into a cytofunnel-filter paper cassette (Thermo Scientific) and spun onto Superfrost plus microscope slides (Thermo scientific) using a Cytospin 4 (Thermo Shandon) at low acceleration, 500rpm for 5min. Samples were

allowed to air-dry before being mounted with ProLong™ Gold and a coverslip. Slides were imaged on a Zeiss LSM880 Airyscan microscope using a 63x oil objective, 4x zoom and z-stacks were generated with images taken every 0.2µm. Images were analysed using Zen software.

Table 5: Primary and secondary antibodies used for confocal microscopy

Primary	Species	Conjugate	Clone	Supplier	Dilution
Thpo	Rabbit	Unconjugated	EPR14948	eBioscience	**1:100**
CD68	Rat	A647	FA-11	Abcam	**1:200**
CD41	Rat	Biotin	MWReg31	Biolegend	**1:200**
B220	Rat	A488	RA3/6B2	Biolegend	**1:200**
F4/80	Rat	A647	BM8	Biolegend	**1:200**
SiglecF	Rat	A488	1RNM44N	eBiosciences	**1:100**
CD31	Rat	Biotin	390	Biolegend	**1:100**
RELMα	Rabbit	Unconjugated	H1717	R&D Biosystems	**1:100**
Laminin	Rabbit	Unconjugated	Polyclonal	Sigma	**1:200**

Secondary	Species	Conjugate	Clone	Supplier	Dilution
α-rabbit IgG	Chicken	A647	NA	Invitrogen	**1:400**
α-rabbit IgG	Goat	A647	NA	Invitrogen	**1:400**
Streptavidin	NA	A546	NA	Biolegend	**1:400**

2.10 Wax embedding

Liver sections were fixed in 4ml 4% PFA/$PBS_{(v/v)}$ solution overnight at 4ºC before being transferred and stored in 70% ethanol at 4ºC. For wax embedding, tissues were dehydrated in an ethanol series, 1x 30min in 70%, 80%, 95% ethanol, 3x 30min in 100% ethanol with agitation. Samples were cleared in Histoclear (National Diagnostics HS202) 3x 30min with agitation and then paraffin wax embedded in molten wax, 3x 1hr at 65ºC. Wax embedded samples were then transferred to moulds and left to set and stored at room temperature.

2.11 Masson's trichrome staining

Paraffin wax embedded samples were sectioned at 10µm thickness on a Leica Microtome onto SuperFrost PlusTM slides, air-dried and stored at room temperature. Slides were deparaffinized in Histoclear for 10min and equilibrated in an ethanol series (100%, 95%, 70%) for 3min each. Samples were washed with dH_2O for 3min before being stained overnight at room temperature in Bouin's solution (Sigma HT10132). Slides were washed in running water to remove yellow colouration and stained in Weigert's iron

haematoxylin working solution i.e. equal parts Solution A (0.01g/ml Haematoxylin in 95% ethanol) and Solution B (29% ferric chloride, 32% HCl in H_2O) for 5min. Slides were washed in running water for 5min and finally stained in Trichrome AB (Sigma HT10516) for 5min. They were transferred to 0.5% acetic acid for 1min to allow for contrasting colour dye staining and rinsed in tap water. Finally, samples were equilibrated in 95% then 100% ethanol for 3min before being cleared in Histoclear for 3min and mounted using Eukitt mounting medium (Fluka 03989). Slides were imaged using an Axio Scan.Z1 slide scanner and analysed using Zen software and Fiji ImageJ.

2.12 Parasitology

To determine parasite egg counts, weighed samples of liver, lung, small and large intestine were digested in $4\%_{(w/v)}$ KOH overnight at 37^{o}C. Small and large intestines were cleaned prior to digestion to prevent the inclusion of faecal eggs. After digestion, 50-100µl of digested tissue solution was added to a gridded container and eggs were counted using a dissecting microscope.

2.13 L929 cell culture

L929 murine fibroblastic cell-line (a gift from Dr. Elmarie Myburgh, University of York) was cultured in cDMEM. Cells were initially grown in T25 and T75 flasks before transfer into T175 ($8.75x10^7$ cells/T175 flask in 50ml media). Cells were cultured in T175 for 7 days before media was removed and replaced with fresh media for 7 more days. Supernatants were collected at 7 and 14 days, filtered through a 0.22µm filter, and frozen at -80^{o}C.

2.14 Generation of bone marrow derived macrophages

Femurs and tibias were harvested from C57BL/6 mice into cDMEM media. Intact bones were briefly sterilised (~30 seconds) with 70% ethanol and returned to fresh complete media. Bones were flushed with cDMEM using a 25G needle until all BM was removed. To remove cell clumps, the BM solution was slowly passed through a 25G needle before being centrifuged 450 xg, 10min at 4^{o}C. Red blood cells were lysed in ACK buffer for 5min, washed, counted on a haemocytometer and re-suspended in macrophage media (DMEM+$30\%_{(v/v)}$ L929 supernatant + $20\%_{(v/v)}$ FCS, 2mM L-glutamine, 100U/ml penicillin G, 100µg/ml streptomycin) and $5x10^6$ cells were seeded in 10cm

dishes (10ml media). Cells were supplemented with fresh macrophage media 3 days later. On days 5-6, media was replaced with cDMEM without L929 supernatant. BM macrophages (BM-Mϕ) were harvested day 6-7 after initial seeding by adding ice-cold cDMEM and scraping. Cells were counted and re-plated at the desired concentration.

2.15 Thioglycollate elicited macrophages

Peritoneal macrophages were harvested 3-5 days after an IP injection with 200µl of 4%$_{(v/v)}$ thioglycollate solution. For termination, mice were given an overdose of anaesthetic (medetomidine and ketamine) and exsanguinated by the brachial artery to limit blood in the peritoneal cavity. The peritoneal cavity was flushed twice with 5ml cDMEM.

2.16 Platelet characterisation from whole blood

Blood was obtained from either a free-flowing tail or saphenous vein into a Microvette® CB 300 K2 EDTA, capillary blood collection tube (Sarstedt, 16.444.100). For Annexin V staining, 5-10µl of blood was transferred into 100µl PBS. As a positive control, some samples were stimulated with PMA (final concentration 25nM) and incubated at 37°C for 1hr. All subsequent steps were performed at room temperature unless otherwise stated and spins were at 350 xg for 5min. All samples were washed in 900µl PBS and stained with CD41-PE (0.2µg) in PBS for 30min. Unbound antibody was washed in PBS and then in 900µl 1x Annexin V Binding Buffer (eBioscience 88-8007-74). Cells were then re-suspended in 100µl Binding Buffer, with 5µl Annexin V - APC/sample. These were incubated in the dark for exactly 15min, washed in Binding Buffer, re-suspended in 450µl Binding Buffer and immediately run on the BD- LSRFortessa.

For assessing desialylation, a positive control was generated from a pooled blood sample (5-10µl) that was digested with neuraminidase (5U/ml Roche 11585886001) for 30min at 37°C. All samples were then washed with 900µl PBS and spun at 350 xg for 5min before being stained with CD41-APC (0.2µg) in PBS for 30min. All samples were stained with the 5µg biotinylated lectin Ricinus Communis Agglutinin I (RCA-I) (Vector laboratories B-1085-5) in MACS buffer (0.5% $_{(w/v)}$ BSA/PBS) for 30min at 37°C. Samples were washed

and stained with 50ng PE-Cy7 conjugated streptavidin (Biolegend 405206), for 30min at room temperature. All samples were washed, re-suspended in MACS buffer and immediately run on the BD-LSRFortessa.

2.17 Platelet isolation

Blood was obtained from terminally anaesthetised (overdose of pentobarbital) donor C57BL/6 mice by direct cardiac puncture and collected into ACD buffer -coated tubes. An equal volume of wash buffer (2%$_{(v/v)}$ FCS/PBS) was added to blood samples before centrifugation at 60 xg for 7min at room temperature without break or acceleration. Platelet rich plasma (PRP) was collected and 500µl wash buffer was added before being centrifuged at 240 xg for 10min at room temperature without acceleration or break in order to pellet the platelets from the plasma. Platelets were re-suspended in 500µl wash buffer and counted on a cell counter.

2.18 Isolated platelet function and characterisation

For macrophage-platelet co-culture, BM-Mϕ were seeded at 1x10^6 cells/well in a 24-well plate and left to adhere for 1-4hr. Macrophages were treated with LPS/IFNγ (100ng/ml, 10ng/ml), IL-4 (20ng/ml) or media alone and platelets were added at a 1:100 ratio (macrophages:platelets). Plates were pulse-spun to aid platelet settling and incubated overnight at 37^{o}C.

For platelet activation, 5x10^7 platelets in wash buffer were treated with PMA or Protease-Activated Receptor 4 (PAR4) agonist (Fisher Scientific 15450997) for 10-30min at room temperature at a final concentration of 30µM and 150µM respectively. Platelet wash buffer was added, and samples centrifuged 240 xg, 10min at room temperature without break or acceleration for subsequent flow cytometry staining.

2.19 Live cell phagocytosis imaging

BM-Mϕ were seeded in 96 well plates (Corning 3603) at 1x10^4 cells/well, allowed to adhere for 1-4hr, then treated with stimuli and platelets and cultured overnight at 37^{o}C. To assess the ability of macrophages to phagocytose *E. coli,* pHrodo® Green *E. coli* Bioparticles (Incucyte 4616) were added to the desired wells at 1-10µg/well in 1x PBS and imaged using a Phase Focus LiveCyte microscope. Imaging began within 1hr of the addition of bioparticles.

An arbitrary fluorescent threshold of mean green intensity was set individually for every independent experiment based on control wells to identify cells that never became fluorescent from those that subsequently lost signal.

To assess the phagocytosis of platelets, cells were re-suspended in PBS/1μM Prostaglandin E1 and labelled with pHrodo™ Red, succinimidyl ester (Thermo, P36600) for 20min. Labelling was quenched by washing cells in PBS/2% FCS and labelled cells were added to the culture at a 1:100 ratio (macrophage:platelets).

2.20 Whole blood impedence aggregometry

Blood was collected as described in **Section 2.17** and diluted 1:2:2, blood : 0.9%$_{(w/v)}$ saline : Ringers buffer, supplemented with 2mM $CaCl_2$. Impendence was measured for 10min, 37^{o}C, with constant stirring on a Chronolog-700 aggregometer.

2.21 Coagulometry

Blood samples (40μl) were pipetted directly from a free-flowing saphenous vein bleed under isoflurane anaesthesia. Samples were immediately transferred to either prothrombin (PT) (06-12895-01) or activated partial thromboplastin time (aPTT) (06-12901-01) cartridge and inserted into an IDEXX Coag Dx* analyser.

2.22 Megakaryocyte ploidy

Femurs were removed from naive and infected mice and collected into ice cold PBS. A single femur from each mouse was carefully cleaned with 70% ethanol and both ends removed. The BM was spun out at 2500 xg for 40s into 100μl ice-cold PBS and gently re-suspended in 5ml ice-cold PBS. Samples were passed through a 100μm cell strainer to remove any bone fragments. Samples were centrifuged at 300 xg, 5min at 4^{o}C. The pellet was re-suspended in 1ml ACK red blood cell lysis buffer for 5min at room temperature. The washed samples were fixed in 150μl ice-cold absolute ethanol for 30min at 4^{o}C. Samples were washed in PBS and re-suspended in 100μl MACS-EDTA buffer (0.5%$_{(w/v)}$ BSA/PBS +2mM EDTA) containing CD41-APC (0.2μg final), propidium iodide (100μg/ml final) (Biolegend 421301) and RNase A (1mg/ml final) (Sigma R6513) for 40min on ice. After staining the cells were

washed in MACS-EDTA buffer and re-suspended in 400µl of MACS-EDTA buffer before being run immediately on the flow cytometer.

2.23 Colony forming unit assays

Femurs and tibias were obtained from naive and infected mice, flushed with a 25G needle before being passed through a 70µm filter and centrifuged at 300 xg for 5min. Red blood cells were lysed as described previously and re-suspended in 2%$_{(v/v)}$ FCS/PBS. For lineage depletion, samples up to 1x10^8 cells/ml were incubated with 20µl/ml EasySep^{TM} mouse Haematopoietic Progenitor Cell Isolation Cocktail (StemCell technologies, 19856) on ice for 15min. Thoroughly vortexed RapidSpheres were added at 50µl/ml and incubated on ice for 15min. Samples were diluted in 2%$_{(v/v)}$ FCS/PBS and added to the EasySep magnet unit for 3min. Enriched flow-through samples were stained for flow cytometry (CD45, EPCR, Sca1, CD48, CD150, 7AAD) as described previously. 1200 ESLAM cells were sorted into 0.1ml StemSpan^{TM} (StemCell Technologies, 09650). 100 ESLAM cells were added to individual wells of a 6-well plate and treated with the appropriate stimulants and added to Methocult before plating out for 10 days culture (StemCell Technologies, 03434) at 37^{o}C. At the assay end-point, plates were imaged using STEMvision^{TM}, before colonies were randomly selected for flow cytometry staining and analysis.

2.24 RNA isolation and quantitative reverse transcription-PCR (qRT-PCR)

BM-Mϕ cultures were washed with 1x PBS, re-suspended in 700µl QIAzol (QIAGEN) and incubated at room temperature for 5min before being stored at -80^{o}C. Small liver tissue samples (~5mm^3) were frozen in QIAzol and stored at -80^{o}C. Prior to RNA extraction, tissue samples were homogenised using metal beads in a TissueLyser (QIAGEN). RNA was extracted using the miRNeasy RNA extraction kit (QIAGEN) following the manufacturer's instructions and eluted in 30µl of RNase free water. Superscript III (ThermoFisher) and random hexamer primers (Promega) were used for cDNA production. mRNA amplification was detected using Fast SYBR Green Master Mix (ThermoFisher) on a StepOnePlus Real Time PCR System

(ThermoFisher) with conditions 95°C for 20s followed by 45 cycles at 95°C for 3s and 60°C for 30s (**Table 6**). Relative transcript levels of genes were calculated using the ΔΔCT method and mRNA expression was normalised to the *Hprt*/*U6* gene (276).

2.25 Enzyme linked immunosorbent assay (ELISA)

TPO ELISA was performed as described by the manufacturer's instructions (R&D systems MTP00) on mouse serum. Briefly, mice were overdosed with anaesthesia (medetomidine and ketamine) before blood collection from the brachial artery. Blood was left to clot at 4°C for 1-5hr before being centrifuged, 5min, at progressively increasing speeds (1000, 5000, 10000 xg), each time transferring the serum to a fresh tube. Serum samples were stored at -20°C and diluted 1 in 5 for use in the ELISA.

2.26 RNA-sequencing analysis

Unprocessed fastq files from RNA sequencing data that has been re-analysed in this thesis is publicly available in the European Nucleotide Archive, accession numbers SAMEA2668137-2668182. We re-analysed the differential expression analysis data from Costain *et al.* (2022) comparing naive and infected mice at 12 week post-infection, available in Supplementary Data (277). Using R 4.2.1 and R Studio 2022.07.1 we filtered the differentially expressed genes for those included in the Mouse gene set, Gene Ontology (GO) biological processes (BP)_BLOOD_COAGULATION_INTRINSIC _PATHWAY (GO:0007597) and GOBP_BLOOD_COAGULATION_FIBRIN _CLOT_FORMATION (GO:0072378). Genes were considered significantly differentially expressed in schistosome-infected mice when the adjusted p value (padj) was < 0.05. The log2fold change in gene expression was plotted or used to express differences.

Table 6: List of primers used for qPCR analysis

Gene	Primer	Sequence (5' – 3') or catalogue number
Hprt	Forward	GCGTCGTGATTAGCGATGATGAAC
	Reverse	ATCTCCTTCATGACATCTCGAGCAAGTC
U6	Forward	CGCTTCGGCAGCACATATAC
	Reverse	TTCACGAATTTGCGTGTCAT
Cxcl12	Forward	GGTTCTTCGAGAGCCAC
	Reverse	TTCTTCAGCCGTGCAACA
Retlna	Forward	TATGAACAGATGGGCCTCCT
	Reverse	GGCAGTTGCAAGTATCTCCAC
Nos2	Forward	CCCGGAAGGTTTGTACAGC
	Reverse	AAGGGGACGAACTCAGTGG
Arg1	Forward	CAGAAGAATGGAAGAGTCAG
	Reverse	CAGATATGCAGGGAGTCACC
Ym1	Forward	CATCTCTTCAGTGTTCTGGTGAA
	Reverse	GGGATCTTGTACCCAGACTTG
Tnf	Forward	CTGTAGCCCACGTCGTAG
	Reverse	TTGAGATCCATGCCGTTG
Il6	Forward	GCTACCAAACTGGATATAATCAGG
	Reverse	CCAGGTAGCTATGGTACTCCAGAA
Cd16	Forward	CTATGTACGGAGAAATCTTCAAACC
	Reverse	GCCTGGTGCTTTCTGATTG
Cd32	Forward	TGCTGTCACTGGGATTGCT
	Reverse	GCTTTTTCTTGAGATAGACCAAGG
Cd64	Forward	TGCTGGATTCTACTGGTGTGA
	Reverse	AAACCAGACAGGAGCTGATGA
Cxcl10	Forward	ATCATCCCTGCGAGCCTATCCT
	Reverse	GACCTTTTTTGGCTAAACGCTTTC
Il10	Forward & Reverse	Mm_IL10_1_SG; QT00106169
Tpo	Forward & Reverse	Mm00437040_m1; 4331182

* Unless stated all primers were designed and optimised by previous Hewitson lab members

3. Assessment of the impact of schistosome-induced type 2 immune responses on platelet production and immune cell interactions

3.1 Introduction

Schistosome-induced inflammatory immune responses, and the associated granulomatous pathology is well understood. However, less well studied are the effects on haematopoiesis and infection associated thrombocytopenia. Thrombocytopenia has been observed in *S. mansoni* infected humans and a number of mouse models (249,278). Whether this feature is caused by elevated platelet clearance because of infection-induced hepatosplenomegaly and increases in macrophages, a reduction in platelet production due to changes in megakaryocytes as a result of peripheral inflammation, or a combination of both is not known (278,279,265).

Platelets are best understood for their involvement in haemostasis and their ability to rapidly bind and aggregate at sites of vascular injury, ultimately forming insoluble clots that prevent excessive bleeding (166). However, platelets also express and contain a multitude of surface molecules and cytokines. These have most likely been acquired from their original MK or scavenged from the circulation. Together these molecules contribute to their immune cell function and signalling and ultimately drive their role in inflammation and infection (205,280–282,203).

Studies into how platelets regulate immune cell function have mostly focused on pro-inflammatory responses to bacterial and viral agonists or inflammatory stimuli *in vitro*. How platelets regulate type 2 immune responses that characterise allergic inflammation, wound healing, metabolic homeostasis and immune responses to helminth parasites are poorly understood. With platelets having an emerging role in host immune responses, regulating monocyte and macrophage activation predominantly in type 1 inflammation (226,217,283), this chapter aims to assess how schistosome infection impacts on platelet levels and if platelets interact with type 2 immune cells. This is particularly relevant to a schistosome infection, given the intravascular localisation of adult worms and infection-induced thrombocytopenia.

A small number of human studies of schistosome infection have demonstrated that serum TPO levels do not correlate with platelet numbers, and therefore enhanced platelet clearance in the periphery has been explored more closely as a mechanism behind depleted platelet numbers (244,245). Murine models of infection have identified potential antibody cross-reactivity between schistosome products and platelets, promoting immune clearance and subsequent thrombocytopenia (278). The majority of murine schistosome studies to date that have assessed thrombocytopenia or platelet function during infection have used very high cercarial doses (100-200 cercariae) and as a result have terminated their experiments at 6-8 weeks post infection, i.e. 1-3 weeks after egg production starts (284,272,285). However, this represents a very acute and indeed fatal infection and does not reflect well the chronic nature of schistosomiasis in infected people. We have instead used a lower dose of cercariae and focused on timepoints that better reflect chronic disease i.e. 10-16 weeks to explore the chronic effects on inflammation and platelet production and clearance.

3.2 Aims

1) To determine the effects of schistosome infection on platelet and MK numbers and their localisation *in vivo*

2) To determine the effects of adult worm clearance on platelet parameters *in vivo*

3) To determine whether platelet production and/or clearance is altered in schistosome infection

4) To determine whether platelets interact with immune cells during schistosome infection

3.3 Results

3.3.1 Does infection dose affect platelet parameters?

Multiple human studies have shown that a diverse range of infections cause thrombocytopenia (238,286,287), including the helminth parasite *S. mansoni* (240–246). However, neither the mechanistic basis nor functional consequences of this reduction in circulating platelets is known. To investigate

this, we used a mouse model of chronic schistosome infection. Mice were infected with varying numbers of infective cercariae (25, 50 or 100) and platelet numbers and platelet-immune cell interactions compared to naive controls (**Figure 3.1A**). In the host, parasites mature into adult worms, and females begin to produce eggs ~5 weeks post initial infection (288). C57BL/6 mice have been shown capable of tolerating this dose range for 8-11 weeks (289–292). In our experiments, mice infected with 100 cercariae became sick (hunched appearance, weight loss) around 8 weeks post-infection and two animals had to be culled due to ill health, so this group was harvested at this point. The remaining infections were allowed to proceed for the full 12 weeks duration. A significant increase in liver and spleen weight was observed with the 25 cercarial infection dose which was further increased in the 50 cercariae infection (**Figure 3.1B-C**). The 100 cercarial infection dose also had elevated liver and spleen sizes, albeit at an early end point. Liver egg counts were also elevated in the 50 cercariae infection compared with 25 cercariae (**Figure 3.1D**). Platelet counts were significantly reduced compared with naive mice across all infection doses, and there was no difference in platelet count between 25, 50 and 100 cercariae (**Figure 3.1E**). Interestingly, mean platelet volume (MPV) increased with infection burden even up to 100 cercariae and MPV was significantly greater after treatment with 100 cercariae compared with 25 cercariae (**Figure 3.1F**). There was a significant negative correlation between platelet count and MPV (**Figure 3.1G**), however there was no trend between platelet count and the number of schistosome eggs in the liver (**Figure 3.1H**).

Platelet glycoprotein IIb (CD41) is a subunit of the glycoprotein IIbIIIa heterodimer primarily expressed on platelets and MK and therefore was used to assess leukocyte interactions with platelets by flow cytometry, as it is not expressed on leukocytes (293). This showed an increase in the percentage of $CD41^+$ $CD45^+$ leukocytes in the liver and spleen, but not the blood of schistosome-infected mice (**Figure 3.2A-B**). Whilst closer examination of the different immune populations in the blood revealed a significant increase in eosinophils, $CD4^+$ and $CD8^+$ T cells during infection (**Figure 3.2C**), the

percentage of platelet-leukocyte aggregates (PLA) in the circulation showed minimal difference during infection (**Figure 3.2D**).

Consistent with previous studies (284,294,295) there was a significant increase in immune cell number in the liver during infection with the eosinophil population increasing approximately 100-fold (**Figure 3.3A-B**)**.** There was also a significant increase in the percentage of eosinophils and neutrophils with bound platelets in the liver of mice infected with 50 cercariae compared with naive mice (**Figure 3.3C**)**.** When considering the absolute number of PLA, there was a significant increase in platelet interactions with all examined cell populations, but little difference between mice infected with 25 or 50 cercariae (**Figure 3.3D-E**). Moreover, there was no significant correlation between the number of schistosome eggs in the liver and the percentage of PLA (**Figure 3.3F**).

Together, these experiments demonstrated that increased schistosome infection burden enhanced hepatosplenomegaly and the number of liver eggs. Moreover, there was a significant increase in hepatic PLA in schistosome infection, however there was not a significant difference between infection with 25 or 50 cercariae.

3.1

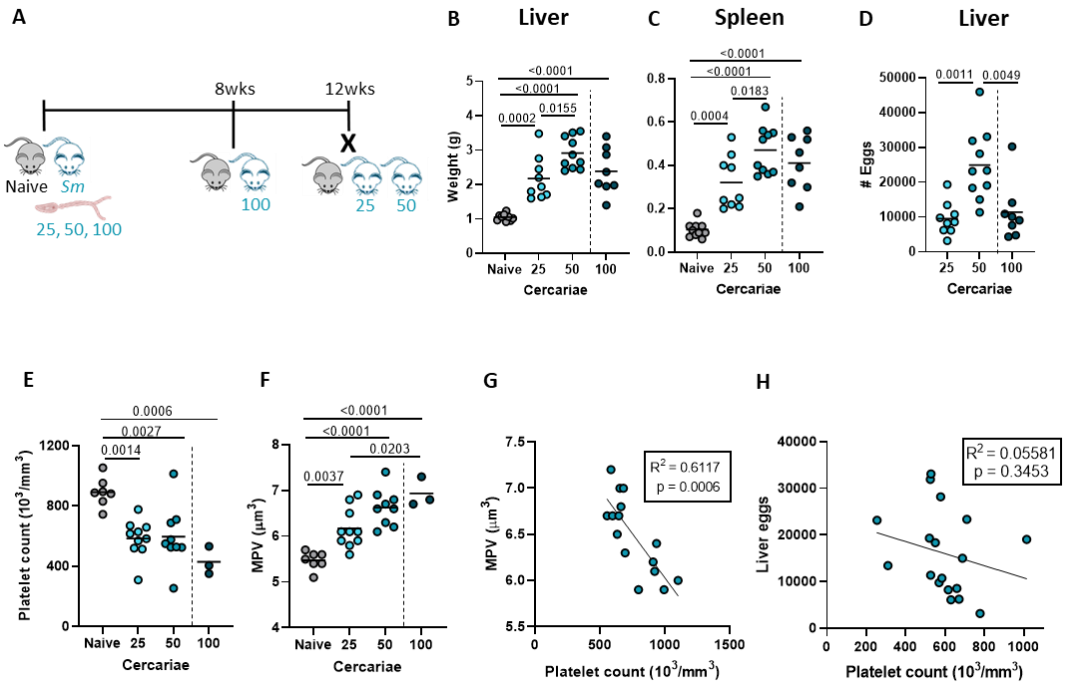

Figure 3.1: Thrombocytopenia in schistosome infection

C57BL/6 mice were percutaneously infected with 25-100 cercariae. A) Experimental schematic showing mice infected with 100 cercariae (n=10) were harvested 8 weeks post infection due to 2 mice being euthanised due to sickness. Mice infected with 25 (n=10) and 50 (n=10) cercariae were harvested at 12 weeks post infection. Naive mice were harvested at both time-points (n=4, n=6). Post-mortem B) liver and C) spleen weights. D) Post-mortem liver tissue from schistosome-infected mice was digested for schistosome egg. E) Platelet count and F) mean platelet volume (MPV) from terminal brachial bleeds. Correlative analysis of G) platelet counts and MPV or H) platelet count and total schistosome liver eggs pooled from the 25 and 50 cercariae infected groups. Data pooled from 2 independent experiments. Statistical significance was determined using one-way ANOVA with post-hoc Tukey's test on the mean of each treatment group. Non-significance ($p > 0.05$) not shown. Simple linear regression was performed to assess any correlation.

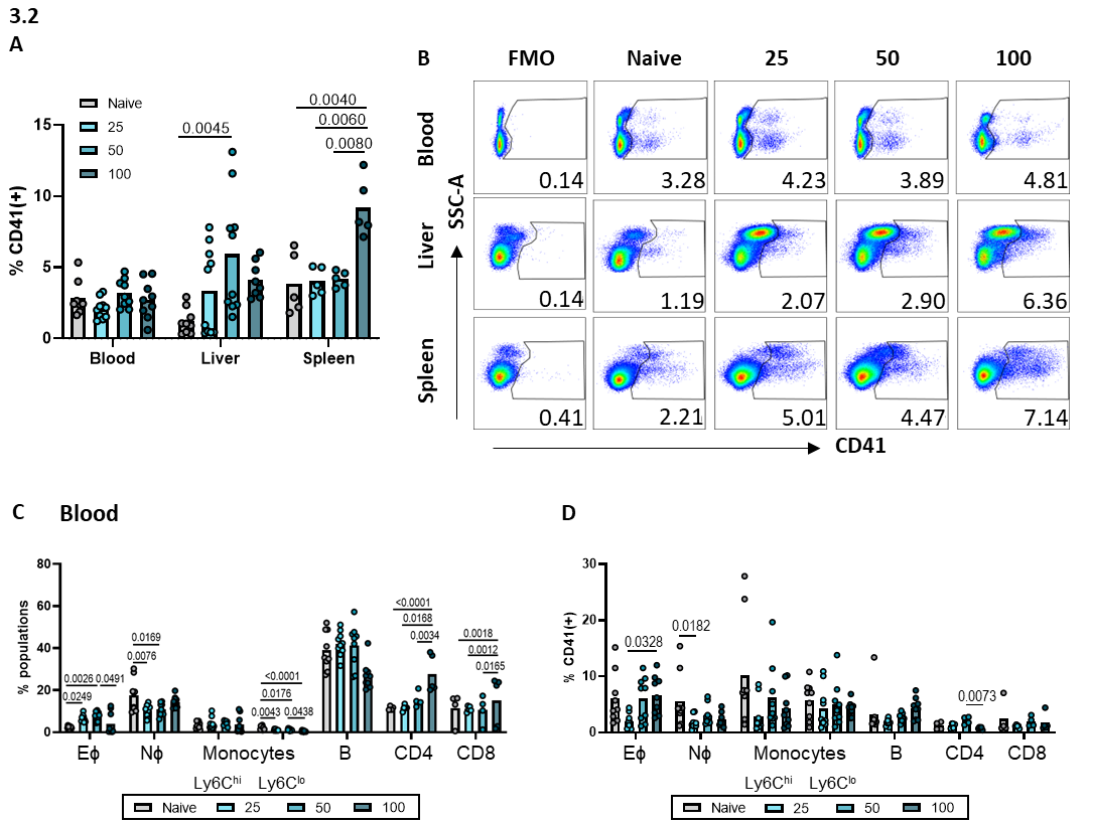

Figure 3.2 Assessment of platelet-leukocyte aggregates (PLA) in schistosome infection with varying infection dose

A) Flow cytometry quantification of CD41⁺ leukocytes (CD45⁺) in the blood (n=10, n=10, n=10, n=8), liver (n=10, n=10, n=10, n=8) and spleen (n=5, n=10, n=5, n=5) of C57BL/6 mice infected with 25-100 cercariae. B) Representative CD41⁺ FACS staining of leukocytes from blood, liver and spleen. Flow cytometry quantification of C) different immune cell populations as a percentage of total blood leukocytes and D) percentage of CD41 expression on the different immune populations. Naive-light grey, 25 cercariae-light blue, 50 cercariae-blue, 100 cercariae-dark blue. Data pooled from 2 independent experiments (blood and liver). Statistical significance was determined using one-way ANOVA with post-hoc Tukey's test on the mean of each treatment group. Non-significance ($p > 0.05$) not shown.

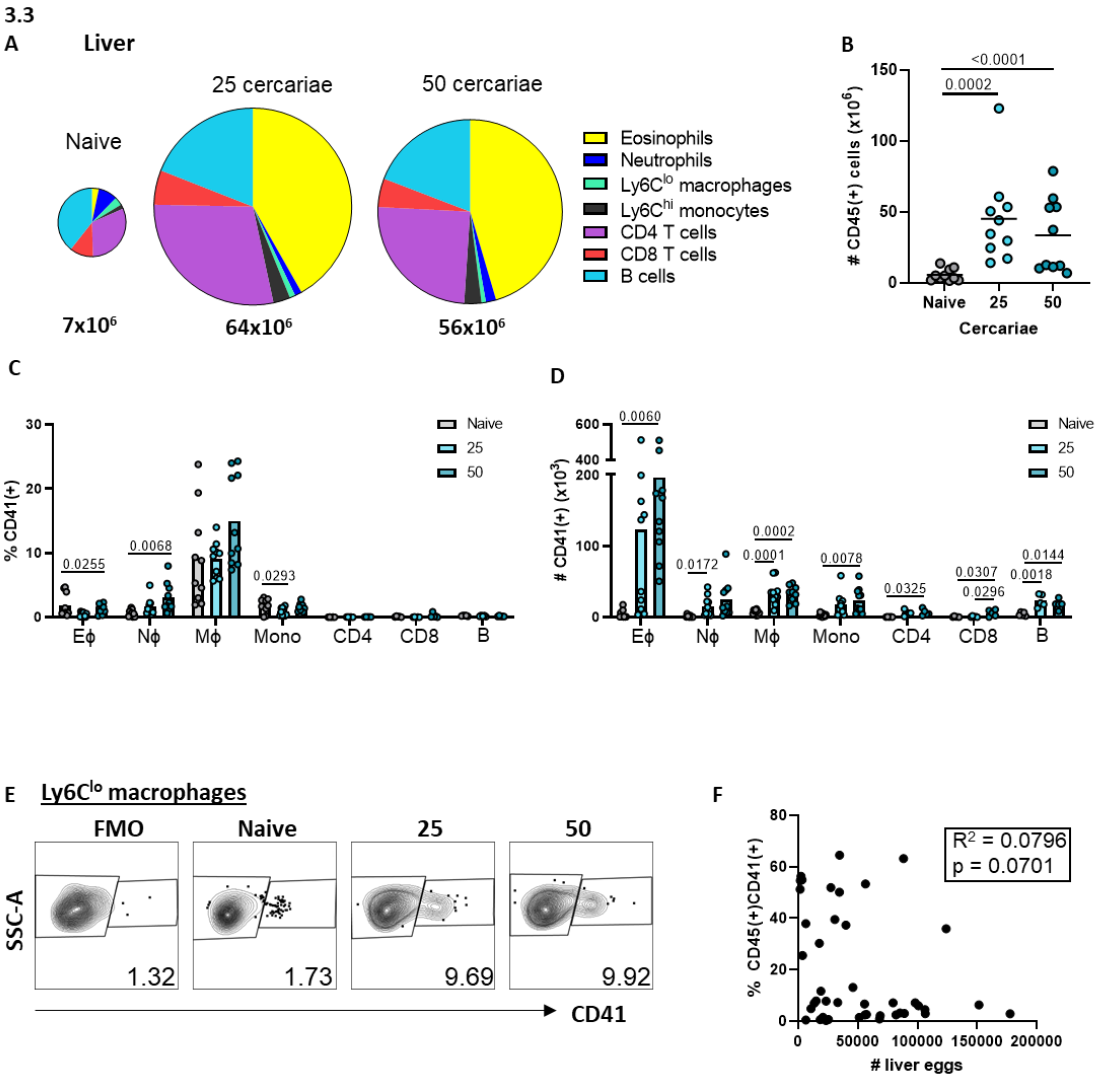

Figure 3.3 Schistosome infection significantly increases the number of PLA in the liver
A) Scaled pie charts, with area proportional to the total immune cell number in the liver at the point of harvest. B) Total number of $CD45^+$ cells in the liver. Flow cytometry quantification of C) the percentage and D) number of $CD41^+$ leukocytes ($CD45^+$) in the liver of C57BL/6 mice infected with 25 or 50 cercariae. E) Representative $CD41^+$ FACS staining on $Ly6C^{lo}$ macrophages. F) Correlative analysis of percentage $CD41^+$ leukocytes in the liver and the total number of schistosome liver eggs pooled from the 25 and 50 cercariae infected groups. (Naive n=10 (grey), 25 cercariae n=10 (light blue), 50 cercariae n=10 (blue)). Data pooled from 2 independent experiments. Statistical significance was determined using one-way ANOVA with post-hoc Tukey's test on the mean of each treatment group. Simple linear regression was performed to assess correlation. Non-significance ($p > 0.05$) not shown.

3.3.2 Does thrombocytopenia persist in chronic schistosome infection after worm clearance?

We next asked whether platelet alterations remained following treatment with the clinically-used chemotherapeutic drug PZQ. PZQ kills adult worms and so prevents continued egg production and worsening of pathology (29). Mice were infected for 12 weeks with 40 cercariae to establish robust platelet changes, treated with PZQ, and then assessed 3-4 weeks later (**Figure 3.4A**). As expected, PZQ treatment led to the clearance of adult worms (**Figure 3.4B**). Furthermore, both the liver and spleen weights of PZQ-treated mice were significantly lower than the infected-untreated group yet had not returned to naive baseline weights (**Figure 3.4C-D**). Pairwise comparisons showed mice treated with PZQ had a range of platelet counts, with ~40% (5/12) showing an increase in platelet counts (≥ 2x SD of the mean at each time point) between 12 weeks (pre-PZQ treatment) and 16 weeks (post-PZQ treatment) (**Figure 3.4E**, **Appendix 1**). Similarly, 75% of PZQ treated mice showed a reduction in MPV between 12 and 16 weeks (**Figure 3.4F, Appendix 1**).

Further analysis of the liver clearly showed PZQ treatment led to a reduction in the number of immune cell populations, particularly eosinophils, Ly6C^{hi} monocytes and lymphocytes (CD4^{+} and CD8^{+} T cells, B cells) compared with the infected-untreated group, with the exception of Ly6C^{lo} macrophages which were unaltered (**Figure 3.5A-B**). The percentage of PLA in the liver was highly variable and showed no significant differences between the infected and PZQ-treated groups (**Figure 3.5C**), however the absolute number of PLA (eosinophils, neutrophils, Ly6C^{lo} macrophages and B cells) were significantly reduced following PZQ treatment (**Figure 3.5D-E**). With the loss of adult worm production of schistosome eggs, we wanted to assess whether there was a reduction in inflammation. In the liver, we showed a modest, but significant reduction in eosinophil RELMα expression, as well as Ly6C^{lo} macrophage Ym1 expression (**Figure 3.6A-C**). In contrast, there was no significant difference in MHCII or RELMα expression by macrophages or monocytes between infected and infected-PZQ treated groups (**Figure 3.6C-D**). When considering liver CD4^{+} T cells, PZQ treatment led to a reduction in intracellular

IL-4, IFNγ and IL-10, with the latter two cytokines significantly decreasing (**Figure 3.7A-C**).

Together these experiments showed the clearance of adult worms by PZQ treatment reduced liver and spleen pathology however, the same improvement was not seen in platelet parameters. The percentage of hepatic PLA did not decrease after PZQ treatment but the total number of PLA did reduce.

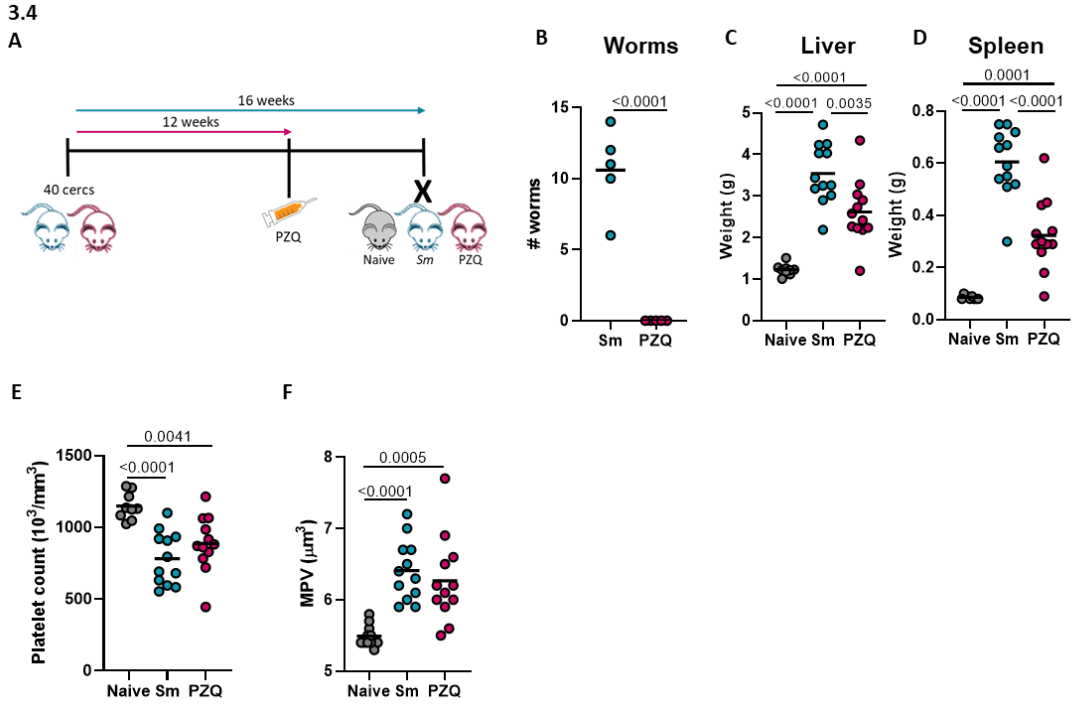

Figure 3.4 Sustained thrombocytopenia after drug-induced worm clearance
C57BL/6 mice were percutaneously infected with 35 cercariae. A) Experimental schematic showing 12 weeks post infection mice were treated with 250mg/kg praziquantel (PZQ) in 10% kolliphor® EL by oral gavage for 3 consecutive days, and all mice were harvested 4 weeks later (16 weeks total post-infection). B) Confirmation of effective treatment regime by worm counts following tissue perfusion of schistosome-infected (n=5) and PZQ treated (n=5) mice. Post-mortem C) liver and D) spleen weights. E) Platelet count and F) mean platelet volume (MPV) from terminal brachial bleeds. Data in C-F) pooled from 2 independent experiments (Naive n=10, *Sm* n=12, PZQ n=12). Statistical significance was determined using one-way ANOVA with post-hoc Tukey's test on the mean of each treatment group. Non-significance ($p > 0.05$) not shown.

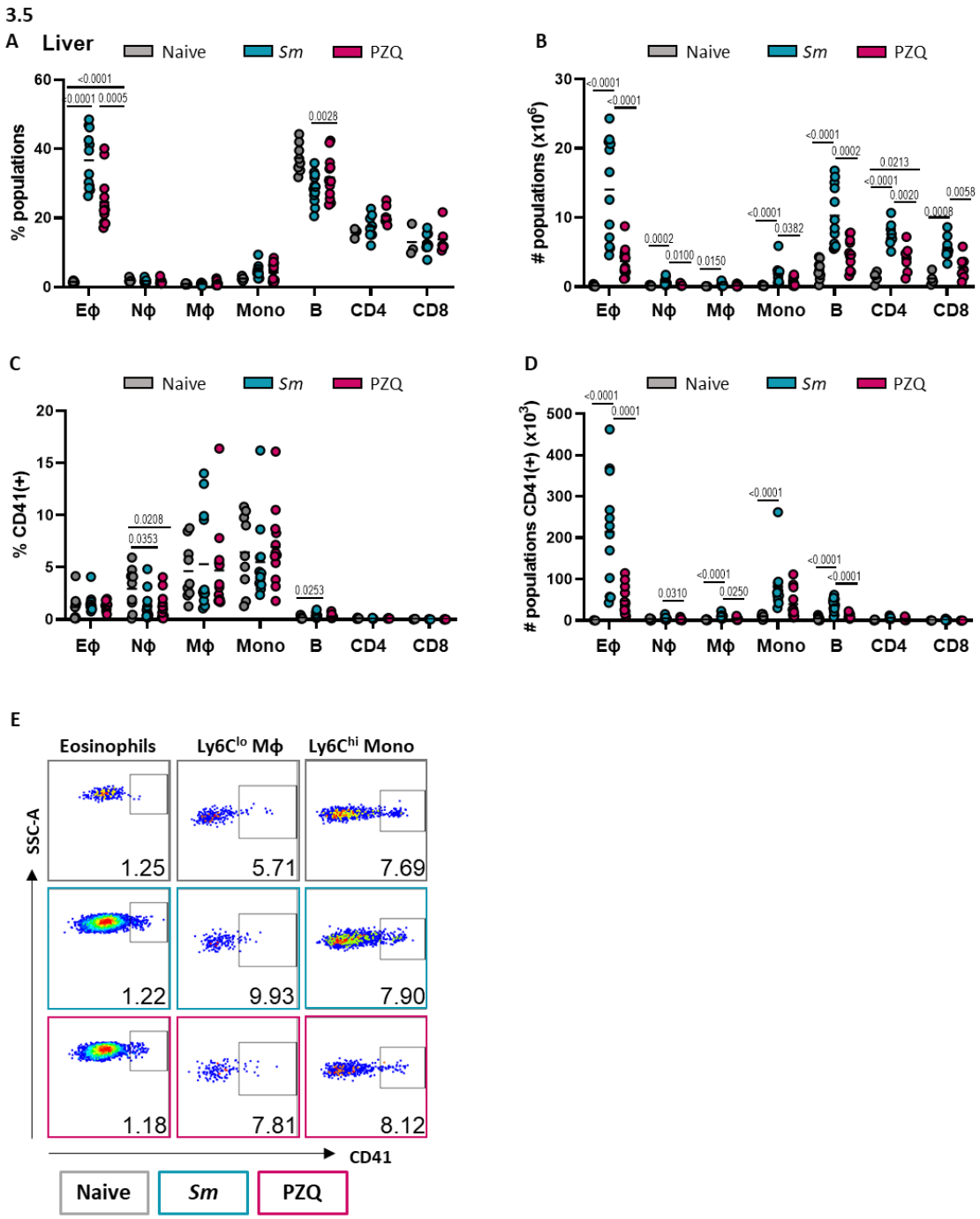

Figure 3.5 PZQ treatment reduces the number of PLA in the liver

Flow cytometry quantification of A) the percentage and B) number of leukocytes ($CD45^+$), C) percentage and D) number of $CD41^+$ leukocytes in the liver. E) Representative $CD41^+$ FACS staining on Eosinophils, $Ly6C^{lo}$ macrophages and $Ly6C^{hi}$ monocytes. Data pooled from 2 independent experiments, Naive (grey) n=10, *Sm* (blue) n=12, PZQ (pink) n=12. Statistical significance was determined using one-way ANOVA with post-hoc Tukey's test on the mean of each treatment group. Simple linear regression was performed to assess correlation. Non-significance ($p > 0.05$) not shown.

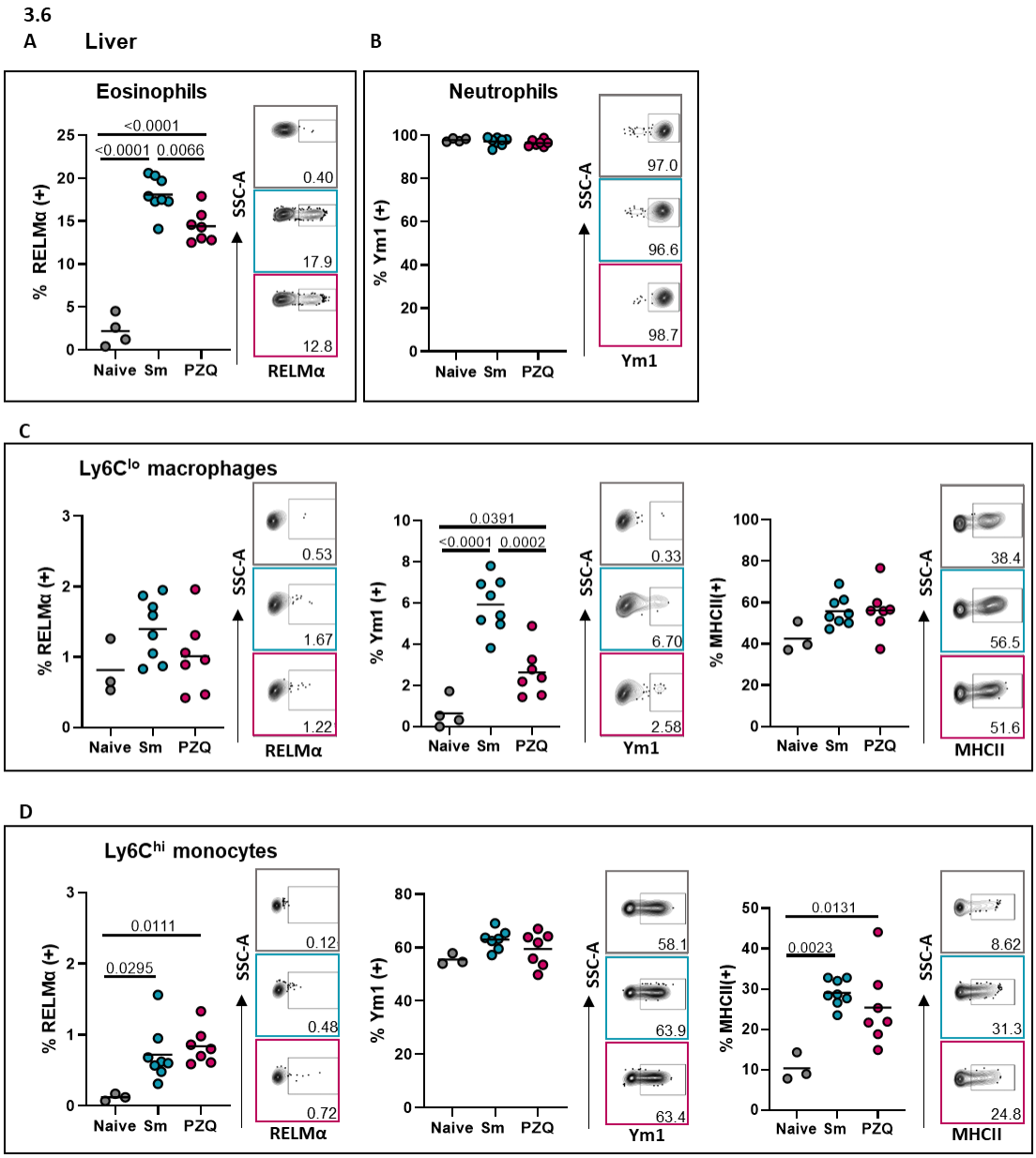

Figure 3.6 PZQ treatment has variable impact on infection-induced myeloid immune cell activation

Flow cytometry quantification and representative FACS staining of A) eosinophil RELMα and B) neutrophil Ym1. Percentage and representative FACS staining for RELMα, Ym1 and MHCII by C) Ly6C^{lo} macrophages and D) Ly6C^{hi} monocytes in the liver. Data representative of 2 independent experiments, Naive (grey) n=4, *Sm* (blue) n=8, PZQ (pink) n=7. Statistical significance was determined using one-way ANOVA with post-hoc Tukey's test on the mean of each treatment group. Non-significance ($p > 0.05$) not shown.

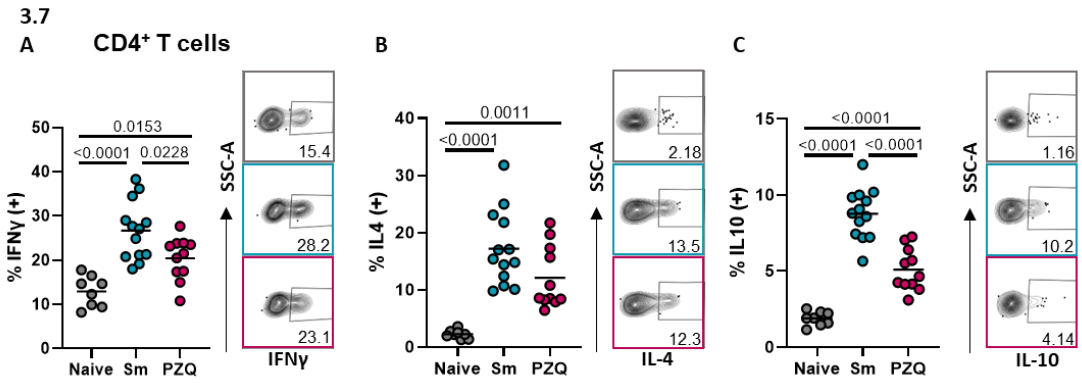

Figure 3.7 PZQ treatment reduces IFNγ and IL-10 by CD4⁺ T cells in the liver
Single cell suspensions (2-4x10^6 cells) from liver isolation processing were cultured *ex vivo* with Ionomycin, PMA and Brefeldin A. Flow cytometry quantification and representative FACS staining of CD4⁺ T cells for A) IFNγ, B) IL-4 and C) IL-10. Data pooled from 2 independent experiments, Naive (grey) n=10, *Sm* (blue) n=12, PZQ (pink) n=12. Statistical significance was determined using one-way ANOVA with post-hoc Tukey's test on the mean of each treatment group. Non-significance ($p > 0.05$) not shown.

3.3.3 Does schistosome infection impair megakaryopoiesis?

To investigate the mechanisms of thrombocytopenia, we asked if infection reduces thrombopoiesis. The main cytokine that regulates platelet production is TPO. TPO is primarily produced by hepatocytes and promotes MK differentiation, maturation and survival (151,145). The liver is the major site of granulomatous inflammation in schistosomiasis, which results in marked hepatomegaly. Confocal analysis of liver sections revealed higher cercarial doses were associated with both greater hepatocyte disorder and also extensive $CD41^+$ staining. As the CD41 staining was larger than a single platelet and also lacked a nuclei, this suggested micro-thrombi formation (**Figure 3.8A**). We also noted that *S. mansoni* granulomas were devoid of TPO^+ cells i.e. hepatocytes (**Figure 3.8A-B**). Higher magnification analysis revealed the presence of MK as well as micro-thrombi in the liver of schistosome-infected mice, and these were distinguished based on the presence or absence of a nucleus and their size (<150μm in diameter) (121) (**Figure 3.8B-C**). MK were also evident in the livers of mice infected with the protozoan parasite *Leishmania donovani* (*L. donovani*) previously shown to induce thrombocytopenia (**Figure 3.8B-E**; (238)). Consistent with reduced TPO^+ hepatocytes, *Tpo* mRNA levels were substantially lower in schistosome livers (**Figure 3.8F**) and circulating TPO protein was also markedly reduced even after PZQ treatment (**Figure 3.8G**). This reduction in circulating TPO was a similar magnitude to that seen in *L. donovani* infection. Despite reduced hepatic TPO production capacity, $CD41^+$ MK were also identified in the spleen (particularly in the red pulp) as well as in the liver, suggestive of extramedullary haematopoiesis (**Figure 3.8H-J**).

Given the BM has been thought of as the primary site of MK production of platelets (121), we next looked to see whether MK number in this location was affected by the reduction in hepatic and circulating TPO. Surprisingly, MK numbers were unchanged (**Figure 3.9A-B**), but schistosome infection led to a small yet significant decrease in $CD41^+$ MK diameter, whereas *L. donovani* increased MK size as in previous studies (**Figure 3.9C,** (238)). Despite no change in the number of BM-resident MK in schistosome infection there was marked reductions in BM $CD68^+$ macrophages, which appeared to start to

revert following PZQ treatment (**Figure 3.9D**). We next explored whether schistosome infection skews the functional programming of MK in the BM. Sun *et al.* (2021) characterised three functionally and phenotypically unique MK populations in the BM: immune (2-8N), HSC-niche maintenance (8-32N) and platelet generating (8-32N) (296). Given the slight reduction in MK size, we wanted to investigate whether this was a result of altered megakaryopoiesis. MK ploidy analysis of BM from naive and schistosome-infected mice showed there was an increase in 4N low-ploidy MK, previously linked to immune roles and a decrease in the higher 8-16N population, associated with HSC-niche maintenance as well platelet production (**Figure 3.9E-F**). There was no significant difference in the percentage of 32N+ MK in BM from naive and infected mice.

Finally, we tested whether schistosome infection affects the differentiation potential of these platelet-producing cells. Endothelial Protein C Receptor ($EPCR^+$) HSC were cell-sorted from the BM of naive and schistosome-infected mice for methylcellulose colony formation assays. This revealed that HSC from naive and infected mice generated a similar number of colonies (**Figure 3.10A-B**), and there was no difference in $CD41^+$ expression, which suggests prior schistosome infection does not alter MK lineage bias (**Figure 3.10C**). In contrast, exogenous IL-4 reduced the overall number of colonies and strongly inhibited $CD41^+$ cell differentiation which is consistent with other reports (297,298). This indicates that whilst exogenous IL-4, characteristic of type 2 immune responses as occurs in schistosome infection, can inhibit megakaryopoiesis, this does not occur with HSC isolated from infected mice.

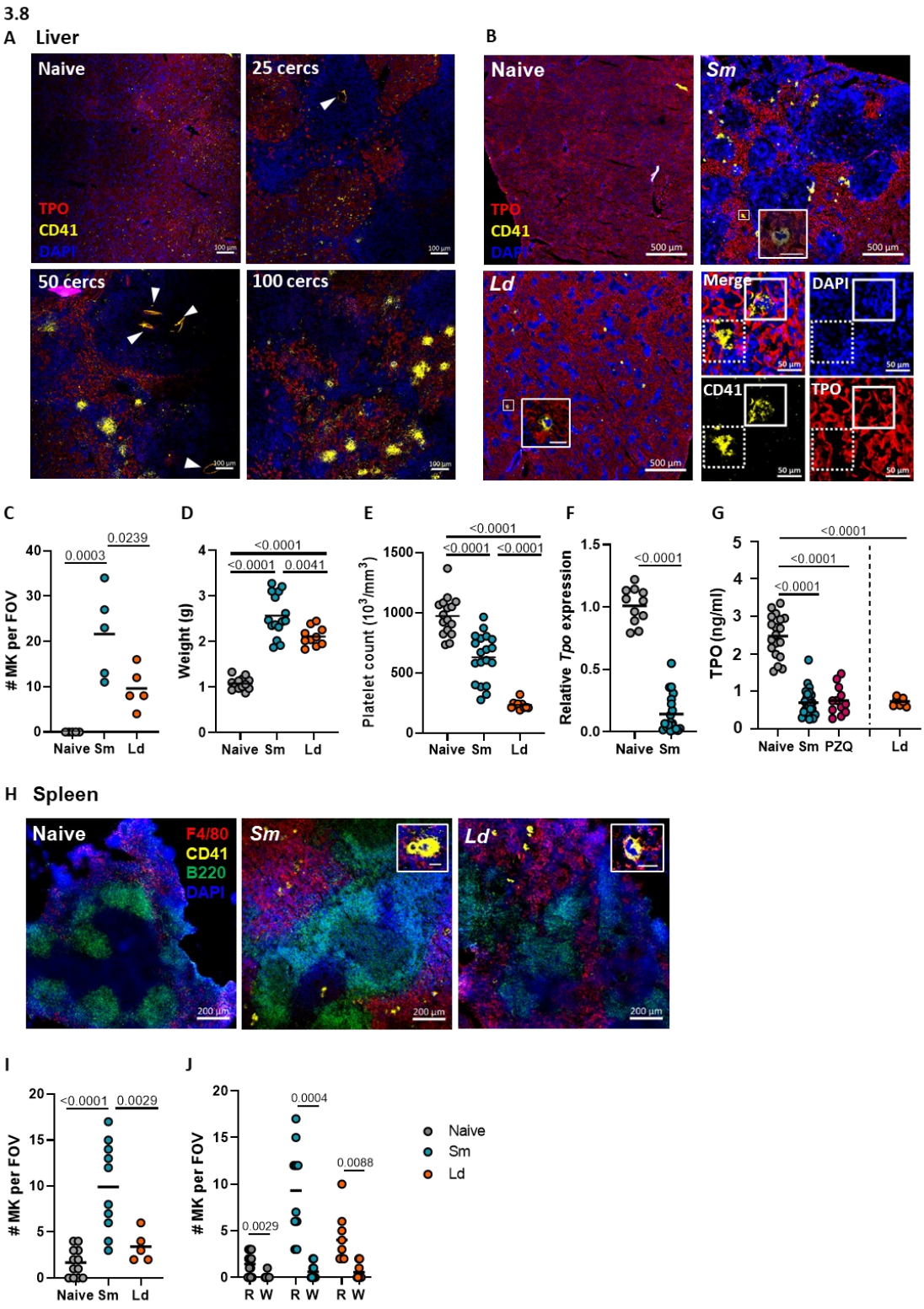

Figure 3.8 Extramedullary haematopoiesis and reduced systemic TPO in schistosome infection

A) Representative fluorescent images of liver tissue from C57BL/6 mice infected with 25 or 50 cercariae (10 weeks) or 100 cercariae (8 weeks) stained for TPO (red), CD41 (yellow) and DAPI (blue) and imaged with a 10x objective. White arrowheads indicate schistosome eggs within granulomas. C57BL/6 mice were infected with 40 *S. mansoni* cercariae for 10 weeks or $5x10^7$ LV9 (*Ld*) for 4 weeks. B) Representative fluorescent images of liver tissue stained

for TPO (red), CD41 (yellow) and DAPI (blue) using a 10x objective with 0.6x zoom. Top left - naive, top right – *S. mansoni,* bottom left – *L. donovani,* bottom right identification of MK (solid white box) from platelet cluster (dotted white box). High magnification image inserts were obtained using a 63x oil-immersion lens. C) Quantification of the number of MK per field of view (Naive n=5, *Sm* n=5, *Ld* n=5). Post-mortem D) liver weight and E) platelet counts (Naive n=13, *Sm* n=15, *Ld* n=10), pooled from 3 independent experiments. F) Hepatic *Tpo* mRNA assessed by qPCR normalised to *Hprt* housekeeping gene (Naive n=11, *Sm* n=20) pooled from 4 independent experiments. G) Serum TPO levels assessed by ELISA (Naive n=19, *Sm* n=25, PZQ n=12, *Ld* n=8), pooled from 4 independent experiments. H) Representative fluorescent images of spleen tissue stained with F4/80 (red), CD41 (yellow), B220 (green) and DAPI (blue) and imaged using a 10x objective lens with 0.6x zoom. High magnification inserts (white boxes) were images using a 63x oil-immersion lens. Quantification of I) all MK and J) distribution of MK in the red (R) and white (W) pulp of the spleen (Naive n=12 (grey), *Sm* n=10 (blue), *Ld* n=9 (orange)), pooled from 2 independent experiments. Statistical significance was determined using one-way ANOVA with post-hoc Tukey's test on the mean of each treatment group (C-E, G and I), unpaired student's t-test (F) and paired t-test (J). Non-significance ($p > 0.05$) not shown.

3.9

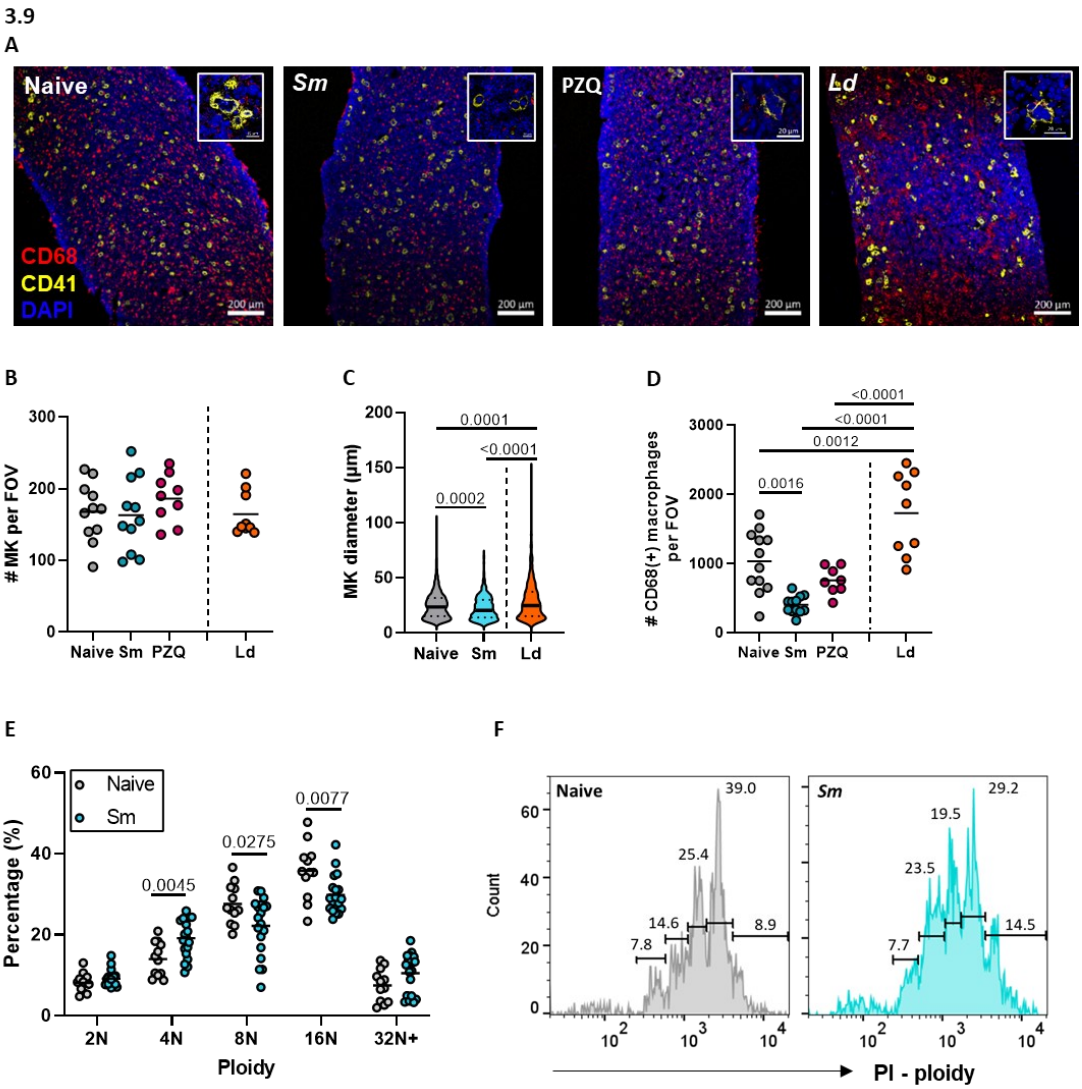

Figure 3.9 Sustained megakaryopoiesis, but lower ploidy MK in schistosome infection
A) Representative fluorescent images of decalcified femurs from C57BL/6 mice infected with ~35 *S. mansoni* cercariae for 16 weeks (*Sm*), PZQ treated schistosome-infected mice at 12 weeks and harvested 4 weeks later (PZQ) or infected with $5x10^7$ *Leishmania donovani* LV9 strain for 4 weeks (*Ld*). Bones were stained with CD68 (red), CD41 (yellow) and DAPI (blue) and imaged using 10x objective or 63x oil-immersion lens (white box inserts). Quantification of B) MK per field of view, C) MK diameter (count Naive=1826, *Sm*= 774, *Ld*=945) and D) $CD68^+$ cells (Naive n=12, *Sm*=11, *Ld*=9). E) Flow cytometry quantification of BM MK ploidy analysis and F) representative histograms (Naive (grey) n=12, *Sm* (blue) n=19), pooled from 3 independent experiments. Statistical significance was determined using one-way ANOVA with post-hoc Tukey's test on the mean of each treatment group (B-D) and unpaired student's t-test (E). Non-significance ($p > 0.05$) not shown.

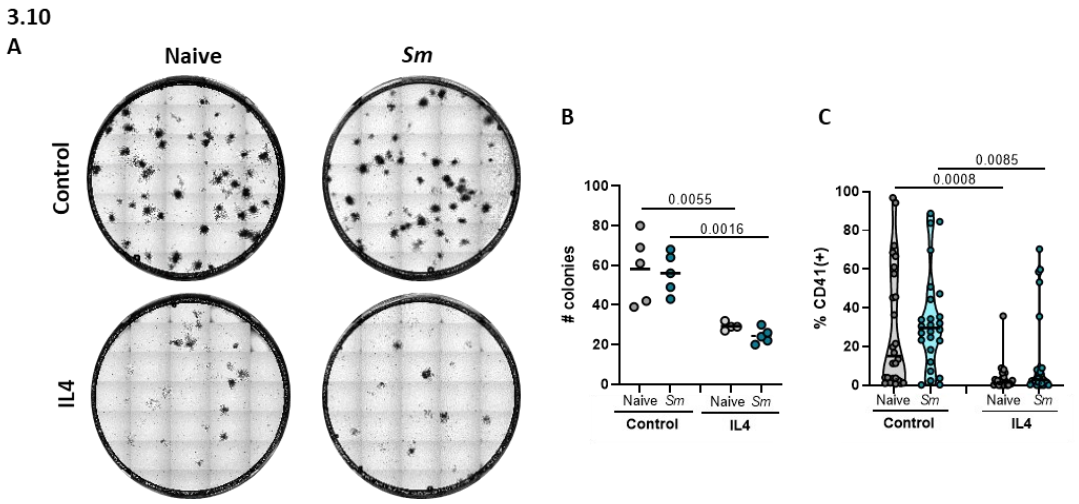

Figure 3.10 Schistosome infection does not alter the production of CD41⁺ colonies from cultured HSC

Bones were isolated from C57BL/6 naive and schistosome-infected mice (~35 cercariae) at 12 weeks post-infection. 100 ESLAM ($Lin^-cKit^+EPCR^+Sca1^+CD48^-CD150^+$) cells were sorted into each well and cultured for 10 days in the absence or presence of 10ng/ml IL-4. A) Representative images of individual wells after 10 days of culture for each treatment group. Quantification of B) the number of colonies per well (5 wells per condition) and C) percentage of all cells $CD41^+$ per colony (each symbol represents individual colonies. Data from a single experiment, representative 3 independent experiments. Statistical significance was determined using unpaired student's t-test (B-C). Non-significance ($p > 0.05$) not shown.

3.3.4 Does schistosome infection enhance platelet clearance?

Having shown that there may be a reduction in platelet-producing 8-16N MK in schistosome infection which may be contributing to the thrombocytopenia, we wanted to assess whether platelet clearance is also accelerated. Initially, we tried to fluorescently label exogenously isolated platelets with a range of markers (acridine orange, Carboxyfluorescein succinimidyl ester and 5-chloromethylfluorescein diacetate), before transferring these back into recipient mice. However, after testing a broad range of dye concentrations, transfer ratios and sampling times we were unable to consistently detect the transferred population to allow monitoring of platelet clearance. Therefore, we tried labelling platelets directly *in vivo*. Here we used a fluorescently conjugated antibody (DyLight649, Emfret X649) which binds the GPIbβ subunit of the platelet/megakaryocyte-specific GPIb-V-IX complex (vWF receptor), from here on referred to as X649. X649 specifically labelled platelets in circulation without driving immune-mediated platelet clearance (**Appendix 2**), thereby allowing us to measure platelet turnover (299). Longitudinal bleeds were taken from schistosome and *L. donovani* infected mice 1hr, 24hr and 48hr post injection of X649 (**Figure 3.11A**). Whole blood was co-stained for CD41, and expression of X649 was normalised to the 1hr time-point. This showed the significant thrombocytopenia and elevated MPV in both schistosome and *L. donovani* infected mice are, at least in part, a result of accelerated platelet clearance (**Figure 3.11B-F**). Increased platelet size may reflect enhanced platelet clearance as it ensures there are proportionally more “newer” larger platelets present in the circulation. Alternatively, infection may cause platelet activation, resulting in larger cells; at this stage we are unable to distinguish between these two possibilities. The half-life of platelets in naive mice was estimated to be ~51hr and this shortened to 39hr and 26hr in schistosome and *L. donovani* infections respectively.

To explore the mechanism of accelerated platelet clearance in schistosome infection, we first asked whether platelets were being opsonised with auto-antibodies which act as “eat-me” signals for phagocytes in immune-mediated thrombocytopenia (300). We used FcRγ$^{-/-}$ mice which lack activating cell surface Fcγ receptors, FcγRI (CD64), FcγRIII (CD16) and FcγRIV, as well as

FcεRI and FcαRI, to assess whether thrombocytopenia could still occur in schistosome-infected mice in the absence of FcRγ-antibody complexes. In a pilot experiment we confirmed that FcRγ$^{-/-}$ mice treated with anti-CD41 IgG antibodies did not become thrombocytopenic compared with wild type (WT) controls (**Figure 3.12A**). In schistosome infection, a significant reduction in platelets and elevated MPV were still observed in FcRγ$^{-/-}$ mice indicating platelet clearance in schistosome infection is not mediated by activating Fc receptors (**Figure 3.12B-C**). There was also no difference in the pathology in terms of liver weight, eggs (**Figure 3.12D-E**) and granuloma formation (**Appendix 3**) between the WT and FcRγ$^{-/-}$ groups. Moreover, the percentage and number of PLA in the blood, liver, spleen and lung (**Figure 3.12F**) and the activation of the different immune populations showed no difference between the WT and FcRγ$^{-/-}$ infected groups (**Appendix 4**).

3.11

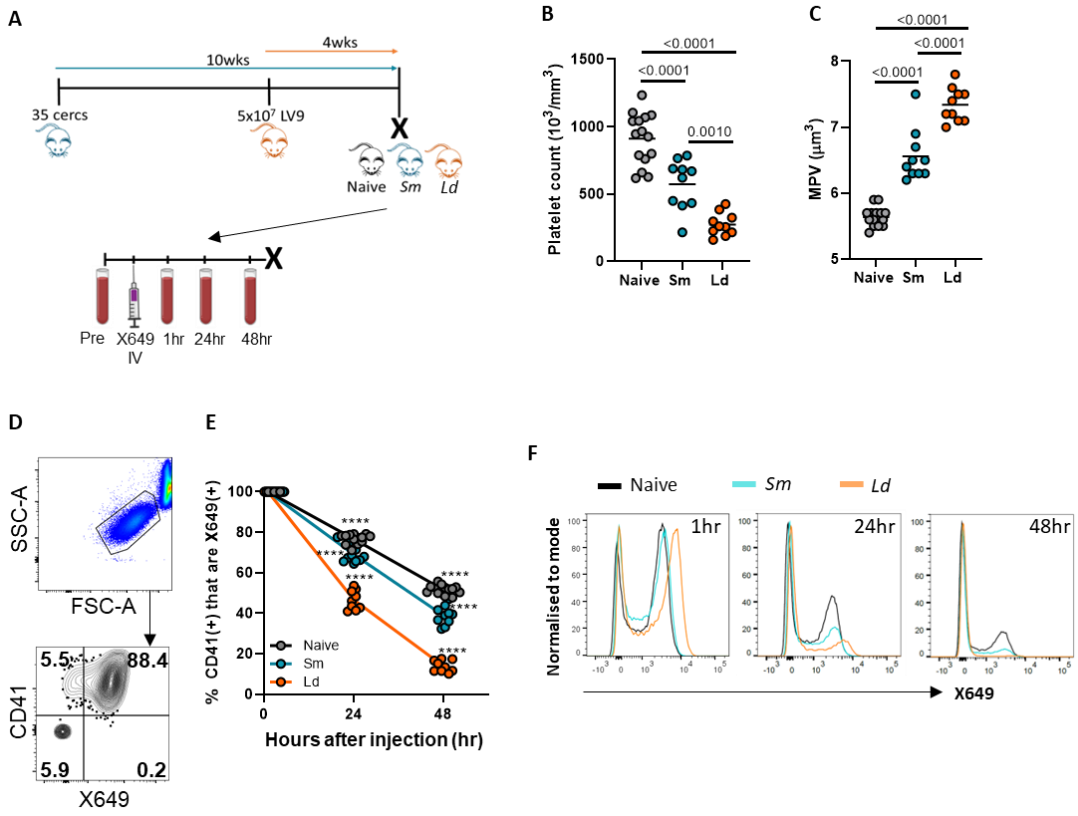

Figure 3.11 Accelerated platelet clearance in schistosome and L. donovani infected mice

A) Schematic showing C57BL/6 mice were infected with 40 *S. mansoni cercariae* (*Sm*) for 10 weeks or 5x10^7 LV9 (*Ld*) for 4 weeks. Tail bleeds were taken prior to IV injection (0.05μg/gram of body weight) of anti-GPIb-V-IX conjugated DyLight 649 (X649). Tail vein blood samples were harvested 1, 24 and 48hr post-injection. Terminal bleed B) platelet count and C) mean platelet volume (MPV). D) Representative FACS staining on platelets at 24hr from a naive mouse. E) Quantification of the percentage of platelets CD41$^+$X649$^+$ from tail bleeds, normalised to the 1hr time-point and F) representative histograms of X649 staining at different time points for naive (black), *Sm* (blue) and *Ld* (orange) platelets. Data pooled from 3 independent experiments (Naive n=15, *Sm* n=10, *Ld* n=10). Statistical significance was determined using one-way ANOVA with post-hoc Tukey's test on the mean of each treatment group (B-C) at each time point (E). Non-significance (p >0.05) not shown.

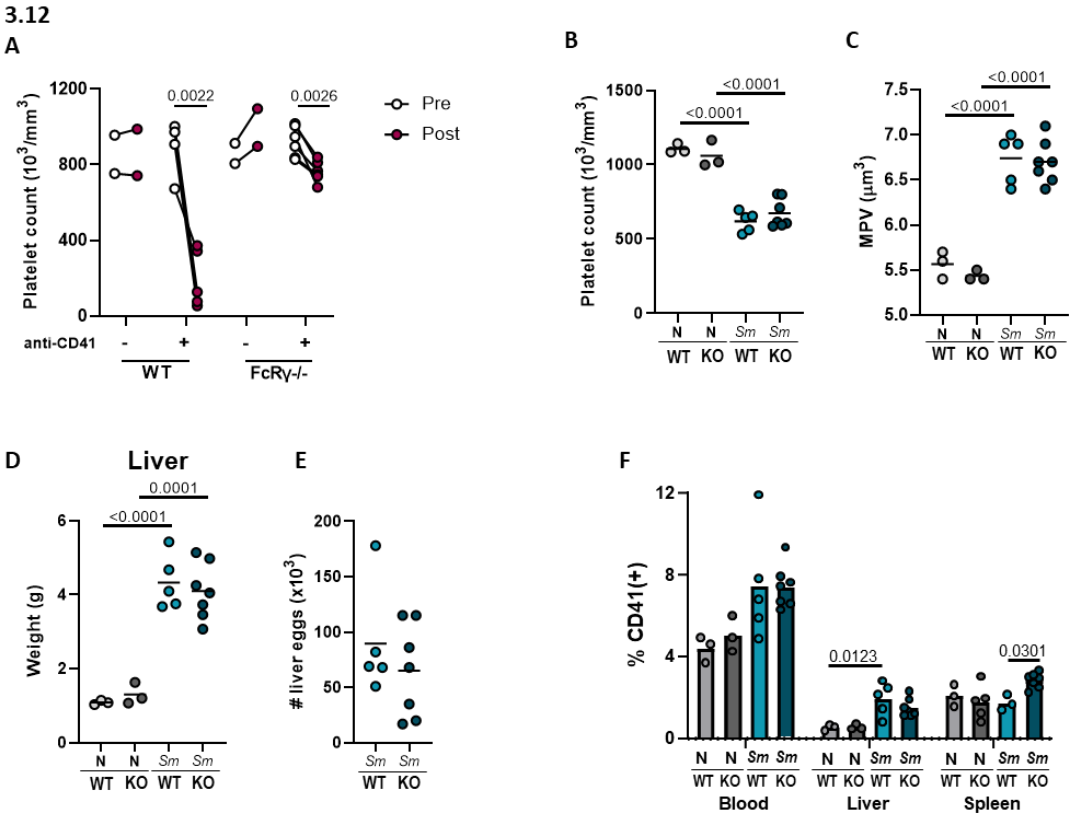

Figure 3.12 No difference in platelet numbers between WT and FcRγ$^{-/-}$ schistosome-infected mice

WT and FcRγ$^{-/-}$ (KO) mice were given a single IP injection with 0.2mg/kg anti-CD41 (MWReg30) antibody or IgG control. A) Terminal bleed platelet count. Representative of a single experiment (WT control n=2, WT anti-CD41 n=5, FcRγ$^{-/-}$ control n=2, FcRγ$^{-/-}$ anti-CD41 n=5) (Pre anti-CD41 treatment = white, post anti-CD41 treatment = pink). WT and FcRγ$^{-/-}$ mice were infected with 40 *S. mansoni* cercariae and harvested 11 weeks later. Terminal B) platelet count and C) mean platelet volume (MPV). Post-mortem liver tissue was D) weighed and E) a section was digested in 4% KOH and schistosome liver eggs were counted. F) Flow cytometry quantification of the percentage of CD41^{+} leukocytes in different tissues (blood, liver and spleen). Data from a single experiment, representative of 2 independent experiments (WT Naive n=3, WT *Sm* n=5, FcRγ$^{-/-}$ Naive n=3, FcRγ$^{-/-}$ *Sm* n=7). Statistical significance was determined using paired t-test (A), one-way ANOVA with post-hoc Tukey's test on the mean of each treatment group (B-D, F) and unpaired student's t-test (E). Non-significance (p >0.05) not shown.

3.3.5 Are platelets surface-bound or phagocytosed by immune cells in schistosome infection?

X649 labelling not only allows us to assess platelet clearance dynamics *in vivo*, but it also indicates cell types that interact with platelets and potentially receive immunomodulatory signals from them (301). We hypothesised that $X649^+$ leukocytes ($CD45^+$) that were also $CD41^+$ (i.e. $X649^+CD41^+$), had surface-bound platelets, whereas leukocytes that had internalised platelets were $CD41^-$ (i.e. $X649^+CD41^-$) as the platelet glycoprotein IIb was no longer accessible to the antibody (**Figure 3.13A**). In order to test this hypothesis, we isolated platelets from naive mice and labelled them with X649 *in vitro* before culturing them for 24hr with BM-derived macrophages at a 100:1 ratio (platelet:macrophage). At multiple time-points we washed plate-bound macrophages to remove platelets in suspension, detached the macrophages and stained the cells for CD11b, CD64 and CD41 to detect the macrophages and any surface-bound platelets. Flow cytometric analysis clearly showed after a short time in culture (<1hr) there was a relatively small percentage of macrophages interacting with platelets (i.e. $X649^+$), but the majority of these were $CD41^+$ representing surface-bound platelets (i.e. $X649^+CD41^+$). In contrast, as culture progressed, whilst the proportion of macrophages that were interacting with platelets increased ($X649^+$), these were predominantly $CD41^-$, suggesting platelet internalisation (**Figure 3.13B-C**).

We next wanted to visually confirm our hypothesis of platelet internalisation based on flow cytometry staining. Using Airyscan microscopy we were able to successfully label and detect platelets labelled with X649 and CD41, which displayed a high degree of co-localisation as anticipated (**Figure 3.14A**). We also confirmed that macrophage cell morphology was maintained after cytospinning onto slides which would enable us to determine the localisation of platelets within, or on the surface of cells (**Figure 3.14B**). A similar co-culture was set up as described previously and cells were stained and harvested at 4hr for both flow cytometry and imaging, in the hope of capturing platelets at all stages of internalisation. 3D reconstruction of z-stacked images and manual orthogonal examination was performed to assess whether the pink X649 signal was located within the yellow, CD45 surface boundary. In

support of our hypothesis, we identified macrophages with cell surface platelets that were X649^{+}CD41^{+}, and macrophages with internalised platelets that were X649^{+}CD41^{-} (**Figure 3.15A-C**).

In order to confirm our finding from *in vitro* co-culture assays we sorted macrophages and monocytes from the livers of 12 week schistosome-infected mice which had been injected with X649 24hr prior to harvesting. However, prior to sorting cells from infected livers we needed to enrich for the population of interest to increase sort efficiency and purity. Initially, we tried F4/80 cell positive-selection on naive liver and spleen samples, however despite enriching monocytes in the liver ~3-fold there was also significant enrichment of the eosinophil population (**Appendix 5**). Given eosinophils are the most abundant cell population in schistosome infection, further enrichment of this population was an issue. We therefore tried CD64 enrichment on naive liver and spleen samples, which showed successful (~4-fold Mϕ, ~7-fold Mono) enrichment and the depletion of eosinophils, B and T cells (**Figure 3.16A-B**). To obtain sufficient cell numbers for downstream imaging and analysis, CD11b^{+}SiglecF^{-}Ly6G^{-}F4/80^{+} cells were sorted based on being X649^{-} or X649^{+}. Given panel complexity and limited cell numbers, we chose not to separate Ly6C^{lo} macrophages and Ly6C^{hi} monocytes in this experiment. After sorting, cells were stained with CD45 and CD41 as in the *in vitro* macrophage experiments, samples were then cytospun and imaged (**Figure 3.17**). This demonstrated that we could distinguish between surface-bound and internalised platelets using *in vivo* X649 labelling and co-staining with fluorescently labelled CD41 *ex vivo*. Double positive (X649^{+}CD41^{+}) monocytes/macrophages had surface-bound platelets, whereas single positive (X649^{+}CD41^{-}) monocytes/macrophages had platelets internalised.

Having demonstrated that we could differentiate between surface-bound and internalised platelets, we were interested to dissect which immune cells were interacting with platelets and whether there was any tissue specificity. Following the same infection and staining regimen as described in **Figure 3.11A** we showed that negligible levels of X649^{+} immune cells were detected in the blood of *L. donovani* infected mice, which is consistent with the severe thrombocytopenia seen in these animals (**Figure 3.11B and Figure 3.18A**).

In contrast, X649$^+$ leukocytes were more readily detectable in the blood of naive and schistosome-infected mice, although there was no significant difference between these two groups. Notably, X649$^+$ leukocytes were elevated in blood compared to liver and spleen (**Figure 3.18A-B**). We did detect a significant increase in liver X649$^+$ leukocytes in schistosome infection compared with naive animals. Examination of individual immune populations in the blood showed the majority of platelets were surface-bound (X649$^+$CD41$^+$) rather than internalised (X649$^+$CD41$^-$). Whilst infection was associated with an increased proportion of Ly6C^{lo} non-classical blood monocytes internalising platelets (**Figure 3.18C**), this population was a relatively minor one as infection skews towards the classical Ly6C^{hi} monocytes. As such, we calculated absolute cell numbers and found infection led to a significant increase in the number of surface-bound platelets on classical monocytes and eosinophils (**Figure 3.18D-E**).

In contrast to the blood, the majority of platelets had been internalised by immune cells in the liver and there was a significantly lower percentage of X649$^+$ leukocytes in *L. donovani* infection compared with naive, and schistosome-infected mice (**Figure 3.19A**). Again, when considering the absolute number of cells that were X649$^+$, there was a significant increase in schistosome infection in multiple cell types (monocytes, eosinophils, CD8$^+$ T cells and B cells) (**Figure 3.19B-D**). The monocyte and eosinophil populations predominated and also showed a significantly greater number of surface-bound, as well as internalised platelets.

Finally, in the spleen, which is the primary site of platelet clearance in ITP (302), there was a reduction in the percentage of monocytes X649$^+$ in both infections compared with the naive mice (**Figure 3.20A**). In *L. donovani* infection, there was a significant increase in absolute number of immune cells (particularly monocytes, neutrophils, B cells and CD4$^+$ T cells) in the spleen (**Figure 3.20B**). It appeared that the majority of platelets were internalised by monocytes and eosinophils in the spleen during *L. donovani* infection, which complements previous data (**Figure 3.20C-D,** (238)). In contrast, there was little difference in platelet interactions with immune cells in the spleen between

naive and schistosome-infected mice, with the exception of an expanded X649^{+} B cell population in schistosome infection.

Together, these data show that there is an increase in surface-bound platelets on multiple blood immune cells in schistosome infection with very little internalisation. However, in the liver of schistosome-infected mice, there is significant platelet internalisation by monocytes and eosinophils, which contrasts with significant platelet internalisation in the spleen in *L. donovani* infection.

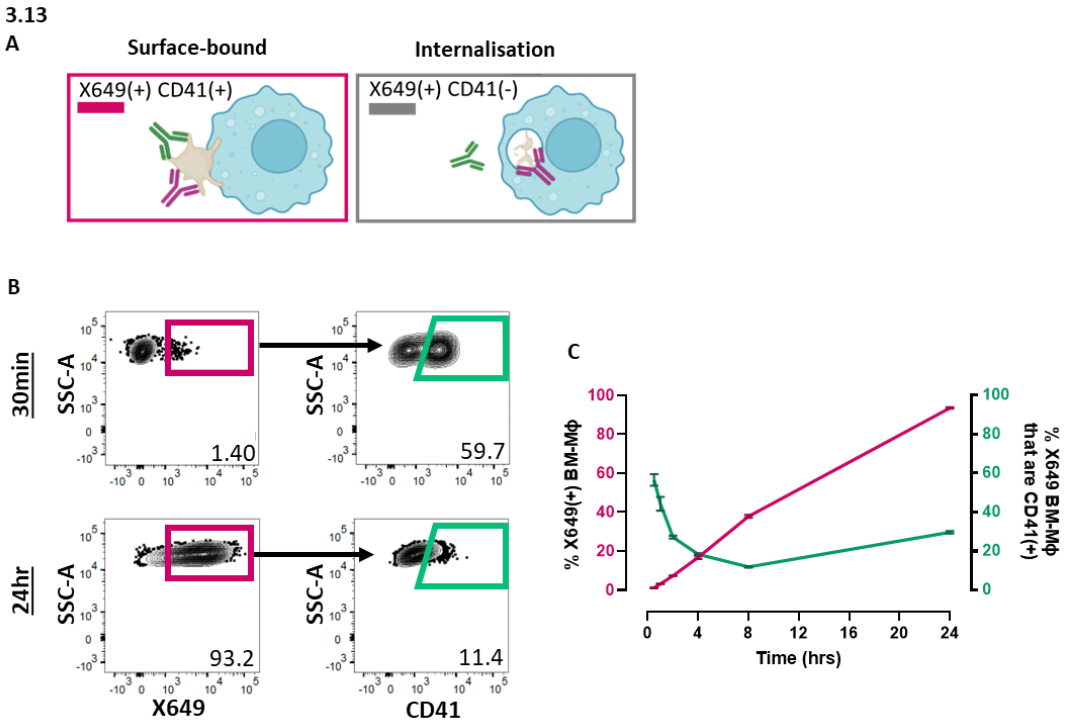

Figure 3.13 Reduction of surface-bound platelets on BM-Mϕ over 24hr
1x10^{6} BM-Mϕ were co-cultured with 1x10^{8} isolated murine platelets labelled with X649. Macrophages were detached at 30min, 1hr, 2hr, 4hr, 8hr and 24hr, and stained for CD11b, CD64 and CD41. A) Hypothesised mechanism of identifying platelet localisation. B) Representative FACS staining of co-cultures at 30min and 24hr. Pink box – percentage of all X649^{+} macrophages (CD11b^{+}CD64^{+}). Green box – percentage of all X649^{+} macrophages that are also CD41^{+}. C) Quantification of FACS stained co-cultures over 24hr. Pink line – percentage of macrophages that are X649^{+}. Green line – percentage of X649^{+} macrophages that are CD41^{+}. Data from a single experiment, with 6 technical replicates for each condition at every time point. Bars represents mean with standard error.

3.14

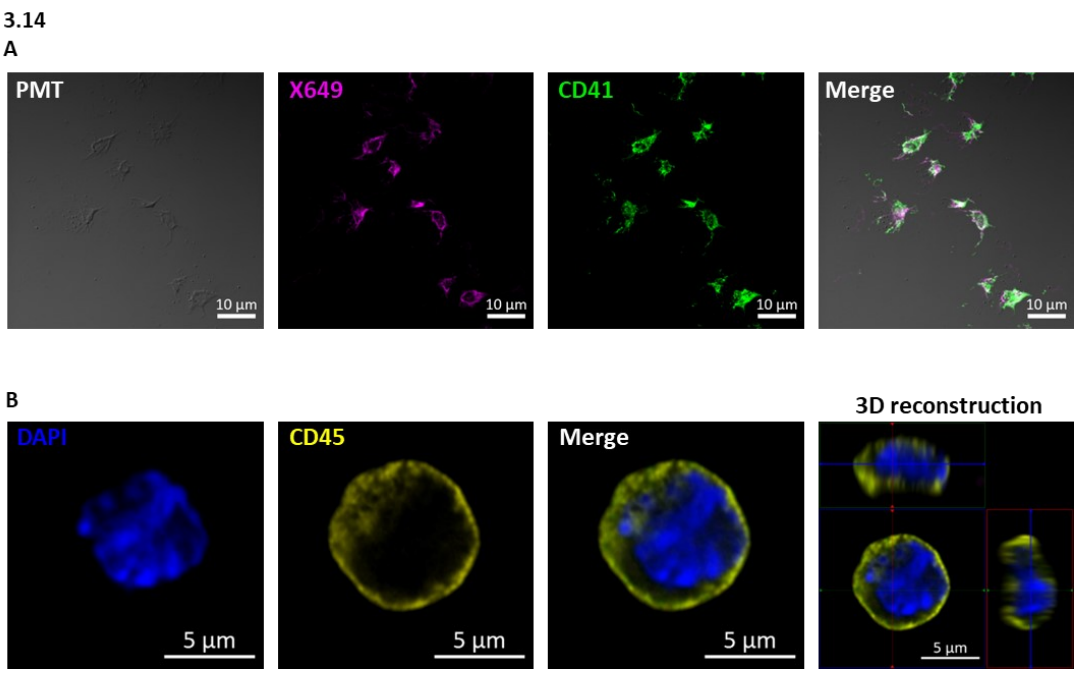

Figure 3.14 Visualisation of platelets and macrophages by confocal microscopy
A) Cytospun isolated murine platelets stained with X649 (pink) and CD41 (green). B) Cytospun BM-Mϕ stained for CD45 (yellow) and DAPI (blue). Z-stack 3D reconstruction orthogonal projection from 0.2µm slices. Images were taken using a 63x oil-immersion lens, with 4x zoom. Images represent a single experiment and >10 FOV.

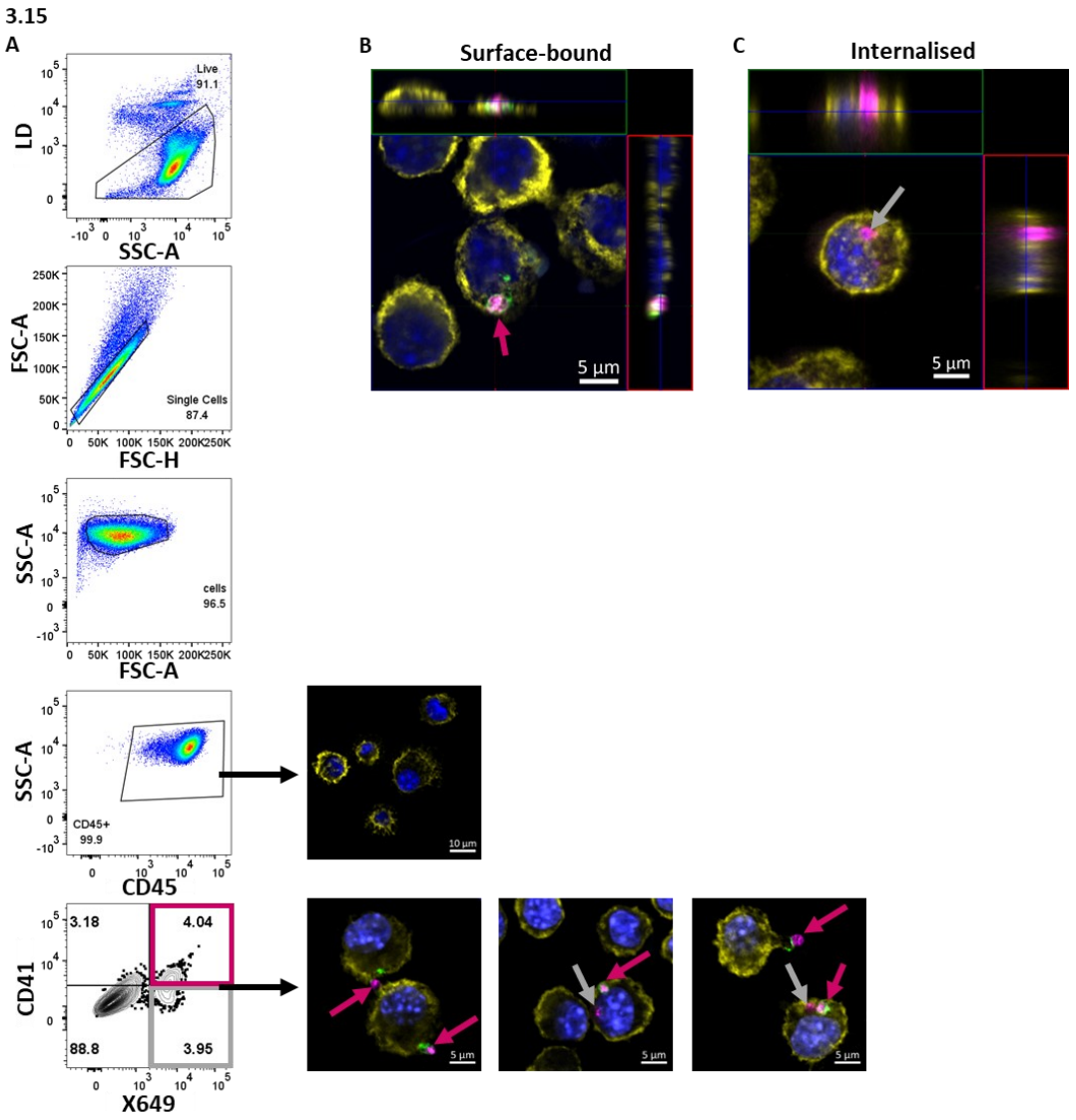

Figure 3.15 Confirmation of surface-bound and internalised platelets by BM-Mϕ in vitro
$1x10^6$ BM-Mϕ were co-cultured with $1x10^8$ isolated murine platelets labelled with X649 (pink). Macrophages were detached at 1hr and stained for DAPI (blue), CD45 (yellow), and CD41 (green). Samples were either A) run on the flow cytometer, or cytospun and imaged using the Zeiss-LSM780 microscope to show B) surface-bound or C) internalised platelets. Black arrows – example fluorescent images corresponding to flow cytometry staining. Pink arrows – surface-bound platelets $X649^+CD41^+$. Grey arrows – internalised platelets $X649^+CD41^-$. Representative of 2 independent experiments with 3 technical replicates in each, >10 FOV were imaged for each condition.

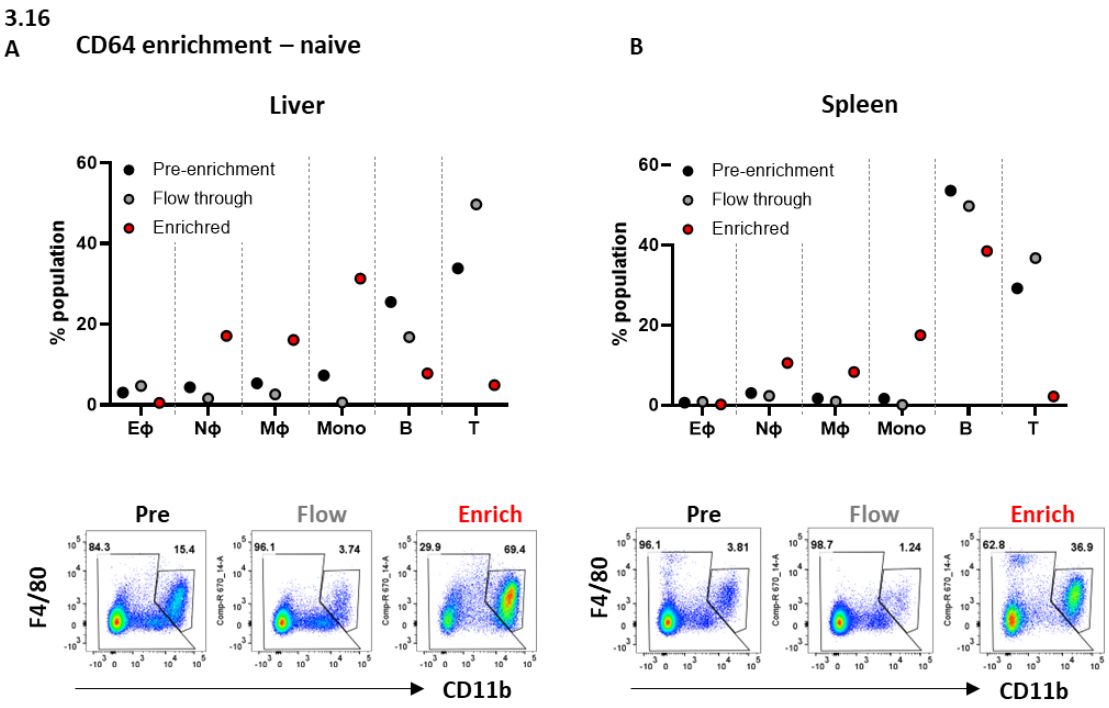

Figure 3.16 Successful enrichment of macrophages and monocytes in the liver and spleen

A liver and spleen were isolated from a C57BL/6 mouse and processed to generate single cell suspensions. Samples were enriched using LS-columns CD64-biotin positive selection. Samples were stained for flow cytometry analysis. Quantification of flow cytometry staining and representative FACS plots of the macrophage/monocyte population in A) the liver and B) the spleen. Black – samples removed pre-CD64 enrichment, grey – samples obtained in the negative column fraction, red – samples positively enriched for CD64 expressing cells. Representative of 3 independent experiments.

3.17

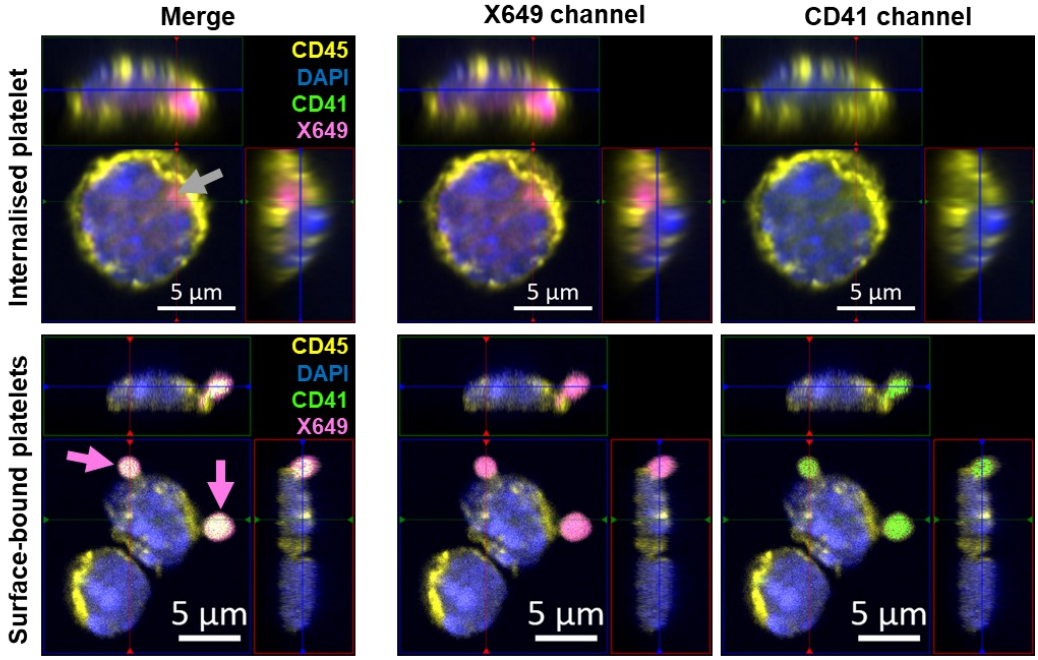

Figure 3.17 Identification of internalised and surface-bound platelets on hepatic macrophages isolated from schistosome-infected mice

Monocytes/macrophages ($CD11b^{+}SiglecF^{-}Ly6G^{-}F4/80^{+}$) isolated from the liver of x2 C57BL/6 mice infected with ~35 *S. mansoni* cercariae for 12 weeks. 24hr prior to tissue harvest mice were *iv* injected with X649 (0.05µg/gram of body weight). Sorted monocytes/macrophages stained with CD45 (yellow), CD41 (green) and DAPI (blue) before cytospin. Samples were imaged using Zeiss LSM-880 Airyscan, 63x oil objective with 4x magnification. Grey arrow – internalised platelet, Pink arrow – surface-bound platelets. Representative of a single experiment with cells from 2 infected mice and >20 FOV.

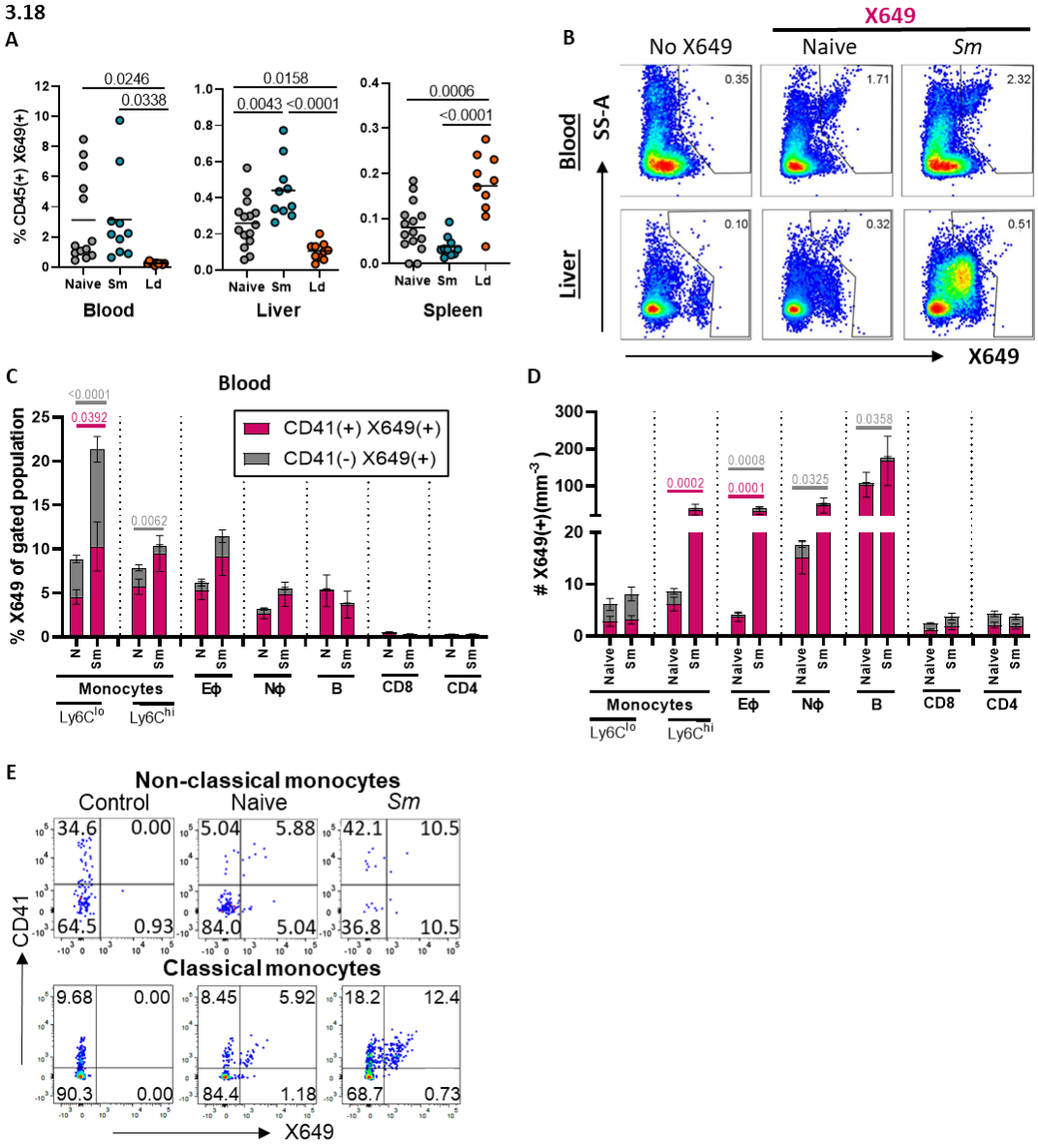

Figure 3.18 Enhanced numbers of PLA in the blood of schistosome-infected mice
C57BL/6 mice were infected with 40 *S. mansoni cercariae* (*Sm*) for 10 weeks or $5x10^7$ LV9 (*Ld*) for 4 weeks. Mice were IV injected with 0.05µg/gram of body weight of anti-GPIb-V-IX conjugated DyLight 649 (X649) 48hrs prior to harvest. A) Quantification of the percentage of $X649^+CD45^+$ leukocytes in the blood, liver and spleen and B) representative FACS plots. Quantification of C) the percentage and D) number of $X649^+$ and $CD41^+$ immune populations in the blood. E) Representative FACS staining of classical and non-classical monocytes in the blood. Data pooled from 3 independent experiments (Naive n=15, *Sm* n=10, *Ld* n=10). Statistical significance was determined using one-way ANOVA with post-hoc Tukey's test on the mean of each treatment group (A) and student's unpaired t-test for each cell type (C-D). Grey: $CD41^-X649^+$, Pink: $CD41^+X649^+$. Error bars represent standard error of the mean, pink comparing $CD41^+X649^+$ populations and grey comparing $CD41^-X649^+$ groups. Non-significance (p >0.05) not shown.

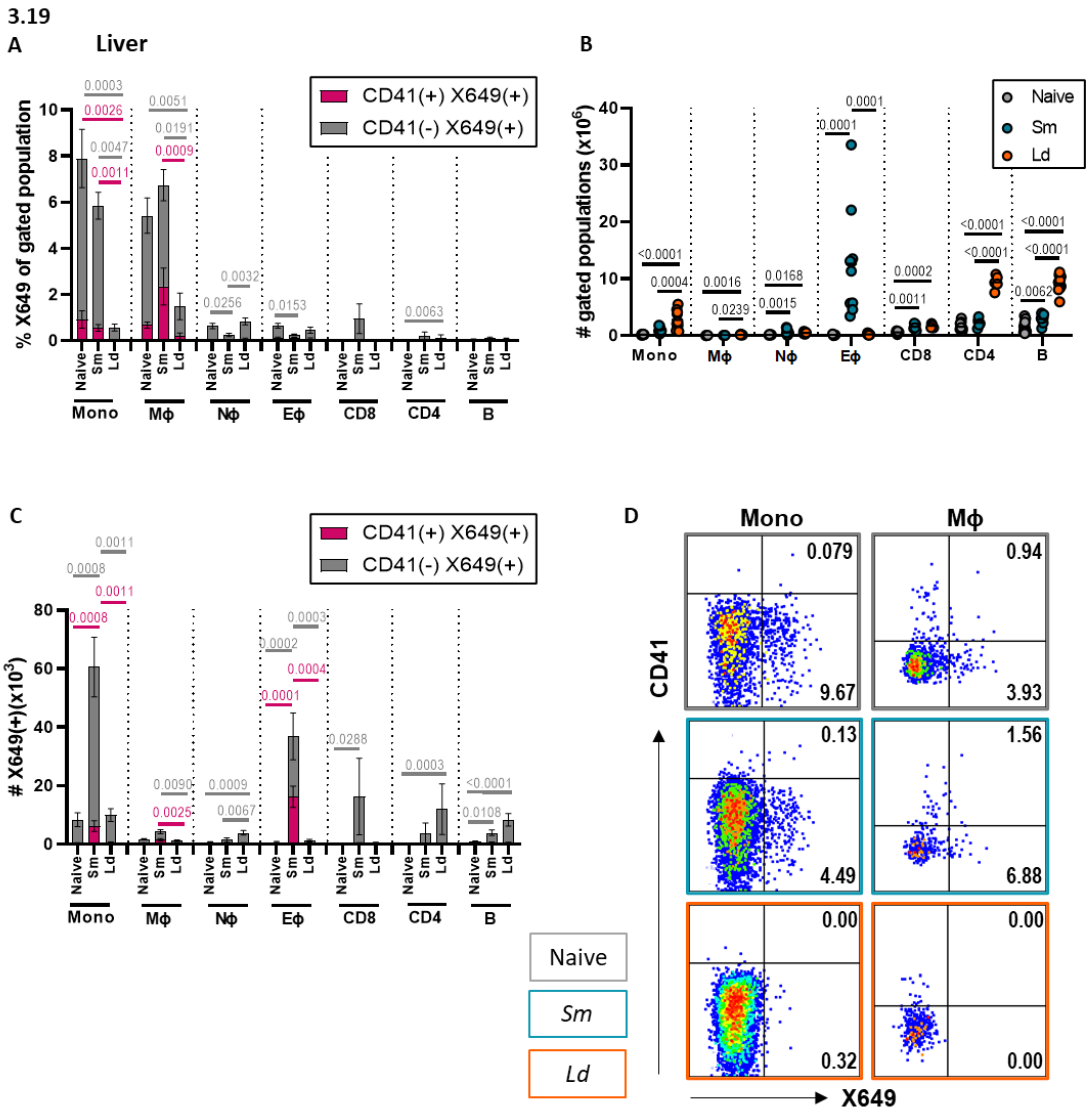

Figure 3.19 Enhanced platelet internalisation in the liver of schistosome-infected mice
C57BL/6 mice were infected with 40 *S. mansoni cercariae* (*Sm*) for 10 weeks or $5x10^7$ LV9 (*Ld*) for 4 weeks. Mice were IV injected with 0.05µg/gram of body weight of anti-GPIb-V-IX conjugated DyLight 649 (X649) 48hr prior to harvest. Quantification of A) the percentage of $X649^+$ and $CD41^+$ leukocytes, B) number of specific immune populations and C) the number of $X649^+$ and $CD41^+$ leukocytes in the liver. D) Representative FACS plots of monocytes and macrophages in the liver. Grey - Naive, Blue - *Sm* and Orange - *Ld.* Data pooled from 3 independent experiments (Naive n=15, *Sm* n=10, *Ld* n=10). Statistical significance was determined using one-way ANOVA with post-hoc Tukey's test on the mean of each treatment group (B) and student's unpaired t-test for each cell type (A, C). Grey: $CD41^-X649^+$, Pink: $CD41^+X649^+$. Error bars represent standard error of the mean, pink comparing $CD41^+X649^+$ populations and grey comparing $CD41^-X649^+$ groups. Non-significance ($p > 0.05$) not shown.

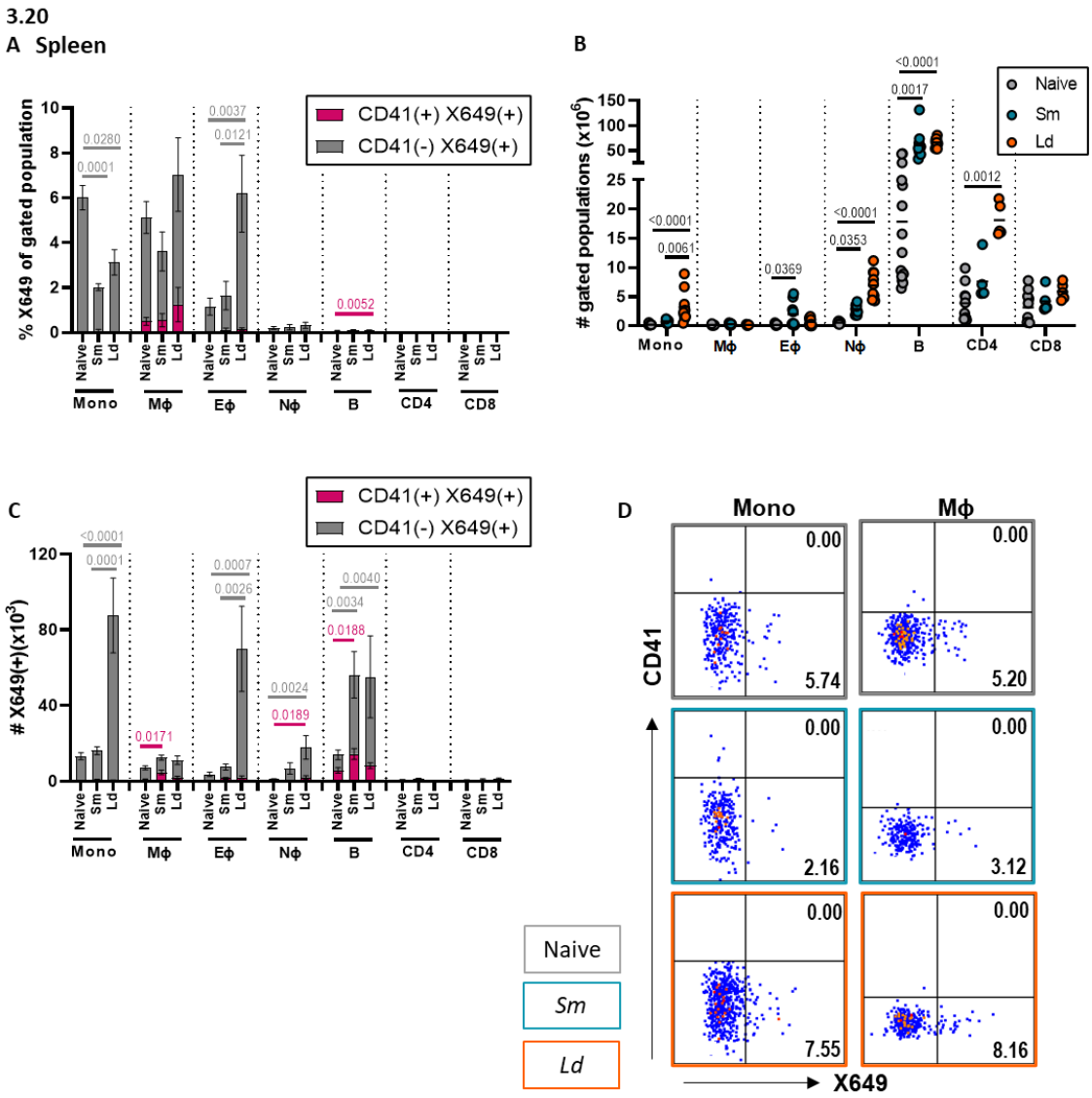

Figure 3.20 Enhanced platelet internalisation in the spleen of L. donovani infected mice
C57BL/6 mice were infected with 40 *S. mansoni* cercariae (*Sm*) for 10 weeks or 5x10^7 LV9 (*Ld*) for 4 weeks. Mice were IV injected with 0.05µg/gram of body weight of anti-GPIb-V-IX conjugated DyLight 649 (X649) 48hr prior to harvest. Quantification of A) the percentage of X649$^+$ and CD41$^+$ leukocytes, B) number of specific immune populations and C) the number of X649$^+$ and CD41$^+$ leukocytes in the spleen. D) Representative FACS plots of monocytes and macrophages in the spleen. Grey - Naive, Blue - *Sm* and Orange - *Ld.* Data pooled from 3 independent experiments (Naive n=15, *Sm* n=10, *Ld* n=10). Statistical significance was determined using one-way ANOVA with post-hoc Tukey's test on the mean of each treatment group (B) and student's unpaired t-test for each cell type (A, C). Grey: CD41$^-$X649$^+$, Pink: CD41$^+$X649$^+$. Error bars represent standard error of the mean, pink comparing CD41$^+$X649$^+$ populations and grey comparing CD41$^-$X649$^+$ groups. Non-significance (p >0.05) not shown.

3.3.6 Do platelets interact with specific subsets of immune cells in schistosome infection?

The consequence of platelet-immune cell interactions appears to be context specific, with little research into how platelets impact type 2 immune cells in a helminth infection. In schistosome infection, Ly6C^{lo} macrophages showed increased MHCII, RELMα and Ym1 expression (**Figure 3.21A-D**). We performed pairwise comparisons of the phenotype of CD41^{-} and CD41^{+} cells in the liver of naive and infected mice, and showed CD41^{+} macrophages in schistosome infection were predominantly MHCII^{lo} RELMα^{hi} Ym1^{hi} compared with CD41^{-} macrophages (**Figure 3.21E-G**). Interestingly, in naive livers, the CD41^{+} subset of macrophages was MHCII^{hi}, which was the opposite to that seen in schistosome infection. Similarly, the monocyte population also showed an increase in the percentage of MHCII^{hi} RELMα^{hi} and Ym1^{hi} cells (**Figure 3.22A-D**), but here CD41^{+} monocytes were MHC^{lo} RELMα^{hi}, with no difference in Ym1 expression between CD41^{-} and CD41^{+} populations (**Figure 3.22E-G**). In contrast to both the macrophages and monocytes, CD41^{+} eosinophils were predominantly RELMα^{lo} (**Figure 3.22H-K**).

In schistosome infection, CD4^{+} T cells in the spleen were predominantly CD62L^{-}CD44^{+} ($T_{E/M}$, T effector/memory) cells and produced significantly more IL-10, IL-4 and IFNγ than naive CD4^{+} T cells (**Figure 3.23A-C**). Pairwise comparison again demonstrated CD41^{+} CD4^{+} T cells were predominantly $T_{E/M}$ cells with positive expression of IL-10, IL-4 and IFNγ (**Figure 3.23D-G**). A similar trend was seen in naive CD4^{+} T cells, however to a lesser extent due to fewer $T_{E/M}$ and lower cytokine production.

We were interested to explore the differences between the CD41^{+} and CD41^{-} macrophage subsets further and therefore sorted schistosome liver samples which had been enriched for CD64^{+} cells (**Figure 3.24A-B**). As discussed previously in **Section 3.3.5**, we did not distinguish between Ly6C^{lo} and Ly6C^{hi} cells in order to obtain sufficient sample. As the monocyte/macrophage populations had different auto-fluorescence with respect to the CD41 fluorophore, a tight gate was drawn to encompass the CD41^{+} populations from both the Ly6C^{lo} and Ly6C^{hi} populations (**Figure 3.24C-D**). After sorting, RNA was extracted, and reverse transcribed for qPCR analysis. For each mouse

liver sample, the relative gene expression between CD41$^-$ and CD41$^+$ macrophage/monocyte subsets was assessed for a range of type 1 and type 2 inflammatory molecules (**Figure 3.25**). We assessed the transcript level of various genes associated with macrophage activation or which had previously been shown to change on exposure to platelets. We found CD41$^+$ liver macrophages showed an unusual phenotype comprising elevated pro- (*Il6*) and anti-inflammatory factors (*Retlna*) alongside downregulation of other facets of pro-inflammatory macrophages (reduced *Tnf*). Moreover, CD41$^+$ liver macrophages/monocytes also expressed more *Cxcl12*, which is highly expressed by perivascular macrophages in some tumours (303). Whilst we lack a global understanding of platelet-induced transcriptomic changes in these macrophages, this experiment provided a strong justification for functional studies examining the consequences of platelet-macrophage interactions (**Chapter 5**).

Sanin *et al.* (2022) have recently shown that monocyte-derived macrophages transition through a RELMα^{hi} phenotype (304). As we have shown that CD41$^+$ monocytes and macrophages in the liver are RELMα^{hi} compared with their CD41$^-$ counterparts, we hypothesised that platelets in schistosome infection are primarily interacting with the newest monocyte-derived macrophages that have most recently exited the platelet-rich circulation. To test this, we first wanted to assess the vascularisation within an infected liver and the granulomas themselves as previous studies in tuberculosis granulomas have shown that granulomas are highly hypoxic (305,306). Whilst we did not directly assess hypoxia in schistosomiasis, we did find formation of a network of CD31$^+$ blood vessels (CD31 staining-white) within the egg-induced granulomas (**Figure 3.26**). Due to the small size of platelets (~5μm diameter), the magnification used for image acquisition and the intensity of CD41 staining from MK and platelet aggregates, it was difficult to visualise the localisation of individual PLA in these images. However, the larger platelet aggregates and MK did not solely co-localise with the endothelial stain, suggesting that the PLA were present deeper within tissues.

Having established granulomas had extensive vascularisation, we performed an *in vivo* CD45 labelling experiment to test whether the

macrophage/monocyte-platelet aggregates were those proximal to circulation (**Figure 3.27A**). We reasoned labelling $CD45^+$ cells *in vivo* for 15min (i.e. extended compared with standard 1-3min labelling (307) prior to sacrificing the animals), would enable strong labelling of both circulating immune cells alongside those close to blood vessels, but would show less penetration into deeper tissues further away from the blood supply (and so labelling cells in these positions less). As expected, we observed >95% CD45 labelling (hi or lo) of blood immune cells (**Figure 3.27-C**), with the hi and lo populations potentially reflecting immune cells exiting and re-entering the circulation during the prolonged 15min labelling period. Despite this, and even with enhanced vascularisation within hepatic tissue, there still appeared to be a reduction in leukocyte labelling in schistosome livers (i.e. cells stained $CD45^+$ *ex vivo* that displayed $CD45^{lo}$ or $CD45^-$ *in vivo* staining) compared with naive animals, and this was observed within all immune cell subsets tested (**Figure 3.27D-E**). We next tested whether $CD41^+$ cells showed any difference in the extent of *in vivo* CD45 labelling and found, contrary to our expectations, that $CD41^+$ monocytes and macrophages displayed reduced CD45 labelling than their $CD41^-$ counterparts. Together, this suggested that, far from being in the process of extravasation and monocyte-macrophage transition, $CD41^+$ monocytes/ macrophages were actually deeper within tissues and so were potentially more mature than their $RELM\alpha^{hi}$ $MHCII^{lo}$ phenotype would suggest (**Figure 3.27F-H**).

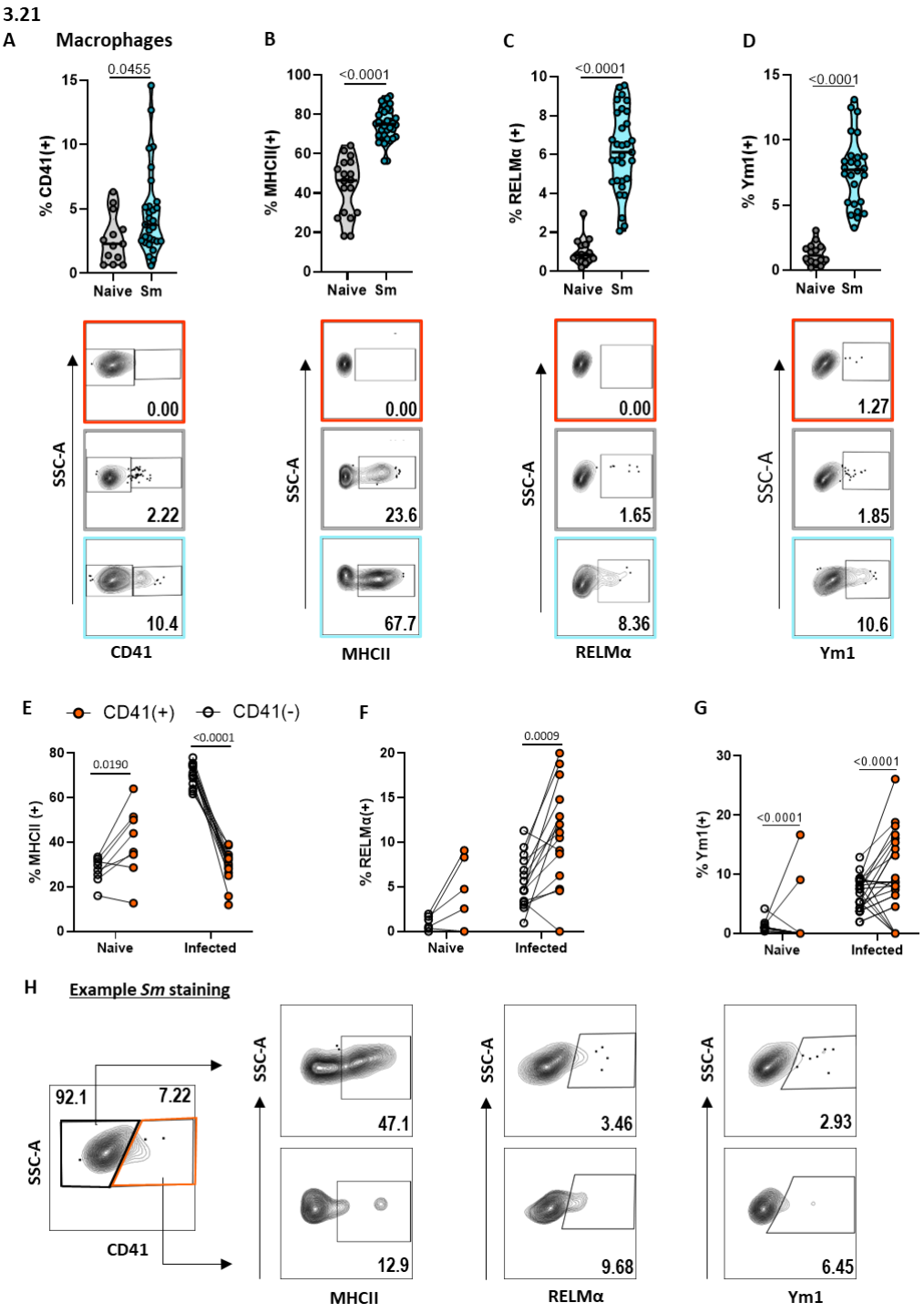

Figure 3.21 Platelets specifically interact with MHCII^{lo} RELMα^{hi} Ym1^{hi} macrophages in the liver in schistosome infection

C57BL/6 mice were infected with 35-50 *S. mansoni cercariae* (*Sm*) for 8-12 weeks. Quantification and representative FACS plots of liver macrophages stained for A) CD41, B) MHCII, RELMα and Ym1. Red-CD41 FMO, Grey-Naive, Blue-Sm. Data pooled from 4 independent experiments (Naive n=16, *Sm* n=30). Paired analysis of CD41^{+} and CD41^{-} macrophages and their expression of E) MHCII, F) RELMα and G) Ym1. H) Representative FACS staining of CD41^{+} and CD41^{-} liver macrophages. Open circles: CD41^{-}, Orange circles: CD41^{+}. Data pooled from 3 independent experiments (Naive n=8, *Sm* n=14). Statistical significance was determined using Student's unpaired (A-D) and paired t-test for each treatment group (E-G). Non-significance (p >0.05) not shown.

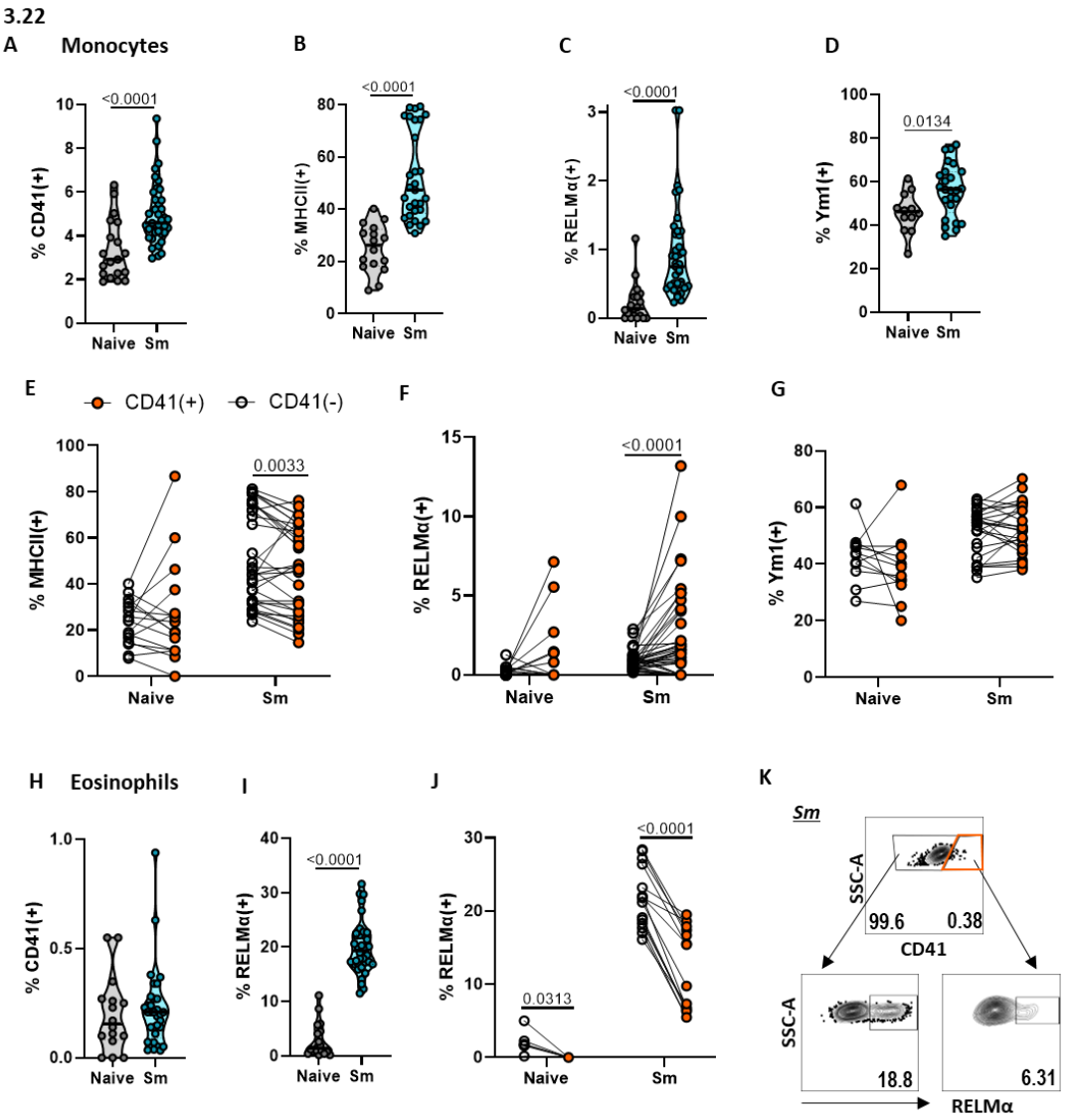

Figure 3.22 Platelets specifically interact with MHCII^{lo} RELMα^{hi} monocytes in the liver
C57BL/6 mice were infected with 35-50 *S. mansoni cercariae* (*Sm*) for 8-12 weeks. Quantification of liver monocytes stained for A) CD41, B) MHCII, C)RELMα and D) Ym1. Data pooled from 4 independent experiments (Naive n=19, *Sm* n=30). Paired analysis of CD41^{+} and CD41^{-} monocytes and their expression of E) MHCII, F) RELMα and G) Ym1. Data pooled from 3 independent experiments (Naive n=12, *Sm* n=25). Quantification of liver eosinophils stained for H) CD41 and I) RELMα. Paired analysis of CD41^{+} and CD41^{-} eosinophils their expression of I) RELMα. K) Representative FACS staining of CD41^{+} and CD41^{-} liver eosinophils. Data pooled from 3 independent experiments (Naive n=12, *Sm* n=25). Open circles: CD41^{-}, Orange circles: CD41^{+}. Statistical significance was determined using Student's unpaired (A-D, H-I) and paired t-test for each treatment group (E-G, J). Non-significance (p >0.05) not shown.

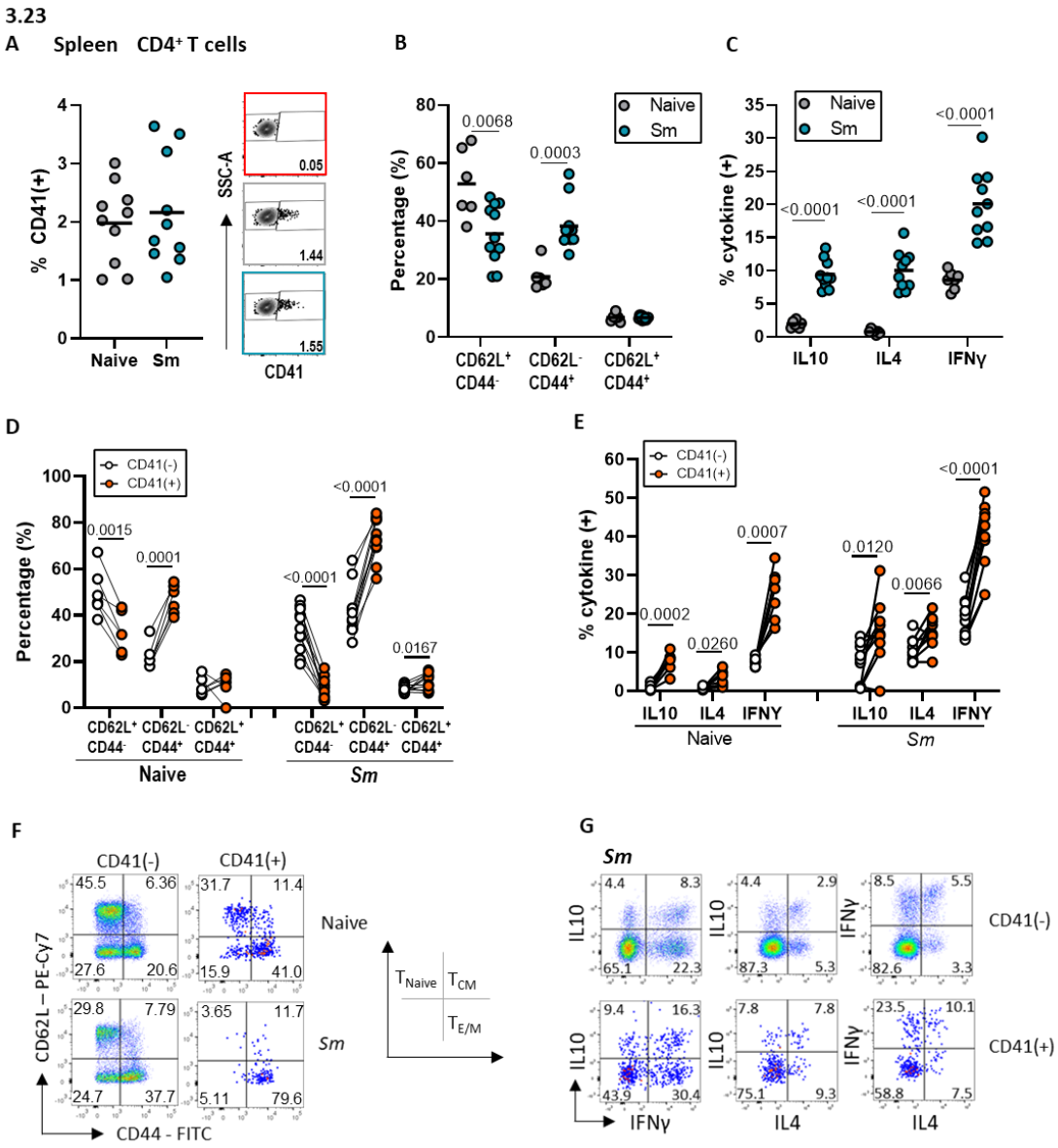

Figure 3.23 Platelets primarily interact with $T_{E/M}$ in the spleen

C57BL/6 mice were infected with 35-50 *S. mansoni* cercariae (*Sm*) for 8-12 weeks. Single cell suspensions (2-4x10^6 cells) from spleen isolation processing were cultured for 4hrs at 37°C with 1µg/ml Ionomycin, 10µg/ml PMA and 10µg/ml Brefeldin A. Flow cytometry quantification of $CD4^+$ T cells for A) CD41, B) T cell subpopulations, naive T cells T_{naive}-$CD44^-CD62L^+$, effector/memory $T_{E/M}$-$CD44^+CD62L^-$ and central memory T_{CM}-$CD44^+CD62L^+$ and C) T cell activation (IL-10, IL-4 and IFNγ). Paired analysis of $CD41^+$ and $CD41^-$ CD4 T cells their expression D) subpopulation markers and E) cytokine expression. Representative FACS plots of F) naive and infected CD4 T cell subpopulation markers and G) infected CD4 T cell expression of IL-10. IL-4 and IFNγ. Data pooled from 2 independent experiments (Naive n=10, *Sm* n=10). Open circles: $CD41^-$, Orange circles: $CD41^+$. Statistical significance was determined using Student's unpaired (A-C) and paired t-test for each marker (E). Non-significance ($p > 0.05$) not shown.

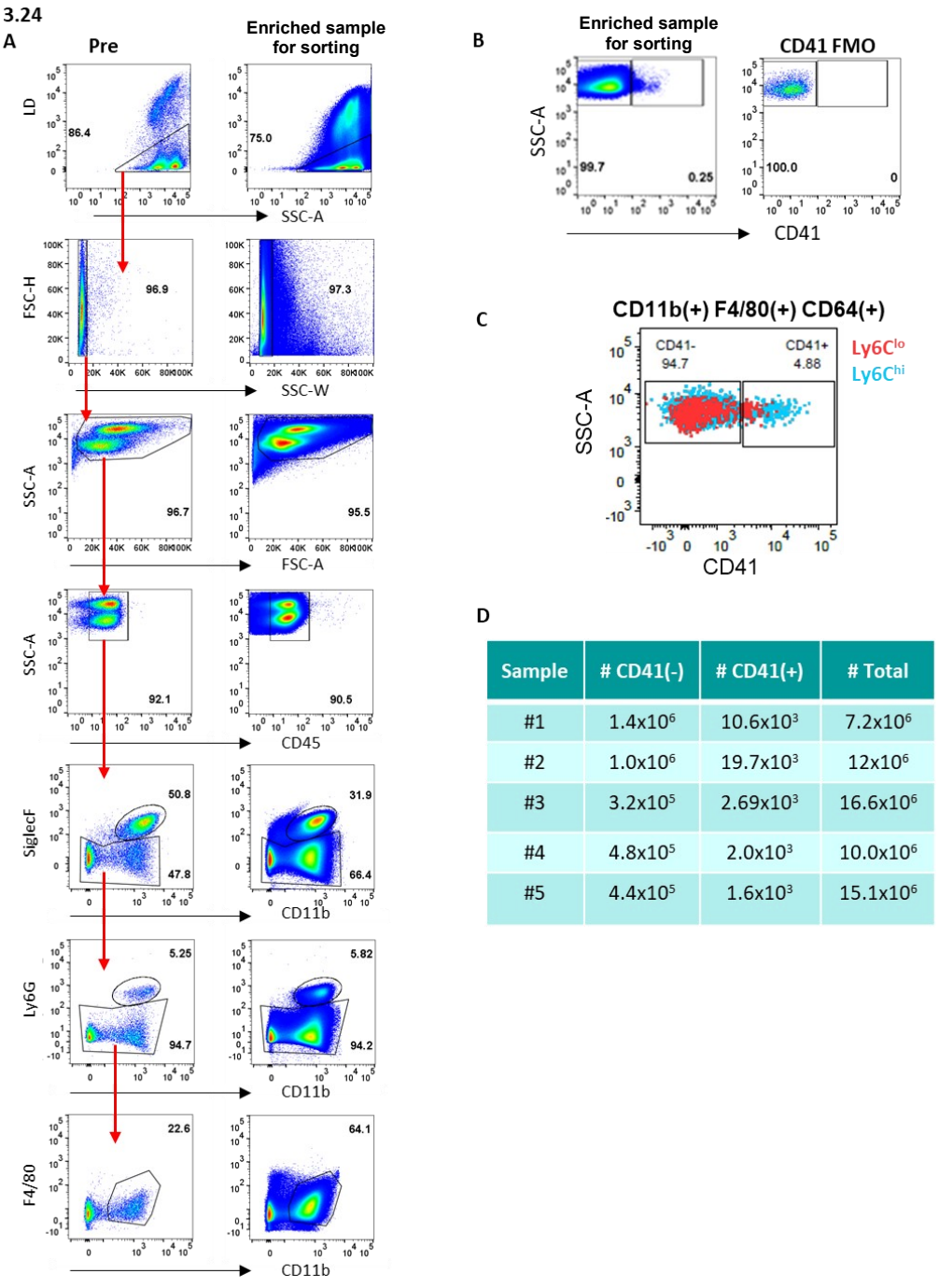

D

Sample	# CD41(-)	# CD41(+)	# Total
#1	$1.4x10^6$	$10.6x10^3$	$7.2x10^6$
#2	$1.0x10^6$	$19.7x10^3$	$12x10^6$
#3	$3.2x10^5$	$2.69x10^3$	$16.6x10^6$
#4	$4.8x10^5$	$2.0x10^3$	$10.0x10^6$
#5	$4.4x10^5$	$1.6x10^3$	$15.1x10^6$

Figure 3.24 Sorted liver macrophages from schistosome-infected mice based on CD41 expression

C57BL/6 mice were infected with 35 *S. mansoni* cercariae (*Sm*) for 12 weeks. Whole livers were processed to generate single cell suspensions. Samples were enriched using LS-columns and CD64-biotin positive selection and $CD45^+CD11b^+SiglecF^-Ly6G^-F4/80^+$ cells were sorted for $CD41^-$ or $CD41^+$. Example FACs staining of A) sorting gating strategy and comparison pre- and post-enrichment, B) $CD41^+$ cell population gating compared with the CD41 control and C) liver macrophages and monocytes and their differing autofluorescence. D) Summary table of sorting output from 5 separate animals from 2 independent experiments.

3.25

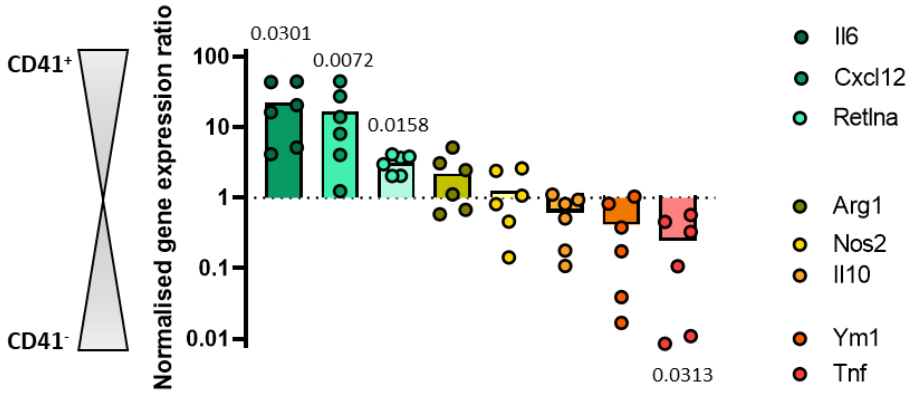

Figure 3.25 Differential gene expression between CD41⁺ and CD41⁻ monocytes/ macrophages from schistosome-infected livers

RNA was extracted from the sorted CD41⁻ and CD41⁺ populations, reverse transcribed and analysed by qPCR. RNA levels were normalised to the average *U6* transcript level from all samples. Gene expression ratio was calculated as CD41⁺ cell transcript level / CD41⁻ cell transcript level. RNA samples from 6 mice, from 2 independent experiments. Significance determined by paired Student's t-test between CD41⁻ and CD41⁺ transcript levels. Non-significance (p >0.05) not shown.

3.26

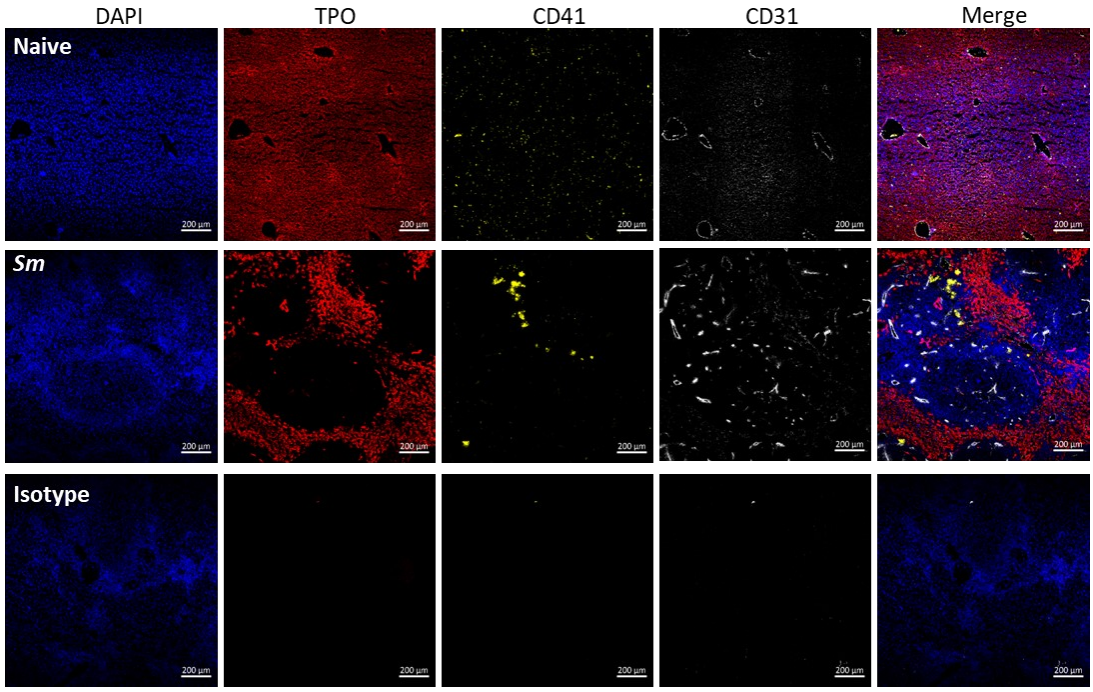

Figure 3.26 Increased vasculature in schistosome-infected livers

Representative fluorescent images of liver tissue from C57BL/6 mice infected with 35-50 cercariae for 10-12 weeks stained for DAPI (blue), TPO (red), CD41 (yellow) and CD31 (white) and imaged with a 10x objective. Data representative of 3 independent experiments.

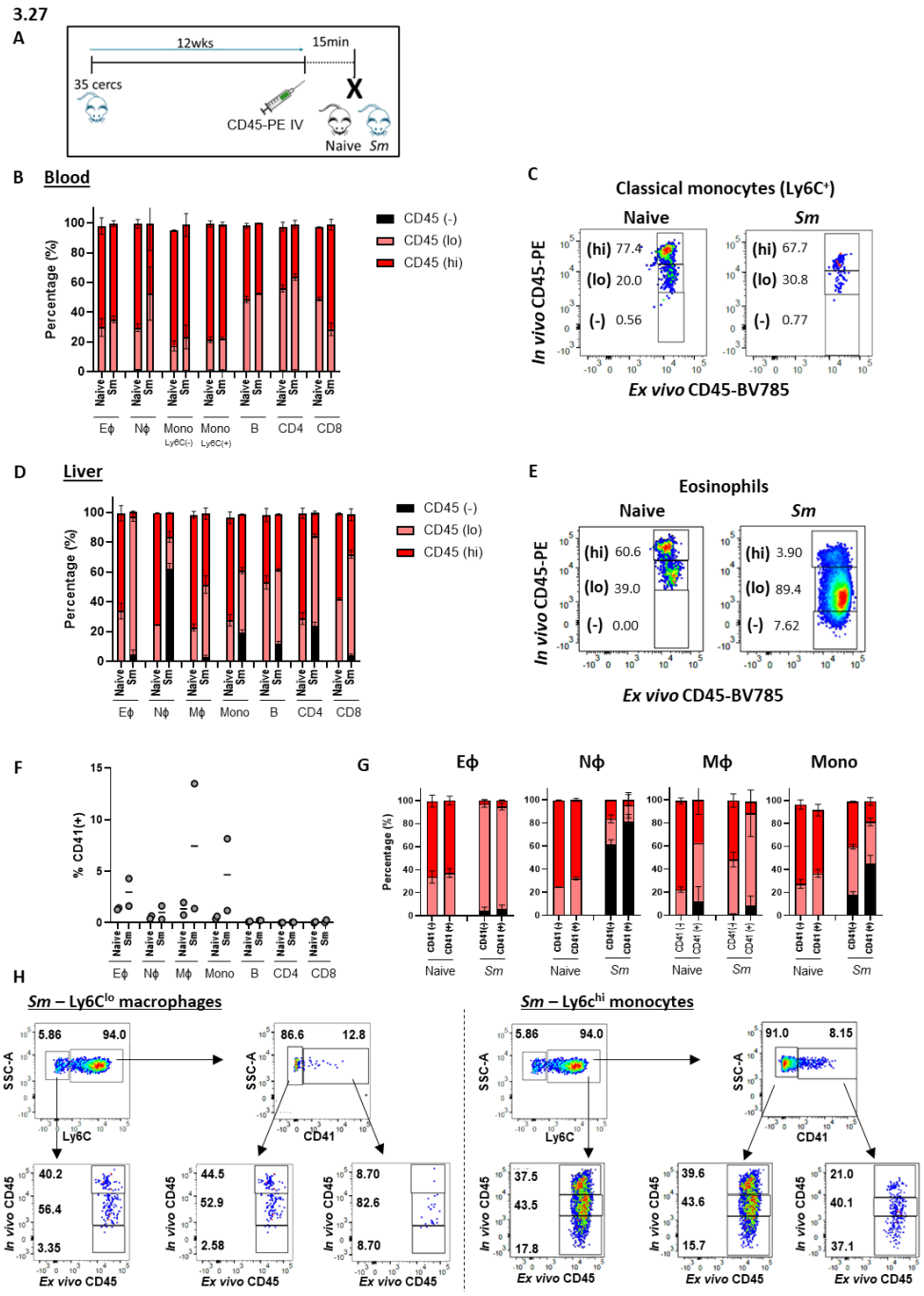

Figure 3.27 Tissue PLA do not represent a population of cells most recently exited from circulation

A) Schematic of C57BL/6 mice infected with 35-50 cercariae for 12 weeks were injected IV with 0.075mg/kg anti-CD45 PE for 15min before being harvested. B) Quantification of FACS staining of the blood showing the percentage of different leukocyte populations that are CD45(-), CD45(lo) or CD45(hi). C) Representative FACS staining of naive and *Sm* classical monocytes (Ly6C$^+$) in the blood. D) Quantification of FACS staining from the liver showing the percentage of different leukocyte populations that are CD45(-), CD45(lo) or CD45(hi). E) Representative FACS staining of naive and *Sm* eosinophils in the liver. Percentage of CD41$^+$ leukocyte populations in the liver. G) Percentage of the myeloid populations in the liver that are CD41$^-$ and CD41$^+$ in terms of their expression of CD45(-)(black), CD45(lo)(peach) and CD45(hi)(red). G) Representative FACS gating of naive and *Sm* Ly6C^{hi} monocytes in the liver. (Naive n=3, *Sm* n=3). Data representative of 2 independent experiments. Error bars represent standard error of the mean.

3.4 Discussion

S. mansoni infection characteristically leads to a type 2 immune response, associated with elevated IgE, mast cell production, eosinophilia, and specific cytokines, i.e. IL-4, IL-13 and IL-5 predominate (308). With platelets having an emerging role in regulating type 1 immune responses, this study set out to investigate the role of platelets in type 2 immunity (217). Whilst platelet function in type 2 immune responses following helminth infection is poorly characterised, there is some evidence for platelets playing a role in type 2 allergic reactions. Allergen sensitisation induces transient thrombocytopenia immediately after stimulation (206). In addition, following allergen exposure in asthma patients, elevated PLA in the lungs have been observed and platelets drive immune cell recruitment and extravasation into inflamed tissues (309). Disruption of platelet-eosinophil aggregates appears beneficial in reducing the airway hyperresponsiveness and inflammation (220,310). Despite this, there is limited understanding of the mechanisms of thrombocytopenia and functional consequences of PLA in type 2 immune responses to helminth infections.

We first assessed the effect of infection burden on pathology and platelet parameters. Thrombocytopenia and elevated MPV was observed in mice infected with as few as 25 cercariae and there was a significant negative correlation between platelet number and size. This may suggest infection-induced BM and haematopoietic stress, which is driving the release of more immature, larger platelets into circulation (311,312). Alternatively, increased clearance of mature, smaller platelets may also give rise to fewer, yet larger platelets in circulation.

Platelet-mediated immune cell infiltration into particular tissues has been reported in allergy, pulmonary inflammation and cardiovascular disease and is dependent on platelet activation by sCD40L and P-selectin interactions (226,313–315). We next explored whether infection burden impacted on PLA formation in schistosome infection (206). Whilst we did not see an overall increase in PLA in the blood of infected mice, we did observe an increase in the liver and spleen at higher infection doses. Due to the blood, liver and spleen being composed of a heterogenous mixture of different immune cell

types each with distinct intrinsic auto-fluorescence, we were concerned about missing subtle shifts in individual immune populations with respect to CD41 staining. We therefore gated and examined these populations separately which again revealed minimal differences in the proportion of blood leukocytes with CD41 staining. However, this did not take into consideration the changes in the immune composition of the blood (i.e. more eosinophils) and so we also recorded the absolute number of blood leukocytes that were $CD41^+$. This showed there was a significant increase in absolute number of PLA in the blood in schistosome infection. With the liver being the major site of pathology in *S. mansoni* infection it was interesting to see a significant increase in both the percentage of multiple leukocyte populations, and the absolute number of the majority increase in $CD41^+$ expression. An increase in platelet-eosinophil and platelet-macrophage interactions in infection may be facilitating immune cell infiltration into tissues to promote parasitic clearance and orchestrate the inflammatory response (316). As we did not see any correlation between platelet count or percentage PLA and liver egg counts, this suggests that PLA may not be driving egg excretion, instead schistosome eggs may be entrapped by platelet-rich thrombi which aids their expulsion (269). However, more functional studies that specifically disrupt PLA would be required to confirm this.

PZQ is effective at killing adult schistosomes and we have shown that immune cell numbers in the liver were also significantly reduced. We wanted to understand whether the haematological changes to platelet number and size were also reversed after treatment. Here we have shown that platelet number and MPV started to return to naive levels, however the percentage of PLA in the liver did not fall to naive levels. The decrease in number of $CD41^+$ immune cells is most likely explained by there being fewer immune cells in total in the liver following PZQ treatment. Therefore, high percentages of PLA suggest that platelet activation or morphology changes that occur during infection facilitate their interaction with leukocytes. Notably, this is sustained even after parasite clearance and a reduction of activated myeloid and lymphoid cells. Interestingly, the only reported treatment regimen given to schistosome-infected mice that prevented thrombocytopenia was 18mg/kg/day PZQ for 28

consecutive days (317). This protection may be due to reduced parasite burden and inflammatory cell infiltration in the liver and spleen thereby reducing platelet sequestration and the resultant thrombocytopenia (317). Future experiments examining a longer period (>4 weeks) post-PZQ treatment and different treatment regimens would enable us to determine whether platelet numbers and size completely return to baseline levels post-PZQ treatment and how this affected PLA formation.

As schistosomiasis causes a peripheral, multi-organ inflammatory response, it was important to establish whether this influenced the production of cells from the BM. Unpublished work in the Hewitson lab, in conjunction with the recent pre-print by Wijshake *et al.* (2023), demonstrate a variety of short- and long-term changes to the BM composition (including massive eosinophilia, reduction of $CD68^+$ macrophages, changes to stem and progenitor populations and alterations to the stem cell stromal niche) (284). Whilst we cannot exclude that *in vivo* BM IL-4 levels are sufficient to prevent $CD41^+$ cell generation, our results suggest this has no long-term consequences on MK potential as equivalent numbers of $CD41^+$ cells were generated *in vitro* from BM from naive and infected mice. Here we have shown using immunofluorescent imaging that, despite a significant and sustained reduction in TPO production thought essential for MK-biased HSC development (318), there was sustained BM megakaryopoiesis alongside infection-associated extramedullary haematopoiesis. Our observation of hepatic extramedullary haematopoiesis complements the work by Francisco *et al.* 2022 (161). TPO is a key regulator of megakaryopoiesis and can act in a feedback loop with platelets sequestering circulating TPO. Therefore, low platelet counts result in increased circulating TPO which stimulates BM HSCs and MK production (148,151). However, given that $TPO^{-/-}$ and $MPL^{-/-}$ mice can still produce ~10% of normal WT platelet levels, this suggests alternative mechanisms of platelet production exist (319). TPO-independent megakaryopoiesis may involve IL-1β and insulin-like growth factor 1 stimulating MK production of platelets to maintain homeostatic levels even when TPO levels are low (121,319).

Individuals can have abnormal platelet counts for a multitude of reasons and display a variety of changes in MK number, size and ploidy in the BM

(122,320). Given the subtle, yet significant change in MK size seen in schistosome-infected mice, we next used ploidy analysis as a proxy marker of MK functionality in the BM. Consistent with the reduced MK diameter there was an increase in 4N and reduction in 8 and 16N MK, suggestive of more inflammatory MK and reduced stem cell supporting- and platelet-producing MK (296). A skewing towards inflammatory MK which are involved in immune surveillance and antigen presentation in schistosome infection may be reducing the number of platelets released into circulation, thereby contributing to the thrombocytopenia. This could be assessed by performing single cell RNA-seq on MK sorted from naive and infected mice and humans in the future.

We next assessed whether platelet clearance was accelerated in schistosome infection, contributing to platelet depletion. Using our novel *in vivo* platelet tracking system, we demonstrated that platelets were cleared more rapidly in schistosome infection, albeit less dramatically than in *L. donovani* infection. Despite schistosome infection causing high levels of antibody production and Stanley *et al.* (2003) demonstrating there to be a degree of cross-reactivity between schistosome egg antigens and platelet antigens, platelet clearance was not mediated by activating Fc receptors as thrombocytopenia still developed in FcRγ$^{-/-}$ mice (278,321). Phenotypic and functional changes to platelets that may act as "eat-me" signals will be explored in more detail in **Chapter 4**.

Having shown there to be increased PLA and accelerated platelet clearance in schistosome infection, we wanted to identify whether the leukocytes were internalising the interacting platelets, thereby contributing to platelet clearance. We were interested to differentiate between surface-bound and internalised platelets because phagocytic uptake may elicit different signals than simply binding to the cell surface, as seen in tumour associated macrophages (322). To visually confirm platelet localisation, we used *in vitro* BM-derived macrophages and sorted liver macrophages/monocytes co-stained for platelets with X649 and CD41.

In vivo platelet tracking in schistosome-infected mice revealed specific PLA occurred during infection. The notable increase in the number of PLA,

particularly by classical monocytes in the blood is characteristic of a pseudo-thrombocytopenia. The co-staining for surface CD41 clearly showed enhanced platelet clearance in the liver by Ly6C^{hi} monocytes in schistosome infection. This observation contrasts with that seen in *L. donovani* infection where PLA (X649^{+} cells) were difficult to detect by flow cytometry in the blood (still detectable in complete blood cell counts) but very low in the liver. However, monocytes in the spleen were internalising platelets, which is consistent with previous studies (238) – characteristic of immune-mediated platelet clearance.

Across multiple experiments we saw that Ly6C^{lo} macrophages and Ly6C^{hi} monocytes in the liver represented the greatest percentage and/or number of CD41^{+} leukocytes compared with other immune cell types. Consistent with previous studies, Ly6C^{lo} macrophages and Ly6C^{hi} monocytes showed elevated expression of MHCII, RELMα and Ym1 following schistosome infection, suggestive of alternative activation and roles in the suppression of pro-inflammatory mediator production and preventing excessive tissue remodelling (114,115,323). The platelet-bound subset of macrophages in schistosome infection expressed less MHCII, and more RELMα and Ym1 compared with the platelet-free subset. In contrast, the CD41^{+} macrophages in naive mice were MHCII^{hi}, suggesting platelet-macrophage interactions may be context specific and dictated by the inflammatory environment. This may facilitate the trafficking of specific macrophage subsets to sites of inflammation or may contribute to their activation. The CD41^{+} monocytes similarly interacted preferentially with a different subset compared with those in a naive liver. Specific analysis at the mRNA level of CD41^{+} and CD41^{-} macrophages/monocytes from infected livers also showed significant differences, with CD41^{+} populations with higher transcript levels of *Il6*, *Cxcl12* and *Retlna*, but lower *Ym1* and *Tnf*. Interestingly, the CD41^{+} macrophage/monocyte population had a range of both pro- and anti-inflammatory mRNA elevated, which is consistent with the liver macrophages displaying hallmarks of both classical and alternate activation, e.g. elevated *Nos2* and *Tnf*, even in a strong Type 2, IL-4 rich environment (324). This mixed response may also represent the complex inflammatory response and

the presence of additional pro-inflammatory stimuli and TLR activation as a result of intestinal perforation and bacterial leakage (11). In the case of eosinophils, the $CD41^+$ subset was the same in both naive and infected livers, however due to the enhanced RELMα expression in schistosome infection there was a far more marked difference with platelets interacting with less-activated eosinophils ($RELM\alpha^{lo}$). In a similar manner, platelets interacted with specific subsets of activated, effector/memory $CD4^+$ T cells. T_{EM} cells primarily reside in the mucosa and circulation enabling rapid migration to sites of inflammation, facilitating rapid antigen recognition and pathogen elimination (325). Furthermore, *in vitro*, platelets have been shown to persistently enhance the responses of T_{EM} cells through a PF4-dependent mechanism (326).

Together, the formation of specific platelet-myeloid interactions raises the questions whether platelets enhance or decrease the expression of these specific activation molecules or alternatively whether platelets preferentially interact with cells that display these activation phenotypes. We will explore this in **Chapter 5**. However, as Sanin *et al.* (2022) have recently shown that all monocyte-derived macrophages transition through a $RELM\alpha^{hi}$ phenotype we wanted to test whether platelets were interacting with the newest monocyte-derived macrophages, that had most recently exited the platelet-rich circulation (304). Having shown increased vascularisation in schistosome -infected livers consistent with Francisco *et al.* 2022 (161), we were surprised to see that there was still poorer circulation in tissues of infected mice compared with their naive controls. It would be of great interest to assess the degree of hypoxia within granulomatous tissue *in vivo* using a reagent such as EF5, which is an injectable compound which labels hypoxic cells and can then be directly targeted with a specific monoclonal antibody (327). This would provide us with a better understanding of the vascularisation and blood supply within these inflammatory environments. Moreover, it has been shown that there are more platelets in the lungs of hypoxic mice and hypoxia induces platelet activation (328). Surprisingly, we showed the $CD41^+$ immune populations were not those most recently exited from circulation, and in fact appeared to represent cells deeper within tissues (i.e. less accessible to *in*

vivo anti-CD45 antibody labelling). This is consistent with platelets facilitating the migration of immune cells within tissues, potentially aiding recruitment and reprogramming of immune cells closer to schistosome eggs, which offers the exciting potential of mediating the inflammatory response and immune cell trafficking within a specific inflammatory environment. Alternatively, platelets may preferentially interact with particular subsets of leukocytes that are more phagocytic, more active, with a unique inflammatory profile, deeper within tissues. In both scenarios, platelets could be used to carry cargo, such as chemotherapeutic drugs to specific immune cells as is starting to be developed in some cancers (329).

In this chapter we have shown that the thrombocytopenia observed in schistosome infection is multi-faceted. Reduced platelet numbers remain even after drug-mediated worm clearance. Platelet production may be impeded due to fewer 8 and 16N MK in the BM, however the number of MK remain constant despite low systemic TPO. Furthermore, we have shown accelerated platelet clearance by liver Ly6C^{hi} monocytes occurs in an activating FcR-independent manner. Finally, our work reveals PLA-mediated pseudo-thrombocytopenia also contributes to schistosome-induced thrombocytopenia.

4. Assessment of the haemostatic consequences of schistosome infection

4.1 Introduction

Platelets are the second most abundant cell type in the blood and are crucial mediators of thrombosis and haemostasis (301). Platelets bind to exposed sub-endothelial matrix proteins, primarily collagen or vWF, following vessel injury via membrane glycoproteins. These interactions initiate changes in platelet shape and activate downstream signalling cascades that result in further recruitment and activation of platelets via granule release (166). Together, this facilitates the activation of the coagulation cascade via proteolytic cleavage of coagulation factors and ultimately the generation of an insoluble fibrin thrombus.

Over recent years, inflammation-associated haemostasis has been identified as a mechanism by which platelets prevent bleeding as a result of leukocyte extravasation and infiltration (330). For example, choriomeningitis virus infection of mice causes haemorrhagic anaemia, thrombocytopenia and dysfunctional platelet aggregation which is at least partially GPIbα, and CD40 ligand dependent (331). Platelet depletion in these mice results in fatal haemorrhaging and a reduced viral-specific cytotoxic T cell response. Treatment with the anticoagulant warfarin, which significantly elongates the prothrombin time, does not worsen haemorrhaging suggesting platelets can prevent vasculature bleeding in infection independently of the coagulation cascade (331). Moreover, inflammatory haemostasis does not solely rely on integrin αIIbβIII -dependent platelet aggregation, instead GPVI and C-type lectin-like type II transmembrane receptors (CLEC2) can be the main drivers as shown in LPS-induced lung inflammation following neutrophil migration (332).

As shown in **Chapter 3**, there is a very close interplay between platelets and immune cells and this is extended further with the inflammatory driven activation of coagulation in order to limit systemic pathogenic dissemination (333). The formation of neutrophil extracellular traps (NETs) are some of the most well characterised examples of immune-thrombosis. Circulating

platelets can scavenge bacteria and present them to neutrophils, which in turn stimulates their activation and the formation of NETs (334). To clear the entrapped bacteria, neutrophils then undergo the cell death process of NETosis (335).

Thrombosis results in the formation of an insoluble thrombus that blocks circulation. Thrombo-inflammation highlights the tight interdependency behind thrombus driven inflammation and inflammation driven thrombosis, it can also be described as excessive activation of immune-thrombosis (333,336). DIC is an example of exaggerated immune-thrombosis, commonly seen in sepsis and stroke patients (337). DIC causes excessive micro-thrombi, consisting of fibrin deposits, platelets and NETs, to form in the microvasculature resulting in oxygen starvation to surrounding cells. This highlights the double-edged sword of immune thrombosis, being good for trapping bacteria, however risks causing fatal thrombi.

The endothelium is an important regulator of thrombo-inflammation through its anticoagulant properties e.g. expression of ecto-adenosine diphosphatase CD39 and production of NO. CD39 converts the platelet stimulatory ATP to adenosine which itself regulates platelet stimulation and aggregation (338), and NO decreases chemokine expression and the transcription of adhesion molecules such as VCAM-1 and ICAM-1 on the endothelial cell surface (336). Pathogenic challenge disrupts these regulatory pathways. In sepsis, bacterial cell surface components bind pattern recognition receptors on the endothelium and stimulate cytokine production, in addition to this endotoxins damage the endothelial surface and drive TF (CD142) expression (339). As mentioned previously, thrombosis can also potentially trigger inflammation through thrombin-mediated cleavage of pro-IL-1α which is expressed on the surface of multiple different cell types including macrophages, keratinocytes and platelets (340). Cleavage of pro-IL-1α causes activation and release of IL-1 into circulation which drives multiple pro-inflammatory effects including increased vascular permeability, leukocyte recruitment and the upregulation of MHC and co-stimulatory molecules (340). This activation of an immune response during coagulation is likely to protect against infection during wound healing.

The intravascular localisation of schistosome parasites, the transit of eggs across endothelium from the blood into the surrounding tissues and the immune cell recruitment, activation, and expansion together highlight three key processes of haemostatic involvement in parasite infection. However, we lack a full understanding of the impact of chronic schistosome infection on coagulation and haemostasis due to the use of short-term, acute infection models and few longitudinal functional studies. As described in **Chapter 1.3.3**, some *S. mansoni* infected individuals have a prolonged clotting time (240,242,246,248). The only whole blood or PRP aggregometry performed on non-human samples were from healthy dogs co-cultured with isolated parasite-associated proteins *ex vivo* to explore the anticoagulant properties of specific schistosome tegument proteins (261). To the best of our knowledge there has only been one murine study of coagulation in schistosome infection, using thromboelastography (TEG) rather than aggregometry, which revealed 7 week-infected blood clotted significantly faster than control blood, but thrombi were far less stable (341). Interestingly, *in vitro* culture of blood with adult schistosomes caused significantly prolonged clotting times and no difference in thrombus stability.

4.2 Aims

1) To assess the functional capacity and phenotypic changes of platelets from schistosome-infected mice

2) To determine the effects of schistosome infection on the coagulation cascade

4.3 Results

4.3.1 Does schistosome infection affect the functional capacity of platelets?

To date, assessment of platelet aggregation in schistosome-infected mice by whole blood aggregometry has not been performed and we wanted to assess whether schistosome infection altered platelet function. This could be caused by the anticoagulant properties of schistosome tegumental phosphatases, which may have a sustained, systemic effect on platelet aggregation. In

addition, the presence of large intravascular worms disturbing blood flow and potentially damaging the endothelium may alter platelet function. Blood was harvested from direct cardiac puncture of mice infected for 12 weeks with ~35 cercariae, or age-matched controls in order to minimise platelet activation and account for changes in platelet activity and immunomodulatory function associated with ageing (342,343). Only blood obtained from first attempt draws was used for whole blood impedance aggregometry analysis to minimise platelet activation through excessive heart endothelial damage. Interestingly, we showed there to be spontaneous platelet aggregation of blood from schistosome-infected animals in the absence of any exogenous agonist (**Figure 4.1A-B**). In some cases, blood from schistosome-infected mice clotted prior to aggregometry analysis even after a successful blood draw (<2 min after sample collection) (**Figure 4.1C**). In contrast, platelets from naive mice were only activated and aggregated following the addition of ADP (**Figure 4.1D-E**). The addition of ADP to infected blood samples did not further increase aggregation (data not shown), but similar aggregates could be seen on the aggregometer probes from infected and activated naive samples (**Figure 4.1F**).

We next asked whether schistosome infection causes platelet activation that leads to spontaneous platelet aggregation. To test this we stained platelets for the active conformation of integrin αIIbβ3 (JON/A) and P-selectin (CD62P) which is usually contained within α-granules but is mobilised to the surface upon activation (344,345). There was no difference in the expression of activation markers between platelets from naive and infected mice, and stimulation with PAR4 agonist induced a similar increase in expression of both markers in both groups (**Figure 4.2A-C**). As there was no significant increase in these activation markers with infection, we next looked at a range of other surface glycoproteins, receptors and ligands which have all been shown to play a role in platelet-platelet and platelet-leukocyte aggregation (CD29, CD42d, CD49b, CD61, CD40L, C5aR) (346–348). However, these also showed no significant difference in their expression between naive and 12 week-infected schistosome mice (**Figure 4.3A-B**).

Experiments in **Chapter 3** showed platelets were cleared faster in schistosome infection, and so we were interested to test whether this was a result of accelerated ageing. To investigate this we examined the expression of terminal galactose residues using the biotinylated lectin Ricinus Communis Agglutinin I (RCA-I) as a surrogate marker of platelet desialylation (349). There was elevated expression of terminal galactose residues on platelets from schistosome-infected mice compared with uninfected controls (**Figure 4.4A-B**). Interestingly, this did not consistently correlate with liver egg counts although there was considerable inter-experiment and intra-group variation (**Figure 4.4C**). Another mechanism of platelet clearance may be due to elevated "eat-me" signals on the platelet surface. We were particularly interested in the exposure of phosphatidylserine (PS) as this not only signals to phagocytes to be cleared but can also drive the intrinsic and common pathway of the coagulation cascade (350–352). Here we showed there was a significant increase in PS exposure on the surface of platelets from infected mice compared with the naive group (**Figure 4.5A**). Moreover, both platelets from naive and infected animals showed significantly greater PS exposure on their surface after Phorbol 12-myristate 13-acetate (PMA) stimulation, but after stimulation the infected group showed a significantly higher exposure compared with the stimulated naive platelets (**Figure 4.5B-C**). There was also a significant positive correlation between annexin V staining and desialylation, so those platelets with more PS on their surface were also more desialylated (**Figure 4.5D**).

Together these experiments showed that platelets from schistosome infected mice spontaneously aggregated in the absence of exogenous agonist, however platelets did not display an overtly activated phenotype in terms of surface marker expression. There was a consistent finding that platelets from infected mice were more desialylated and did have greater PS exposure on their surface than their naive counterparts.

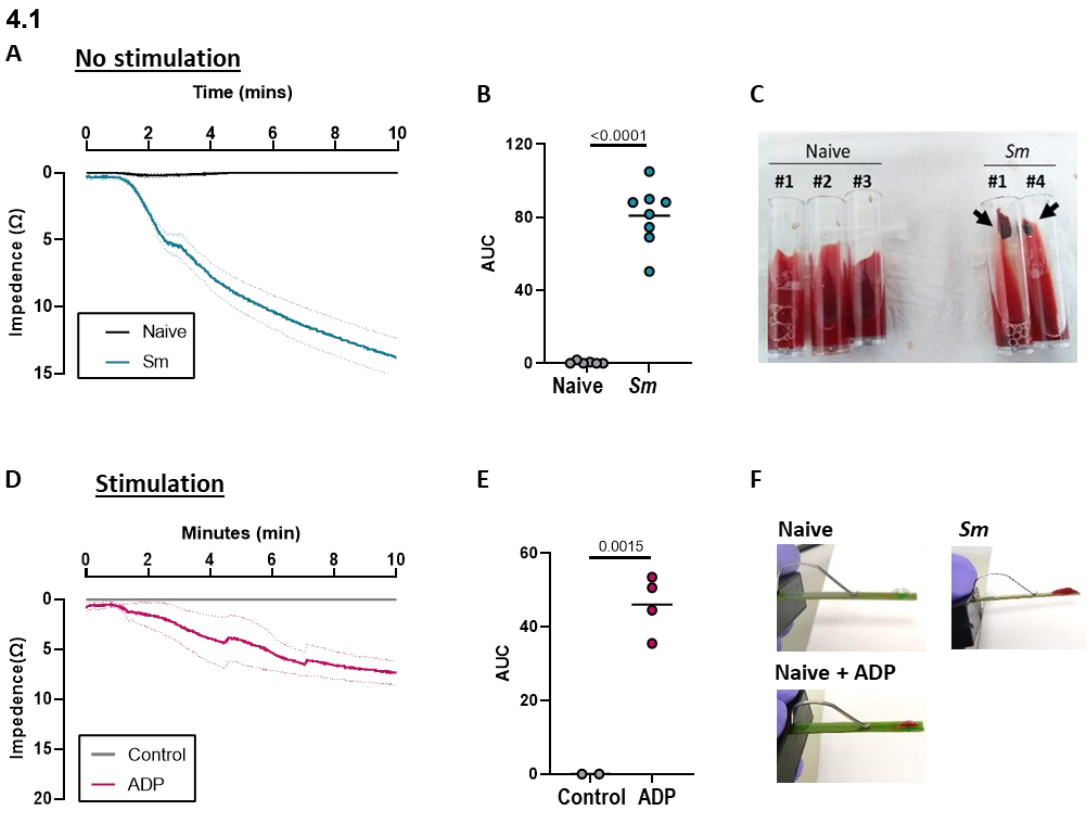

Figure 4.1 Spontaneous platelet aggregation in schistosome infection
C57BL/6 mice were infected with 35-50 *S. mansoni* cercariae and harvested 12 weeks later. A) Whole blood aggregometry following direct cardiac bleed in the absence of exogenous stimulation, B) quantification of the area under the curve of the impedance and C) example blood samples of naive and infected mice at the assay endpoint in the absence of agonist. Arrows indicate clots that formed not on the probe (Naive n=6 (grey), *Sm* n=8 (blue)). D) Whole blood aggregometry from naive mice in the absence (grey) or presence of ADP (30μM) (pink) and E) the area under the curve (Control n=2, ADP n=4). F) Representative images of the aggregometry probe at the end of the assays. Significance determined by unpaired t-test (B, E).

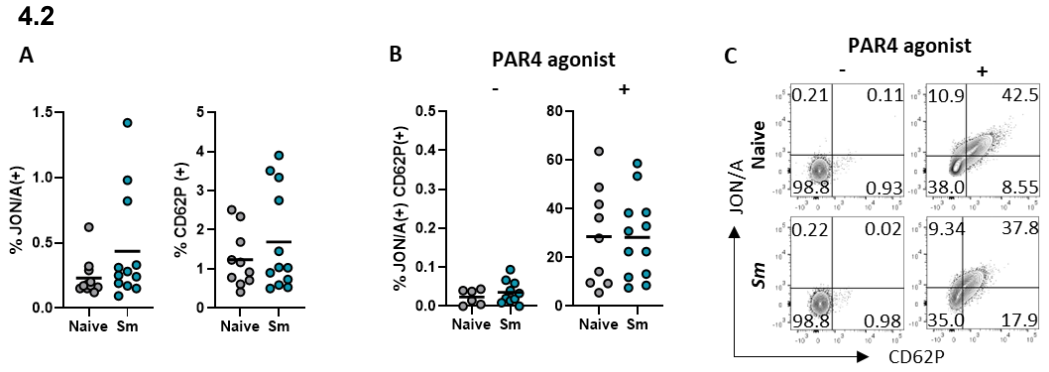

Figure 4.2 No difference in activation markers between platelets from naive and infected mice

C57BL/6 mice were infected with 40 cercariae and 12 weeks post infection blood was harvested by cardiac puncture. Isolated platelets were A) directly stained or B) stimulated with AYPGKF-NH2 (PAR4 agonist) for 20min and then stained for integrin αIIbβ3 (JON/A) and CD62P (Naive n=10, *Sm* n=12). C) Representative FACS plots of naive and infected platelets with and without stimulation. Data pooled from 3 independent experiments. Significance determined by unpaired t-test of the mean (A-B). Non-significance (p>0.05) not shown.

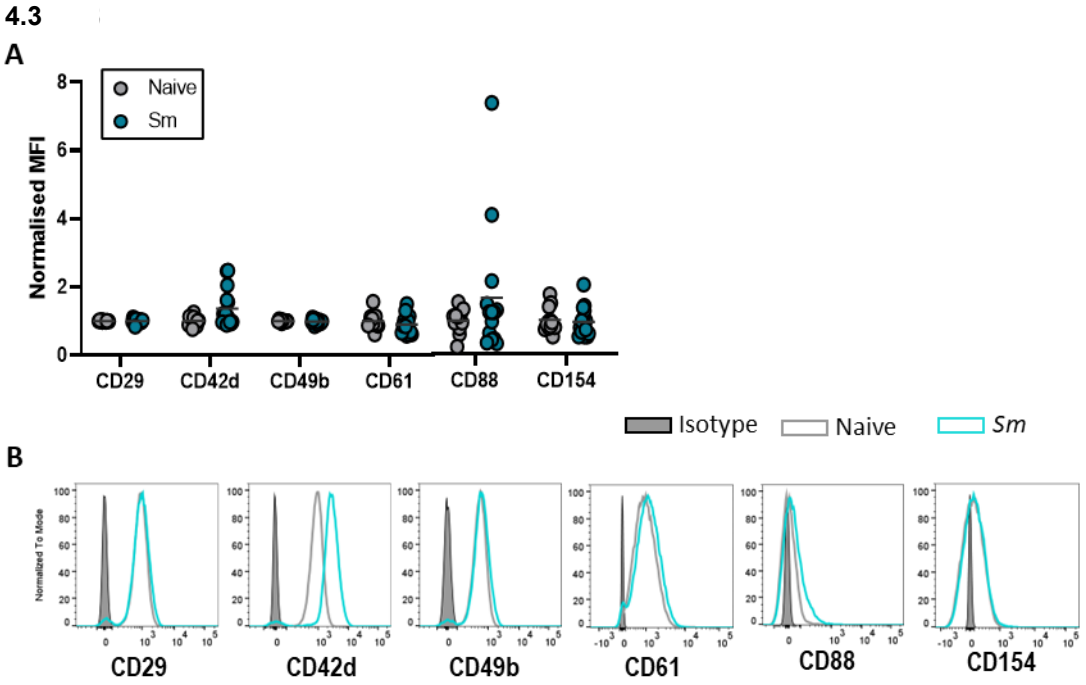

Figure 4.3 No difference in the expression of multiple surface molecules on platelets from naive and infected mice

Whole blood from the peripheral tail vein of naive and 12 weeks schistosome-infected mice. A) Expression of multiple molecules on CD41⁺ platelets were examined and normalised to the mean MFI of the naive group for each marker. B) Representative histograms for each marker (Naive n= 12, *Sm* n= 15). Data pooled from 3 independent experiments. Naive – grey outline, *Sm* – blue outline, Isotype – filled grey histogram. Significance determined by unpaired t-test of the mean raw MFI (A). Non-significance (p>0.05) not shown.

4.4

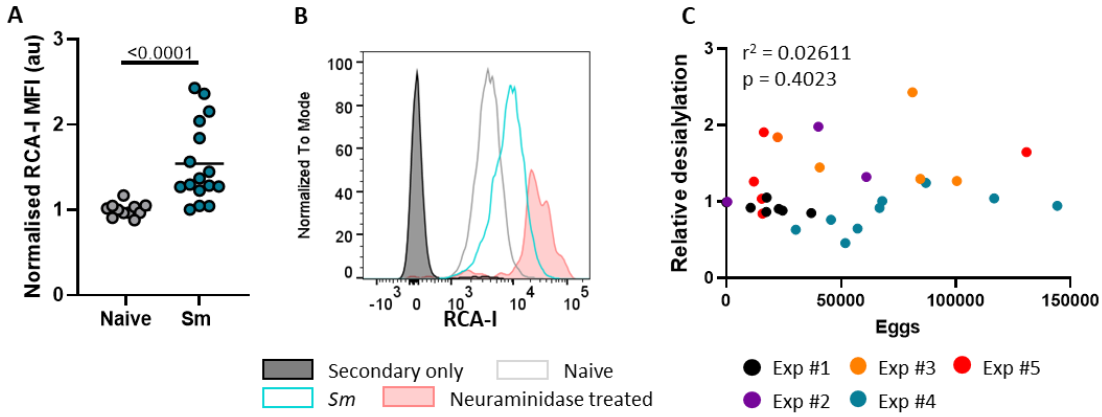

Figure 4.4 Greater exposure of terminal galactose sugars on platelets from schistosome-infected mice

Whole blood from the peripheral tail vein of naive and 12 weeks schistosome-infected mice was stained with anti-CD41 antibody and biotinylated lectins RCA-I. A) MFI of RCA-I$^+$ cells normalised to the mean of naive mice and B) representative histogram with neuraminidase (5U/ml) positive control (red) (Naive n=10 (blue), *Sm* n=16 (grey outline)). C) Correlative analysis of relative RCA-I MFI (desialylation) and total liver egg counts from schistosome-infected mice. Coloured symbols represent 5 independent experiments. Significance determined by unpaired t-test of the mean (A). Non-significance (p>0.05) not shown. Simple linear regression was performed to assess correlation.

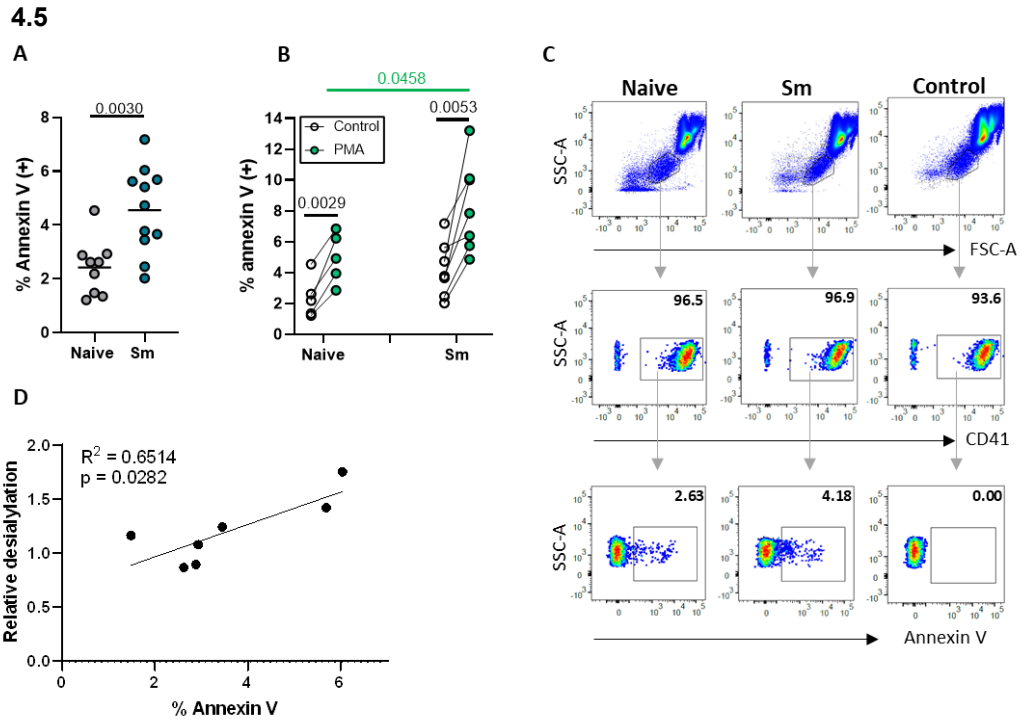

Figure 4.5 Elevated phosphatidylserine expression on the surface of platelets from schistosome-infected mice

Whole blood from the peripheral tail vein of naive and 12 week schistosome-infected mice was stained with anti-CD41 antibody and fluorescently labelled Annexin V. A) Percentage of Annexin V$^+$ platelets (Naive n=8, *Sm* n=11). B) Paired comparison of Annexin V expression following PMA (green) stimulation (25nM, 1hr, 37^{o}C) (Naive n=5, *Sm* n=7) and C) representative FACS plots. Data pooled from 2 independent experiments. D) Correlation analysis of desialylation and Annexin V staining. Significance determined by unpaired t-test of the mean (A) and N vs *Sm* (B) or paired t-test +/- PMA (B). Simple linear regression was performed to assess correlation (D).

4.3.2 Is the coagulation cascade affected by schistosome infection?

Given platelets from schistosome-infected mice spontaneously aggregated in the absence of platelet activation and had more PS on their surface, we were interested to explore changes that may be occurring to the coagulation cascade. As the liver is the site for production of the majority of coagulation factors and is also the main site of pathology in *S. mansoni* infection we first re-analysed a publicly available bulk RNA-sequencing dataset of livers from naive and 12 week schistosome-infected mice. We filtered the differentially expressed genes for those associated with coagulation (GO: (BP) BLOOD_COAGULATION_ INTRINSIC_ PATHWAY and BLOOD_ COAGULATION_FIBRIN_CLOT_FORMATION and showed there were considerably more genes upregulated (87/183, 48%) in schistosome infection compared with those downregulated (24/183, 13%), with 38% remaining unchanged (**Figure 4.6**). Of those upregulated, more than 79% (69/87) had a padj <0.01 and a log2fold change >1. We next looked at specific genes encoding components of the coagulation cascade as shown in **Figure 4.7** to establish whether they showed significant differential gene expression (padj <0.05). Individual genes encoding components of the intrinsic pathway were either up- or down-regulated following schistosome infection, however the only significant changes in components of the extrinsic and common pathways were the downregulation of genes encoding Factor VII, V and XIII. This contrasted with the fibrinolytic pathway which only had the upregulation of genes encoding urokinase and tissue plasminogen activators which ultimately drive the degradation of a fibrin clot (**Figure 4.7**). Finally, we systematically assessed the remaining significantly differentially expressed genes as to their role in the coagulation cascade and direction of regulation (**Figure 4.8 - Figure 4.9**). Despite there being more activating than inhibitory genes upregulated in schistosome-infected livers, the complexity and tightly regulated coagulation cascade has its own inhibitory pathways (**Figure 4.8**). For example, an upregulation of the gene encoding the protein C receptor is likely to promote greater thrombomodulin signalling, more activated protein C, which in turn inhibits the activation of FVIII and progression to the common pathway. Moreover, in terms of the genes downregulated, there is almost an equal proportion of activating and inhibitory genes (**Figure 4.9**), but their log2fold

change is generally less marked than seen for up-regulated genes. Together this shows that whilst schistosome infection has a significant impact on expression of genes associated with all stages of the coagulation cascade, the downstream consequences of this are difficult to predict given the multitude of activating and inhibitory factors that control this cascade.

To dissect the coagulation cascade more closely we developed the first protocol, to the best of our knowledge, for measuring changes to the intrinsic and extrinsic pathway longitudinally in mice. We carried out saphenous bleeds on naive and schistosome-infected mice and measured the prothrombin time (PT), to assess the extrinsic pathway, and activated partial thromboplastin time (aPTT) to assess the intrinsic pathway. Interestingly, as infection progressed both the PT and aPTT were prolonged, with the PT showing significant elongation by 10 weeks and the aPTT by 12 weeks (**Figure 4.10**). This revealed that whilst neither PT nor aPTT were changed in acute infection (8 weeks), there was a progressive increase in both these parameters as infection progressed. Together, this shows that despite platelets being more capable of aggregation in schistosome infection the coagulation cascade was significantly impeded.

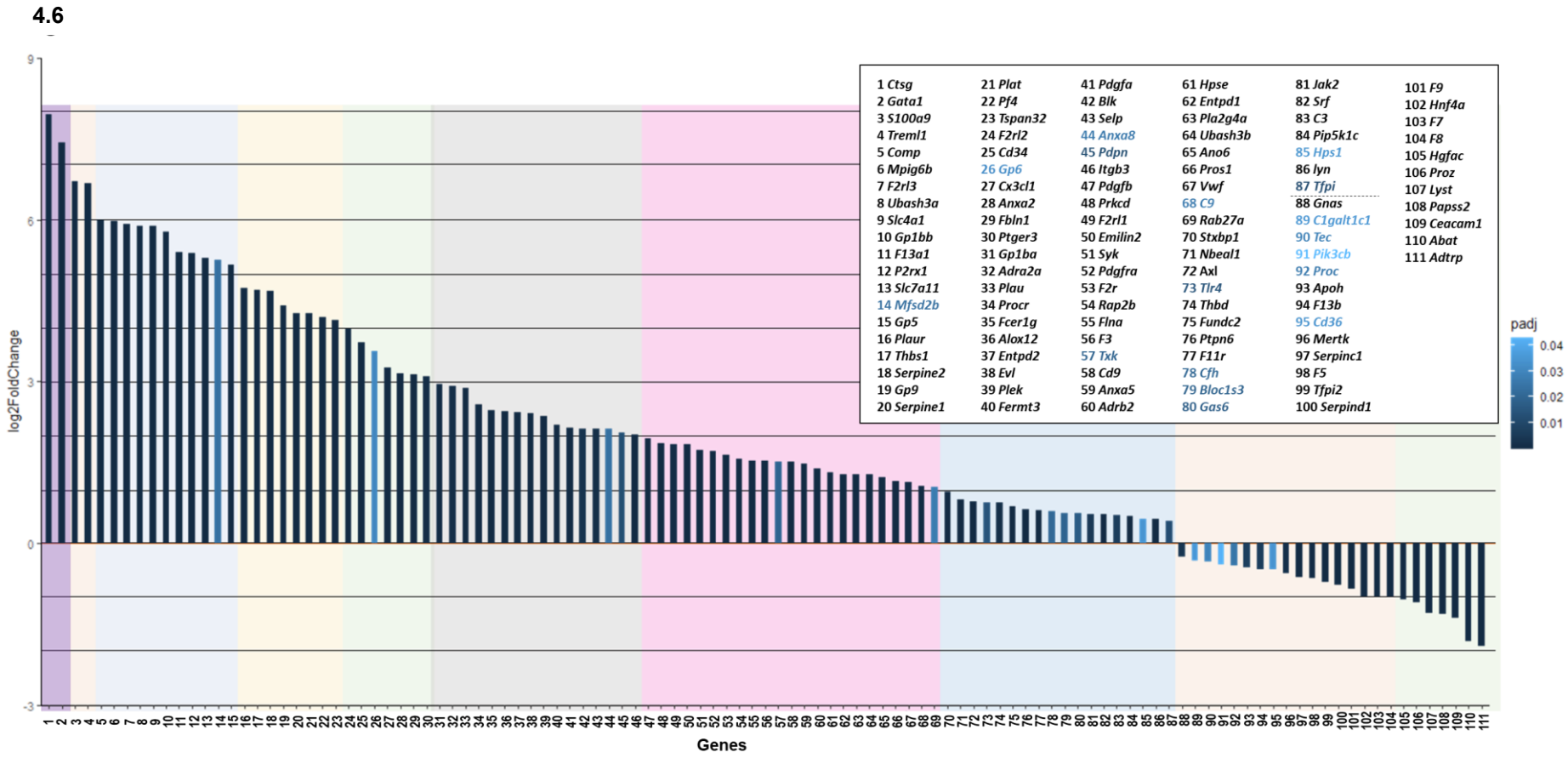

Figure 4.6 Many significant changes in genes associated with coagulation in schistosome infection

Differentially expressed genes were filtered based on the genes found in the GOBP_blood_coagulation_intrinsic_pathway and blood_coaguation_ fibrin_clot_formation. Individual bar colours represent significance based on adjusted p-value, genes were considered significantly differentially expressed in schistosome infection when padj <0.005.

4.7

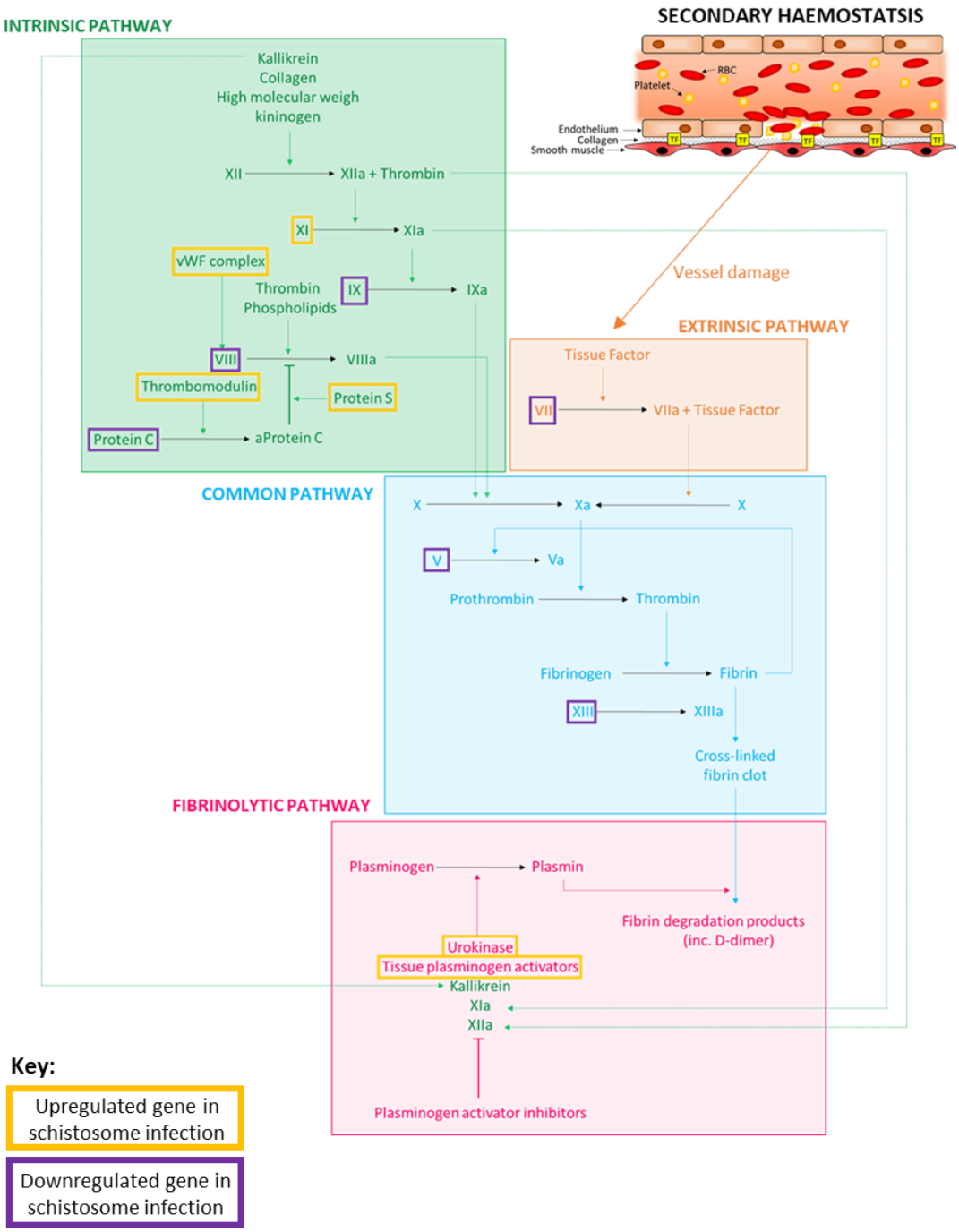

Figure 4.7 Significantly upregulated and downregulated genes in the liver encoding components of the coagulation cascade

Significantly upregulated genes highlighted in yellow and downregulated genes highlighted in purple. Significance determined as padj<0.05 and >log2fold change.

4.8

UPREGULATED

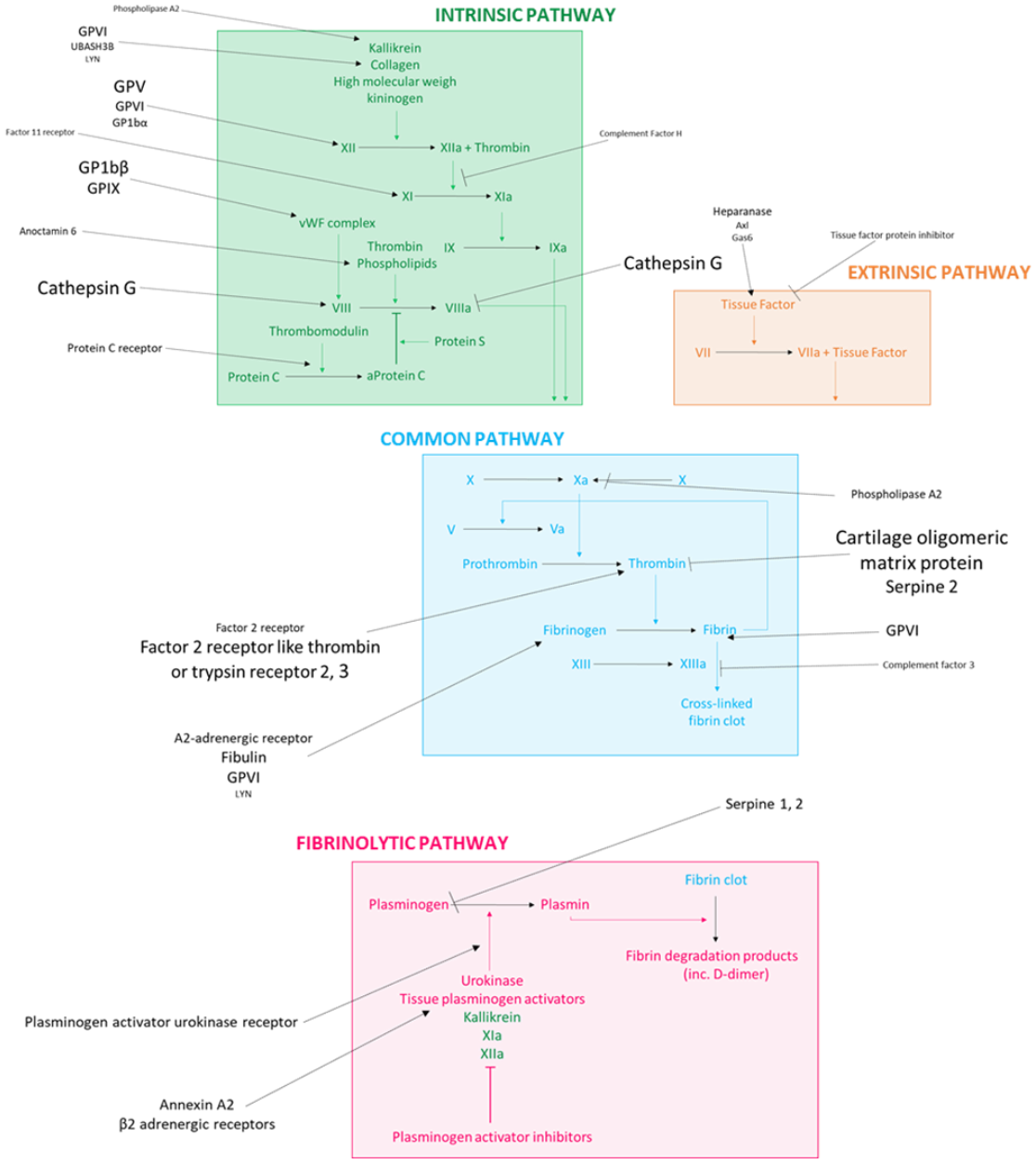

Figure 4.8 Significantly upregulated genes in schistosome infection encoding molecules which both drive and inhibit coagulation

Font size represents log2fold change of gene expression in schistosome infection.

4.9

DOWNREGULATED

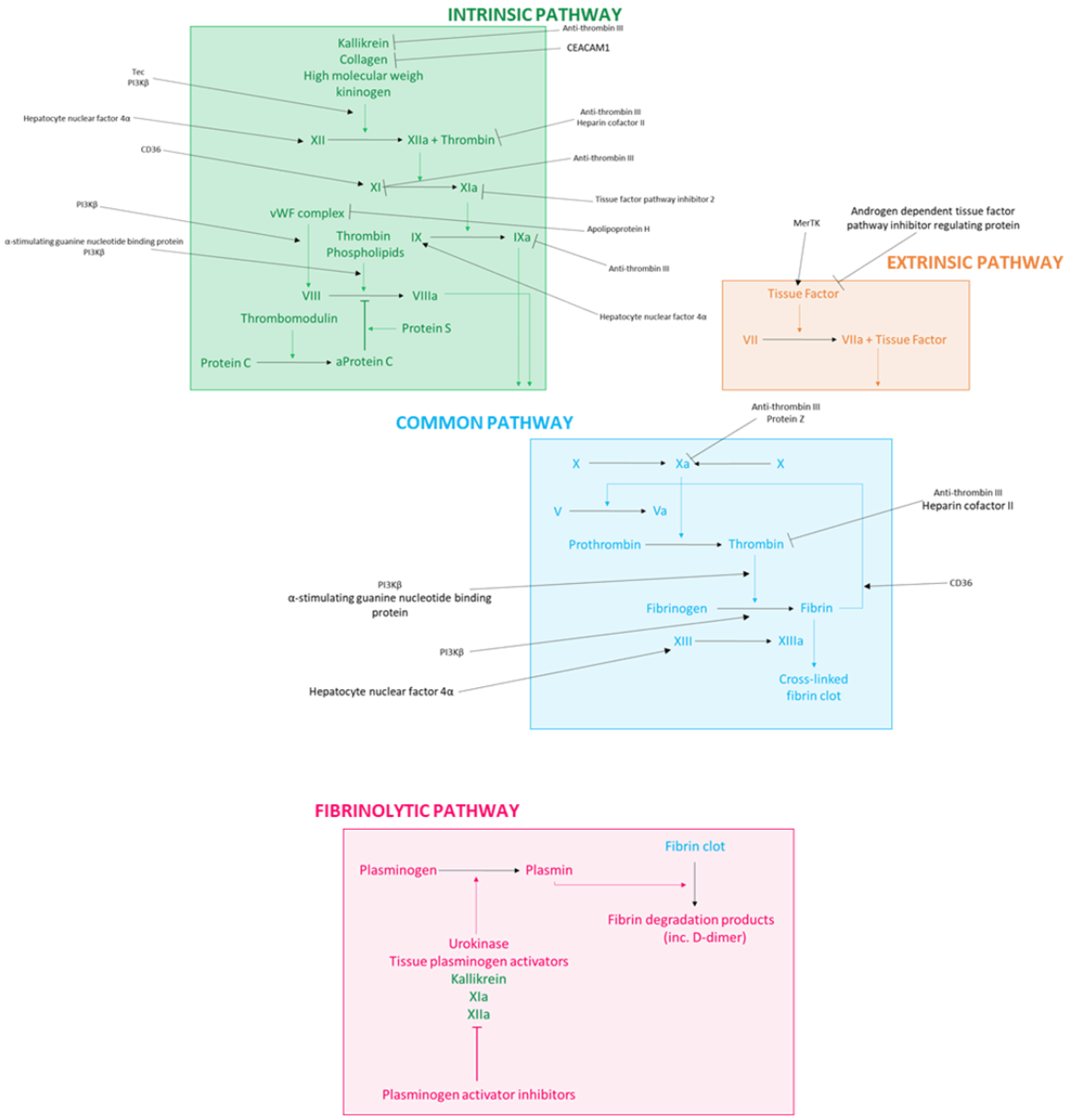

Figure 4.9 Significantly downregulated genes in schistosome infection encoding molecules which both drive and inhibit coagulation

Font size represents log2fold change of gene expression in schistosome infection.

4.10

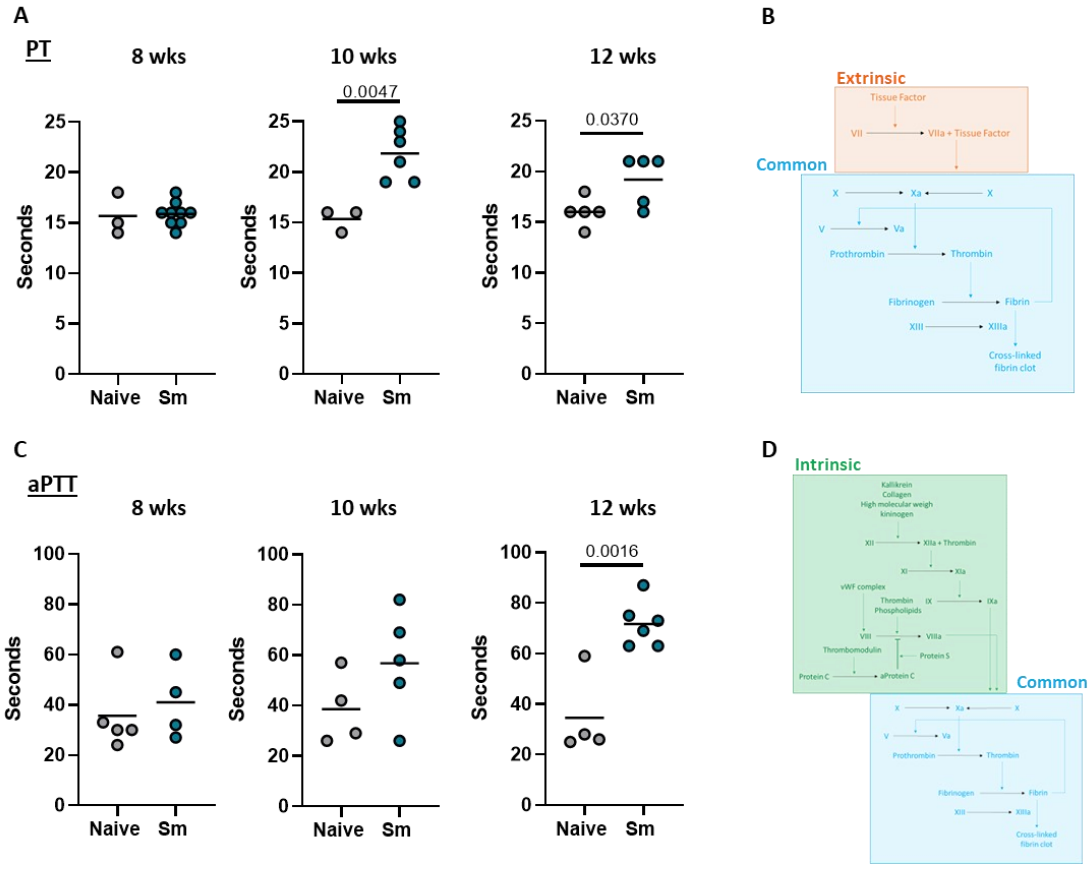

Figure 4.10 Prolonged clotting times from 10 weeks post-schistosome infection
C57BL/6 mice were infected with 40 *S. mansoni* cercariae. Mice were bled from the saphenous vein and 40ul blood directly transferred into A) prothrombin time (PT) or C) activated partial thromboplastin time (aPTT) coagulometry cassette. Schematic of B) extrinsic and common pathway assessed by PT and D) intrinsic and common pathway assessed by aPTT. (Naive, n=5, *Sm* n=6). Significance determined by unpaired t-test of the mean. Non-significance (p>0.05) not shown.

4.4 Discussion

The haemostatic role of platelets is tightly regulated to ensure platelet activation and coagulation are supressed until they are required following vascular injury. However, loss of this regulation, for example in the case of infection can be severe and result in either insufficient aggregation or exaggerated activation (353).

We first observed that schistosome infection led to spontaneous platelet aggregation in the absence of any exogenous stimuli. Despite this, the platelets themselves did not appear to be overtly activated yet maintained their propensity to become activated following stimulation with a PAR4 agonist. We therefore hypothesised that schistosome infection was driving the coagulation cascade leading to a hypercoagulable phenotype. It was surprising that schistosome-infected mice displayed a hypocoagulable phenotype with prolonged PT and aPTT as infection progressed. Spontaneous platelet aggregation has been associated with cardiovascular disease, however the underlying mechanism remains unclear (354). We looked at a range of surface molecules associated with platelet activation (including activated integrin αIIbβ3, CD62P and multiple integrins and glycoproteins involved in platelet adherence) but none showed any significant difference in schistosome infection. This was not an exhaustive list as such, other molecules may be driving spontaneous aggregation. In humans, FcγRIIA (CD32A) has been shown to drive spontaneous platelet aggregation, but FcγRIIA is not present in mice so is not a driver here (355). Moreover, increased GPVI has also been linked to spontaneous platelet activation in diabetes and stroke patients, however we have not assessed levels in our mouse model (356). One potential explanation for spontaneous platelet aggregation in both mouse and humans is a result of erythrocyte fragility. In whole blood aggregometry, the blood sample is subjected to constant stirring which can cause erythrocyte lysis and release of ADP/ATP. Elevated ADP/ATP then activates platelets by binding P2Y1 and P2X1 receptors, which in turn stimulates intracellular Ca^{2+} influx, granule release and a positive feedback loop leading to platelet-platelet aggregation (357). Moreover, as red blood cells lyse and are broken down

they may release free haem which has recently been shown to induce platelet activation through CLEC-2 in both mice and humans (358).

In schistosome infection, mature adult worms perform haematophagy as their primary source of nutrient acquisition. During this process, erythrocytes are degraded and release their contents, such as the highly toxic haem which is immediately converted to less toxic hemozoin crystals, released into host circulation and cleared by macrophages and neutrophils that are then released into host circulation (359,360). An *in vitro* study has shown that platelets drive neutrophil-mediated clearance of hemozoin which may mean in the cases of thrombocytopenia (as occurs in schistosome infection) that there is a higher concentration of hemozoin in circulation, especially given increased production due to worm feeding (361). It is not known what effect hemozoin has on platelets and whether this binds to CLEC-2 like haem causing platelet activation. To assess the intrinsic aggregatory capacity of platelets from schistosome-infected mice, in the absence of any erythrocyte lysis or extrinsic signalling molecules, washed platelet aggregometry could be performed. To further dissect the mechanism of action, *in vitro* transfer of isolated platelets from naive mice into the platelet poor plasma of infected mice and vice versa would demonstrate whether spontaneous aggregation was directly platelet-driven or a result of plasma components.

The prolonged coagulation times are consistent with infected patient samples (240,242,246,248). Importantly, our coagulometry assays of PT and aPTT consider all the procoagulant and anticoagulant factors due to the use of whole blood (362). However, they do not provide any information about the stability of the thrombus as they only measure fibrogenesis and not fibrinolysis. Analysis of publicly available data also showed a significant reduction in multiple genes encoding coagulation factors such as FIX, FVIII, FVII, FV and FXIII as well as an increase in the genes encoding thrombomodulin and protein S, both of which contribute to inhibition of the coagulation cascade. Interestingly, Da'dara *et al.* (2016) used TEG to show blood from schistosome-infected mice clotted faster than naive animals, however the thrombi were rapidly degraded (341). The differences with our experiments showing prolonged clotting time, may be as a result of the other studies' earlier time-

point of blood collection (7 weeks) compared with our more chronic stages (prolonged at 10-12 weeks), lack of differentiation between intrinsic and extrinsic coagulation pathways and/or the higher cercarial infection dose and associated excessive pathology (~125 compared with 40 cercariae) (341). Whilst we did not measure clot stability directly, our analysis of an existing RNA-seq dataset of schistosome liver did show an increase in gene expression of urokinase and tissue plasminogen activators, both of which promote fibrinolysis (277).

Prolonged coagulation may also be caused by impeded production of coagulation factors from the liver due to granulomatous inflammation during schistosome infection or excessive consumption of coagulation factors or a combination of both processes (363). DIC often manifests with prolonged PT and aPTT alongside micro-thrombi in tissues (364). In **Chapter 3** we found enhanced $CD41^{+}$ staining in the liver of schistosome-infected mice representing both micro-thrombi and MK. Micro-thrombi may have formed in the liver in response to vascular damage following schistosome egg and immune cell migration. This in turn could have induced excessive activation of the extrinsic pathway and thrombin production which drives a feed-forward loop and coagulation factor consumption (364). If this was the case, it may explain the faster coagulation time observed by Da'dara *et al.* (2016) at 7 weeks, i.e. prior to severe coagulation factor consumption, and may also be contributing to thrombocytopenia as platelets are consumed within these micro-thrombi (341). To understand these changes occurring in coagulation better, longitudinal analysis of individual coagulation factors in the liver at the protein level would be required, i.e. unbiased serum proteomics or more targeted western blotting could be used to assess protein expression in naive mice, prior to schistosome egg laying as granulomatous inflammation develops and eventually leads to liver fibrosis. In addition, other markers of DIC could be tested e.g. circulating D-dimer levels as a measure of fibrin degradation. Vasculature damage/activation and exposure of TF on both immune cells and endothelium can drive DIC initiation and therefore it would be interesting to assess this by fluorescence microscopy and flow cytometry looking for both TF as well as inflammatory markers such as ICAM-1 and

VCAM-1 (365). Indeed, our own pilot studies and previously published literature suggest there is an increase in the expression of ICAM-1 and VCAM-1 in the liver of schistosome-infected mice which would be consistent with the initiation of DIC (366–368).

An interesting finding was that platelets from schistosome infection expressed more PS on their cell surface. PS is known to have pro-coagulant properties through driving the activation of FVIII and generation of FXa, and the subsequent activation of FV (369). Despite PS driving coagulation, if there was less FVIII and FV (as shown by RNA-seq at the mRNA level) it would have fewer binding partners and would have less of a pro-coagulant effect. However, it may still drive platelet aggregation (370). Expression of PS also acts as an “eat-me” signal for phagocytes and therefore is likely to contribute and provide a potential mechanism for the accelerated platelet clearance described in **Chapter 3** (350). Given the FcR-independent thrombocytopenia we have observed in schistosome infection (**Chapter 3**), we were also interested to explore whether platelets expressed any other “eat-me” signals which would enhance their clearance. Here we showed there was enhanced desialylation in infected animals which is likely to contribute further to platelet clearance as the terminal galactose sugars can be recognised by Ashwell-Morell receptors on hepatocytes (371). Whether schistosome infection impacts on platelet phagocytosis will be tested in **Chapter 5**.

In summary, we have highlighted the complex relationship and tight balance between aggregation and coagulation and the multitude of factors that feed into these interdependent pathways. Platelets from schistosome-infected mice spontaneously aggregate in the absence of exogenous agonist and do not possess an overtly active phenotype. Thus, the increased propensity to aggregate may be, at least in part, a result of additional blood factors rather than an intrinsic ability of the platelets to aggregate. Alongside this, infected mice displayed a prolonged coagulation time for both the intrinsic and extrinsic pathways suggesting a multi-faceted coagulopathy which may be due to inflammation and fibrosis impeded coagulation factor production, and/or a result of DIC-induced coagulation factor consumption. We have also identified that schistosome infection increases both platelet PS exposure and

desialylation that likely contribute to accelerated clearance. As we were only able test a fraction of the potential molecules that may change during schistosome infection, global transcriptomic, proteomic and metabolomic analysis of isolated platelets from naive and schistosome-infected mice could be performed to identify more broadly the molecules responsible for spontaneous platelet aggregation and clearance.

5. Assessment of the immunomodulatory capacity of platelets on macrophages

5.1 Introduction

Our studies have revealed that schistosome infection results in an increase of platelet-leukocyte interactions, particularly with monocytes and macrophages (**Chapter 3**). In this chapter, an *in vitro* approach was used to better understand the downstream consequences of these interactions.

Increased PLA have been observed both in clinic and in many *in vivo* animal models of infection and disease (372,373). The consequences of these interactions are complex and often contradictory, which may reflect context-specific roles of platelets (217,227,283,374–376). Several groups have shown platelets promote survival in mouse models of sepsis, although there is controversy over the mechanism. Xiang *et al*. (2013) proposed platelets limit macrophage activation, with excessive macrophage activation being associated with poor sepsis survival (283). Conversely, Carestia *et al*. (2019) showed platelets actually promote the polarisation of macrophages towards a pro-inflammatory phenotype, thereby enhancing phagocytosis and bacterial clearance (227). Other studies have shown platelets variously induce macrophage expression of CD16 (374,375), reduce phagocytosis of *E. coli* and apoptotic Jurkat cells (217), and decrease macrophage pro-inflammatory cytokine and chemokine production (377). Some of these discrepancies may be explained by differences in the exact cell types used, for instance mouse or human cells, BM-derived or thioglycollate-elicited macrophages and characterisation using distinct activation markers (e.g. CD16, CD64, iNOS, CD163, CD206 as well as cytokines such as IL-6 and IL-10). Notably, despite BM-derived and thioglycollate-elicited macrophages both being of BM origin, they exhibit distinct responses following activation with cytokines or microbial products (376).

Given the elevated macrophage-platelet interactions observed in our murine *S. mansoni* infection model, in this chapter we test whether platelets from naive or infected mice affect the polarisation and activation of BM-derived macrophages. As schistosome infection leads to thrombocytopenia (**Chapter**

3), we also investigate phagocytosis of platelets by macrophages of different origins and after stimulation with pro- and anti-inflammatory stimuli.

5.2 Aims

1) To determine whether platelets affect macrophage polarisation
2) To determine whether platelets affect macrophage phagocytosis
3) To determine whether platelets from naive or infected mice have distinct effects on macrophage activation and phagocytosis

5.3 Results

5.3.1 Do platelets modulate macrophage polarisation?

In **Chapter 3** we showed platelets interact with a specific subset of liver macrophages and monocytes (MHCII^{lo} RELMα^{hi}) in schistosome infection. Our aim here is to take a reductionist *in vitro* approach to probe the consequences of platelet-macrophage interactions. We initially tested two well characterised murine macrophage populations, thioglycollate-elicited peritoneal macrophages (Thio-Mϕ) and *in vitro* BM-derived macrophages generated by culture of BM cells with L929-supplemented media (BM-Mϕ) (378). Our initial experiments demonstrated that BM-Mϕ were a more homogeneous final population compared with Thio-Mϕ, with a higher proportion of live intact cells and CD11b^{+}F4/80^{+} cells (**Figure 5.1**). Both populations were treated overnight with LPS/IFNγ to generate classically activated (M1-like) cells, or IL-4 which favours alternative (M2-like) activation. We used iNOS, an enzyme required for arginine metabolism to citrulline and NO, as the main marker for classical activation (98). Ym1 and RELMα were used as markers of alternative activation (103–105) (**Figure 5.2**). Despite both macrophage populations being of BM origin they expressed different facets of M2 activation in response to IL-4, with BM-Mϕ producing significantly more RELMα than Thio-Mϕ, and Thio-Mϕ producing significantly more Ym1 than BM-Mϕ (**Figure 5.3**). We focused on BM-Mϕ as IL-4 treatment induced high levels of RELMα that is shared with liver macrophages that interact with platelets *in vivo* (**Chapter 3**). Additionally, BM-Mϕ generated a greater yield

which offered the potential to freeze down excess macrophages from each experiment.

To assess the effects of platelets on macrophages, we co-cultured BM-Mϕ overnight +/- platelets from naive mice at 100:1 (platelet:macrophage) ratio that mimics physiological levels (379). Macrophages were left either unpolarised (no further treatment) or with M1 or M2 stimuli. Across four independent experiments, platelets did not impact on iNOS expression by LPS/IFNγ induced M1 macrophages (**Figure 5.4A**). In contrast, platelets had much less consistent effects on IL-4-dependent Ym1 and RELMα expression i.e. in two experiments platelets promoted Ym1 and inhibited RELMα, yet had no effect in two other repeats (**Figure 5.4B-C**). Since we were able to generate and freeze excess macrophages from BM cultures, we were able to re-test these, culturing them with a single, common, naive platelet sample. This revealed platelets from naive mice had only marginal inhibitory effects on IL-4 stimulated RELMα expression (1 of 4 macrophage cultures) and instead suggests the strong immune modulatory effects of platelets observed in experiments 1 and 2 reflects differences in starting platelet population, perhaps as a result of differences in platelet activation or purity during the isolation process (**Figure 5.4D**). There were also no consistent differences observed at the mRNA level in the presence or absence of platelets with respect to *Retlna, Ym1, Nos2, Cd16, Cd32, Cd64, Tnf* and *Cxcl10* (**Figure 5.5**). These markers encompass the majority of those investigated in the literature to explore the effects of platelets on both human and murine macrophage polarisation and activation (227,375). Together, this demonstrates that naive resting platelets do not consistently affect macrophage polarisation with respect to RELMα or Ym1.

We next investigated whether activated platelets affected macrophage polarisation. The PAR4 agonist triggers intracellular G-protein signalling (380) in platelets (**Chapter 4**), resulting in inside-out signalling and granule release, measured here by the activated conformation of integrin αIIbβIII (detected by JON/A mAb reactivity) and P-selectin (CD62P) expression (**Figure 5.6A**). Phillips *et al*. (1991) and Lee *et al*. (2021) have shown that activated platelets cause human $CD14^{+}$ monocytes to upregulate CD16 and decrease CXCL10

and TNF. In our BM-Mϕ co-cultures, initial experiments suggested activated platelets reduced RELMα and Ym1, whilst iNOS levels were unaffected (**Figure 5.6B-D**). However, we carried out a control experiment using the PAR4 agonist treatment in the absence of platelets (at the same concentration present in the washed platelet samples) and found the same changes. This suggested that the altered RELMα and Ym1 expression was caused by a direct effect of PAR4 agonist on the macrophages, rather than specifically via the activated platelets (**Figure 5.6**) (381,382). Introducing additional platelet washing steps after PAR4 agonist stimulation caused the loss of any platelet-induced changes to classical or alternative activation markers by flow cytometry (**Figure 5.7**) and qPCR (*Retlna, Ym1, Nos2, Cd16, Cd32, Cd64, Tnf* or *Cxcl10* not shown).

Having established that neither resting nor activated platelets from naive mice consistently altered macrophage polarisation, we next wanted to test whether platelets from infected mice were immunomodulatory. As discussed in **Chapter 4**, platelets from 9-12 week infected mice did not express elevated surface activated integrin αIIbβIII or CD62P (**Figure 5.8A**). Co-culture of platelets from infected mice with BM-Mϕ caused a reproducible increase in CD64 MFI in the presence of LPS/IFNγ but did not cause a change in iNOS levels (**Figure 5.8B-C**). IL-4 stimulated macrophages co-cultured with platelets from infected mice showed a small but consistent reduction in RELMα, although this did not reach statistical significance (**Figure 5.8D**). Transcript analysis was very variable with no reproducible differences in *Cd64* and *Retlna*, in contrast to protein level changes (**Figure 5.9**).

We next assessed whether platelets would have stronger immunomodulatory effects at suboptimal concentrations of M1/M2 stimuli as high concentrations of stimuli may mask more subtle changes. Having normalised expression levels to the highest IL-4 concentrations (10ng/ml) in the absence of platelets, we found that platelets from infected mice induced subtle, yet significant, increases in Ym1 expression when macrophages were stimulated with 1-3ng/ml IL-4 (**Figure 5.10**). Initially, 4 half-log dilutions of LPS/IFNγ were tested, however even with the lowest concentration (1ng/ml LPS, 0.1ng/ml IFNγ) ~80% BM-Mϕ were iNOS^{+} (**Figure 5.11**). To allow for any changes in

iNOS to be observed, a lower concentration range was tested. This demonstrated that M1 differentiation, with respect to iNOS was an "all or nothing" response with iNOS expression increasing from <5% in 0.3ng/ml LPS, 0.03ng/ml IFNγ to ~60% iNOS$^+$ with 1ng/ml LPS, 0.1ng/ml IFNγ. Platelets did not have any effect on any M1 markers (including CD68 and MHCII not shown) even at the lower concentrations (**Figure 5.11**).

In **Chapter 3**, we showed that CD41$^+$ macrophages in the liver of naive mice are MHCII^{hi} RELMa^{hi} Ym1^{hi} compared with MHCII^{lo} RELMa^{hi} Ym1^{hi} in schistosome-infected mice. However, our *in vitro* co-culture assays did not show consistent, significant, down- or up-regulation of these markers following exposure to platelets. Therefore, we hypothesised that rather than directly promoting macrophage polarisation, platelets instead preferentially bound to these activated macrophages. To test this, we differentially polarised BM-Mϕ *in vitro* to M1 or M2-like populations using sub-optimal concentrations of stimuli in order to generate both polarised (i.e. M1 iNOS$^+$, M2 RELMa$^+$ Ym1$^+$) and non-polarised cells. We then assessed whether X649-labelled platelets preferentially bound to the polarised cells compared with non-polarised cells *in vitro* (**Figure 5.12A-D**). After 20hr of co-culture of platelets with polarised macrophages, more platelets had been internalised (i.e. X649$^+$CD41$^-$, grey) than remained surface-bound (X649$^+$CD41$^+$, pink) and M1-like macrophages had internalised significantly more than unpolarised M0 or IL-4 treated M2 macrophages (**Figure 5.12E-F**). Importantly, regardless of the nature of stimulation (IL-4 or LPS/IFNγ), polarised macrophages internalised more platelets than their unpolarised counterparts (**Figure 5.12G-I**). This finding is consistent with platelets preferentially binding to (or being phagocytosed by) activated macrophages, rather than platelets directly driving macrophage polarisation.

5.1
A

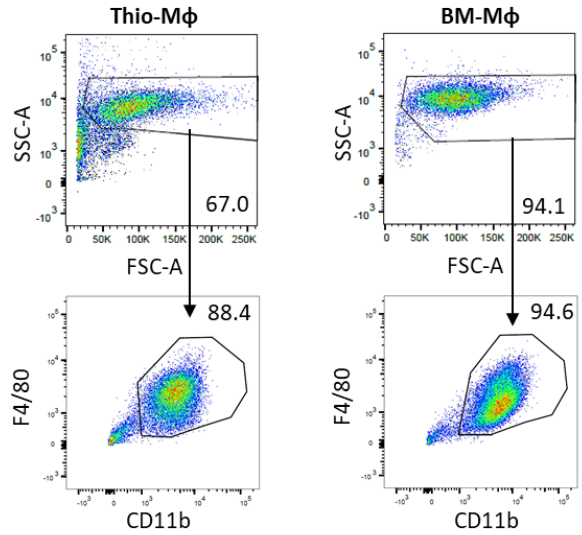

Figure 5.1 Greater heterogeneity in thioglycollate-elicited macrophages compared with BM-cultured macrophages

Example FACS plots of murine peritoneal macrophages harvested 3 days after injection with 4% thioglycollate broth (Thio-Mϕ) and BM cells cultured in L929-supplemented media for 6 days (BM-Mϕ). Representative of 4 independent experiments with 3 technical replicates in each.

5.2
A

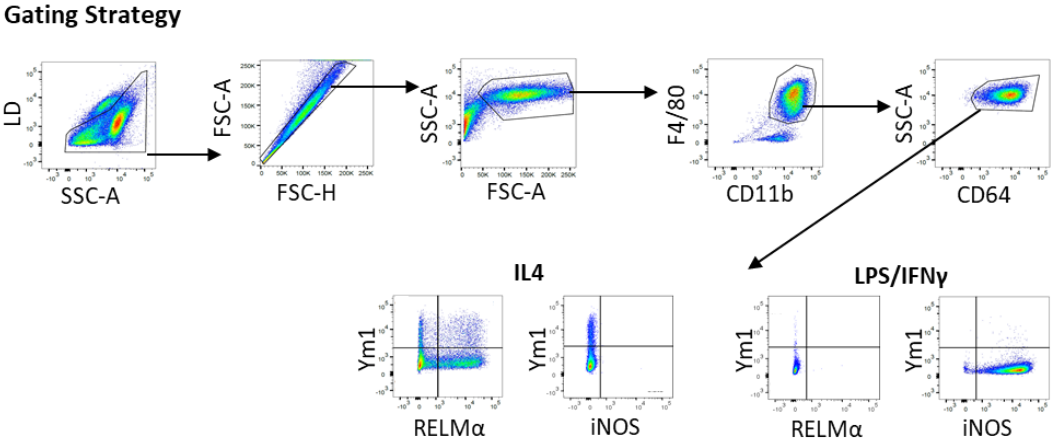

Figure 5.2 Identification of polarised macrophages gating strategy

Example flow cytometry gating and staining associated with BM-Mϕ stimulated overnight with IL-4 (20ng/ml) or LPS/IFNγ (100ng/ml 10ng/ml).

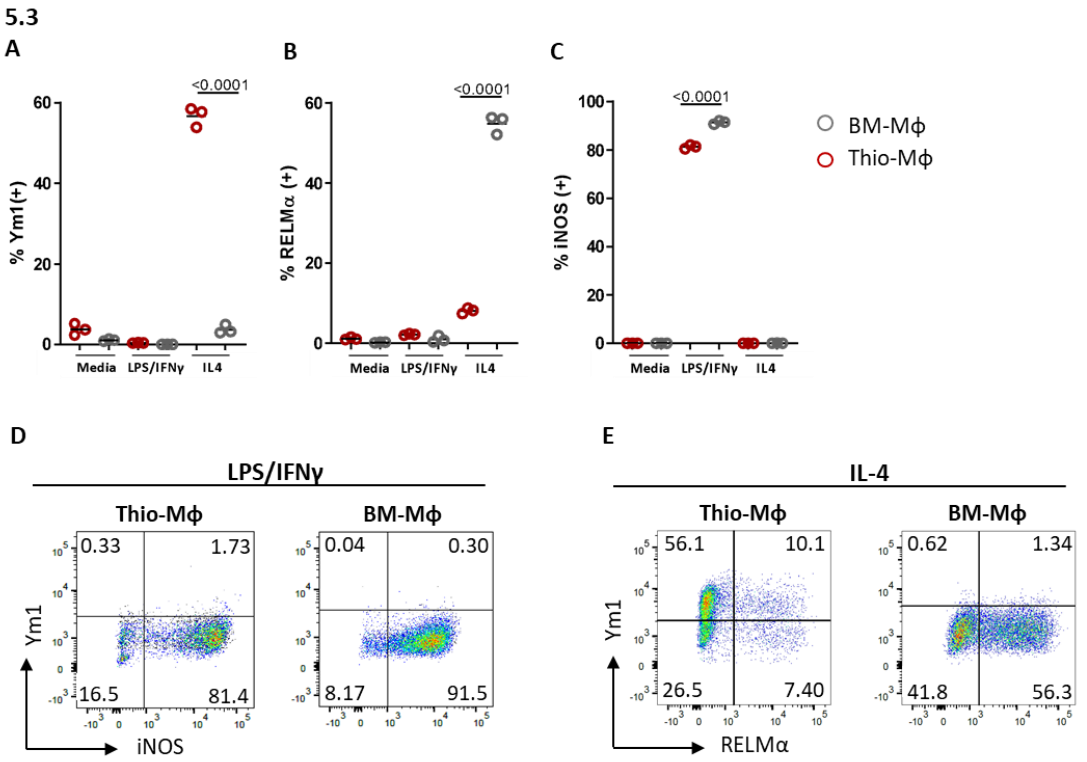

Figure 5.3 Thio-Mϕ and BM-Mϕ respond differently to IL-4 stimulation

Thio-Mϕ and BM-Mϕ stimulated with LPS/IFNγ (100ng/ml 10ng/ml) or IL-4 (20ng/ml) overnight and analysed by flow cytometry for A) Ym1, B) RELMα and C) iNOS. Representative FACS plots following D) LPS/IFNγ or E) IL-4 stimulation. Statistical significance was determined using unpaired t-tests between BM-Mϕ and Thio-Mϕ groups. Non-significance ($p>0.05$) not shown. Symbols indicate technical replicates, representative of 3 independent experiments.

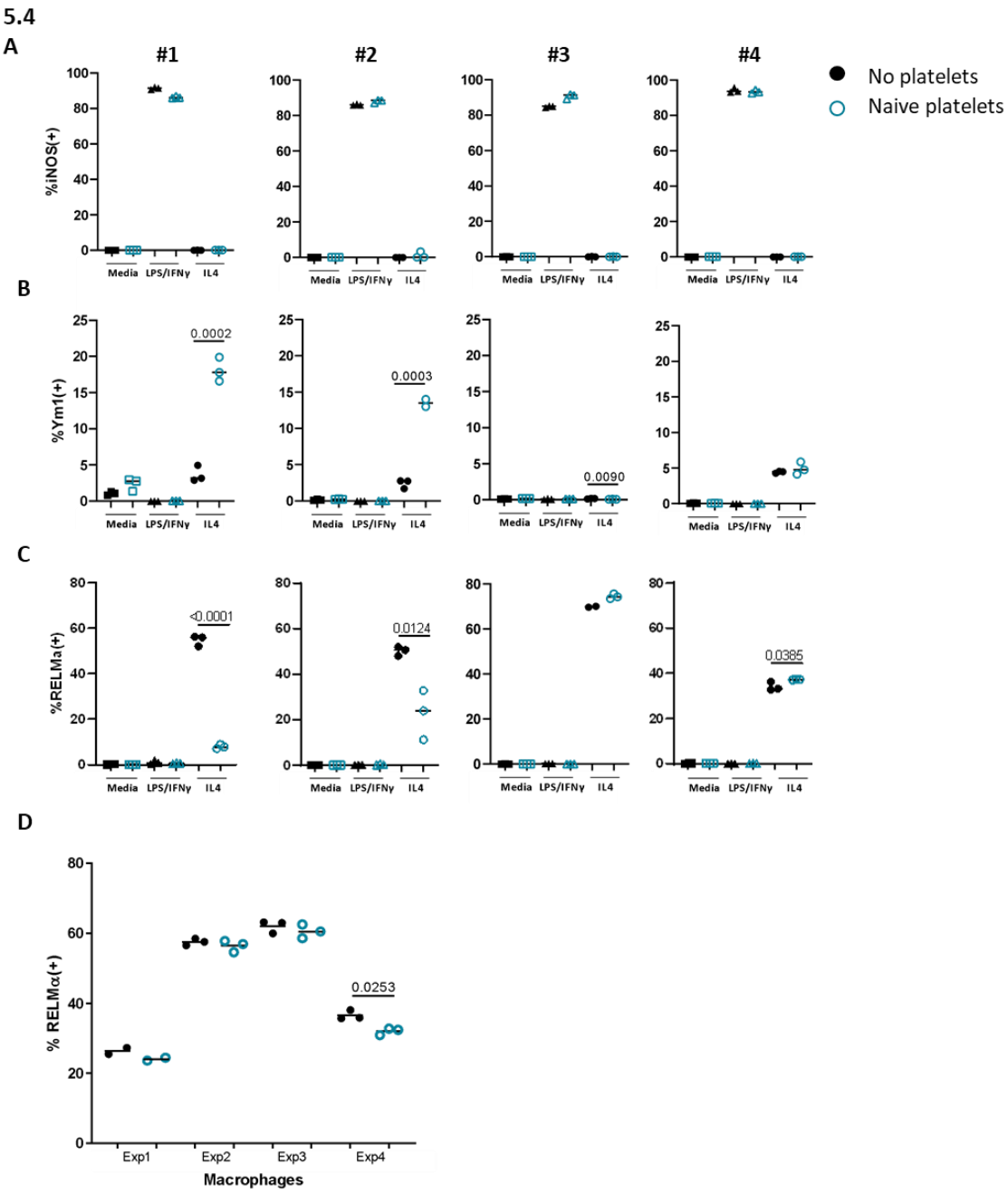

Figure 5.4 Naive platelets do not affect expression of RELMα by IL-4 stimulated BM-Mϕ
BM-Mϕ stimulated with LPS/IFNγ (100ng/ml 10ng/ml) or IL-4 (20ng/ml) and co-cultured overnight with naive platelets (1:100 macrophages : platelets). Flow cytometry analysis from 4 independent experiments of the percentage expression of A) iNOS, B) Ym1 and C) RELMα. Percentage expression of RELMα by IL-4 stimulated BM-Mϕ in the presence (blue) or absence (black) of naive platelets (1:100) from frozen stock samples of BM-Mϕ from the 4 independent experiments and co-cultured with the same murine platelet sample. Statistical significance was determined using unpaired t-tests between BM-Mϕ with/without platelets with each stimulation. Symbols indicate technical replicates, representative of 4 independent experiments. Non-significance ($p>0.05$) not shown.

5.5

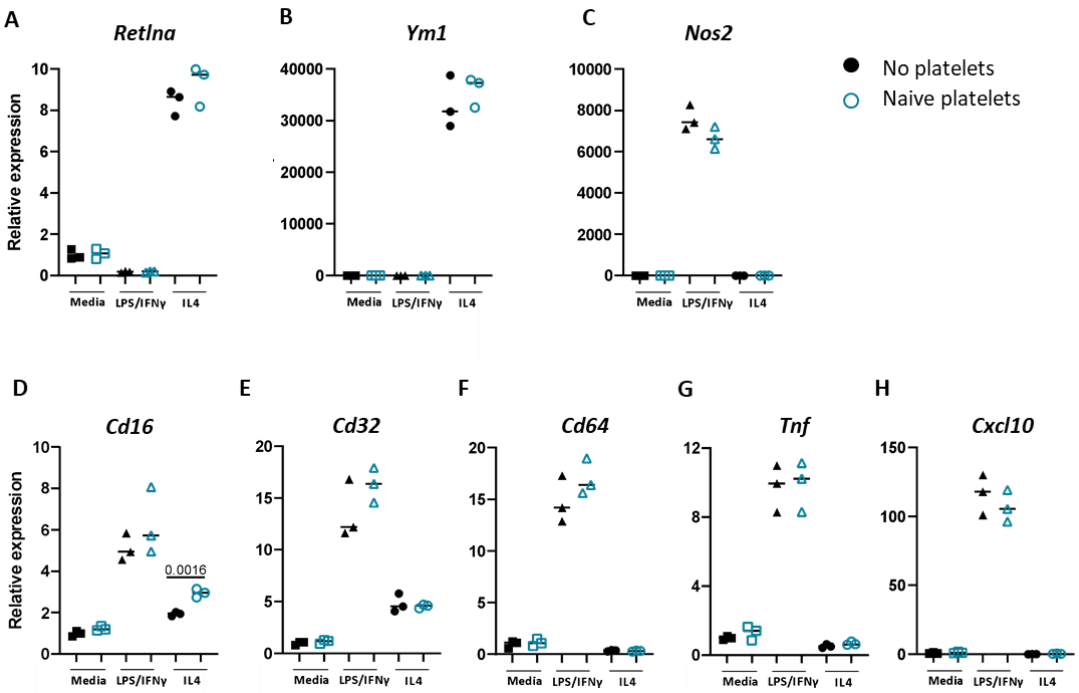

Figure 5.5 No reproducible differences in expression of markers at the transcriptional level in the presence of platelets

BM-Mϕ stimulated with LPS/IFNγ (100ng/ml 10ng/ml) or IL-4 (20ng/ml) and co-cultured overnight with naive platelets (1:100 macrophages : platelets). Relative mRNA transcript levels of A) *Retlna,* B) *Ym1*, C) *Nos2,* D) *Cd16*, E) *Cd32,* F) *Cd64*, G) *Tnf* and H) *Cxcl10* normalised to *Hprt* housekeeping gene. Representative of 2 independent experiments with the exception of *Cd16* which showed no significant difference upon repetition. Statistical significance was determined using unpaired t-tests between BM-Mϕ with/without platelets with each stimulation. Symbols represent technical replicates. Non-significance ($p>0.05$) not shown.

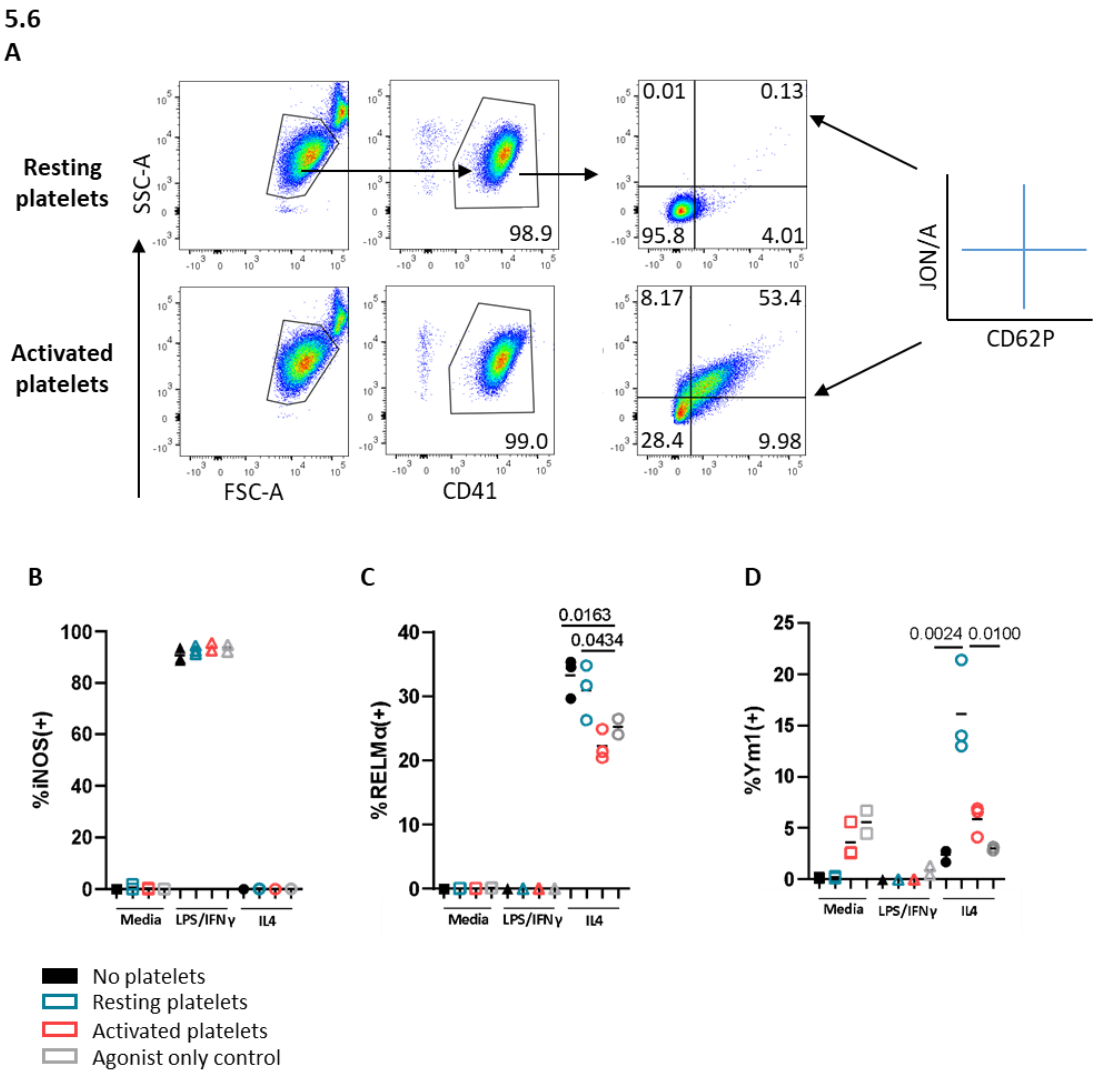

Figure 5.6 PAR4 agonist inhibits RELMα and Ym1 expression by IL-4 stimulated BM-Mϕ

A) Isolated murine platelets activated with 150μM PAR4 agonist for 30min before analysis by flow cytometry. BM-Mϕ stimulated with LPS/IFNγ (100ng/ml 10ng/ml) or IL-4 (20ng/ml) and co-cultured overnight with naive resting or PAR4 activated platelets (1:100 macrophages : platelets). Percentage expression of B) iNOS, C) RELMα, and D) Ym1 on BM-Mϕ. No platelets (black), resting platelets (blue), activated platelets (pink), agonist only (grey). Statistical significance was determined using one-way ANOVA with post-hoc Tukey's test on the mean of each stimulation group. Representative of a single experiment. Symbols indicate technical replicates. Non-significance ($p>0.05$) not shown.

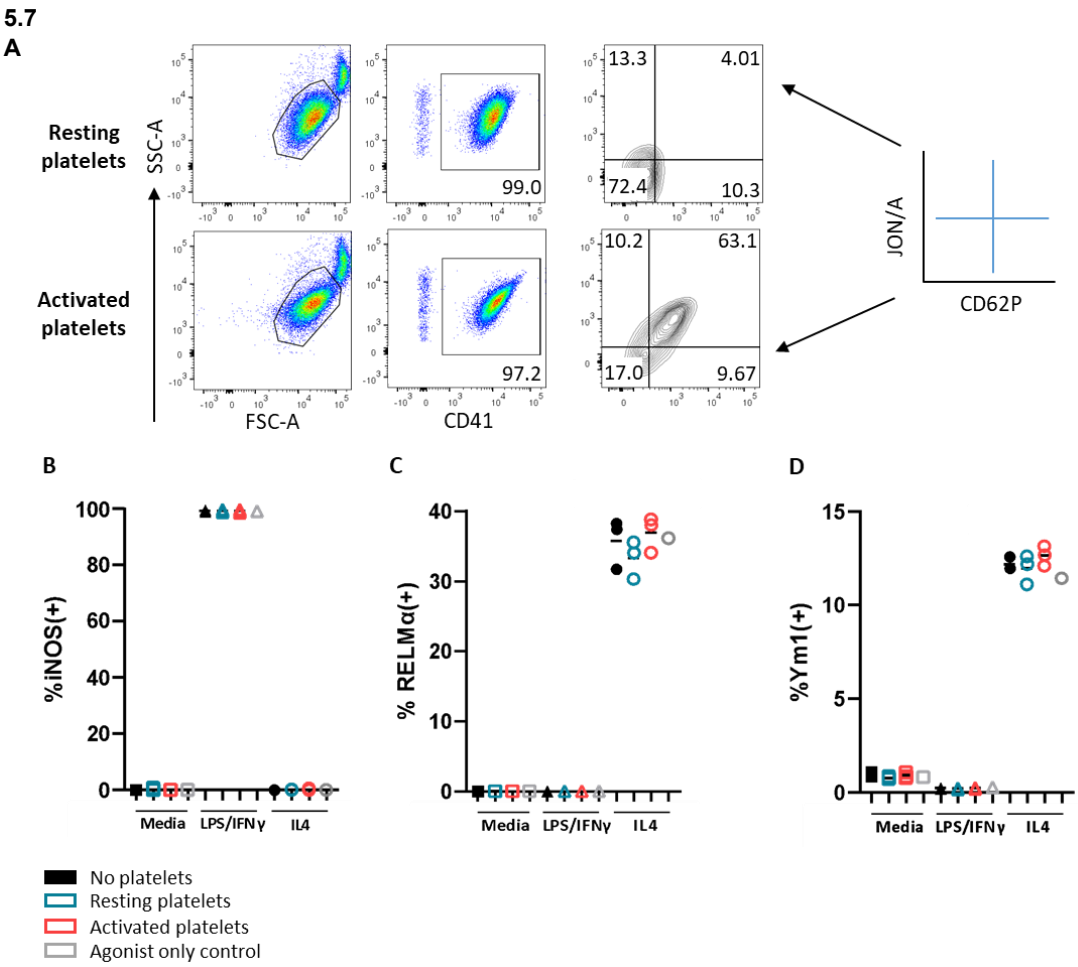

Figure 5.7 Activated platelets do not affect polarisation of BM-Mϕ

A) Isolated murine platelets activated with 150μM PAR4 agonist for 30min before analysis by flow cytometry. BM-Mϕ stimulated with LPS/IFNγ (100ng/ml 10ng/ml) or IL-4 (20ng/ml) and co-cultured overnight with naive resting or PAR4 activated platelets (1:100 macrophages : platelets). Activated platelets were thoroughly washed prior to addition to BM-Mϕ. No platelets (black), resting platelets (blue), activated platelets (pink), agonist only (grey). Representative of 2 independent experiments. Statistical significance was determined using one-way ANOVA with post-hoc Tukey's test on the mean of each stimulation group. Non-significance ($p>0.05$) not shown. Symbols indicate technical replicates.

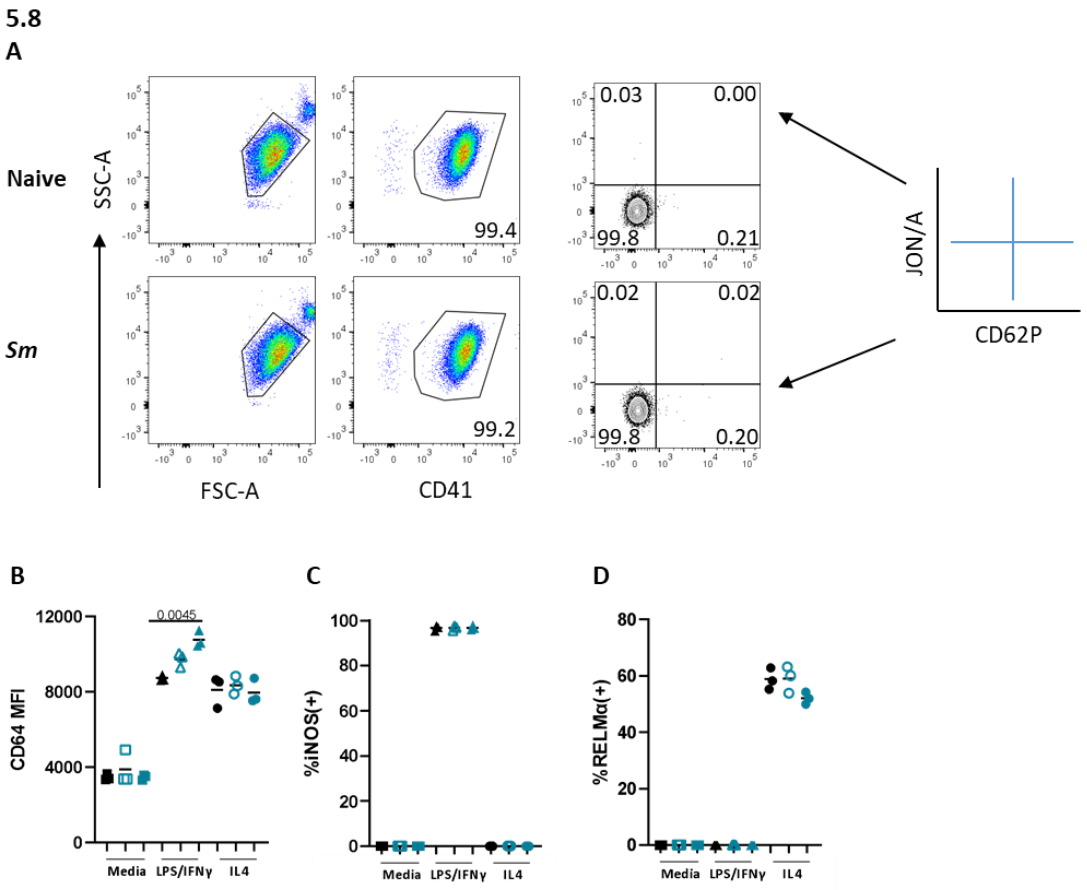

Figure 5.8 Infected platelets do not significantly affect the polarisation of IL-4 stimulated BM-Mϕ

A) Isolated platelets from naive and 10-12 week schistosome-infected mice analysed for activation by flow cytometry. BM-Mϕ stimulated with LPS/IFNγ (100ng/ml 10ng/ml) or IL-4 (20ng/ml) and co-cultured overnight with naive or infected platelets (1:100 macrophages : platelets). Mean fluorescent intensity of B) CD64 and percentage expression of C) iNOS and D) RELMα from 3 independent experiments. Symbols indicate technical replicates. Statistical significance was determined using one-way ANOVA with post-hoc Tukey's test on the mean of each stimulation group. Non-significance ($p>0.05$) not shown.

5.9

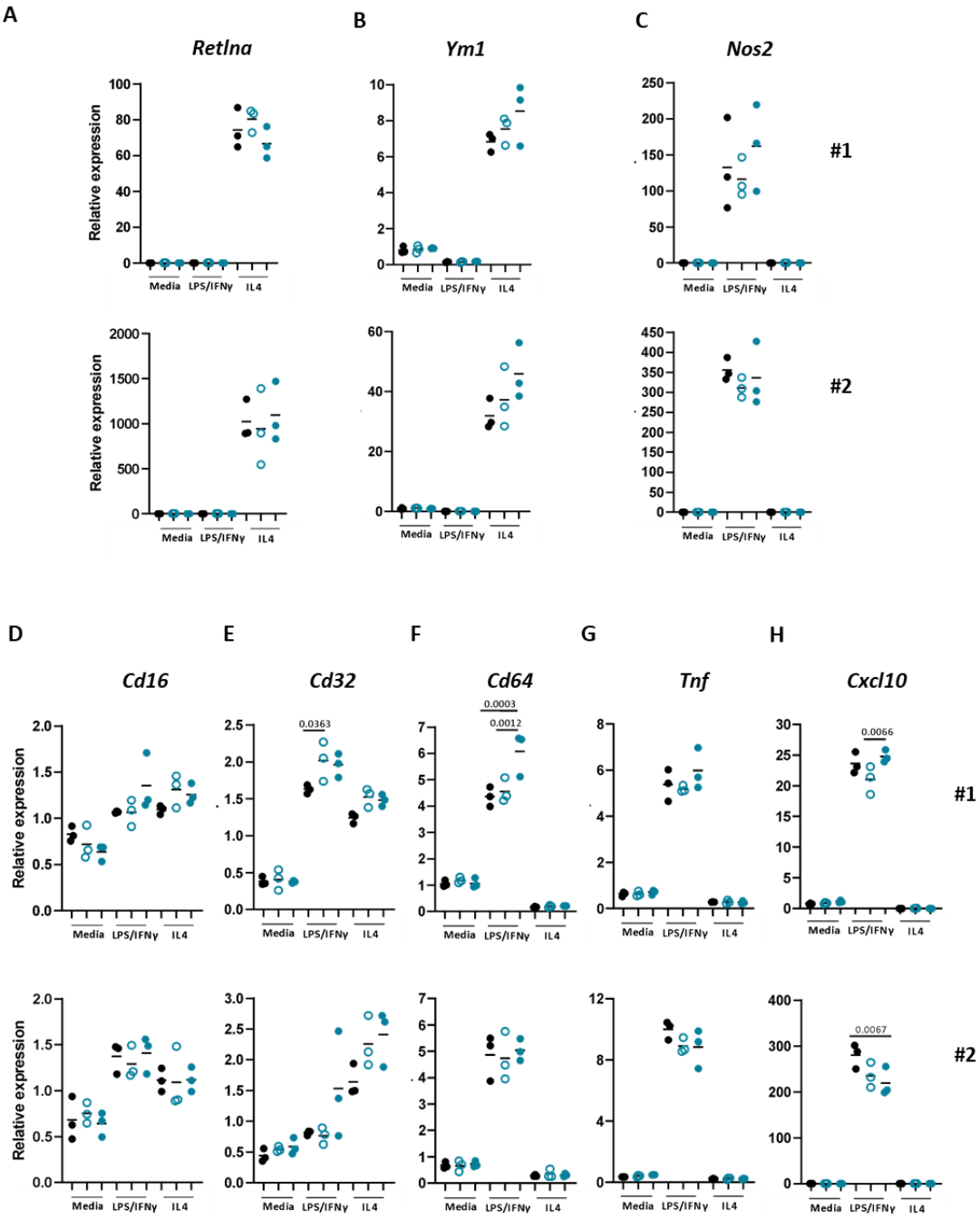

Figure 5.9 No reproducible differences of markers at the transcriptional level in the presence of platelets

BM-Mϕ stimulated with LPS/IFNγ (100ng/ml 10ng/ml) or IL-4 (20ng/ml) and co-cultured overnight with naive or infected platelets (1:100 macrophages : platelets) from 2 independent experiments (#1 and #2). Relative mRNA levels of A) *Retlna,* B) *Ym1*, C) *Nos2,* D) *Cd16*, E) *Cd32,* F) *Cd64*, G) *Tnf* and H) *Cxcl10* normalised to *Hprt* housekeeping gene. Symbols indicate technical replicates. Statistical significance was determined using one-way ANOVA with post-hoc Tukey's test on the mean of each stimulation group. Non-significance ($p>0.05$) not shown.

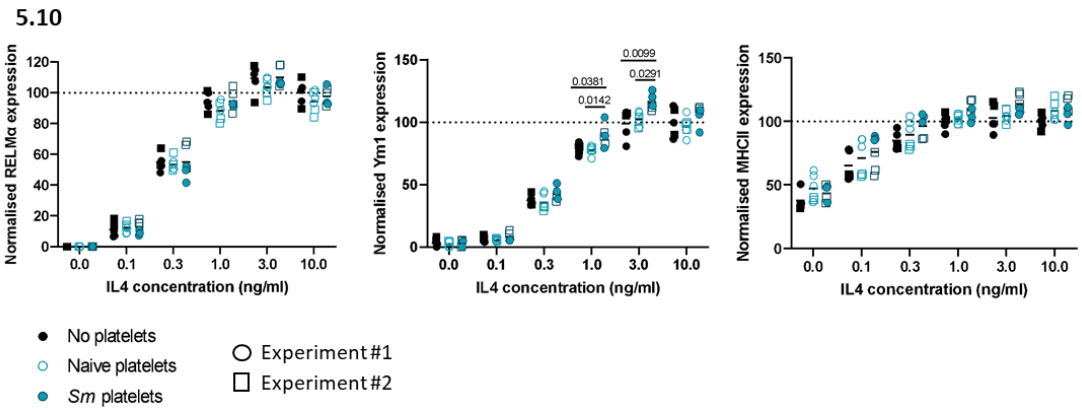

Figure 5.10 Naive and infected platelets have minimal effect on BM-Mϕ polarisation following stimulation with a range of IL-4 concentrations

BM-Mϕ stimulated with varying concentrations of IL-4 (0.1-10ng/ml) and co-cultured overnight with naive or infected platelets (1:100 macrophages : platelets). Protein expression of RELMα, Ym1 and MHCII from 2 independent flow cytometry experiments normalised to 10ng/ml IL-4, no platelet control group. No platelets (black), Naive platelets (blue outline), *Sm* platelets (blue), circles (experiment #1), squares (experiments #2). Symbols indicate technical replicates. Statistical significance was determined using one-way ANOVA with post-hoc Tukey's test on the mean at each IL4 concentration. Non-significance (>0.05) not shown.

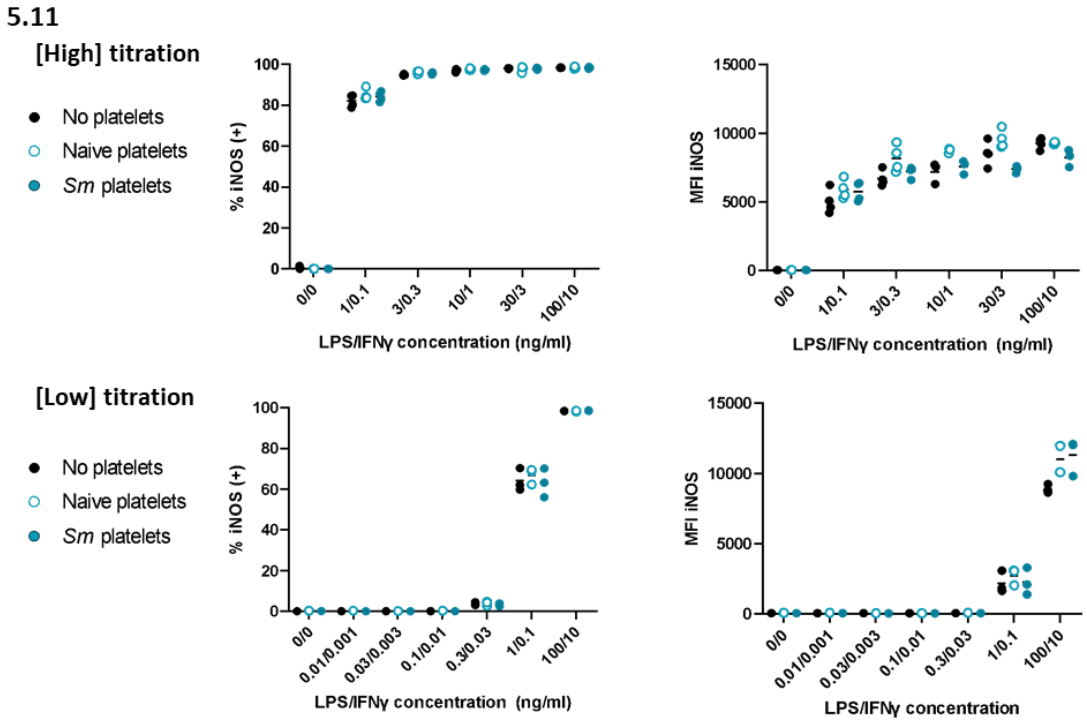

Figure 5.11 No effect of platelets on LPS/IFNγ-induced iNOS by macrophages

BM-Mϕ stimulated with varying concentrations of LPS/IFNγ, [High] – 1ng/ml LPS 0.1ng/ml IFNγ or [Low] 0.01ng/ml LPS 0.001ng/ml. 0.1-10ng/ml IFNγ. Samples co-cultured overnight with naive or infected platelets (1:100 macrophages : platelets). Percentage and MFI of iNOS. Representative of 2 independent experiments. No platelets (black), Naive platelets (blue outline), Sm platelets (blue). Symbols indicate technical replicates. Statistical significance was determined using one-way ANOVA with post-hoc Tukey's test on the mean at each LPS/IFNγ concentration. Non-significance (p>0.05) not shown.

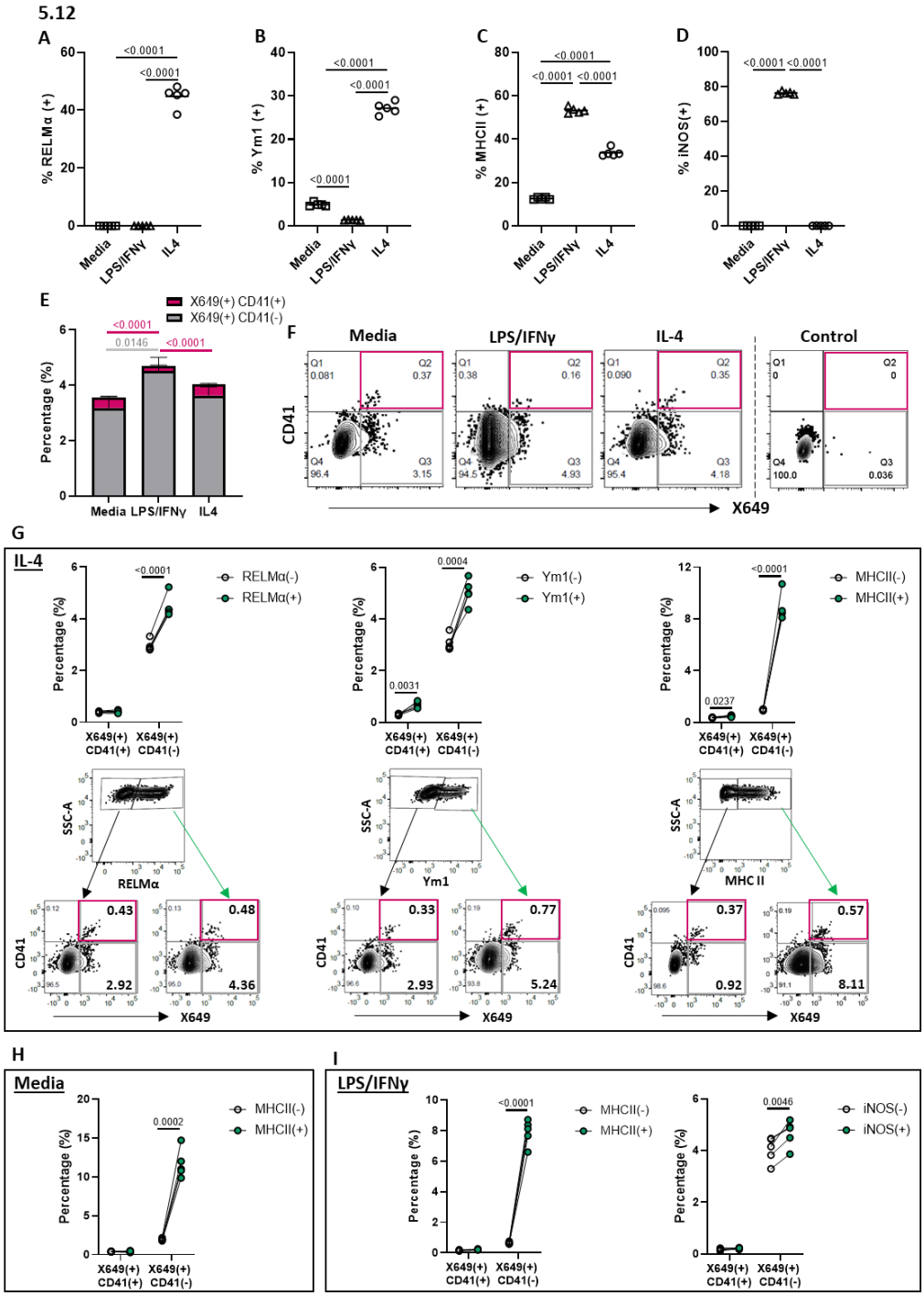

Figure 5.12 Platelets are preferentially internalised by activated macrophages regardless of polarisation signal

1x10^6 BM-Mϕ were stimulated with 1ng/ml LPS, 0.1ngml IFNγ, or 10ng/ml IL-4 overnight. 1x10^8 platelets from naive mice were cultured for 20hr and samples assessed by flow cytometry. Percentage expression of A) RELMα, B) Ym1, C) MHC II and D) iNOS. E) Percentage expression and F) representative FACS plots of X649 and CD41 expression on detached macrophages. (Grey – internalised X649$^+$CD41$^-$, Pink – surface-bound X649$^+$ CD41$^+$) Percentage expression and representative FACS plots of G) IL-4, H) media alone and I) LPS/IFNγ stimulated macrophages. Statistical significance was determined using one-way ANOVA with post-hoc Tukey's test on the mean for each treatment group (A-E) and paired t-test (G-I). Symbols represent 5 technical replicates from a single experiment. Non-significance (p>0.05) not shown.

5.3.2 Do platelets affect the ability of differentially polarised macrophages to phagocytose *E. coli*?

Having shown that platelets from naive and schistosome-infected mice had subtle effects on macrophage polarisation in terms of their expression of markers such as iNOS, Ym1 and RELMα, we next explored whether platelets affected the phagocytic capacity of differentially polarised macrophages. Our *in vivo* experiments showed there to be increased platelet-macrophage interactions in schistosome infection, thereby offering multiple opportunities for platelets to modulate macrophage activity. Altered phagocytosis *in vivo* during infection could be both beneficial and detrimental. For example, if macrophages were able to phagocytose opportunistic pathogens as a result of intestinal breach following egg transit, this would support host survival by reducing excessive inflammation and immunopathology (227). However, enhanced phagocytosis of cells/debris as a result of inflammation may "switch-off" macrophages preventing their anti-microbial capacity and ability to attack parasites or limiting their tissue-repair and wound healing response (322).

In initial experiments, we used FITC-conjugated latex beads to measure macrophage phagocytosis (**Figure 5.13**). However, this approach is not suitable for longitudinal studies, and it is difficult to distinguish between beads binding to the macrophage surface versus beads internalised by phagocytosis. To circumvent these problems we switched to using pH-sensitive *E. coli* bioparticles (383). We first optimised the concentration of *E. coli* bioparticles in macrophage co-cultures to identify a level of bioparticles that gave clear signal to noise ratio for quantification (**Figure 5.14**). Despite the strongest green-fluorescent signal being detected with 10μg of *E. coli* bioparticles (50μg/ml), segmentation analysis was difficult at this high bioparticle concentration due to the settling and aggregation of un-phagocytosed bioparticles. As a consequence, clumps of bioparticles were mis-identified as macrophages and due to the neutral pH of the media, and lack of phagocytosis they did not show any green fluorescence. This gave rise to a bimodal green-fluorescent intensity. As such, we used 5μg of bioparticles in all subsequent experiments to ensure a strong fluorescent phagocytic signal, but with less background noise. Of note, LPS/IFNγ-stimulated macrophages phagocytosed

to a greater degree than IL-4-stimulated populations in these initial optimisation experiments.

In order to examine the phagocytic capacity of individual cells over the 20hr time-course, we looked at single-cell fluorescent trajectories. We established an experiment-specific fluorescent threshold using *E. coli*-only and macrophage-only control wells (**Figure 5.15A-C**). Cells that passed this threshold were classed as having phagocytosed a sufficient number of bioparticles to be detected as fluorescent. Using this gating strategy, we were also able to identify a number of cells that passed the threshold but subsequently fell below it, as well as those that never passed the threshold (**Figure 5.15D-F**). This revealed that 10μg *E. coli* bioparticles was potentially too high for the more-phagocytic LPS/IFNγ-stimulated macrophages which showed the greatest percentage of cells that passed the threshold but then fell below it (**Figure 5.15G**). Interestingly, it demonstrated that with bioparticles in excess (10μg), more than 90% of all cells passed the fluorescent threshold at some point during the time course (**Figure 5.15H-J**). With all concentrations of *E. coli* bioparticles M2-like macrophages being the slowest to reach maximum phagocytic capacity.

We next explored whether platelets affected the ability of macrophages to phagocytose *E. coli* bioparticles. Macrophages were stimulated and cultured overnight with platelets (100:1 platelets:macrophages) before adding *E. coli* bioparticles and imaging longitudinally (**Figure 5.16A-D**). We observed a large degree of variation in both mean green intensity and percentage passing the fluorescent threshold across four independent experimental replicates (**Figure 5.17**). The macrophages, particularly those lacking additional cytokine stimulation, failed to survive as well in experiments 3 and 4, and there was significantly less phagocytosis. This was the case despite fresh reagents (including new bioparticles) being used. However, taking all the experiments into consideration, it can be concluded that both M1 and M2 polarised macrophages phagocytosed *E. coli* bioparticles to a greater extent than the control M0 population, with M1 being more phagocytic than M2-like macrophages. Direct comparisons of mean green intensity and percentage of macrophages passing the fluorescent threshold in the presence or absence of

platelets showed a minor, yet significant increase in phagocytic capacity of M0 macrophages in the presence of platelets (**Figure 5.17A, D**). In contrast, platelets did not alter phagocytosis of M1 macrophages (**Figure 5.17B, E**). Importantly, co-culture of IL-4 stimulated macrophages with platelets consistently resulted in significantly enhanced phagocytosis of bioparticles, showing that platelets did indeed alter the activity of M2 macrophages (**Figure 5.17C, F**). Individual cell trajectories for the different treatments and conditions were compared with respect to cells passing a fluorescent threshold, but this did not reveal significant differences (data not shown).

Having shown that platelets could significantly increase the ability of M2 macrophages to phagocytose targets, we next asked whether platelets from infected mice had similar effects to those from naive mice. We reasoned this could result in enhanced phagocytic activity in a schistosome infection where platelet-macrophage interactions are elevated. As before, macrophages were polarised to M1-like or M2-like phenotypes, this time in the presence or absence of platelets from naive and infected mice prior to bioparticle addition (**Figure 5.18A-C**). The three experimental repeats showed there was very little difference in the phagocytosis of bioparticles by media and LPS/IFNγ treated macrophages in the presence of platelets from naive or infected mice (**Figure 5.18D-E**). Whilst we again found enhanced phagocytosis by IL-4 stimulated macrophages in the presence of platelets from naive mice, platelets from schistosome-infected mice did not enhance phagocytosis of M2-like macrophages to the same extent, so revealing an important difference between platelets from naive and schistosome-infected animals (**Figure 5.18F**).

Given both phagocytosis and motility involve cytoskeletal reorganisation, we next wanted to explore whether changes in phagocytic ability -/+ platelets from naive and infected mice were coincident with altered macrophage motility. Single cell analysis of macrophage displacement over the 20hr, within each well after normalisation to the origin (0,0) was assessed (each cell represented by a different coloured line) (**Figure 5.19A-C**). This showed M0 macrophages to be more motile than both M1- and M2-like populations. In the case of both the media alone and IL-4 stimulation conditions, the presence of platelets

inhibited the displacement of macrophages over the time-course, however platelets had no effect on LPS/IFNγ-stimulated macrophage motility **(Figure 5.19D)**.

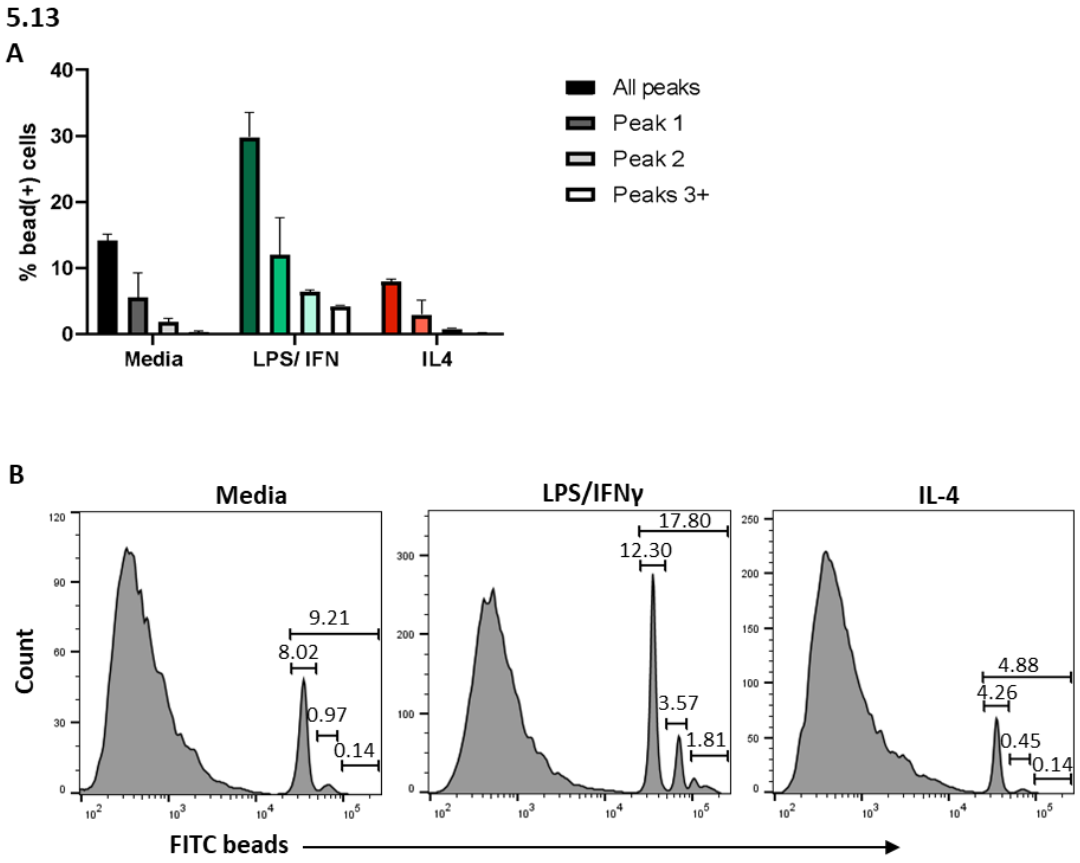

Figure 5.13 M1-like macrophages phagocytose latex beads to the greatest extent
1x10^6 BM-Mϕ stimulated with LPS/IFNγ (100ng/ml 10ng/ml) or IL-4 (20ng/ml) overnight. FITC-latex beads (2μm) added at a ratio of 1:10 (macrophages:beads) for 1.5hr. A) Percentage of bead uptake and B) example flow cytometry histograms of bead uptake. Gates were drawn from trough to trough. Data representative of 3 independent experiments. Symbols indicate technical replicates. Statistical significance was determined using one-way ANOVA with post-hoc Tukey's test on the mean for each peak between stimulation treatments. Non-significance ($p>0.05$) not shown.

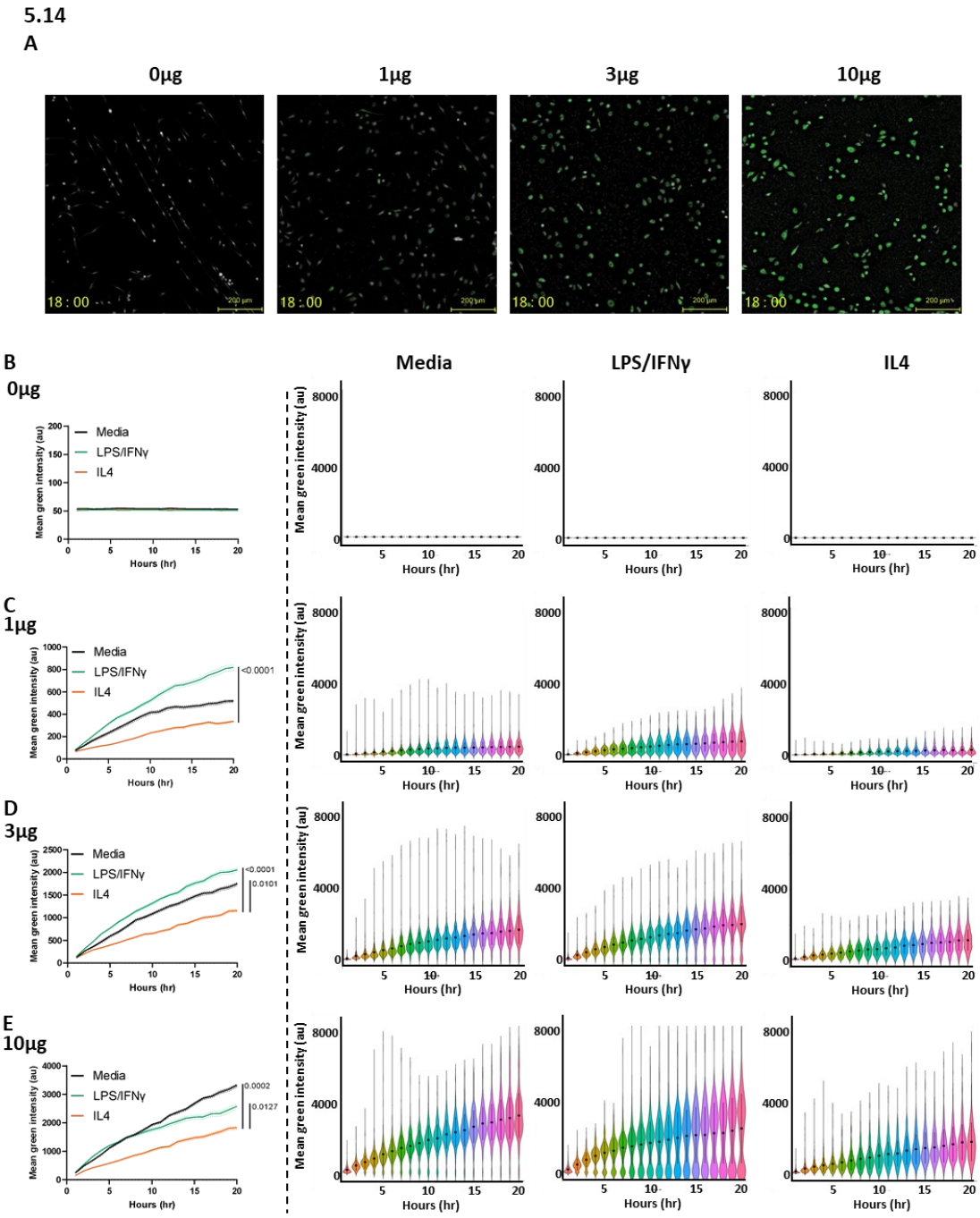

Figure 5.14 10µg E. coli bioparticles was too high for phagocytosis quantification
1x10^4 BM-Mϕ stimulated with LPS/IFNγ (100ng/ml 10ng/ml) or IL-4 (20ng/ml) overnight. Varying concentrations (1-10µg) of *E. coli* bioparticles were added per well and immediately imaged every 15min on the LiveCyte for 18hrs. A) Representative end-frame still images from IL-4 stimulated macrophages. Mean green intensity and treatment well variation were calculated for B) 0µg, C) 1µg, D) 3µg and E) 10µg *E. coli* bioparticles. Representative of a single experiments. Line represents mean and dotted lines represent SE of the mean for 4 technical replicates. Statistical significance was determined using one-way ANOVA with post-hoc Tukey's test on the area under the curve. Non significance (p>0.05) not shown.

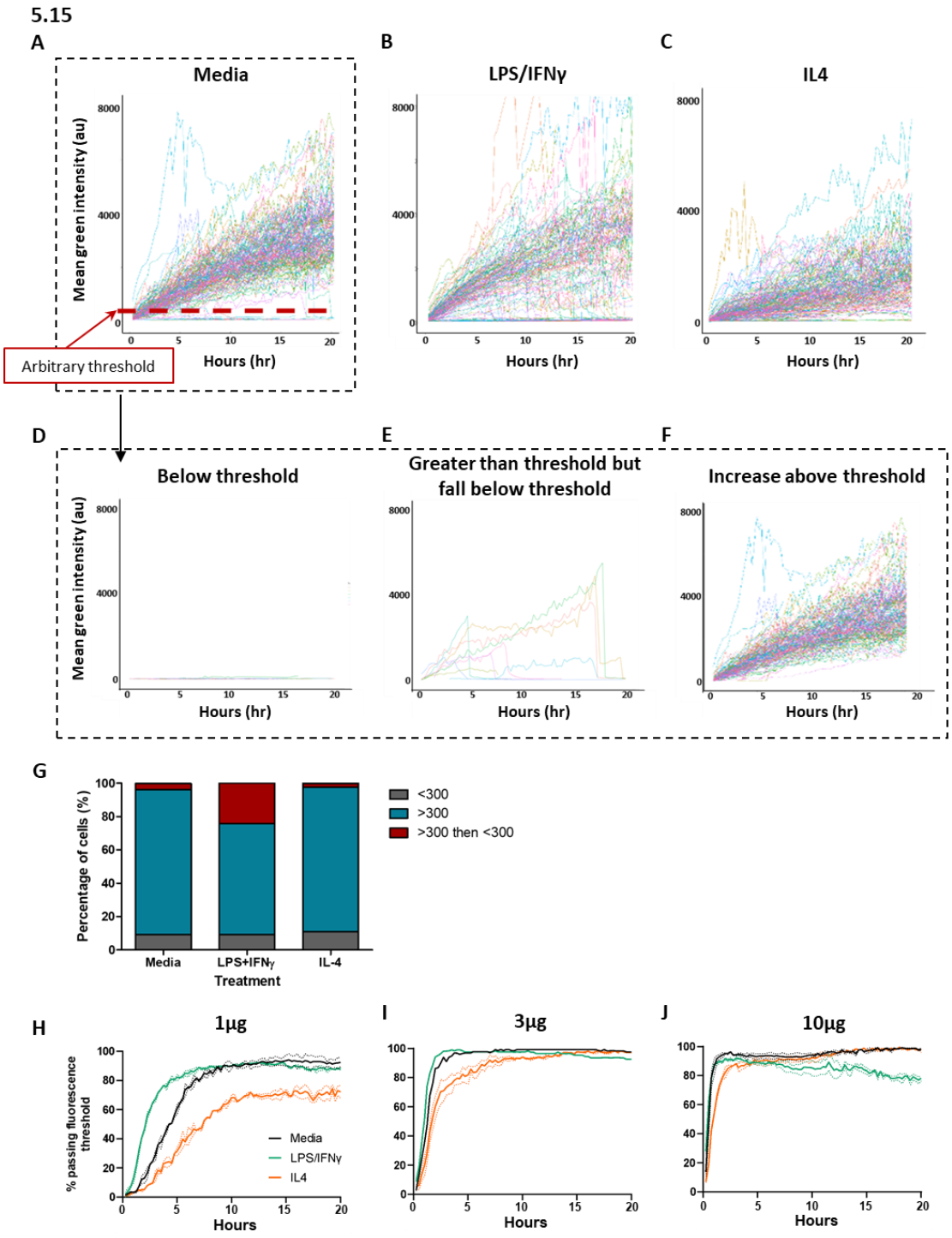

Figure 5.15 Individual cell fluorescent trajectories over 18hr

Mean green intensity of every cell within a well for each frame of the 18hr time-course following A) no, B) LPS/IFNγ or C) IL-4 treatment. This allowed for calculation of percentage cells passing fluorescent threshold over the time course. Example trajectories of cells which D) never pass the threshold, E) pass the threshold but fall below it, or F) cells which pass the threshold and remain above it. G) Percentage of cells falling within the three threshold categories after stimulation. Comparison of cells which pass the threshold and remain above it when cultured with H) 1µg, I) 3µg or J) 10µg *E. coli* bioparticles. Representative of a single independent experiment with 4 technical replicates for each condition.

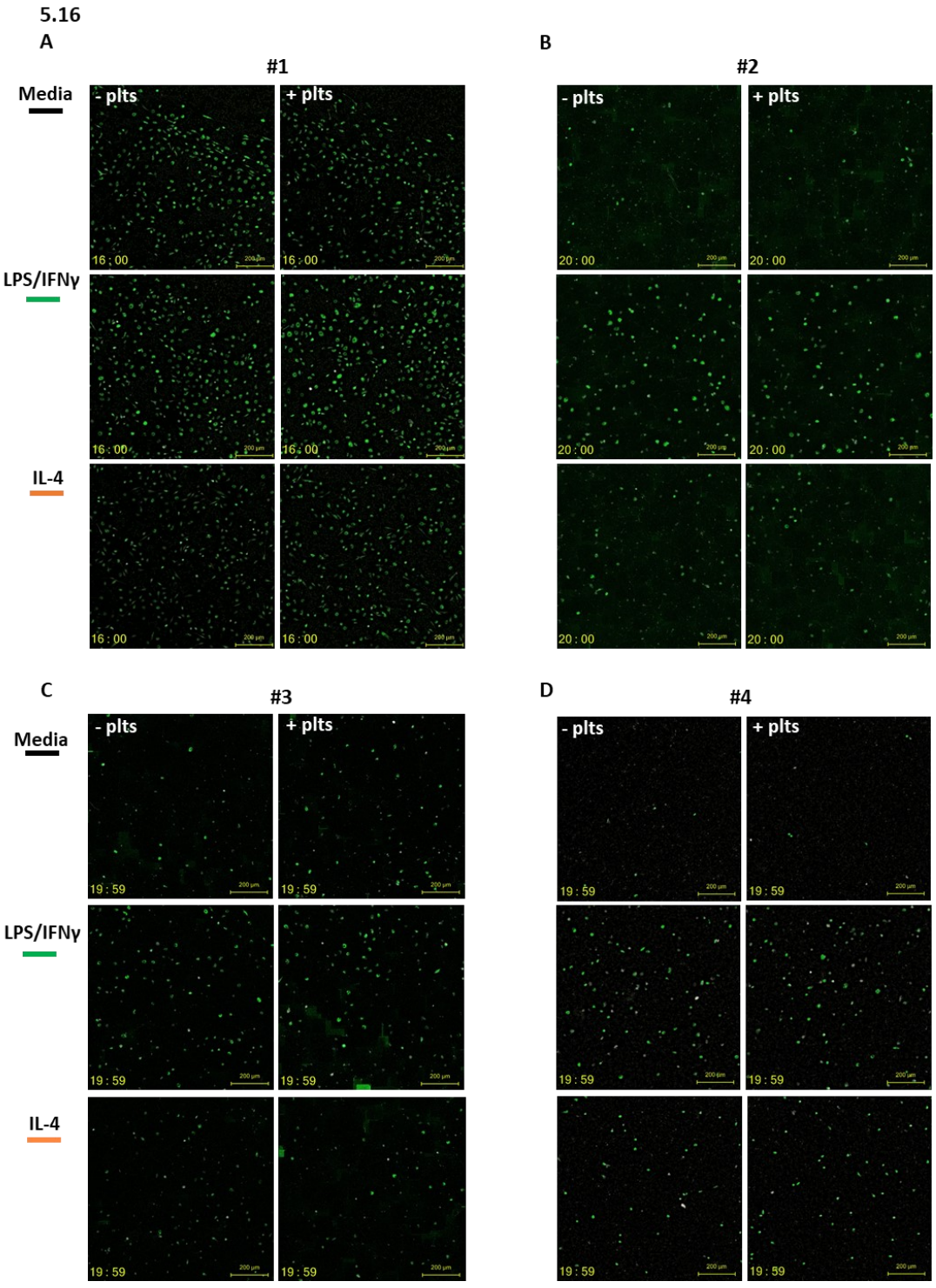

Figure 5.16 Polarised macrophages phagocytose E. coli to a greater extent than M0 populations

1x10^4 BM-Mϕ stimulated with LPS/IFNγ (100ng/ml 10ng/ml) or IL-4 (20ng/ml) overnight followed by treatment with 5µg *E. coli* bioparticles. Wells imaged every 15min on the LiveCyte for 20hr. Representative end-frame still images from 4 independent experiments in the presence or absence of platelets (A-D).

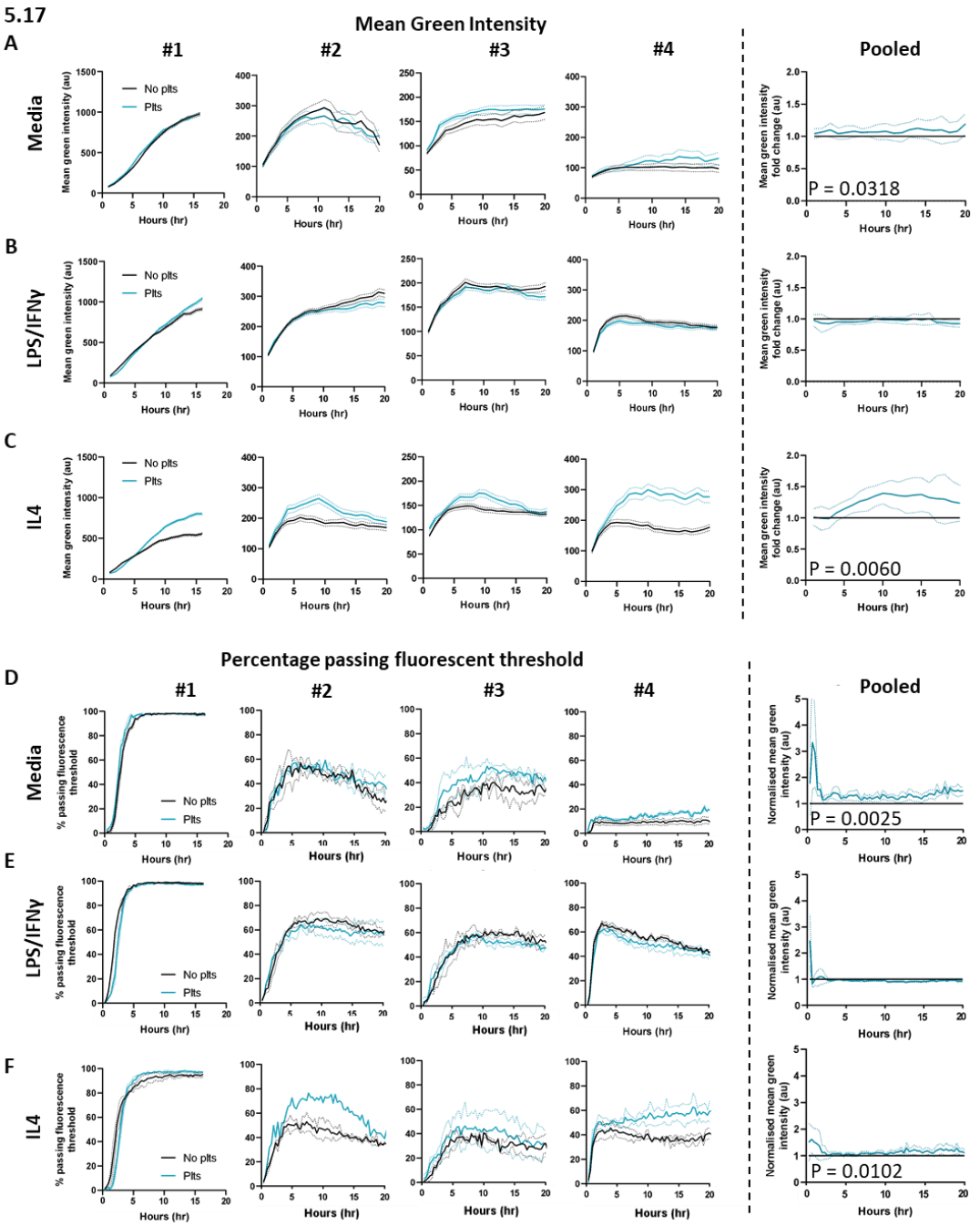

Figure 5.17 Platelets enhance IL-4 polarised macrophages phagocytosis of E. coli bioparticles 1.5 fold

1x10^4 BM-Mϕ stimulated with LPS/IFNγ (100ng/ml 10ng/ml) or IL-4 (20ng/ml) overnight followed by treatment with 5µg *E. coli* bioparticles. Wells imaged every 15min on the LiveCyte for 20hr. Mean green intensity and normalised mean green intensity for A) media, B) LPS/IFNγ and C) IL-4 treated macrophages from 4 independent experiments. Percentage passing threshold and normalisation for D) media, E) LPS/IFNγ and F) IL-4-treated macrophages. Solid line represents mean of 3-4 technical replicates with standard error (dotted line). Statistical significance was determined using unpaired t-tests, assuming unequal variance on the area under the curve. Non significance (p>0.05) not shown.

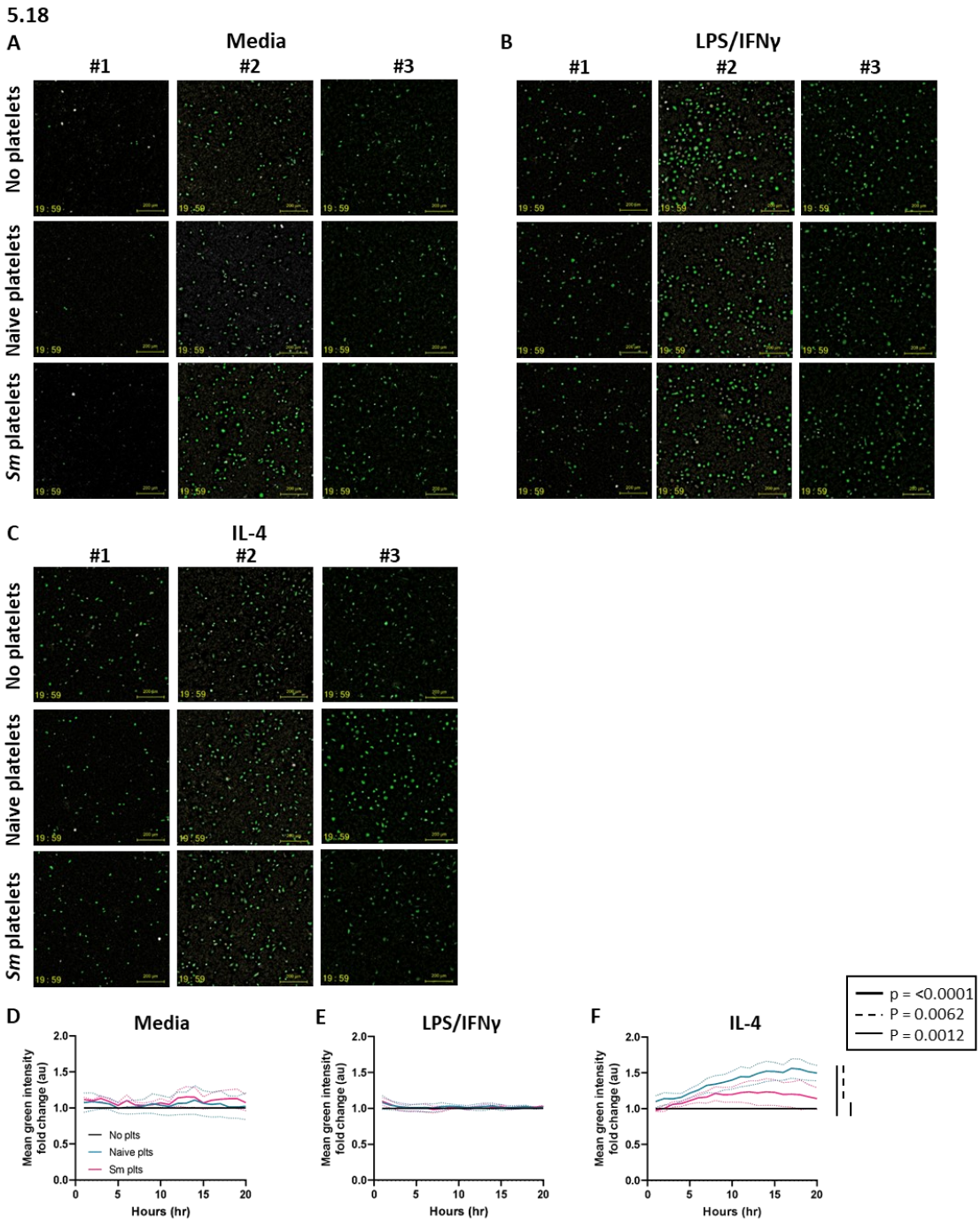

Figure 5.18 Both naive and infected platelets enhance IL-4 polarised macrophages phagocytosis of E. coli bioparticles

1x10^4 BM-Mϕ stimulated with LPS/IFNγ (100ng/ml 10ng/ml) or IL-4 (20ng/ml) and co-cultured with 1x10^6 naive or schistosome infected platelets overnight followed by treatment with 5μg *E. coli* bioparticles. Wells were imaged every 15min on the LiveCyte for 20hr. Representative end-frame still images of A) media, B) LPS/IFNγ and C) IL-4 treated macrophages. Mean green intensity normalised to the no platelet control group from 3 independent experiments, from D) media, E) LPS/IFNγ and F) IL-4 treated macrophages. Solid line represents mean of 3-4 technical replicates with standard error (dotted line). Statistical significance was determined using one-way ANOVA with post-hoc Tukey's test on the area under the curve. Non-significance not shown (p>0.05).

5.19

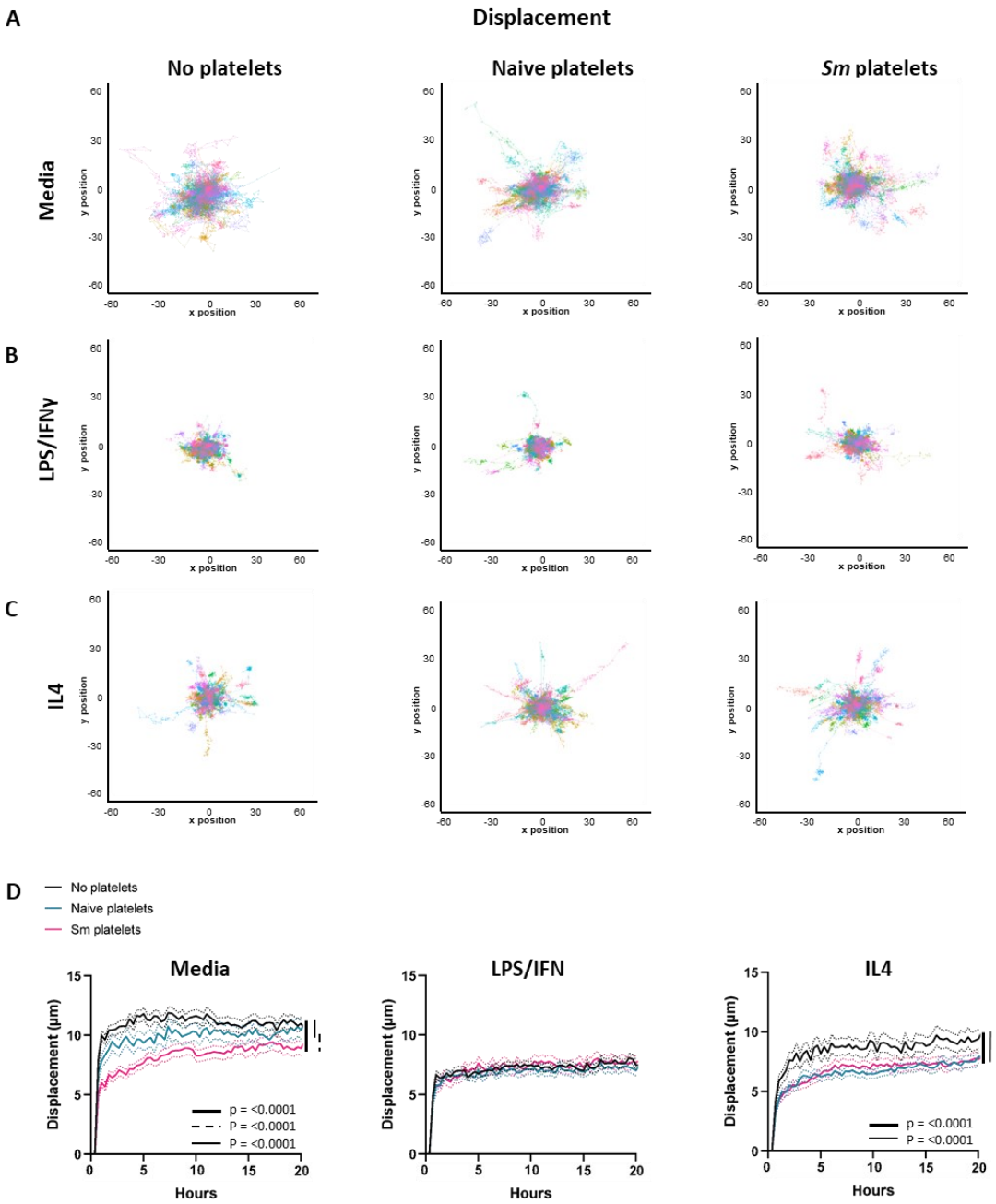

Figure 5.19 Subtle differences in macrophage displacement

Mean green intensity normalised to media control treatment from each of the 4 independent experiments. Solid line represents mean of 3-4 technical replicates with standard error (dotted line). Statistical significance was determined using one-way ANOVA with post-hoc Tukey's test on the area under the curve. Non-significance not shown (p>0.05).

5.3.3 Do differentially polarised macrophages phagocytose platelets?

Having observed the impact of platelets on the ability of M2 macrophages to phagocytose *E. coli* bioparticles, we wanted to assess whether this was a result of differences in platelet uptake by the M2-like population. To do this, we again used live-cell imaging to examine whether specifically polarised macrophage subsets had a different propensity for phagocytosing platelets. To visualise the phagocytosis of platelets over time, and to differentiate between internalised platelets compared with those adhered to the surface, we labelled platelets with a pH sensitive rhodamine fluorescent (pHrodo) dye. As with pH-sensitive *E. coli* bioparticles, pHrodo-labelled platelets do not fluoresce at neutral pH in culture media, but a fluorescent signal is detected following entry into the acidic phagolysosome of the macrophages (384).

Initial experiments revealed platelet labelling with the pHrodo dye caused a significant shift in FSC-A and SSC-A (**Figure 5.20A**). Lower pHrodo dye concentrations and DMSO controls (0.2-1% $_{(v/v)}$) were tested to reduce these morphological changes. In addition, markers of activation (activated integrin αIIbβIII (JON/A) and CD62P) were also included to check for platelet activation as an artefact of the isolation and labelling process. This showed that even half the initial concentration (0.1mM pHrodo dye) resulted in a significant upregulation of JON/A and CD62P (**Figure 5.20B-D**). As these changes in size and activation were not observed in the DMSO control (**Figure 5.20B**), it suggested the incorporation of pHrodo dye itself was causing platelet activation. To avoid this, we labelled with a further 5-fold reduced concentration of pHrodo dye (0.02mM) and included prostaglandin E1 during labelling to minimise the risk of platelet activation occurring at any other stages throughout the process. Together, this resulted in minimal platelet activation. Notably, whilst platelets labelled in this way exhibited substantial fluorescence even at neutral pH when measured by flow cytometry (blue histogram peak), there was still a substantial shift at lower pH with MFI increasing 6-fold (blue to red histogram peaks) (**Figure 5.20E-F**). This fluorescence detected in neutral conditions likely reflects the greater sensitivity of flow cytometry compared with LiveCyte microscopy used for longitudinal live-cell imaging assays (384).

A preliminary platelet phagocytosis assay was performed comparing the phagocytosis of resting versus PAR4-activated platelets. It is known that exogenously activated platelets express more surface PS (352,385), which is recognised by macrophages and drives phagocytosis (386). Here we showed that all subsets of macrophages phagocytosed platelets and this was enhanced when cultured with activated platelets (**Figure 5.21A-B**). Interestingly, the percentage of macrophages passing the red fluorescent threshold (<15%) was less than the percentage phagocytosing *E. coli* bioparticles (up to 100%). In **Chapter 4**, we showed schistosome infection did not cause any changes in platelet activated integrin αIIbβIII, CD62P, or multiple other surface markers, but did cause a moderate increase in PS alongside desialylation. Moreover, in **Chapter 3** we found that platelets were cleared more rapidly during schistosome infection. As such, we wanted to test whether platelets from infected mice were cleared faster than platelets from naive mice, and whether this was impacted by differential macrophage polarisation. Here, M1-like macrophages took up platelets from naive and infected mice significantly more than resting or M2-like macrophages (**Figure 5.22A**). There was no significant difference in uptake of platelets from naive and infected mice for M0 and M1-like macrophages, but despite experiment-to-experiment variation, data normalised across multiple experiments revealed a significant increase in uptake of platelets from infected mice compared with naive platelets by M2-like macrophages (**Figure 5.22B**).

Finally, we were interested to look at the effects of platelets and their phagocytosis on macrophage motility. In these experiments we showed IL-4-stimulated macrophages to be the most motile in all platelet conditions and platelets from naive or infected mice did not affect macrophage motility during the 20hr imaging time-course (**Figure 5.23**). Visual inspection of the individual cells in M1 conditions revealed that despite M1-like macrophages having minimal displacement, cells were still motile and moved small distances back and forth which was not accounted for by displacement analysis. However, there was no significant difference in the total track length over 20hr between different macrophage populations in the presence or absence of platelets from naive or infected mice (**Figure 5.24A**). We also confirmed that after

phagocytosing platelets and “becoming red” the track length remained unchanged (**Figure 5.24B**). Together, indicating that platelet phagocytosis did not alter macrophage motility.

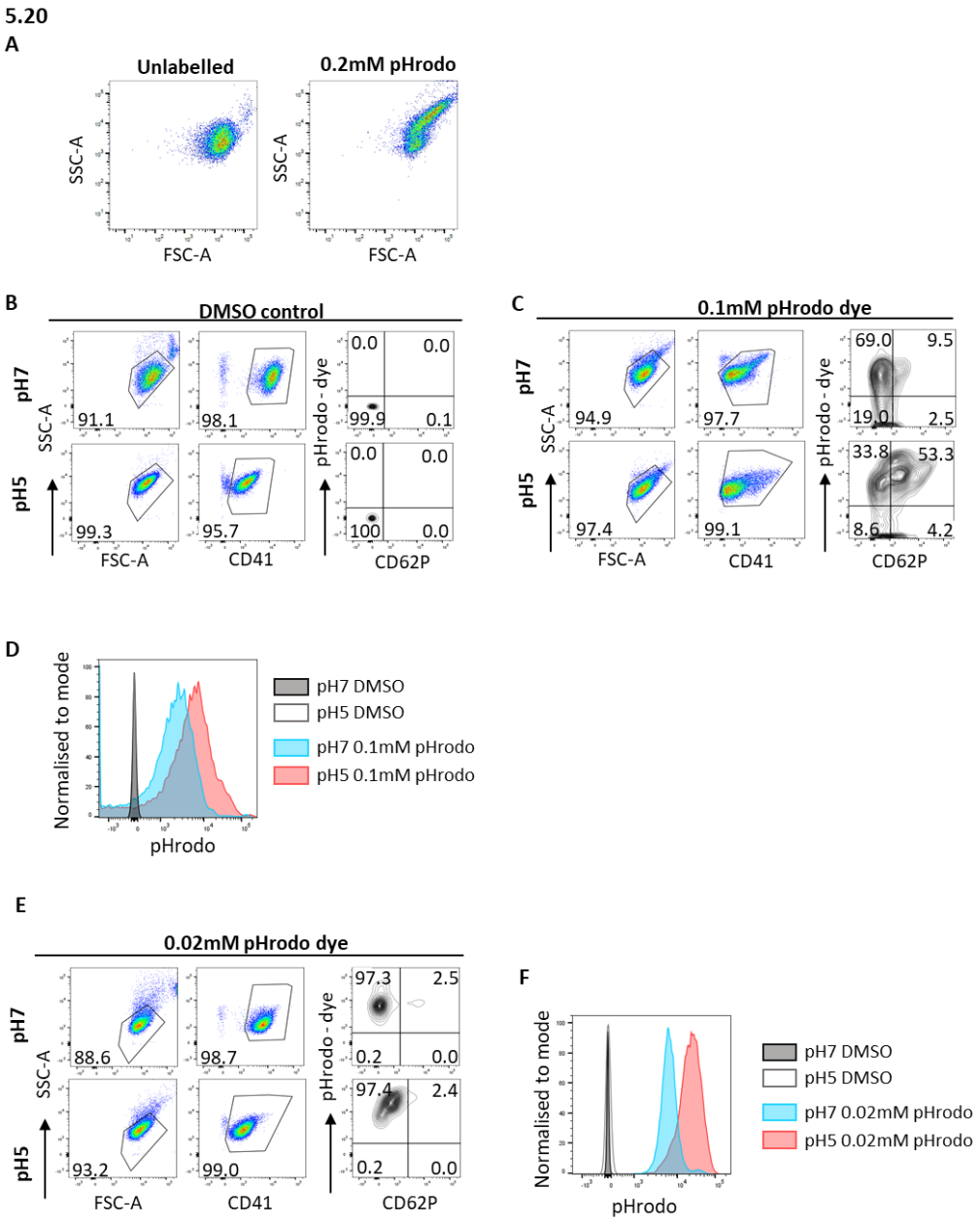

Figure 5.20 Reduced pHrodo concentration and PGE1 allows for labelling in the absence of platelet activation

Whole blood harvested by cardiac puncture and platelets isolated by sequential centrifugation. A) Example FACS staining of $1x10^8$ isolated platelets stained 20min with 0.2mM pHrodo™ Red, succinimidyl ester (pHrodo). Example FACS plots of B) DMSO treated platelet control and C) 0.1mM pHrodo-stained platelets. D) Example histogram overlay of pHrodo-stained platelets at neutral and acidic pH. E) Example FACS plots of platelets stained 20min RT with 0.02mM in PBS/1µM Prostaglandin E1 (PGE1) and F) histogram overlay of pHrodo-stained platelets at neutral and acidic pH.

5.21

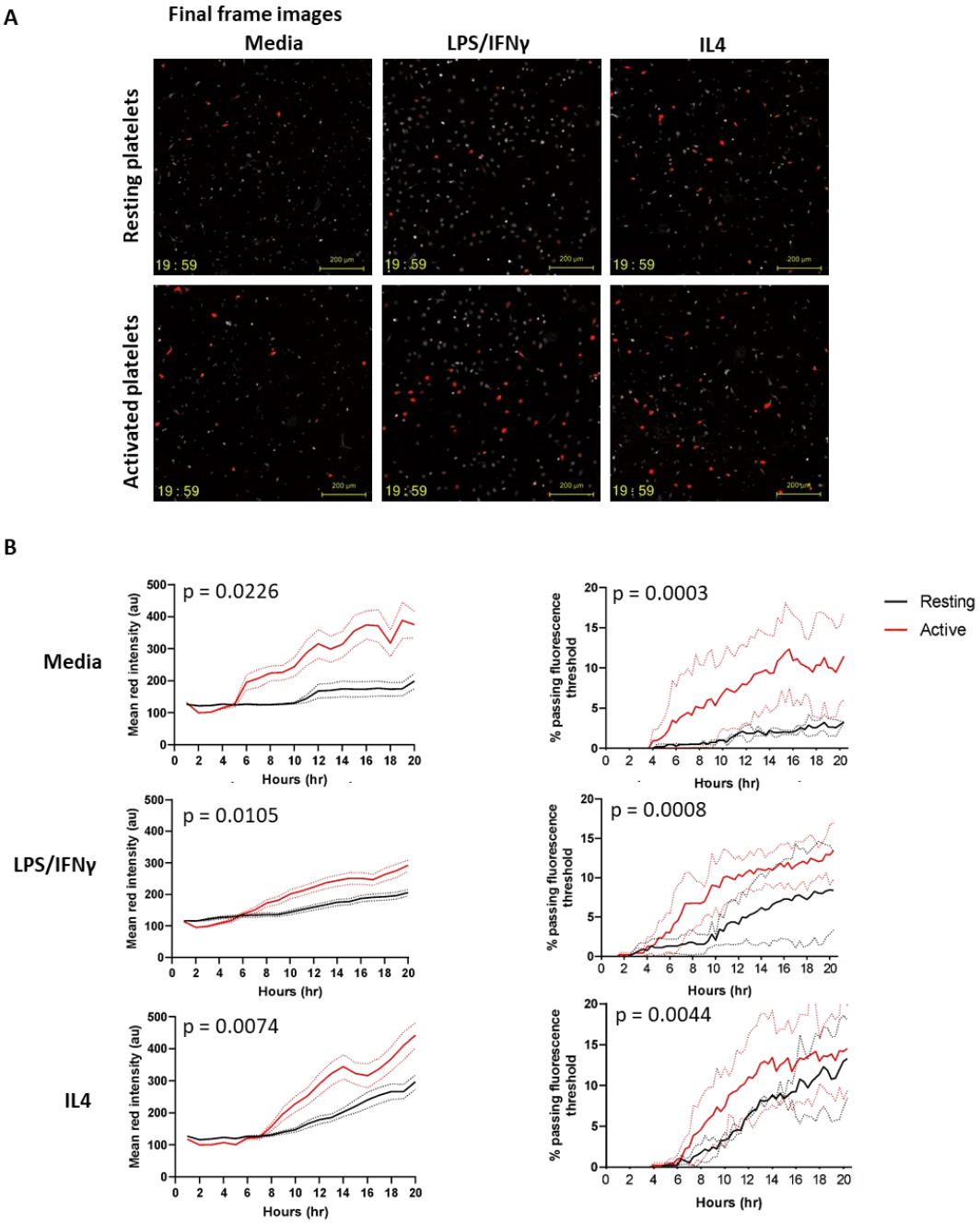

Figure 5.21 All macrophage populations phagocytose activated platelets to a greater extent than resting platelets

1x10^4 BM-Mϕ stimulated with LPS/IFNγ (100ng/ml 10ng/ml) or IL-4 (20ng/ml) overnight. 1x10^6 naive platelets, activated with 150μM PAR4 agonist, labelled with 0.02mM pHrodo dye and added to the macrophages. Wells were imaged every 15min on the LiveCyte for 20hr. A) Representative end-frame still images. B) Mean red intensity and percentage passing fluorescent threshold for resting or activated platelets. C) Direct comparison of phagocytosis of resting and activated platelets by the differentially polarised macrophages. Representative of 2 independent experiments. Solid line represents mean of 3-4 technical replicates with standard error (dotted line). Statistical significance was determined using unpaired t-tests, assuming unequal variance on the area under the curve. Non significance (p>0.05) not shown.

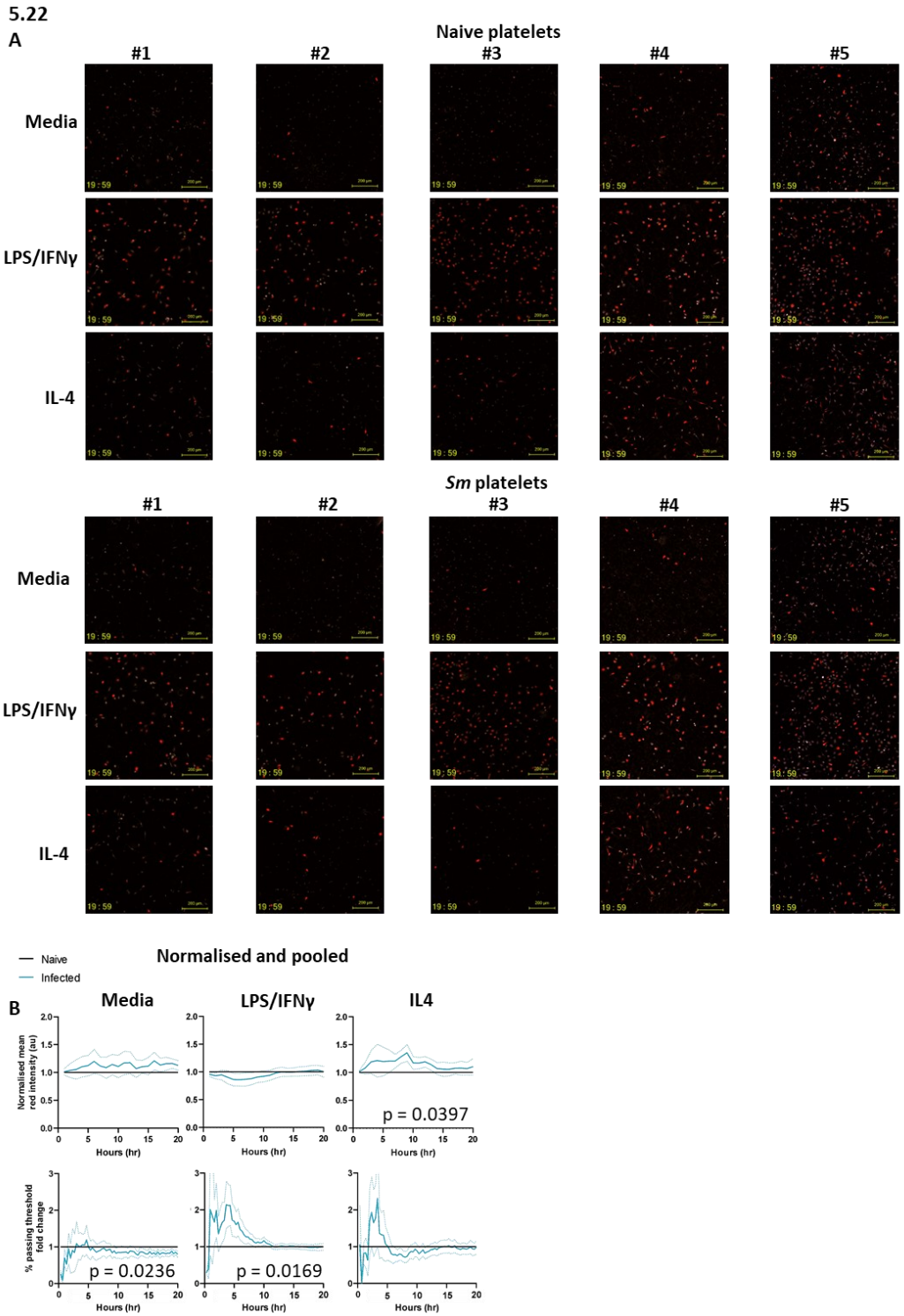

Figure 5.22 Minimal difference in the ability of polarised macrophages to phagocytose naive platelets

$1x10^4$ BM-Mϕ stimulated with LPS/IFNγ (100ng/ml 10ng/ml) or IL-4 (20ng/ml) overnight. $1x10^6$ naive platelets, labelled with 0.02mM pHrodo dye and added to the macrophages. Wells were imaged every 15min on the LiveCyte for 20hr. A) Representative end-frame still images. B) Mean red intensity and percentage passing fluorescent threshold normalised to naive platelet control treatment from each of the 5 independent experiments. Solid line represents mean of 3-4 technical replicates with standard error (dotted line). Statistical significance was determined using unpaired t-tests, assuming unequal variance on the area under the curve. Non significance (p>0.05) not shown.

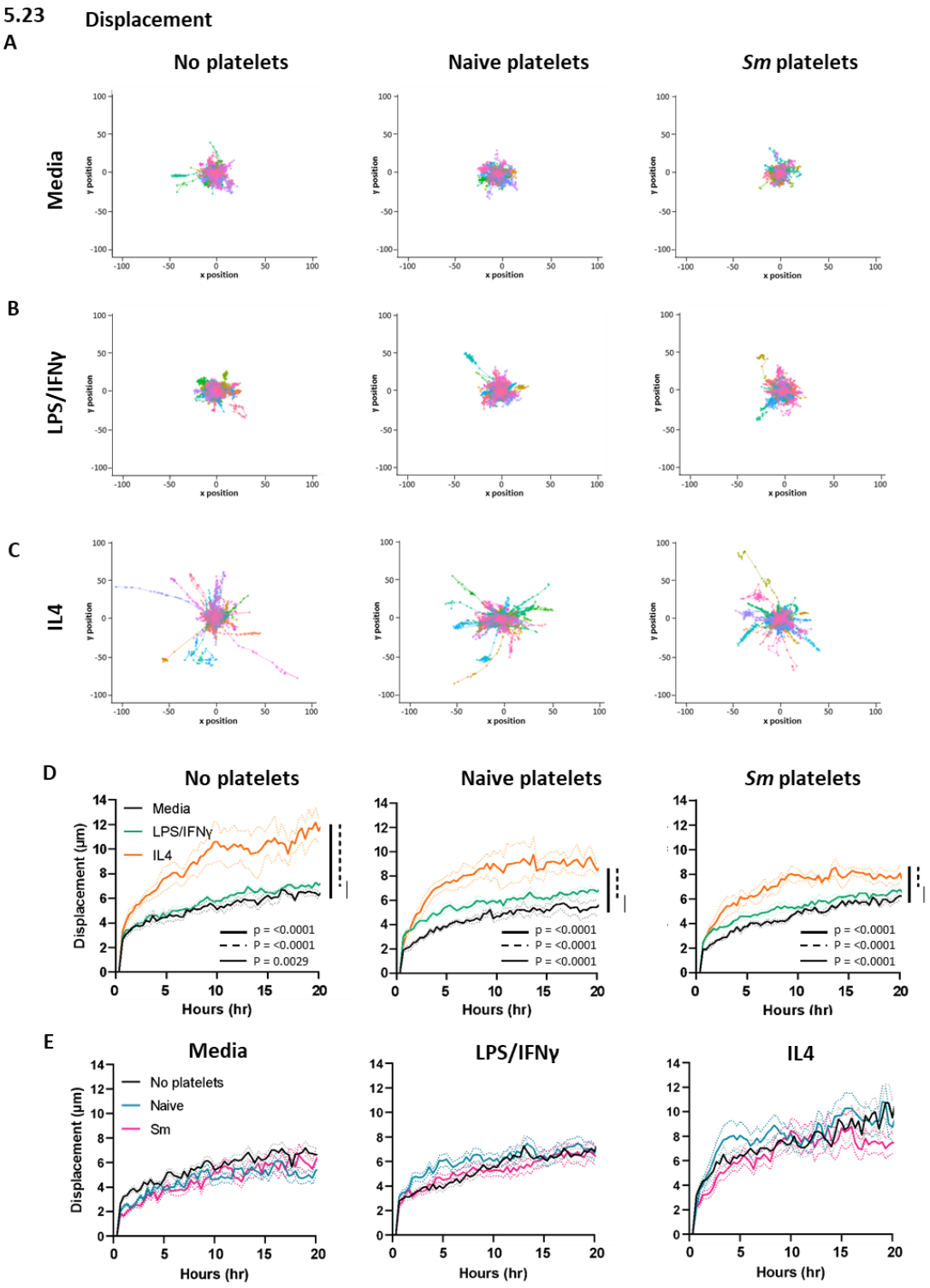

Figure 5.23 Macrophage displacement remains unchanged after co-culture with platelets

Representative displacement plots of individual macrophages, normalised to the origin 0,0 within a well after A) no treatment, LPS/IFNγ, or C) IL-4 treatment. D-E) Mean macrophage displacement in the presence of naive or infected platelets. Solid line represents mean of >50 individual cells, representative of 5 independent experiments with SE (dotted line). Statistical significance was determined using one-way ANOVA with post-hoc Tukey's test on the mean for each macrophage stimulation. Non-significance ($p>0.05$) not shown.

5.24

A

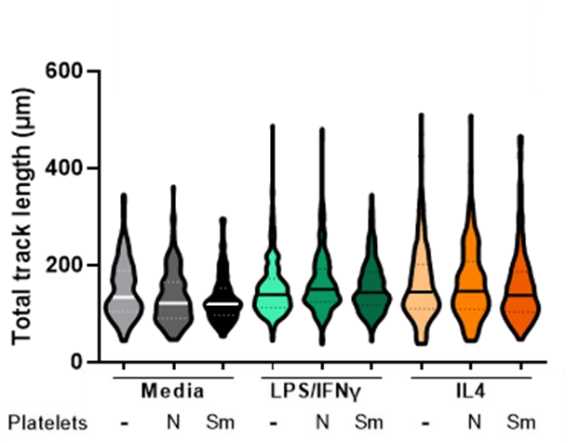

B

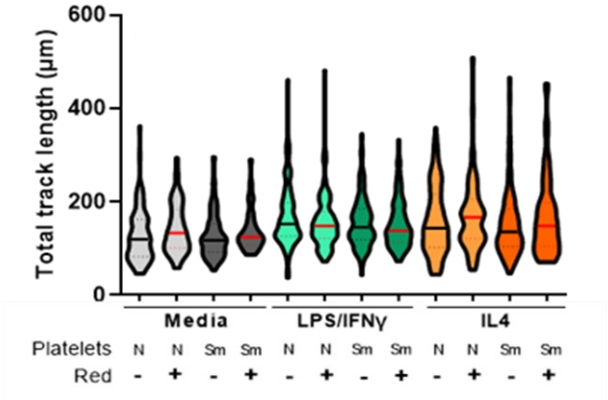

Figure 5.24 No significant difference in macrophage movement after platelet phagocytosis

A) Total track length of individual macrophages in the presence of naïve, or infected platelets. B) Total track length of macrophages which have not phagocytosed a platelet (black mean line), or one that have phagocytosed a platelet (red mean line). Bold line represents mean track length of >50 individual cells, dotted lines representative of upper and lower quartile. Representative of 3 independent experiments. Statistical significance was determined using one-way ANOVA with post-hoc Tukey's test on the mean for each macrophage stimulation. Non-significance ($p>0.05$) not shown.

5.4 Discussion

Since platelets have been shown to have immunomodulatory functions alongside their roles in haemostasis, several groups have investigated their direct interactions with more traditional immune cells (predominantly macrophages and monocytes) using different *in vitro* models. However, the production and functionality of monocytes and macrophages is highly heterogeneous (387). De Sousa *et al*. (2019), showed that the inflammatory environment can result in completely different macrophage fates (325). Furthermore, the classification of M1 and M2 macrophages is far less "black and white" and is now better understood as a long, continuous spectrum of macrophages with subtle differences in phenotype and functionality (388). The M1-M2 paradigm also does not reflect the full spectrum of macrophage activation, for example Mreg cells respond to TLR agonists, immune complexes and apoptotic cells; and M4 respond to CXCL4 (389,99,390). Together, the differences in methods for macrophage/monocyte generation and isolation, culture conditions and the markers used for classification has resulted in a lack of consensus regarding the effects of platelets on these immune cells.

As we have already shown that platelets primarily interacted with MHCII^{lo} RELMα^{hi} macrophages in the liver in schistosome-infected mice and that platelets were cleared more rapidly during infection (**Chapter 3**), we firstly wanted to assess whether platelets drove differential macrophage polarisation and secondly to determine if platelets from infected mice were preferentially phagocytosed compared with naive controls.

During schistosome infection the resident Kupffer cell macrophage population is replaced by inflammatory monocyte-derived macrophages that derive from BM precursors (391). We therefore chose to use BM-derived macrophages for our *in vitro* experiments. In agreement with other studies, we found Thio-Mϕ to be highly heterogeneous (392). Furthermore, as has been explored previously, Thio-Mϕ and BM-Mϕ responded in distinct manners to polarising stimuli (376). We observed IL-4 treated BM-Mϕ to express high levels of RELMα, whilst Thio-Mϕ to have high levels of Ym1. The functional significance of this divergent expression of differential facets of M2 activation is not known,

but it suggests that macrophage phenotype is controlled by extrinsic factors in addition to cytokines, including environmental and tissue specific cues that may be missing *in vitro.* As **Chapter 3** revealed RELMα expression distinguished $CD41^+$ and $CD41^-$ liver macrophages, we primarily used BM cells differentiated with L929-supplemented media given their higher expression of RELMα in response to IL-4 treatment compared with Thio-Mϕ. Our results demonstrated that platelets from naive or schistosome-infected mice did not cause consistent changes in macrophage activation or polarisation.

The lack of reproducible changes in macrophage polarisation following co-culture of macrophages with platelets *in vitro* may indicate that platelets are not driving the changes in liver macrophage phenotypes in schistosome infection. Instead, platelets may be preferentially binding to the specific subset of macrophages i.e. $RELMα^{hi}$ $MHCII^{hi}$ *in vivo* in naive mice and $RELMα^{hi}$ $MHCII^{lo}$ in schistosome infection. Our *in vitro* binding assay, with M0 macrophages and platelets from naive mice, is consistent with this hypothesis of preferential binding to activated macrophages. In our IL-4 stimulated macrophage cultures used to mimic M2 macrophages found during schistosome infection, we continued to see preferential platelet interactions with polarised macrophages. These differences between our *in vitro* and *in vivo* experiments may reflect the reductionist nature of these cultures and highlight the need for more complex communication between multiple cell types in a particular inflammatory environment. Minutti *et al.* (2017), showed the important role of tissue-specific factors, such as surfactant protein A and C1q to drive the most effective type 2 macrophage response in the lung to *Nippostrongylus brasiliensis* (393). More recently, and in a different type 1 inflammatory environment, Rossaint *et al*. (2021) showed that following *Klebsiella pneumonia* infection the composition of platelet-leukocyte aggregates varies during infection progression and resolution i.e. platelets interact with neutrophils at the onset of infection, and then Treg cells during the resolution phase of infection (226). Furthermore, they also showed that Treg-platelet aggregation was required for the transcriptional reprogramming of macrophages towards a more wound healing-like phenotype. Therefore,

our *in vitro* macrophage cultures may be lacking signals from other immune or non-immune cells. We considered sorting macrophages from naive and schistosome-infected hepatic tissue and performing similar *in vitro* assays (as shown in **Chapter 3**) but we could only isolate limited cell numbers (~1-4x10^6) from infected mice and naive livers would be substantially less, meaning this was not practical.

In chronic schistosome infections, individuals sometimes present with high levels of circulating endotoxins and can suffer from endotoxemia as a result of damage to the intestinal walls following the transit of schistosome eggs into the gut (24,394). We wanted to explore whether the increased platelet-macrophage aggregates observed in schistosome infection were potentially beneficial or detrimental to bacterial clearance. Previously, studies have shown that peritoneal macrophages isolated from schistosome-infected mice were less capable of phagocytosing *Salmonella typhimurium* compared with cells from naive mice (395). Consistent with these findings we have shown that M2-like macrophages (IL-4-stimulated), as observed in schistosome infection, were less able to phagocytose the pH sensitive *E. coli* bioparticles compared with the LPS/IFNγ-stimulated cells. Despite substantial experimental variation, IL-4 treated BM-Mϕ polarised in the presence of platelets consistently showed an enhanced ability to phagocytose *E. coli* bioparticles compared with M2 macrophages cultured without platelets. This is consistent with Carestia *et al*. (2019) who showed enhanced M2-like human macrophage phagocytosis of GFP-*E. coli* in the presence of platelets (227). Given the results of Muniz-Junqueira *et al*. (1992), who showed macrophages from schistosome-infected mice were less capable of phagocytosing bacteria, we tested whether platelets from infected mice were still able to enhance M2-like macrophage phagocytosis of *E. coli* (395). We demonstrated that these platelets did enhance M2-like macrophage phagocytosis, albeit to a lesser extent than naive platelets, thereby highlighting important differences between these platelet populations in naive and schistosome-infected mice. It appears that platelets may be involved in maintaining the M2-like phenotype, associated with tissue repair following damage to the intestinal wall whilst enhancing the macrophage phagocytic capacity which minimises the risk of

sepsis. The interaction of platelets, even in schistosome infection, are able to enhance the phagocytic ability of macrophages to clear any pathogenic material that does leak through, without impeding the beneficial tissue repair function associated with RELMα and Ym1 expression (288). Moreover, platelets preferentially interacted with activated macrophages, rather than directly promoting their polarisation. However, it may be the case that platelets are promoting other facets of macrophage activation that we did not assess in these experiments. For example, the adhesion and phagocytosis of platelets from naive and infected mice may induce metabolic reprogramming which drives the enhanced ability to phagocytose *E. coli* bioparticles. This has been shown in tumour associated macrophages after phagocytosis of neoplastic cells (322).

In **Chapter 4** we showed that platelets in schistosome infection did not show any significant differences in expression of a wide range of surface molecules, including those for activated integrin αIIbβIII and CD62P. However, *in vivo* platelet tracking revealed that platelets were cleared faster during infection. We hypothesised that M2-like macrophages may have an increased propensity to phagocytose platelets from schistosome-infected animals given elevated PS and desialylation. Here we have shown that polarised macrophages phagocytosed platelets to a greater degree than M0 cells, and that M2-like macrophages did in fact phagocytose platelets from schistosome-infected mice to a significantly greater degree than platelets from naive mice. Translating this *in vivo* to schistosome infection suggests there is greater platelet phagocytosis due to both M2 polarisation and infection-induced increases in macrophage numbers. We could use intravital microscopy to visualise the interactions between fluorescently labelled circulating platelets within a GFP-macrophage mouse (e.g. CX3CR1-GFP, CD68-GFP)(396,397). This would allow us to assess the differences in macrophage-platelet interactions and clearance *in situ* with all the inflammatory cytokines and molecules (e.g. IL-4, IL-10, schistosome egg antigen) associated with schistosome infection. We could also assess platelet surface adherence versus internalisation by dual labelling platelets with pH-sensitive dyes as with our *in vitro* experiments. A further *in vitro* experiment could be performed

using pHrodo-labelled platelets and pHrodo *E.coli* bioparticles, this would allow the identification of macrophages that have phagocytosed platelets (i.e. “red” macrophages) or not and then assess whether they have phagocytosed *E. coli* bioparticles (i.e. “turned green”). These different macrophage populations could be sorted and analysed for behavioural, phenotypic or metabolomic changes.

Together, these *in vitro* experiments have shown significant differences in the way platelets from naive and schistosome-infected mice interact with M2-like macrophages. Naive platelets significantly enhance the ability of M2-like macrophages to phagocytose *E. coli* bioparticles, however platelets from infected mice are less able to enhance the levels of phagocytosis. Furthermore, we have shown that all three macrophage populations (M0, M1 and M2) are capable of phagocytosing platelets but M2-like populations phagocytose platelets from schistosome-infected mice to a greater extent than naive platelets. Interestingly, these changes in macrophage activity in response to platelets are not associated with significant changes in the activation markers examined. This is in contrast to Carestia *et al.* (2019), Lee *et al.* (2021), Barrett *et al.* (2019) and Uchiyama *et al.* (2021) who all show platelets induce macrophage polarisation either to pro- or anti-inflammatory phenotypes *in vitro* (217,227,375,377). Whilst these studies used cells from different origins i.e. human monocytes/macrophages or Thio-Mϕ, as well as different subtype classification parameters, our results clearly show that platelets do not strongly impact on BM-Mϕ polarisation in multiple *in vitro* assays, but they do enhance the ability of M2 macrophages to phagocytose which is consistent with Carestia *et al.* (2019) and Lee *et al.* (2021) (227,375).

6. Assessment of the effect of modulating platelet number in murine schistosomiasis

6.1 Introduction

Experiments in **Chapter 3** revealed schistosome infection caused enhanced platelet clearance, formation of platelet-macrophage aggregates, and that platelet-associated macrophages showed a distinct maturation profile. Despite this, *in vitro* studies using a range of assays in **Chapter 5** indicated platelets had only limited impact on macrophage phenotype. To address this discrepancy, in this chapter we experimentally manipulated platelet levels *in vivo* to test the immunomodulatory capacity of platelets directly in schistosome infection. We wanted to assess whether platelet depletion or enhancement altered the immune response to schistosome infection given the context specific effects of platelets in other inflammatory diseases.

For instance, PLA (primarily platelet-eosinophil aggregates) drive leukocyte recruitment to the lung in type 2 inflammation that occurs in allergic asthma (206). Here, activated platelets interact with leukocytes in a P-selectin – PSGL-1 dependent manner (313). In both mouse and rabbit models, antibody-mediated platelet depletion reduces eosinophil lung infiltration and hyperresponsive airway inflammation (398,222). However, there is minimal clinical evidence suggesting anti-platelet drugs such as aspirin, or the P2Y12 antagonist clopidogrel have any beneficial effects on asthma patients (206). This may reflect that these drugs reduce platelet activation rather than numbers e.g. low-dose aspirin treatment in thrombocythaemia patients with any microvasculature disturbances (399).

Platelets also control immune responses to *Klebsiella pneumoniae* infection in the lung. Rossaint *et al.* (2021) demonstrate that platelets help in the recruitment of neutrophils to the lung during the initial stages of infection (226). Subsequently, platelets switch binding partners to interact primarily with Tregs which reduce pathological inflammation and support M2 macrophage-mediated wound-healing and tissue repair. Platelet depletion using anti-GPIbα antibodies results in a sustained pro-inflammatory alveolar neutrophil response (226). Moreover, use of inducible platelet deficient mouse models

(Pf4Cre; RosaiDTR) allows platelet depletion at different times during infection. These models have revealed platelet depletion prior to bacterial infection causes mouse death due to the lack of neutrophil recruitment to the lung at the onset of infection, whereas platelet depletion after bacterial clearance prevents M2 macrophage-mediated tissue remodelling (226).

To the best of our knowledge, the only previous study to manipulate platelet levels in schistosomiasis involved platelet depletion in CBA mice infected with a high dose of cercariae (150-200 per mouse). Mice treated with rabbit anti-mouse platelet serum at 5 weeks post-infection had significantly reduced schistosome egg excretion, whereas similar treatment at 6 weeks post-infection resulted in death of 2 out of 3 mice in the group (269). In this chapter we will assess the impact of platelet depletion in the more chronic stages of schistosome infection as well as identifying specific immunomodulatory roles of platelets which have not previously been explored.

An alternative approach to assess the immune regulatory role of platelets is to boost their numbers by enhancing TPO signalling using recombinant TPO or TPO receptor agonists, of which three are clinically approved for administration to ITP patients: Romiplostim, Eltrombopag and Avatrombopagelon (400). As described in **Chapter 1.2**, TPO acts through binding to its cognate MPL receptor on HSC, MK and platelets themselves. Detection by MK results in signalling via the JAK2/STAT3/5 pathway and increases MK number (151). Recombinant TPO drives MPL receptor dimerization and an increase in platelet count, however this can also lead to the development of anti-TPO antibodies that cross-react with and neutralise native TPO, leading to reduced platelet levels (401). In contrast, TPO peptide mimetics do not share sequence homology with endogenous TPO which minimises the risk of cross-reactivity of anti-TPO auto-antibodies (401).

Whilst platelet depletion reduces allergic lung inflammation (222,398), enhancing platelet levels with romiplostim leads to significant increases in lung inflammation and mortality in mouse models of allergy (402). To date, there are very few studies examining the efficacy of treating bacteria, virus or parasite-induced thrombocytopenia with TPO receptor agonists (287,403).

Instead, TPO mimetics are primarily given to the most severe thrombocytopenic patients, when there is a high risk of bleeding and they have not responded to other treatments (404). In this regard, whilst platelet depletion causes bleeding phenotypes, raising levels can promote thrombosis (166). As such, these potentially detrimental haemostatic complications must also be considered if platelet levels are manipulated to modulate immune responses. In order to test the immunomodulatory capacity of platelets during *in vivo* type 2 immune responses, we trialled multiple experimental strategies to deplete or increase platelet numbers in schistosome infection, and subsequently measured both immunological and parasitological parameters.

6.2 Aims

1) To determine the effects of platelet depletion in schistosome infection

2) To determine whether enhanced TPO signalling can restore platelet numbers and impact the immune response in schistosome infection

6.3 Results

6.3.1 Does platelet depletion affect the immunological response to schistosome infection – antibody-mediated platelet depletion?

Previous studies have shown platelet depletion causes extensive mortality following infection with high doses of schistosome cercariae (269). To reduce this risk and permit assessment of the role of platelets in immune cell function in chronic schistosomiasis, we reduced our standard infective dose (upper limit 35 vs. standard limit of 40 cercariae) and harvested infections at earlier time points (10 weeks vs. standard 12 weeks) (**Figure 6.1A**). We treated naive and infected mice with increasing concentrations of anti-CD41 mAb (MWReg30) or isotype control three times a week with 0.2mg/kg anti-CD41 and increased to 0.4mg/kg for a further week, corresponding to weeks 8 and 9 post-infection to induce sustained and severe thrombocytopenia (405). Given the lower infection dose and earlier time-point we observed only a relatively mild thrombocytopenia (700-800x10^3/mm^3) in the schistosome IgG control group in these experiments (**Figure 6.1B**). However, there was still a significant increase in MPV with schistosome infection (**Figure 6.1C**). Naive mice treated

with anti-CD41 showed substantial reductions in platelet number over the first week, but platelet depletion was significantly impaired in schistosome-infected mice (**Figure 6.1B**). Anti-CD41 treatment increased MPV in naive animals as well as schistosome-infected mice which already had an elevated MPV (**Figure 6.1C**). Despite our precautions and only partial platelet depletion, 50% of mice given anti-CD41 (3/6 vs 1/7 in the IgG group) developed symptoms of severe disease (weight loss, hunched appearance, pallor) and needed to be culled prior to experimental harvest (**Figure 6.1D**). Even with the earlier time-point and lower infection dose there was significant hepatosplenomegaly and egg deposition which was not exacerbated by platelet depletion (**Figure 6.1E-F**).

Having used anti-CD41 MWReg30 mAb to deplete platelets *in vivo*, we decided it would be problematic to identify PLA in the isolated cell suspensions with fluorescently labelled MWReg30. This would also be the case with other anti-CD41 mAb clones that may target overlapping epitopes. Instead, 24hr prior to tissue harvesting we fluorescently labelled the remaining platelets *in vivo* with X649 as described in **Chapter 3**. Unfortunately, this meant we were unable to distinguish between internalised and surface-bound platelets in different tissues. There was no significant difference in the percentage of $X649^+$ leukocytes in the blood, liver or spleen, however in both the spleen and liver of naive mice there was a general trend of increase with anti-CD41 treatment, and this was not observed in schistosome infection (**Figure 6.2A**). Whilst there was an increase in the total number of $X649^+$ leukocytes in schistosome infection in both liver and spleen compared with naive mice, there was no difference +/- anti-CD41 treatment (**Figure 6.2B-C**). When considering individual cell populations, there was a significant increase in the percentage of $X649^+$ neutrophils and classical monocytes in the blood in naive mice treated with anti-CD41, but this was not seen in schistosome infection (**Figure 6.2D**). There was no difference in $X649^+$ staining in the liver with or without anti-CD41 treatment (**Figure 6.2E**). In the spleen, anti-CD41 treatment caused a significant increase in $X649^+$ macrophages and B cells in naive mice, but again this was not seen in schistosome infection (**Figure 6.2F**).

In **Chapter 3** we showed platelets interacted with specific subsets of hepatic monocytes/macrophages (MHCII^{lo} RELMα^{hi}) and eosinophils (RELMα^{lo}) *in vivo* in schistosome infection. *In vitro* experiments in **Chapter 5** indicated that platelets do not strongly drive macrophage polarisation and instead bind preferentially to cells that have an activated phenotype. Consistent with platelets not directly modulating immune cell activation, anti-CD41-mediated platelet depletion did not impact on eosinophil RELMα (**Figure 6.3A**) or macrophage/monocyte MHCII expression following schistosome infection, both of which were elevated compared with naive mice (**Figure 6.3B-C**). Conversely, anti-CD41 treatment led to a reduction in RELMα expression by monocytes, and to a lesser extent macrophages in schistosome-infected mice. Although, this was not significant potentially due in part to the small group size due to culling 3/6 anti-CD41 treated mice (**Figure 6.3B-C**). Pairwise analysis of X649^{+} and X649^{-} immune populations showed no difference after anti-CD41 treatment, however in this experiment the X649^{+} macrophages and monocytes were MHCII^{hi} in schistosome infection compared with the MHCII^{lo} CD41^{+} populations previously shown in **Chapter 3** (**Figure 6.4**).

In ITP, antigen presenting cells (APC) such as macrophages, monocytes and DC present integrin αIIbβIII peptides to CD4^{+} T cells which then drive B cell production of more anti- integrin αIIbβIII IgG (406). As such we wanted to assess whether the APC in this model were impacting the CD4^{+} T cell response. Splenic CD4^{+} T cells showed an increase in the production of IL-4, IL-10 and IFNγ in schistosome infection and this was not affected by anti-CD41 treatment (**Figure 6.5A-C**).

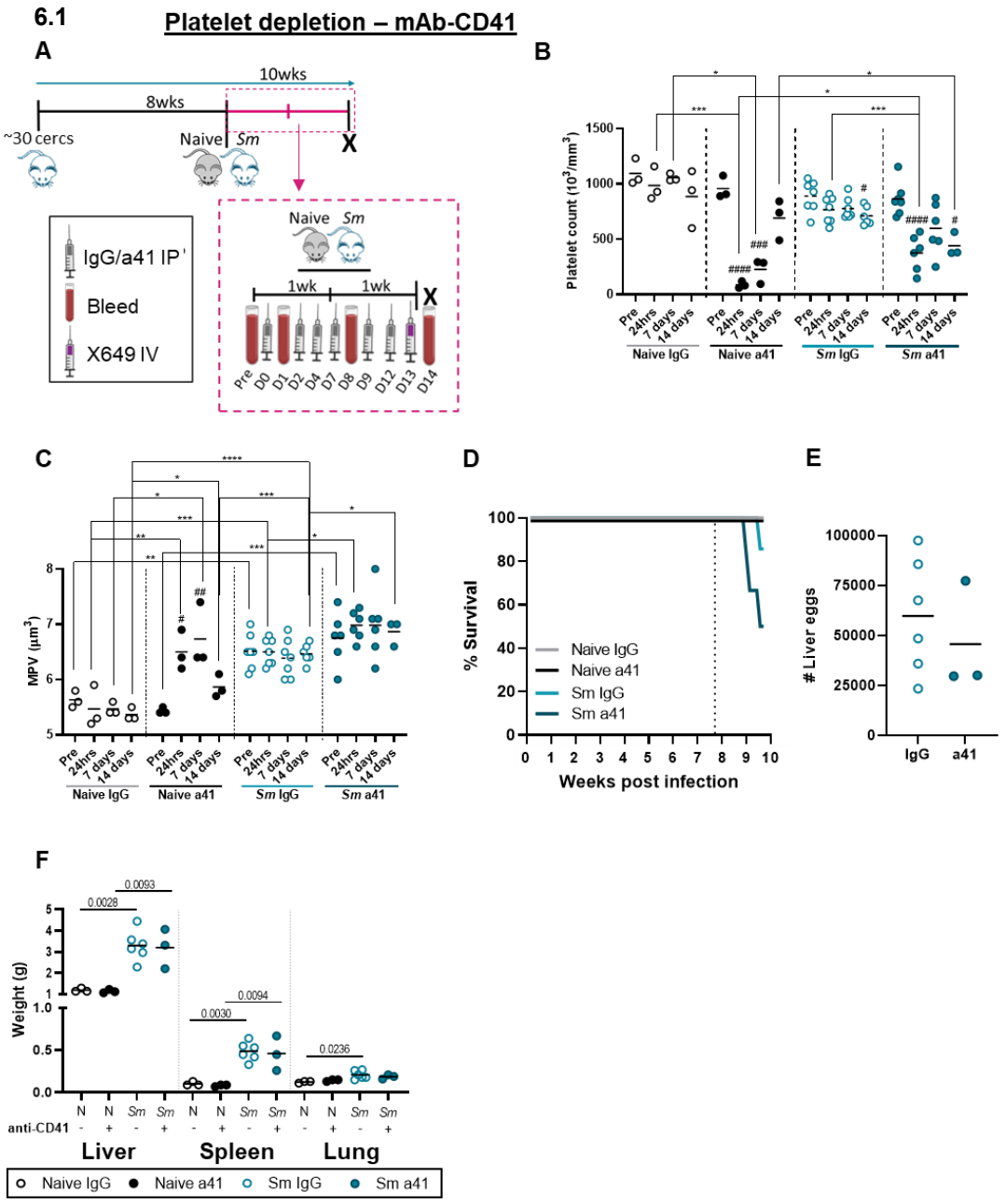

Figure 6.1 Partial platelet reduction in schistosome infection with anti-CD41 treatment
A) C57BL/6 were infected with 30-35 *S. mansoni* cercariae (*Sm*) at 8 weeks post-infection mice were injected with 0.2mg/kg anti-CD41 (MWReg30) or IgG control IP 3 times per week and then with 0.4mg/kg for a further week. 24hr prior to tissue harvesting all mice were injected IV with X649 (0.05µg/g of body weight). Longitudinal tail bleed B) platelet count and C) mean platelet volume. # represents significance to pre-bleed within each treatment group, * represent significance between treatment groups at different time-points. (*# p<0.05, **## p<0.01, ***### p<0.001, ****#### p<0.0001). D) Survival curve during infection, dashed line represents start of anti-CD41 treatment (Naive IgG n=3 (white), Naive anti-CD41 n=3 (black), *Sm* IgG n=7(6)(light blue), *Sm* anti-CD41 n=6(3)(dark blue)) Post-mortem E) hepatic schistosome eggs from KOH digested livers and F) liver, spleen and lung weights. Data representative of 2 independent experiments. Statistical significance determined by one-way ANOVA with post-hoc Tukey's test on the mean of each group (B-D, C) or unpaired Student's unpaired t-test (E). Non-significance (p>0.05) not shown.

6.2

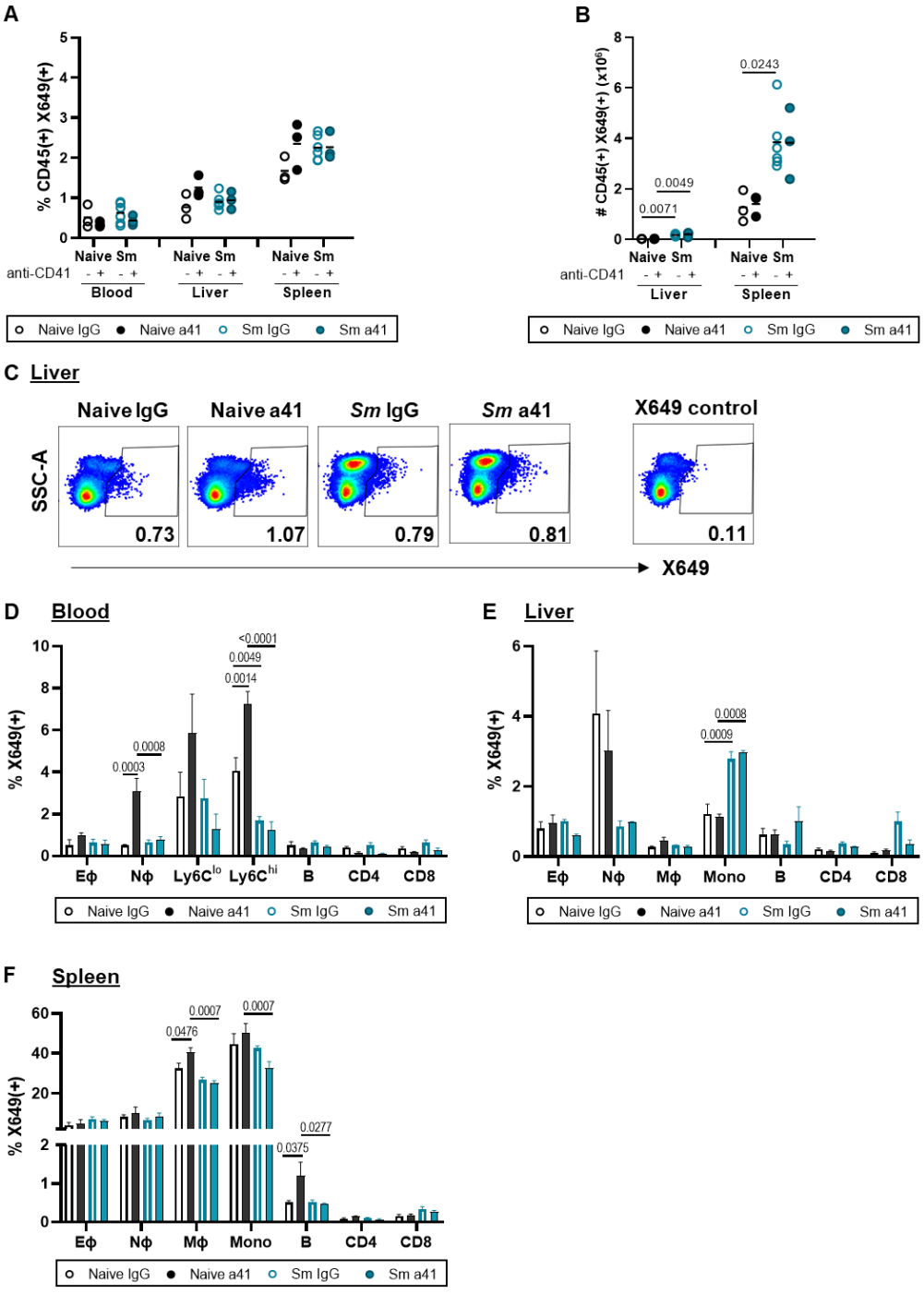

Figure 6.2 No significant difference in PLA in schistosome infected mice after anti-CD41 treatment

C57BL/6 were infected with 30-35 *S. mansoni* cercariae (*Sm*) at 8 weeks post-infection mice were injected with 0.2mg/kg anti-CD41 (MWReg30) or IgG control IP 3 times per week and then with 0.4mg/kg for a further week. 24 hours prior to tissue harvesting all mice were injected IV with X649 (0.05µg/g of body weight). A) Percentage and B) number of X649+ CD45+ cells in the liver, spleen and blood and C) representative FACS plots. Percentage of X649+ individual immune cell populations in the D) blood, E) liver, and F) spleen. (Naive IgG n=3 (white), Naive anti-CD41 n=3 (black), *Sm* IgG n=6 (light blue), *Sm* anti-CD41 n=3 (dark blue)). Statistical significance determined by unpaired Student's unpaired t-test (A-B) and one-way ANOVA with post-hoc Tukey's test (D-F) on the mean of each group. Non-significance (p>0.05) not shown.

6.3 Liver

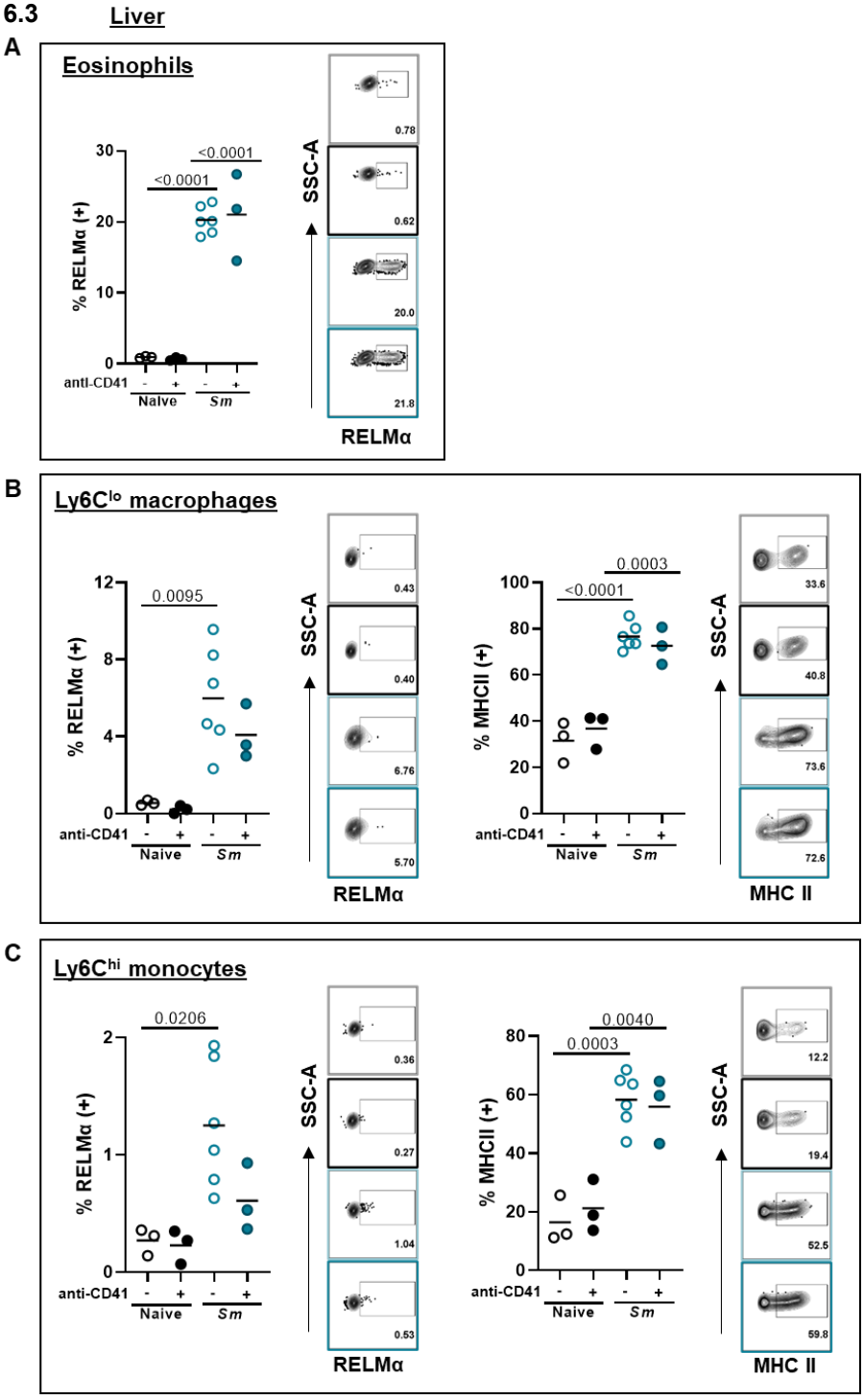

Figure 6.3 No significant difference in activation markers on eosinophils, macrophages and monocytes in schistosome-infected mice after anti-CD41 treatment

C57BL/6 were infected with 30-35 *S. mansoni* cercariae (*Sm*) at 8 weeks post-infection mice were injected with 0.2mg/kg anti-CD41 (MWReg30) or IgG control IP 3 times per week and then with 0.4mg/kg for a further week. 24hr prior to tissue harvesting all mice were injected IV with X649 (0.05µg/g of body weight). A) Percentage of RELMα and representative FACS plots in hepatic eosinophils. Percentage of RELMα and MHCII and representative FACS plots by B) hepatic Ly6C^{lo} macrophages and C) hepatic Ly6C^{hi} monocytes. (Naive IgG n=3 (grey), Naive anti-CD41 n=3 (black), *Sm* IgG n=6 (light blue), *Sm* anti-CD41 n=3 (dark blue)). Statistical significance determined by one-way ANOVA with post-hoc Tukey's test (A-C) on the mean of each group. Non-significance ($p>0.05$) not shown.

6.4

A Liver

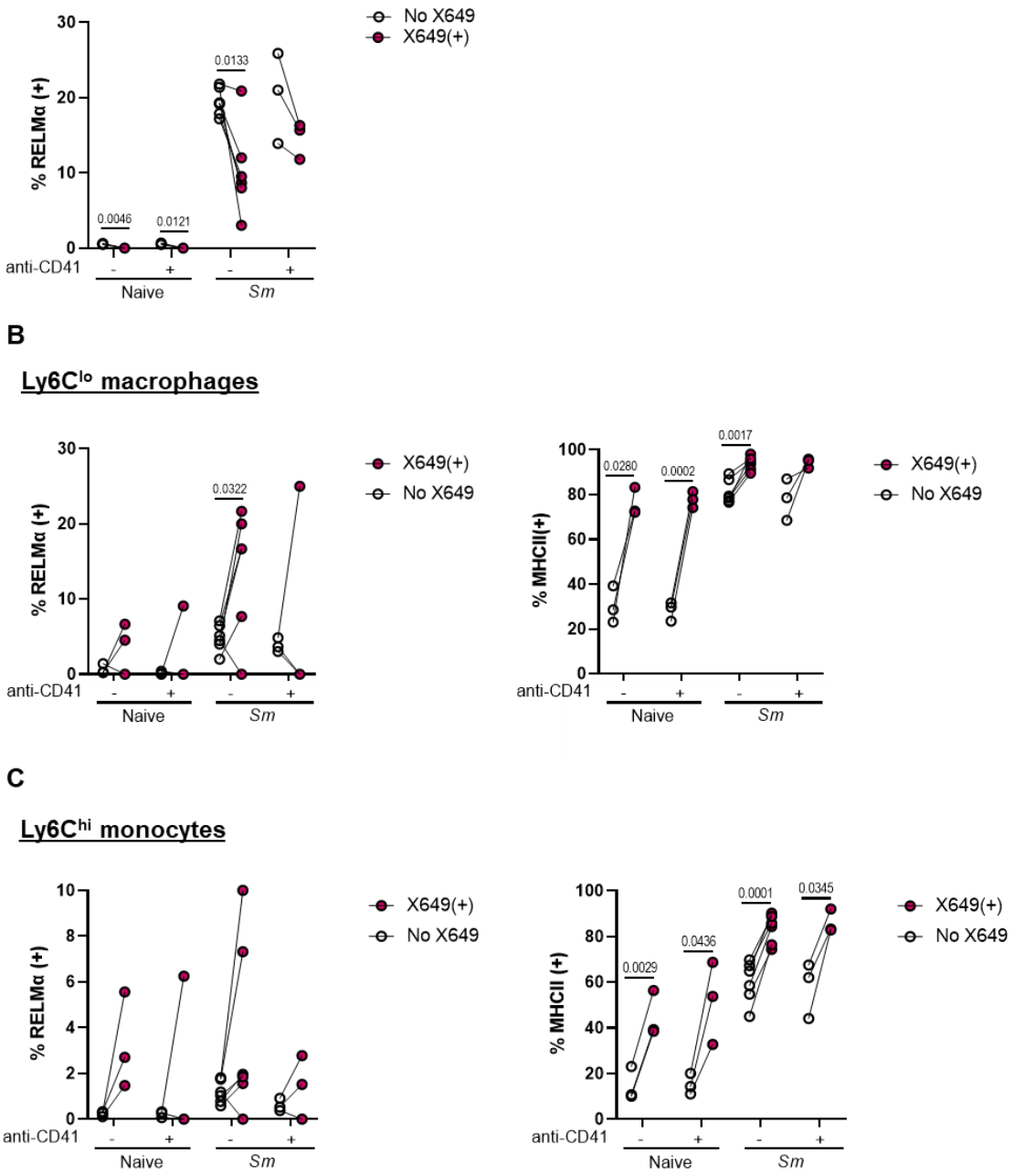

Figure 6.4 No difference in X649 pairwise comparisons after anti-CD41 treatment

C57BL/6 were infected with 30-35 *S. mansoni* cercariae (*Sm*) at 8 weeks post-infection mice were injected with 0.2mg/kg anti-CD41 (MWReg30) or IgG control IP 3 times per week and then with 0.4mg/kg for a further week. 24hr prior to tissue harvesting all mice were injected IV with X649 (0.05µg/gram of body weight). A) Pairwise comparison of RELMα expression by $X649^+$ (pink) and $X649^-$ (white) eosinophils in the liver. Pairwise comparison of RELMα and MHCII by $X649^+$ (pink) and $X649^-$ (white) B) macrophages and C) monocytes in the liver. (Naive IgG n=3, Naive anti-CD41 n=3, *Sm* IgG n=6, *Sm* anti-CD41 n=3). Statistical significance determined by paired t-test between $X649^+$ and $X649^-$ subsets (A-C). Non-significance ($p>0.05$) not shown.

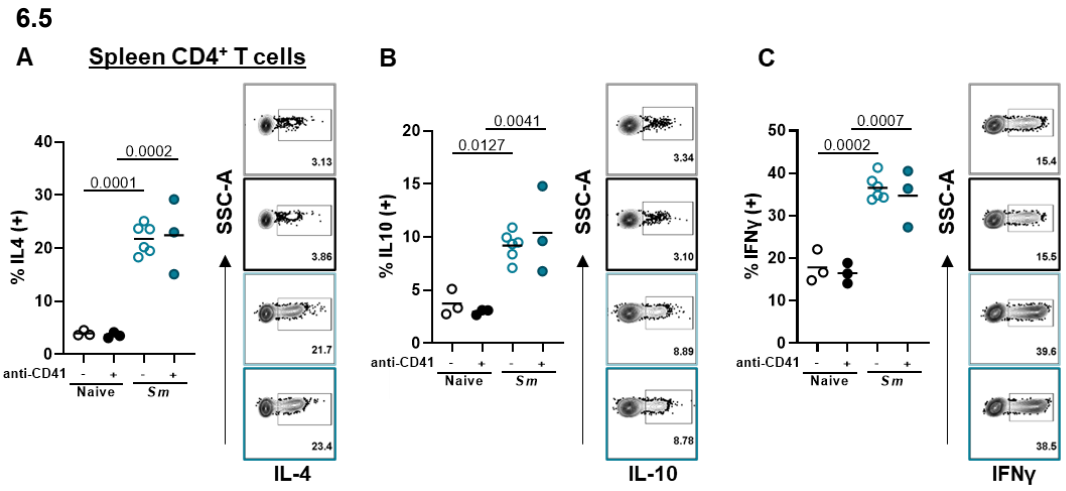

Figure 6.5 No significant difference in cytokine production by CD4⁺ T cells in schistosome infected mice after anti-CD41 treatment

C57BL/6 were infected with 30-35 *S. mansoni* cercariae (*Sm*) at 8 weeks post-infection mice were injected with 0.2mg/kg anti-CD41 (MWReg30) or IgG control IP 3 times per week and then with 0.4mg/kg for a further week. 24hr prior to tissue harvesting all mice were injected IV with X649 (0.05µg/g of body weight). Single cell suspensions (2-4x10^6 cells) from spleen isolation processing were cultured for 4hr at 37°C with 1µg/ml Ionomycin, 10µg/ml PMA and 10µg/ml Brefeldin A. Percentage of A) IL-4, B) IL-10 and C) IFNγ by CD4⁺ T cells and representative FACS plots. (Naive IgG n=3 (grey), Naive anti-CD41 n=3 (black), *Sm* IgG n=6 (light blue), *Sm* anti-CD41 n=3 (dark blue)). Statistical significance determined by one-way ANOVA with post-hoc Tukey's test (A-C) on the mean of each group. Non-significance (p>0.05) not shown.

6.3.2 Does platelet depletion affect the immunological response to schistosome infection – MPL$^{-/-}$ mice?

Given we were only able to partially reduce platelet numbers in schistosome infection with anti-CD41 treatment and monoclonal antibody treatment drives immunological activation (407), we turned to an alternative approach for assessing the impact of platelet depletion in schistosome infection. MPL$^{-/-}$ mice lack the TPO receptor resulting in severe thrombocytopenia (148,151,152,408). Due to health concerns with platelet-deficient mice, we again infected with a lower dose of parasites and harvested at an earlier time-point of 7.5 weeks post-infection (**Figure 6.6A**). Whilst this did not lead to infection-induced thrombocytopenia in WT mice, MPV was still significantly elevated (**Figure 6.6B-C**). As expected, MPL$^{-/-}$ mice were severely thrombocytopenic, and platelets were slightly, but non-significantly reduced further after infection (p=0.053) (**Figure 6.6B**). In all parameters measured there were no differences observed between male and female mice and therefore the data from these two independent experiments were pooled for all analysis. Infected MPL$^{-/-}$ mice also displayed marked reductions in circulating red blood cells and elevated red cell distribution width, suggestive of infection-induced anaemia (**Figure 6.6D-E**). This may reflect a failure to stem intestinal bleeding caused by parasite egg transit across the tissue, consistent with intestinal haemorrhaging observed in some infected MPL$^{-/-}$ mice (**Figure 6.6F**). As MPL is also expressed on a range of HSC and progenitor cells (409), we wanted to assess whether these were also impacted after schistosome infection. We showed a significant infection-induced expansion of LSK (Lin^{-}Sca1^{+}cKit^{+}) cells in schistosome infection compared with naive mice. As previously reported, the naive MPL$^{-/-}$ mice had a very small LSK population and in schistosome infection there was a failure of the LSK population to expand (**Figure 6.7A-B,** (410)). This was due to a reduction in all progenitor populations between schistosome-infected WT and MPL$^{-/-}$ mice, from the most immature LT-HSC to the MPP2 population which gives rise to the MK and erythroid lineages (**Figure 6.7C-D**).

Despite the low infection dose and early time-point harvest, both WT and MPL$^{-/-}$ infected mice developed hepatosplenomegaly to a similar extent

(**Figure 6.8A-B**). Similarly, there was no difference in schistosome egg levels in the liver (**Figure 6.8C**). Despite the reduction in all MPP populations and LT-HSC populations, there was no significant difference in the frequency or absolute number of immune cells in the liver (**Figure 6.8D-E**). Consistent with reduced circulating platelet counts, myeloid cells from MPL$^{-/-}$ mice showed reduced (but not absent) CD41 expression, consistent with fewer PLA (**Figure 6.8F-H**).

Next, we assessed whether platelet depletion in MPL$^{-/-}$ mice affected the immune response, particularly the expression of RELMα and MHCII. The expression of RELMα by eosinophils in MPL$^{-/-}$ mice was higher compared with WT animals, however this was not significant given the spread of data and group size (**Figure 6.9A**). Schistosome infection also induced a significant increase in RELMα expression in eosinophils, macrophages and monocytes in both WT and MPL$^{-/-}$ animals compared with their naive counterparts (**Figure 6.9A-C**). Interestingly, there was significantly less MHCII expression by both macrophages and monocytes in schistosome-infected MPL$^{-/-}$ mice compared with their WT counterparts (**Figure 6.9B-C**). Given these changes in activation, we next explored whether differential MHCII expression by myeloid cells influenced the T cell response in the liver and spleen. This revealed liver CD4^{+} T cells from MPL$^{-/-}$ mice had a similar capacity to their WT counterparts to produce IL-4, IL-10 and IFNγ in response to schistosome infection (**Figure 6.10A-B**). In contrast, splenic CD4^{+} T cells from infected MPL$^{-/-}$ mice had an overall trend towards elevated cytokine production compared with WT animals but this was only significant ($p<0.05$) for IFNγ (**Figure 6.10B**).

Together, our platelet depletion experiments reveal that platelets play an important haemostatic role in schistosome infection by stemming intestinal bleeding after schistosome eggs transit the gut wall. Moreover, severe thrombocytopenia in our MPL$^{-/-}$ mice resulted in fewer PLA alongside lower MHCII expression by macrophages and monocytes but an elevated pro-inflammatory CD4^{+} T cell response.

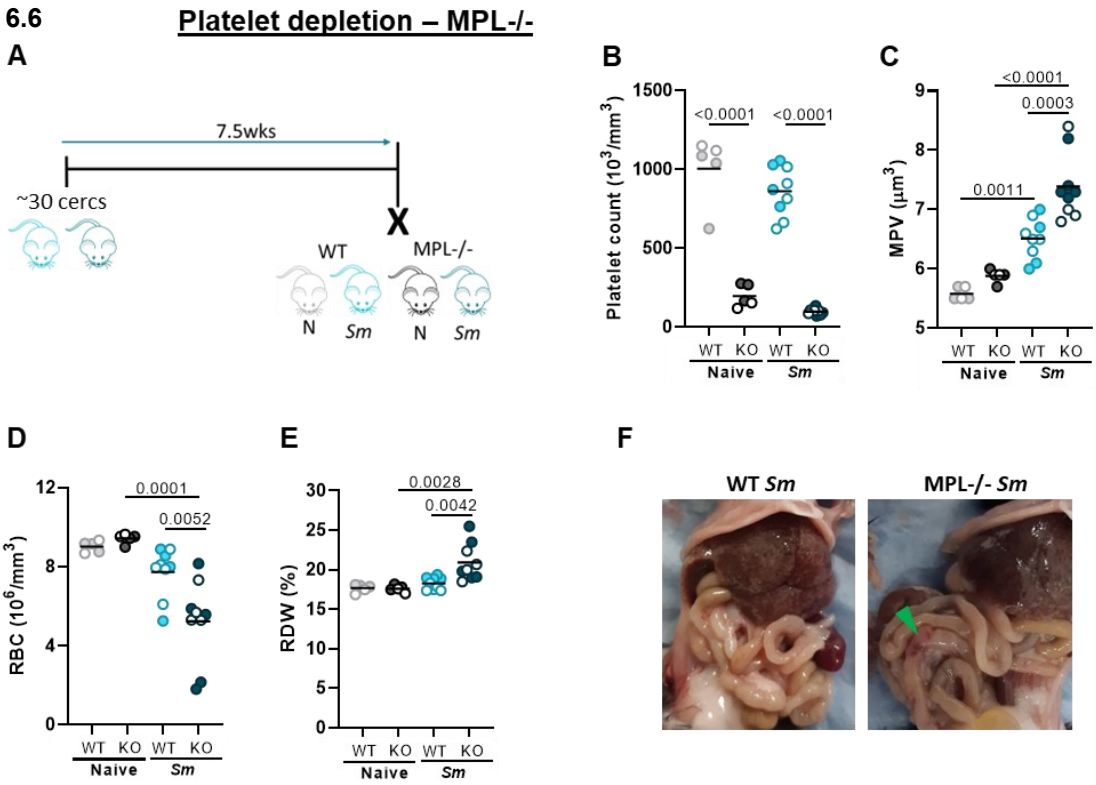

Figure 6.6 Signs of anaemia in schistosome-infected MPL$^{-/-}$ mice

A) C57BL/6 and MPL$^{-/-}$ mice were infected with 30-35 *S. mansoni* cercariae (*Sm*) and harvested at 7.5 weeks (open circles = male, closed circles = female). Terminal brachial tail bleed B) platelet count, C) mean platelet volume, D) red blood cell count and E) percentage red cell distribution width. F) Representative images of *Sm* WT and MPL$^{-/-}$ mice post-mortem, intestinal bleeding identified by green arrow. (WT Naive n=5, KO Naive n=5, WT *Sm* n=9, KO *Sm* n=9). Data pooled from 2 independent experiments, representative of 3 independent experiments. Statistical significance determined by one-way ANOVA with post-hoc Tukey's test on the mean of each group (B-E). Non-significance ($p>0.05$) not shown.

6.7

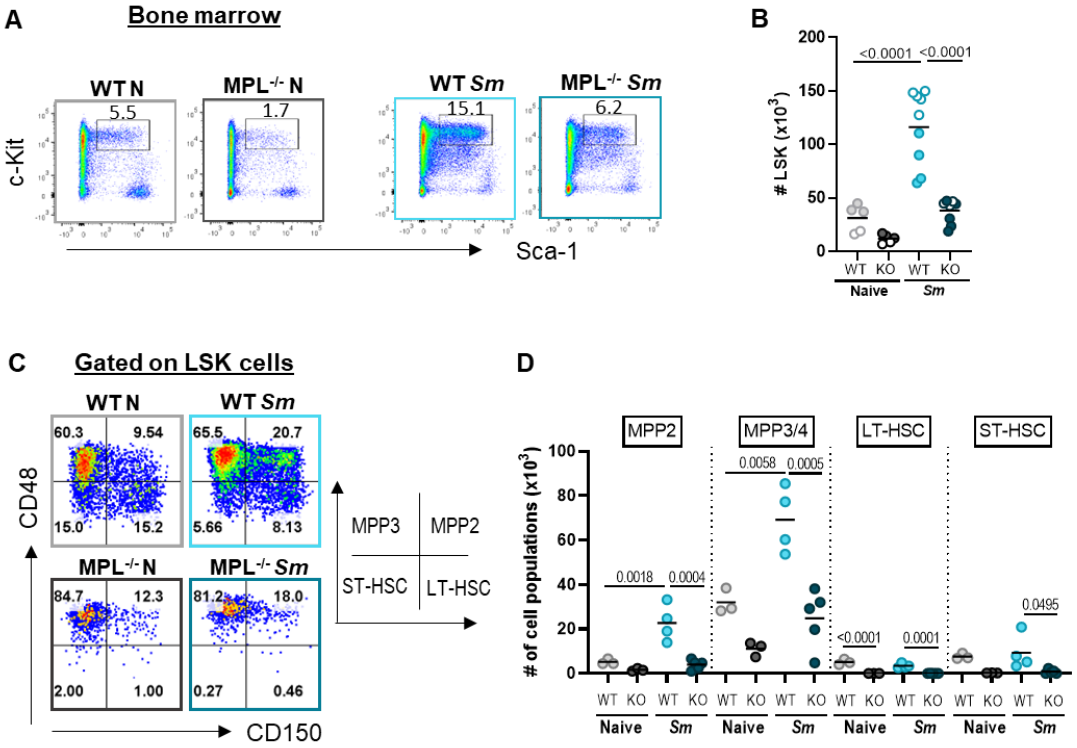

Figure 6.7 Failure of BM stem cell expansion in schistosome-infected MPL$^{-/-}$ mice
C57BL/6 and MPL$^{-/-}$ mice were infected with 30-35 *S. mansoni* cercariae (*Sm*) and harvested at 7.5 weeks (open circles = male, closed circles = female). A) Representative FACS staining and B) percentage of LSK cells in the BM. C) Representative FACS staining and D) flow cytometry quantification of multipotent progenitor (MPP) cell subsets (MPP2-CD48^{+}CD150^{+}, MPP3/4-CD48^{+}CD150^{-}, LT-HSC-CD48^{-}CD150^{+}, ST-HSC-CD48^{-}CD150^{-}). (WT Naive n=5, KO Naive n=5, WT *Sm* n=9, KO *Sm* n=9). Data pooled from 2 independent experiments, representative of 3 independent experiments. Statistical significance determined by one-way ANOVA with post-hoc Tukey's test on the mean of each group (B, D). Non-significance ($p>0.05$) not shown.

6.8

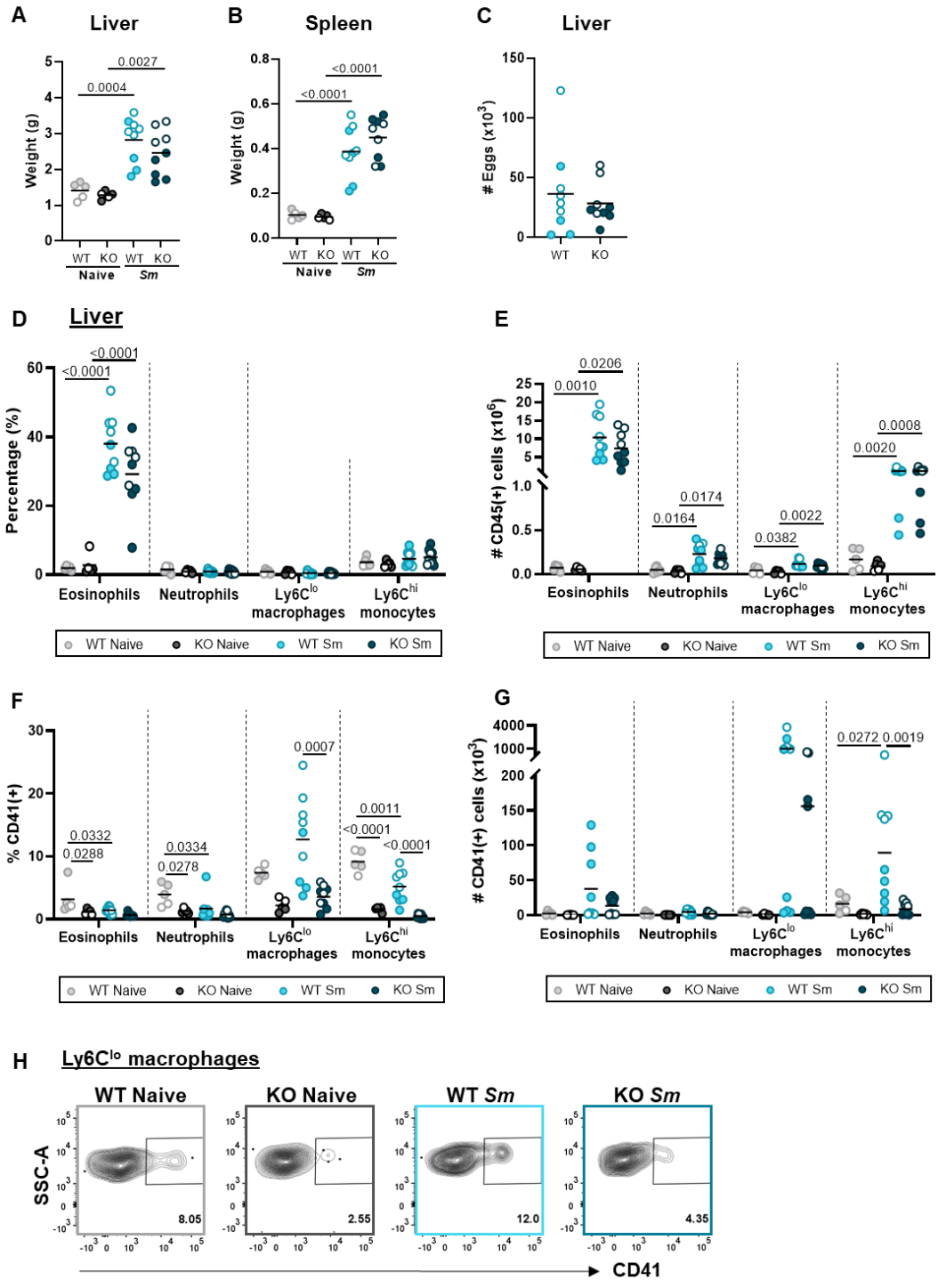

Figure 6.8 Fewer hepatic PLA in schistosome-infected MPL$^{-/-}$ compared with WT mice
C57BL/6 and MPL$^{-/-}$ mice were infected with 30-35 *S. mansoni* cercariae (*Sm*) and harvested at 7.5 weeks (open circles = male, closed circles = female). Postmortem A) liver, B) spleen weights and C) hepatic schistosome egg counts. D) Percentage and E) number of leukocyte populations in the liver and F) percentage and G) number of CD41^{+} leukocyte populations. H) Representative FACS plots of macrophage CD41 staining. (WT Naive n=5 (grey), KO Naive n=5 (black), WT *Sm* n=9 (light blue), KO *Sm* n=9 (dark blue)). Data pooled from 2 independent experiments, representative of 3 independent experiments. Statistical significance determined by one-way ANOVA with post-hoc Tukey's test on the mean of each group (A-B, D-G) or unpaired Student's t-test (C). Non-significance (p>0.05) not shown.

6.9 Liver

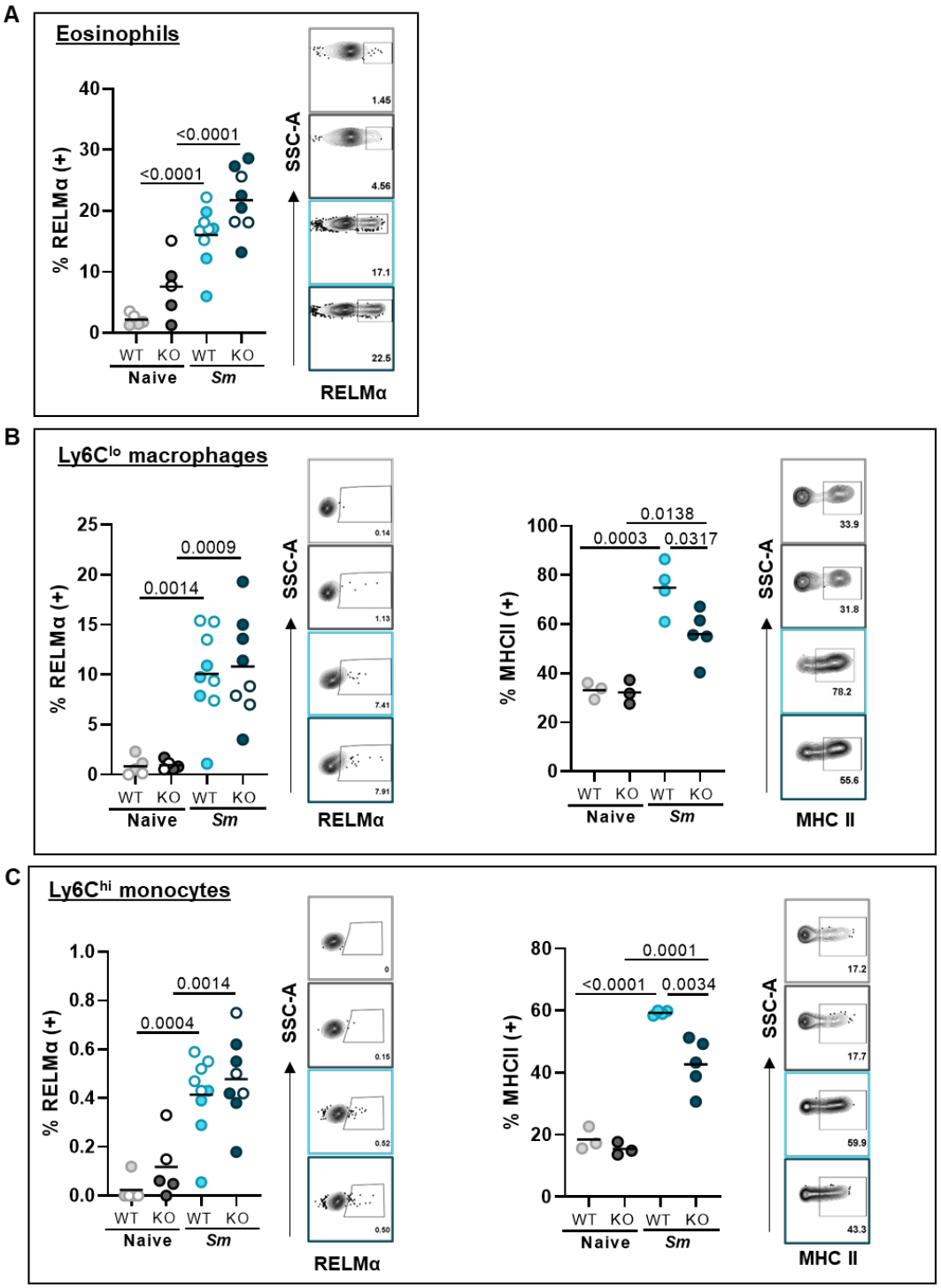

Figure 6.9 Reduction of MHCII on hepatic macrophages and monocytes in schistosome-infected MPL$^{-/-}$ compared with WT mice

C57BL/6 and MPL$^{-/-}$ mice were infected with 30-35 *S. mansoni* cercariae (*Sm*) and harvested at 7.5 weeks (open circles = male, closed circles = female). A) Percentage of RELMα and representative FACS plots in hepatic eosinophils. Percentage of RELMα and MHCII and representative FACS plots by hepatic B) Ly6C^{lo} macrophages and C) Ly6C^{hi} monocytes. (WT Naive n=5 (grey), KO Naive n=5 (black), WT *Sm* n=9 (light blue), KO *Sm* n=9 (dark blue)). Data pooled from 2 independent experiments, representative of 3 independent experiments. Statistical significance determined by one-way ANOVA with post-hoc Tukey's test on the mean of each group (A-C). Non-significance ($p>0.05$) not shown.

6.10

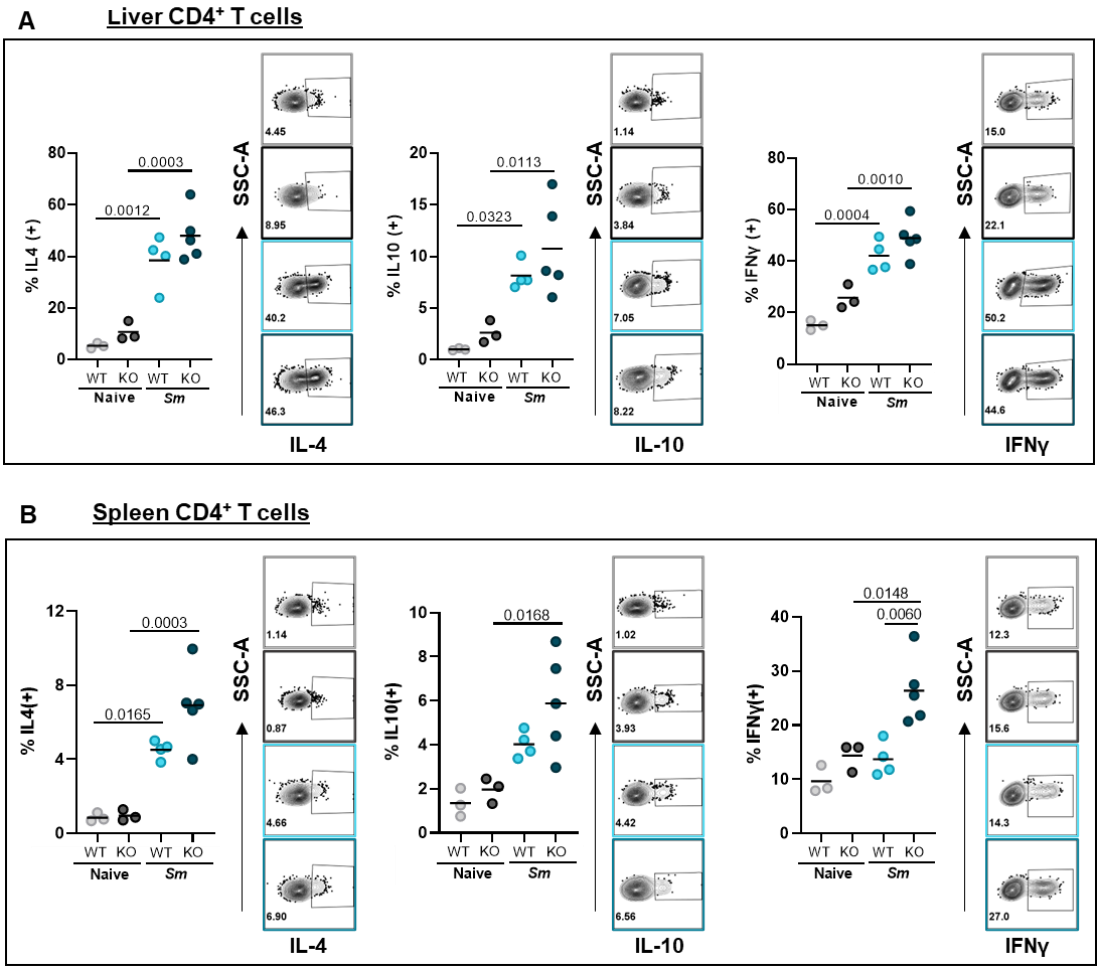

Figure 6.10 Elevated IFNγ production by CD4⁺ T cells in MPL$^{-/-}$ infected mice

C57BL/6 and MPL$^{-/-}$ mice were infected with 30-35 *S. mansoni* cercariae (*Sm*) and harvested at 7.5 weeks (open circles = male, closed circles = female). Single cell suspensions (2-4x10^6 cells) from liver and spleen isolation processing were cultured for 4hr at 37^{o}C with 1μg/ml Ionomycin, 10μg/ml PMA and 10μg/ml Brefeldin A. Percentage of IL-4, IL-10 and IFNγ by CD4⁺ T cells and representative FACS plots in the A) liver and B) spleen. (WT Naive n=5 (grey), KO Naive n=5 (black), WT *Sm* n=9 (light blue), KO *Sm* n=9 (dark blue)). Data pooled from 2 independent experiments, representative of 3 independent experiments. Statistical significance determined by one-way ANOVA with post-hoc Tukey's test on the mean of each group (A-B). Non-significance (p>0.05) not shown.

6.3.3 Do elevated platelet counts effect the immune response in schistosome infection - rTPO?

Both our models of platelet depletion in schistosome infection resulted in ill-health, likely reflecting a bleeding phenotype. Given the caveats and lack of specificity of both these models as well as the ethical implications of increased mortality in further platelet depletion systems, we decided to take an alternative approach and look at the role of platelets in schistosome infection by enhancing platelet numbers.

In our experiments we used both recombinant mouse TPO (rTPO) and Romiplostim to enhance platelet production. Romiplostim is a 60-kDa molecule peptidbody that has four 14-amino acid peptides attached to an Fc heavy chain that enables a 10,000-fold increase in activity, greater stability and a longer half-life than rTPO (411). Romiplostim, unlike Eltrombopag and Avatrombopagelon competes with endogenous TPO at the distal region of the MPL receptor (**Figure 6.11**)(401).

To test the importance of platelets *in vivo* in anti-schistosome immune responses, we treated mice with rTPO three times a week for 2 weeks at weeks 9 and 10 post-infection based on a previously optimised dosing regimen (Hitchcock lab, data not shown) (**Figure 6.12A**). Surprisingly, these repeated rTPO injections only led to a subtle and non-significant increase in circulating platelets in both naive and 11 week schistosome-infected mice, and did not reverse infection-induced thrombocytopenia (**Figure 6.12B**). Our rTPO regimen also did not influence platelet size judged by MPV (**Figure 6.12C**). As platelet numbers only subtly increased, we next looked in the BM at the number of MK and their ploidy. We showed rTPO significantly enhanced both 2N and >32N MK in naive mice, whilst decreasing 16N MK (**Figure 6.12F-G**). Whereas rTPO only significantly enhanced 32N MK in schistosome-infected mice.

We next looked at whether enhanced rTPO affected the gross pathology associated with schistosome infection. We observed no significant difference in hepatosplenomegaly or liver egg burdens in the presence or absence of rTPO (**Figure 6.13A-C**). There were also no significant changes in the

percentage of immune cell populations in the liver between control and rTPO-treated mice (**Figure 6.13D**). However, there was a general increase in the number of all immune cell populations after rTPO treatment in schistosome infection with the eosinophil population reaching significance ($p<0.05$) (**Figure 6.13E**). Similarly, there was no difference in the percentage of $CD41^+$ aggregates after rTPO treatment but the total number of eosinophil and macrophage PLA was significantly increased in schistosome-infected mice treated with rTPO (**Figure 6.13F-G**). Despite the increase in total number of platelet aggregates there was no difference in RELMα or MHCII expression by eosinophils, macrophages or monocytes in the liver (**Figure 6.14A-C**). As there were more PLA following rTPO treatment we were able to perform pairwise comparison of $CD41^+$ and $CD41^-$ populations. Consistent with our findings in **Chapter 3**, $CD41^+$ eosinophils in schistosome infection were $RELM\alpha^{lo}$ compared with the $RELM\alpha^{hi}$ $CD41^-$ sub-population, and this was also the case in the presence of rTPO (**Figure 6.15A**). Moreover, when considering the $CD41^+$ macrophage populations in schistosome infection with rTPO treatment, these showed a similar trend with the $CD41^+$ macrophages being $RELM\alpha^{hi}$ $MHCII^{lo}$ (**Figure 6.15B**). In this experiment there was little difference between the $CD41^+$ and $CD41^-$ subsets of hepatic monocytes in terms of their RELMα and MHCII expression in the presence or absence of rTPO (**Figure 6.15C**). We also looked at the $CD4^+$ T cell populations in the liver and spleen to see whether enhanced PLA with APC impacted on T cell activation. However, this did not appear to be the case as no difference was seen in $CD4^+$ T cell production of IL-4, IL-10 and IFNγ in the presence of rTPO (**Figure 6.16A-B**).

6.11

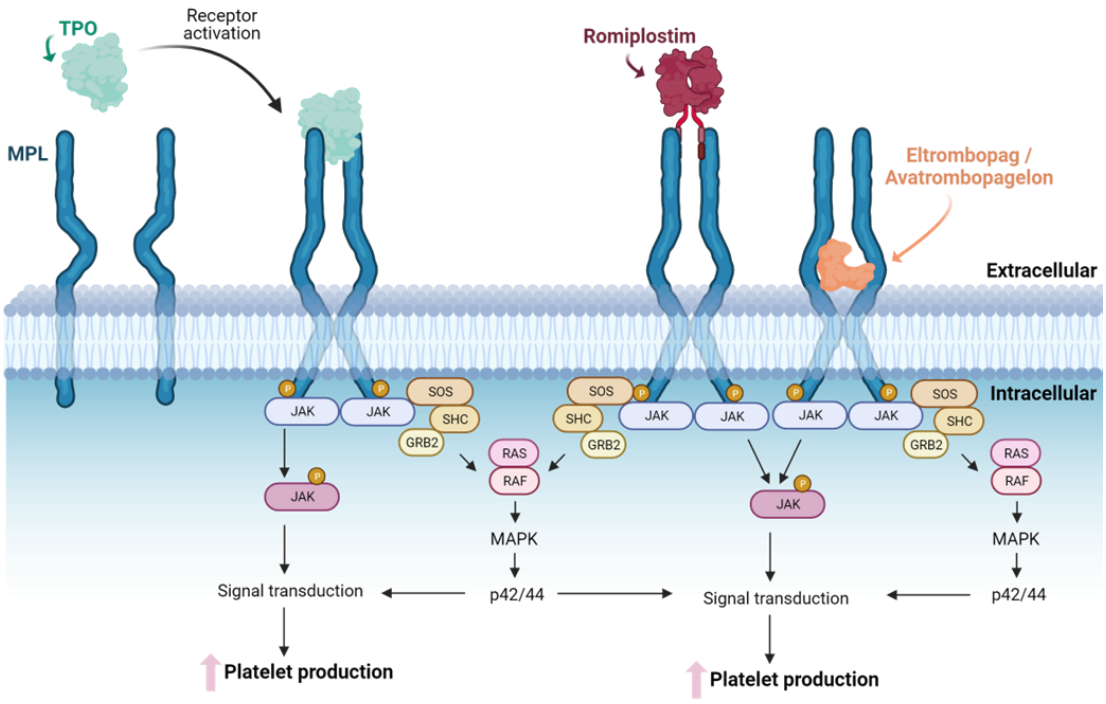

Figure 6.11 TPO and TPO mimetic signalling via MPL receptor
Simplified representation of TPO (green), Romiplostim (red) and Eltrombopag/ Avatrombopagelon (orange) interactions at different sites of the MPL receptor and one of the downstream signalling pathways that is stimulated. Based on (412).

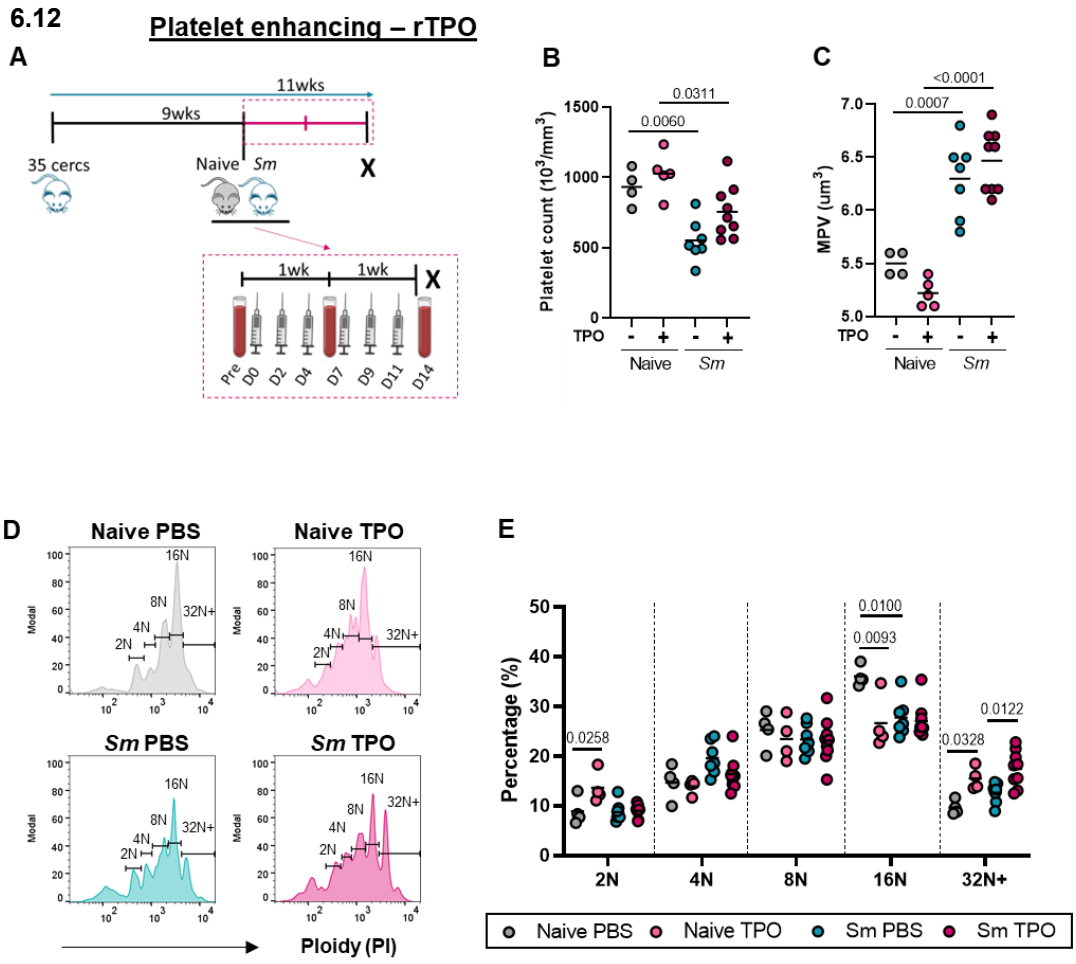

Figure 6.12 Partial platelet enhancement with rTPO treatment

A) C57BL/6 mice were infected with ~35 *S. mansoni* cercariae (*Sm*), at 9 weeks mice were injected IP with 10ug/mouse recombinant mouse TPO or PBS 3 times per week for 2 weeks. Mice were harvested at 11 weeks post-infection. Terminal brachial tail bleed B) platelet count, C) mean platelet volume. D) Representative ploidy histograms and E) quantification of $CD41^{+}$ MK in the BM of 1 femur. (Naive PBS n=4 (grey), Naive rTPO n=4 (light pink), *Sm* PBS n=7 (blue), *Sm* rTPO n=9 (pink)). Data representative of 2 independent experiments. Statistical significance determined by one-way ANOVA with post-hoc Tukey's test on the mean of each group (B-C, G). Non-significance ($p>0.05$) not shown.

6.13

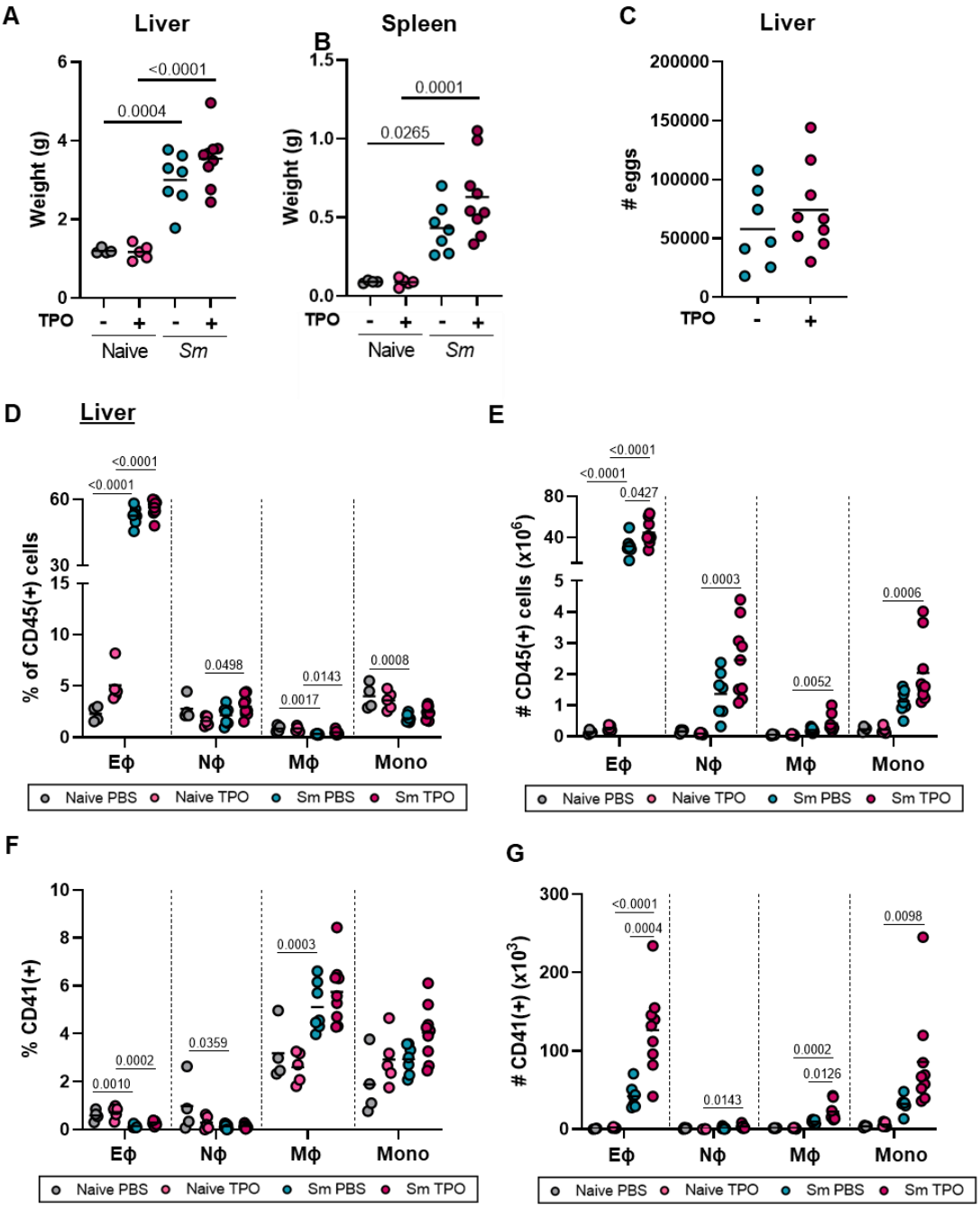

Figure 6.13 Significant increase in the number of PLA in the liver in schistosome infection with rTPO

C57BL/6 were infected with ~35 *S. mansoni* cercariae (*Sm*), at 9 weeks mice were injected IP with 10ug/mouse recombinant mouse TPO or PBS 3 times per week for 2 weeks. Mice were harvested at 11 weeks post-infection. Post-mortem A) liver, B) spleen weights and C) schistosome egg counts in the liver. D) Percentage and E) number of leukocyte populations in the liver and F) percentage and G) number of CD41^{+} leukocyte populations. (Naive PBS n=4 (grey), Naive rTPO n=4 (light pink), *Sm* PBS n=7 (blue), *Sm* rTPO n=9 (pink)). Data representative of 2 independent experiments. Statistical significance determined by one-way ANOVA with post-hoc Tukey's test on the mean of each group (A-B, D-G) or unpaired Student's t-test (C). Non-significance ($p>0.05$) not shown.

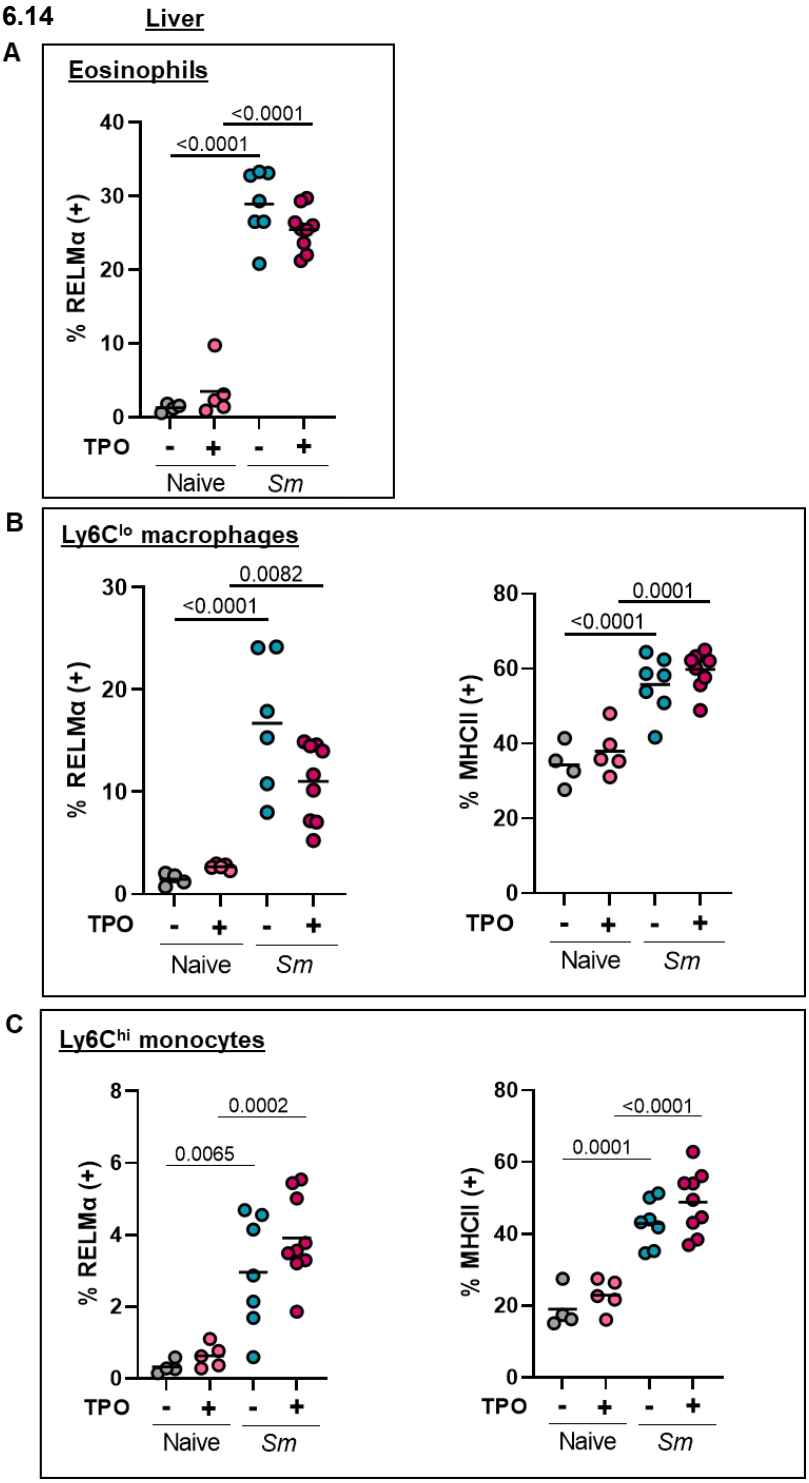

Figure 6.14 No difference in activation marker expression in the presence or absence of rTPO

C57BL/6 were infected with ~35 *S. mansoni* cercariae (*Sm*), at 9 weeks mice were injected IP with 10ug/mouse recombinant mouse TPO or PBS 3 times per week for 2 weeks. Mice were harvested at 11 weeks post-infection. A) Percentage of RELMα in hepatic eosinophils. Percentage of RELMα and MHCII by hepatic B) Ly6C^{lo} macrophages and C) Ly6C^{hi} monocytes. (Naive PBS n=4, Naive rTPO n=4, *Sm* PBS n=7, *Sm* rTPO n=9). Data representative of 2 independent experiments. Statistical significance determined by one-way ANOVA with post-hoc Tukey's test on the mean of each group (A-B, D-G) or unpaired Student's t-test (C). Non-significance (p>0.05) not shown.

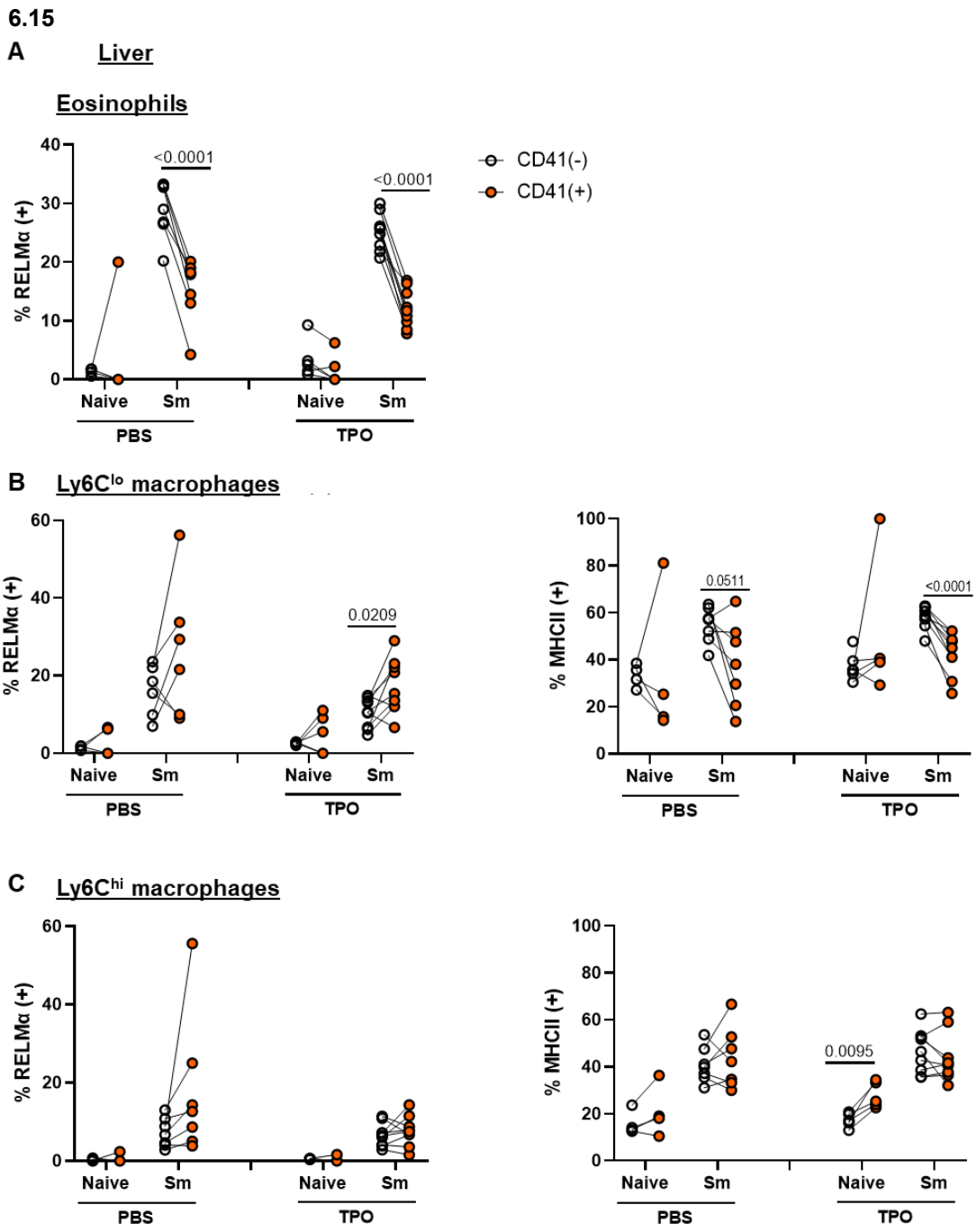

Figure 6.15 Eosinophil, macrophage and monocyte subsets interact with platelets to the same extent in the presence or absence of rTPO

C57BL/6 were infected with ~35 *S. mansoni* cercariae (*Sm*), at 9 weeks mice were injected IP with 10ug/mouse recombinant mouse TPO or PBS 3 times per week for 2 weeks. Mice were harvested at 11 weeks post-infection. A) Pairwise comparison of $CD41^{-/+}$ hepatic eosinophils with respect to RELMα expression. Pairwise comparison of $CD41^{-/+}$ hepatic B) $Ly6C^{lo}$ macrophages and C) $Ly6C^{hi}$ monocytes with respect to RELMα and MHCII. (Naive PBS n=4, Naive rTPO n=4, *Sm* PBS n=7, *Sm* rTPO n=9). $CD41^{-}$-white, $CD41^{+}$-orange. Data representative of 2 independent experiments. Statistical significance determined by paired t-test of the mean between $CD41^{-/+}$ groups (A-C). Non-significance ($p>0.05$) not shown.

6.16

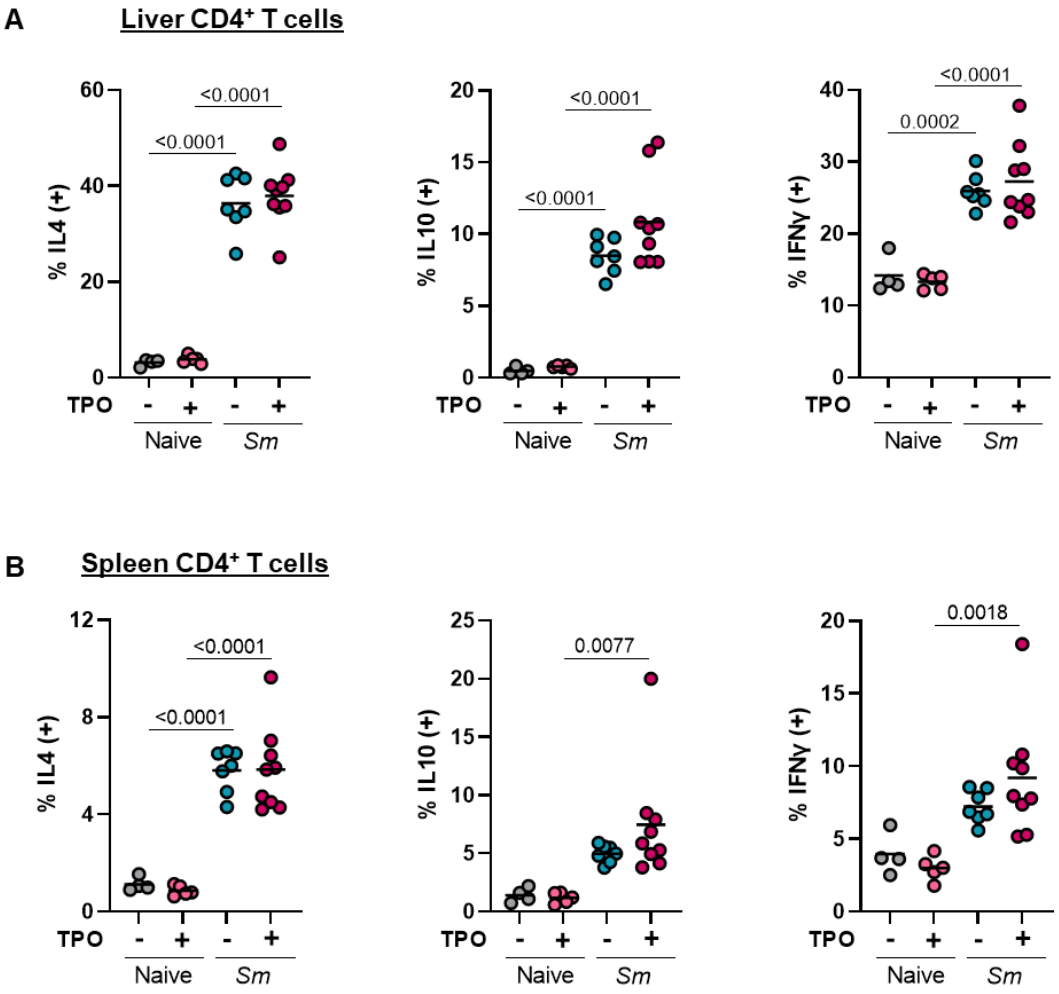

Figure 6.16 No difference in hepatic or splenic CD4+ T cell responses after rTPO treatment

C57BL/6 were infected with ~35 *S. mansoni* cercariae (*Sm*), at 9 weeks mice were injected IP with 10ug/mouse recombinant mouse TPO or PBS 3 times per week for 2 weeks. Mice were harvested at 11 weeks post-infection. Single cell suspensions (2-4x10^6 cells) from liver and spleen isolation processing were cultured for 4hr at 37°C with 1µg/ml Ionomycin, 10µg/ml PMA and 10µg/ml Brefeldin A. Percentage of IL-4, IL-10 and IFNγ by $CD4^+$ T cells in the A) liver and B) spleen. (Naive PBS n=4, Naive rTPO n=4, *Sm* PBS n=7, *Sm* rTPO n=9). Data representative of 2 independent experiments. Statistical significance determined by one-way ANOVA with post-hoc Tukey's test on the mean of each group (A-B). Non-significance ($p>0.05$) not shown.

6.3.4 Do elevated platelet counts affect the immune response in schistosome infection - Romiplostim?

Having observed only a subtle increase in platelet number *in vivo* following 2 weeks treatment with rTPO we next tried sustained treatment with the TPO mimetic Romiplostim. Here naive and schistosome-infected mice were given Romiplostim once a week for 4 weeks beginning at week 6 post-infection based on pilot optimisation experiments (**Figure 6.17A, Appendix 6**). We wanted to examine whether elevated platelet counts from the point of schistosome egg laying (~6 weeks post-infection) to the more chronic stages impacted on infection-induced immune response and pathology. Platelets and MPV were significantly and substantially elevated from as early as 1 week of treatment in both naive and schistosome-infected mice given Romiplostim (**Figure 6.17B-C**). Interestingly, at all time-points the platelet count in schistosome-infected mice treated with Romiplostim was lower than that in naive Romiplostim controls, but the MPV was significantly higher.

In **Chapter 3** we showed that despite a significant reduction in circulating and hepatic TPO there was still sustained numbers of MK in the BM, but that these were skewed towards lower ploidy (predominantly 4N). Here we see that Romiplostim massively increased the number of MK in the BM to the same extent in both naive and schistosome-infected mice (**Figure 6.17D-E**). Moreover, the percentage of $CD68^{+}$ macrophages was depleted in the BM of infected mice regardless of Romiplostim treatment (**Figure 6.17D, F**). In naive mice most notably, Romiplostim caused a significant reduction in 16N MK but increased 4N and 32N MK (**Figure 6.17G-H**). However, in schistosome infection Romiplostim did not significantly increase 32N MK but increased 2N, 4N and 8N populations alongside reduced 16N (**Figure 6.17G-H**).

With Romiplostim being a TPO mimetic and having significant effects on BM MK we were interested to assess whether other stem cell and progenitor populations were also impacted. Romiplostim caused a significant increase in the percentage of LSK cells in the BM which was further increased in schistosome infection (**Figure 6.18A-B**). This was primarily a result of expanded MPP2, MPP3 and LT-HSC populations, and was consistent with the

reverse phenotype (i.e. reduced numbers of LSK cells) seen before in MPL$^{-/-}$ mice (**Figure 6.18C** and **Figure 6.7D**).

Given the significant changes at the BM level and in circulating platelet number, we next assessed gross pathological changes. Whilst there was no difference in hepatomegaly, the spleen was significantly larger in schistosome-infected mice treated with Romiplostim (**Figure 6.19A-B**). There was no significant difference in schistosome egg counts in the liver or intestines, however there were trends of elevation in the liver (**Figure 6.19C-D**). There was also no difference in the percentage of granuloma coverage or in the average granuloma diameter in the liver indicating boosting platelet numbers did not substantially impact on disease pathology (**Figure 6.19E-G**). Treatment of both naive and schistosome-infected mice with Romiplostim led to an increase in liver CD41^{+} MK compared with their untreated counterparts, although this was only significant for naive mice (**Figure 6.20A-B**). Perhaps surprisingly given that infection caused elevated liver MK numbers, Romiplostim treatment led to significantly more MK in the liver of naive mice compared with infected mice. These differences in hepatic MK number may reflect the higher platelet levels in naive mice following Romiplostim treatment compared with schistosome infection (**Figure 6.20B**).

As circulating platelets increased over 3-fold with Romiplostim treatment we next examined whether this led to increased PLA and altered the recruitment of inflammatory cells to the liver, as has been observed in other tissue sites (206,222,226,313,398). Romiplostim did not alter the proportion or number of liver eosinophils following infection but did lead to increases in neutrophils and monocytes in both naive and infected animals (**Figure 6.21A-B**). In terms of PLA, Romiplostim increased the percentage of CD41^{+} leukocytes of all myeloid cells in naive and infected animals and reached significance ($p<0.05$) for eosinophils and macrophages (**Figure 6.21C**). Moreover, there were significantly more CD41^{+} macrophages, monocytes and B cells in Romiplostim-treated schistosome-infected mice compared with those that were untreated (**Figure 6.21C, E**). This was also reflected in total cell number with there being significantly more CD41^{+} eosinophils, neutrophils and monocytes (**Figure 6.21D-E**).

As there were more PLA, we next assessed the phenotype and activation of these immune cell populations. Here we showed eosinophils, macrophages and monocytes expressed RELMα to the same extent in the presence or absence of Romiplostim (**Figure 6.22A-C**) and this was also the case for MHCII expression by macrophages. In contrast, Romiplostim treatment of infected mice led to reduced monocyte MHCII expression compared with control infected mice (**Figure 6.22C**). Furthermore, monocyte/ macrophages that were $CD41^{+}$ from infected, Romiplostim-treated mice were no longer $MHCII^{lo}$ compared with their $CD41^{-}$ $MHCII^{hi}$ counterparts, instead there was no difference between the $CD41^{+/-}$ subsets and MHCII expression. We also tested whether macrophages and monocytes responded similarly to LPS stimulation. We were only able to examine schistosome-infected liver samples because of the low cell numbers recovered from naive mice. This showed that Romiplostim did not affect the ability of macrophages or monocytes to produce IL-10, IL-6 or TNFα following LPS stimulation (**Figure 6.23A, C**). We also performed pairwise comparisons of the $CD41^{+}$ and $CD41^{-}$ populations and showed that even though there were more PLA after Romiplostim treatment the direction of the immune response by monocytes and macrophages remained unchanged with respect to IL-10, IL-6 and TNFα (**Figure 6.23B, D**). There was a relatively high degree of variation between samples due to low cell numbers that were analysed because some platelet interactions were lost during the detachment process of the monocytes and macrophages. Despite this, when we examined the macrophage and monocyte populations together $CD41^{+}$ cells were $IL\text{-}6^{hi}$ $TNF\alpha^{lo}$, and there was no difference in IL-10 expression (**Appendix 7**). This was consistent with qPCR transcript level analysis in **Figure 3.25**.

Although we saw no significant increase in aggregates between T cells and platelets after Romiplostim treatment, we were again interested to see whether platelet binding to myeloid cells that can be $MHCII^{hi}$ offers a mechanism by which platelets can influence the T cell response. Moreover, as platelets have now been shown to express MHCII and present antigen to T cells in some pathological states we next examined the lymphoid response in these mice, focusing primarily on $CD4^{+}$ T cells which predominate during schistosome

infection (413). Again, due to limited cell numbers we only assessed schistosome-infected samples and showed liver $CD4^+$ T cells from Romiplostim-treated mice responded the same extent to PMA/Ionomycin stimulation with respect to IL-4, IL-10, IL-13 and IFNγ (**Figure 6.24A**). Pairwise comparisons of $CD41^+/CD41^-$ populations demonstrated how platelets were interacting with specific subsets of $CD4^+$ T cells i.e. IL-4^{lo}, IL-10^{lo}, IL-13^{lo} and IFNγ^{hi} and this was unchanged after Romiplostim treatment (**Figure 6.24B-C**). We next assessed whether the surface phenotype of activation markers in $CD4^+$ T cells was impacted by Romiplostim treatment. Schistosome infection induced a marked expansion of $T_{E/M}$ ($CD44^+CD62L^-$) cells, and these were also expanded in schistosome-infected mice treated with Romiplostim (**Figure 6.24D-E**). Whilst Romiplostim did not alter the response in infection it did cause changes in the surface phenotype of $CD4^+$ T cells from naive mice, with loss of $CD62L^-$ $CD44^-$ cells and replacement with $T_{E/M}$ cells (**Figure 6.24D-E**). There was a lot of sample variation and little difference was seen in the interaction of platelets and the different populations of $CD4^+$ T cells (**Figure 6.24F**).

Having examined the pathological and immunological changes occurring in the liver, we next wanted to assess whether the spleen had become a reservoir for excess platelets and whether this was contributing to the enhanced splenomegaly following schistosome infection and Romiplostim treatment (**Figure 6.19B**). Fluorescence microscopy of the spleen from both naive and schistosome-infected mice treated with Romiplostim showed a significant increase in $CD41^+$ staining, with the majority being nucleated, suggestive of MK (**Figure 6.25A-D**). All MK were localised within the red pulp and infection did not further increase the number of MK associated with Romiplostim treatment. Given the significant increase in MK in the spleen and their potential immunological roles we looked to see whether the immune cell fractions of the spleen were impacted by Romiplostim treatment. In naive mice, Romiplostim increased the percentage of neutrophils, macrophages and monocytes in the spleen, but this was not seen in schistosome infection or reflected in total cell number (**Figure 6.26A-B**). However, in schistosome infection Romiplostim caused a significant reduction in both percentage and

number of B cells as well as a reduction in the number of $CD4^+$ T cells (**Figure 6.26A-B**). Romiplostim significantly increased the percentage of $CD41^+$ eosinophils, macrophages and monocytes in naive mice, and this extended to all immune cell populations except neutrophils in schistosome infection (**Figure 6.26C**). The total number of $CD41^+$ immune cells was also elevated in all cell populations after Romiplostim treatment of schistosome-infected mice, with eosinophils, monocytes, B cells and CD4 T cells reaching significance ($p<0.05$) (**Figure 6.26D**). In **Chapter 3.23** we showed platelets preferentially interacted with a specific subset of spleen $T_{E/M}$ cells that were IL-4^{hi} IL-10^{hi} IL-13^{hi} and IFNγ^{hi}. Given the significant increase in platelet interactions after Romiplostim treatment we wanted to assess whether these impacted on immune cell activation. We showed splenic $CD4^+$ T cells still produced elevated IL-4, IL-10 and IL-13 in schistosome infection after Romiplostim treatment, however the previously observed increase in IFNγ production was less marked after Romiplostim suggesting the immune response may be more strongly type 2-polarised (**Figure 6.27A**). Comparisons of the $CD41^+$ and $CD41^-$ subsets were consistent with our findings in **Figure 3.23** showing that platelets preferentially interacted with cytokine-producing $CD4^+$ T cells in the spleen and this remained the case for all cytokines, even IFNγ production that was lower after Romiplostim treatment (**Figure 6.27B**). Given the significant difference in T cell surface phenotype in the liver with Romiplostim treatment it was surprising to see that this was not the case in the spleen and that there were no significant differences in naive versus activated T cell populations in the presence or absence of Romiplostim (**Figure 6.27C-D**). It was however, more evident in the spleen that $CD41^+$ T cells were primarily $T_{E/M}$ or T_{CM} (**Figure 6.27E**).

Our "platelet-boosting" experiments have shown that mice do not die prematurely as a result of excessive spontaneous thrombus formation. Moreover, schistosome-infected mice showed less of an increase in circulating platelets after treatment but enhanced PLA. Whilst platelet boosting did not induce profound changes in immune cell phenotype, together these experiments have highlighted infection-induced PLA that arise in the liver and spleen.

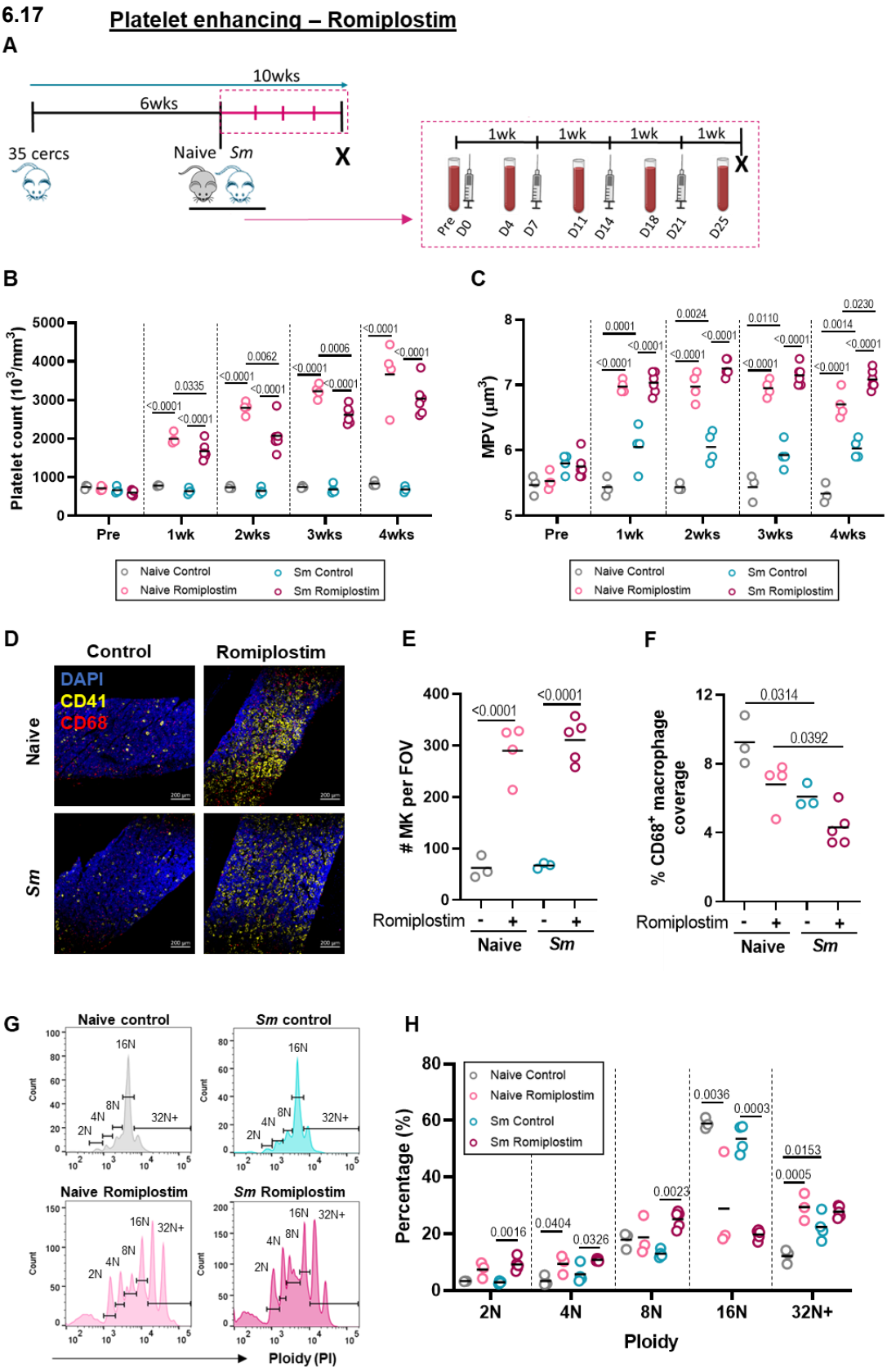

Figure 6.17 Infected mice respond less well to Romiplostim than naive mice

A) C57BL/6 mice were infected with ~35 *S. mansoni* cercariae (*Sm*), at 6 weeks mice were injected subcutaneously with 2.2µg/mouse Romiplostim or PBS once a week for 4 weeks, with weekly tail bleed monitoring. Mice were harvested at 10 weeks post-infection. Terminal

brachial tail bleed B) platelet count, C) mean platelet volume. D) Representative fluorescent images and quantification of the E) number of MK per field of view and F) percentage of $CD68^+$ macrophages in the BM. G) Representative ploidy histograms and H) quantification of $CD41^+$ MK in the BM of 1 femur. (Naive PBS n=3 (grey), Naive Romiplostim n=4 (light pink), *Sm* PBS n=4 (blue), *Sm* Romiplostim n=6 (pink)). Data representative of a single experiment. Statistical significance determined by one-way ANOVA with post-hoc Tukey's test on the mean of each group (B-C, E-F G). Non-significance (p>0.05) not shown.

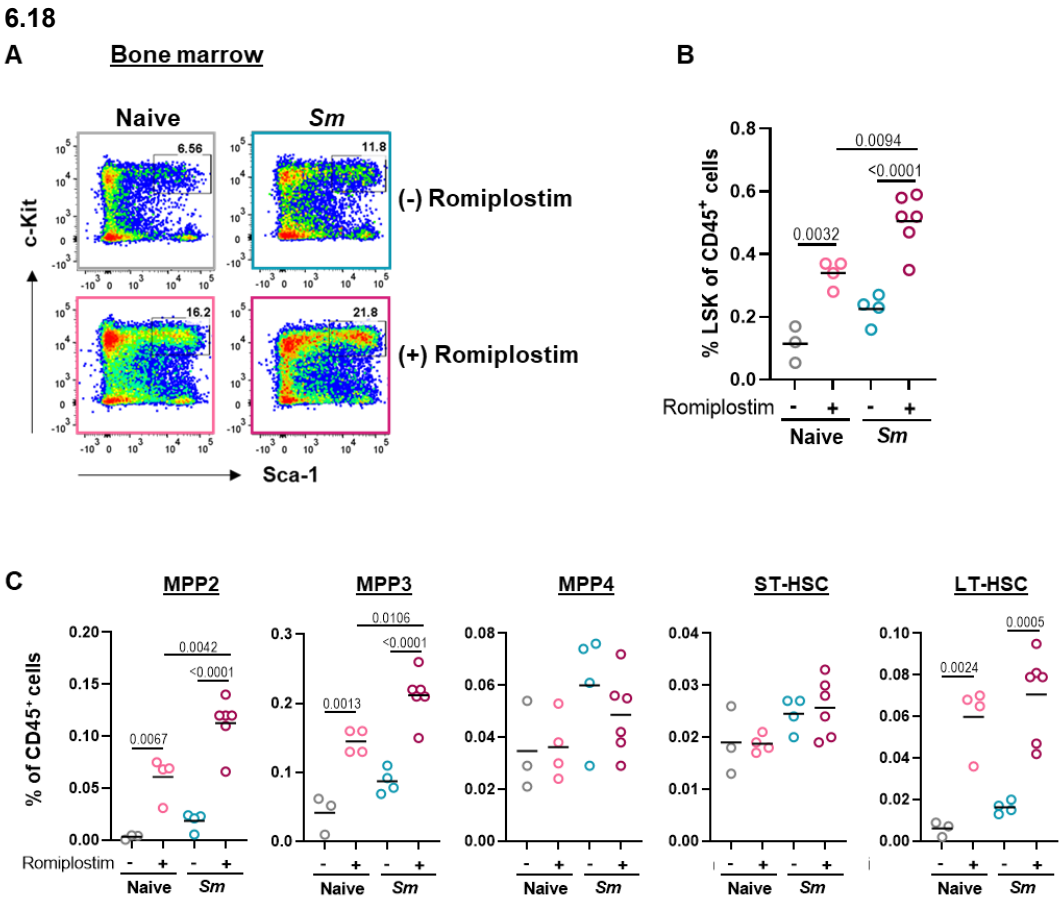

Figure 6.18 Expansion of LSK cells and progenitor populations after Romiplostim treatment

C57BL/6 mice were infected with ~35 *S. mansoni* cercariae (*Sm*), at 6 weeks mice were injected subcutaneously with 2.2µg/mouse Romiplostim or PBS once a week for 4 weeks, with weekly tail bleed monitoring. Mice were harvested at 10 weeks post-infection. A) Representative FACS staining and B) percentage of LSK cells in the BM. C) Flow cytometry quantification of progenitor cell subsets (MPP2-$CD48^+CD150^+$, MPP3/4-$CD48^+CD150^-$, LT-HSC-$CD48^-CD150^+$, ST-HSC-$CD48^-CD150^-$). (Naive PBS n=3, Naive Romiplostim n=4, *Sm* PBS n=4, *Sm* Romiplostim n=6). Data representative of a single experiment. Statistical significance determined by one-way ANOVA with post-hoc Tukey's test on the mean of each group (B-C, E-F G). Non-significance (p>0.05) not shown.

6.19

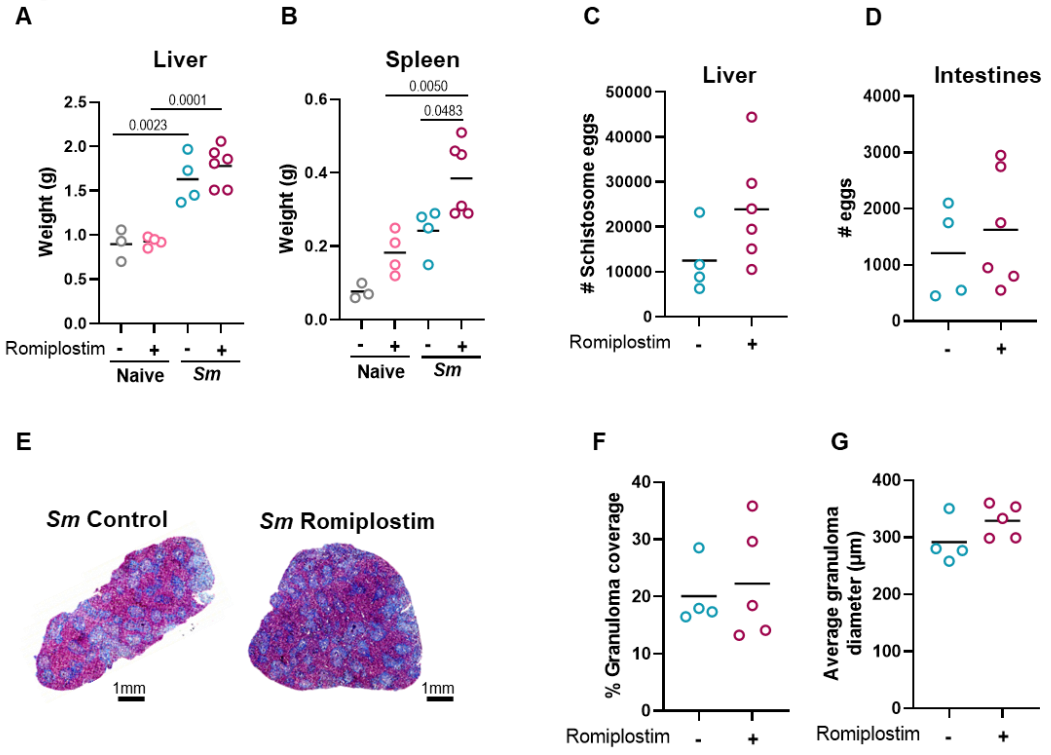

Figure 6.19 Enhanced splenomegaly in schistosome mice treated with Romiplostim
C57BL/6 mice were infected with ~35 *S. mansoni* cercariae (*Sm*), at 6 weeks mice were injected subcutaneously with 2.2µg/mouse Romiplostim or PBS once a week for 4 weeks, with weekly tail bleed monitoring. Mice were harvested at 10 weeks post-infection. Postmortem A) liver, B) spleen weights and C) hepatic schistosome egg counts. E) Representative images of Masson's Trichrome stained infected livers and quantification of F) the percentage of granuloma coverage and G) the average granuloma diameter. (Naive PBS n=3, Naive Romiplostim n=4, *Sm* PBS n=4, *Sm* Romiplostim n=6). Data representative of a single experiment. Statistical significance determined by one-way ANOVA with post-hoc Tukey's test on the mean of each group (A-B) or student's unpaired t-test (C-D, F-G). Non-significance ($p>0.05$) not shown.

6.20

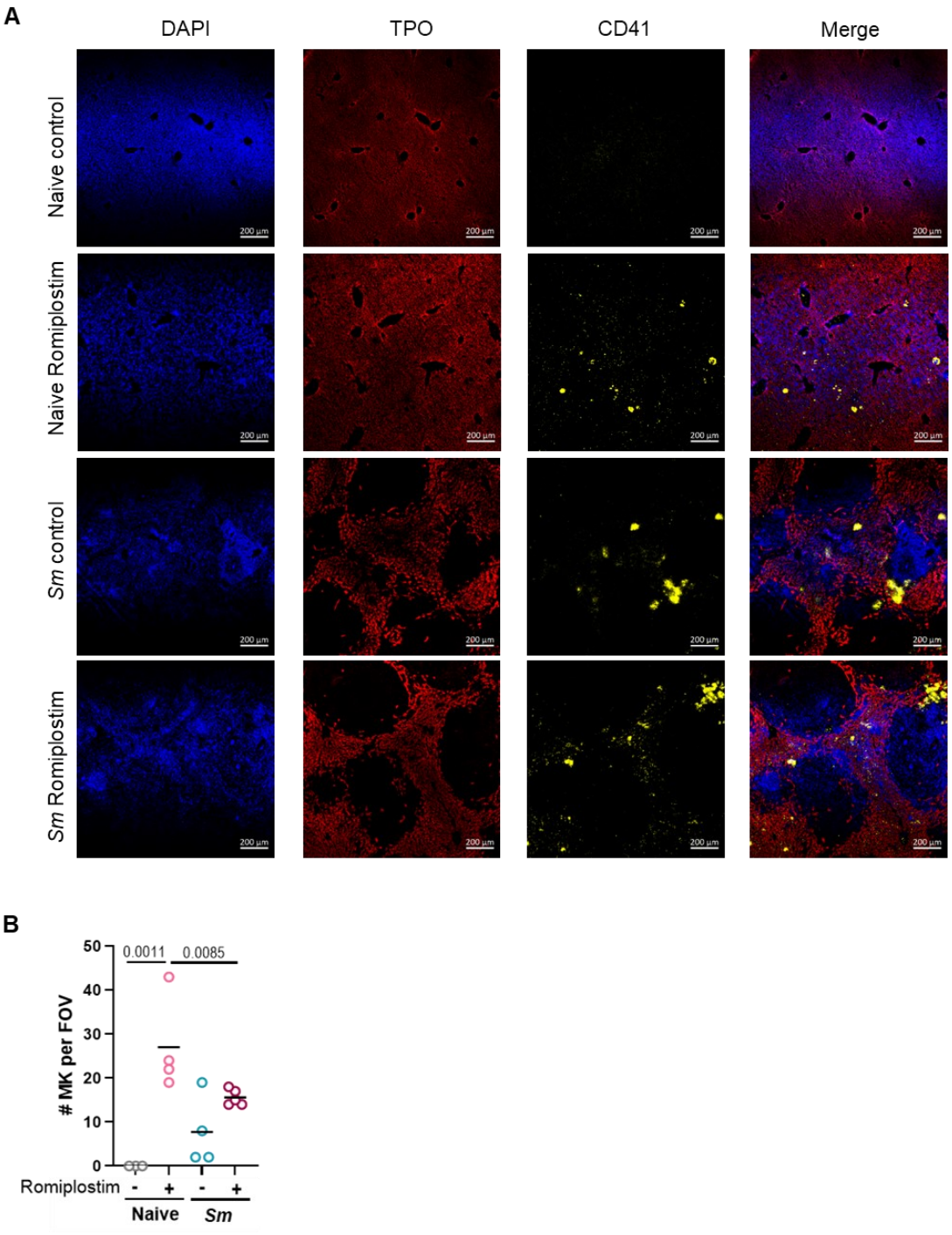

Figure 6.20 Fewer MK in the liver of schistosome-infected mice with Romiplostim compared with naive mice

C57BL/6 mice were infected with ~35 *S. mansoni* cercariae (*Sm*), at 6 weeks mice were injected subcutaneously with 2.2µg/mouse Romiplostim or PBS once a week for 4 weeks, with weekly tail bleed monitoring. Mice were harvested at 10 weeks post-infection. A) Representative fluorescent staining of livers with DAPI (blue), TPO (red) and CD41 (yellow). Images taken using 10x objective and 0.6x zoom. B) Quantification of fluorescent images of the number of MK per field of view. (Naive PBS n=3, Naive Romiplostim n=4, *Sm* PBS n=4, *Sm* Romiplostim n=6). Data representative of a single experiment. Statistical significance determined by one-way ANOVA with post-hoc Tukey's test on the mean of each group (B). Non-significance (p>0.05) not shown.

6.21

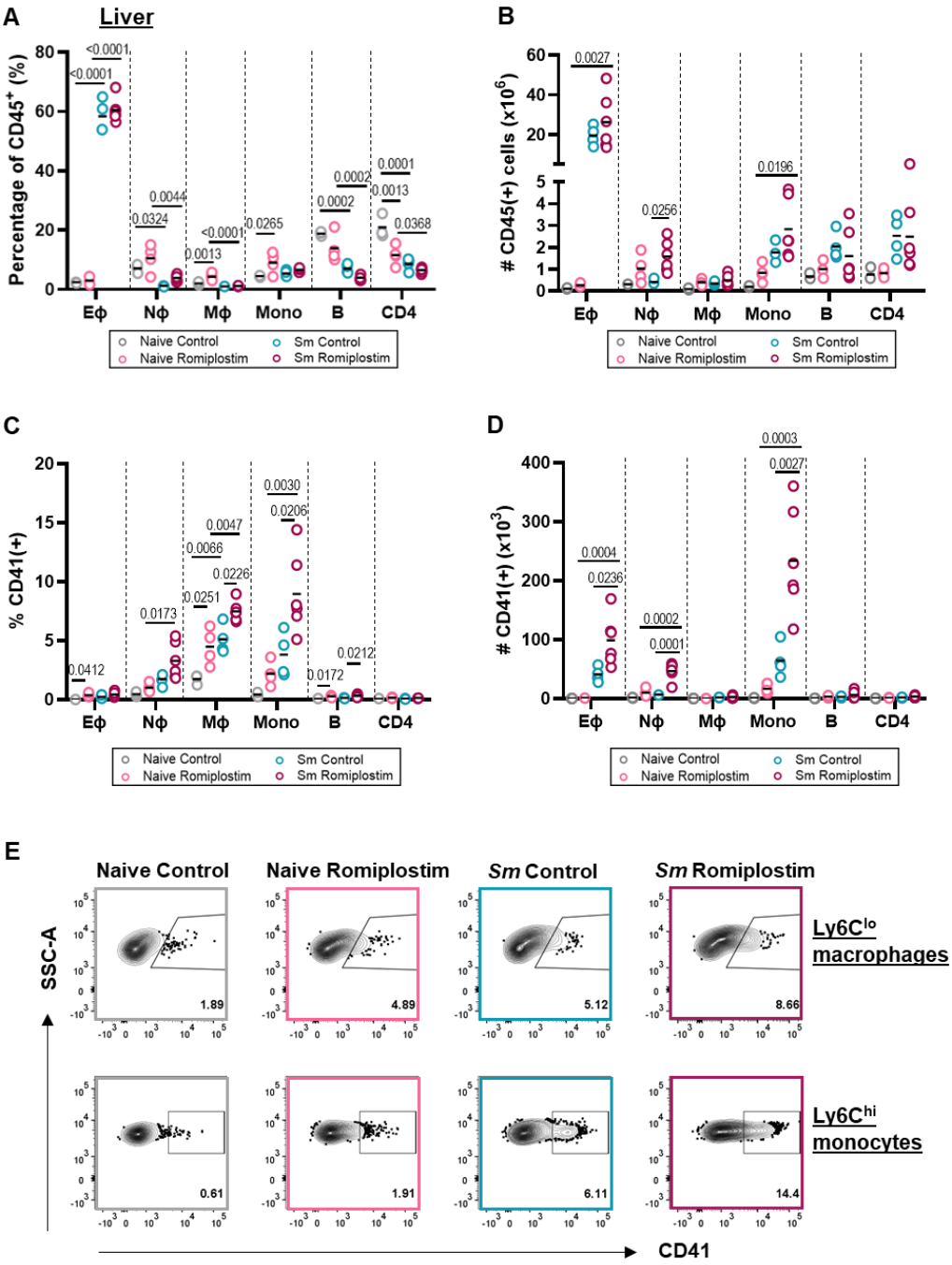

Figure 6.21 Romiplostim significantly increases the percentage and number of PLA in the liver

C57BL/6 mice were infected with ~35 *S. mansoni* cercariae (*Sm*), at 6 weeks mice were injected subcutaneously with 2.2µg/mouse Romiplostim or PBS once a week for 4 weeks, with weekly tail bleed monitoring. Mice were harvested at 10 weeks post-infection. A) Percentage and B) number of leukocyte populations in the liver and C) percentage and D) number of $CD41^+$ leukocyte populations. E) Representative CD41 staining of macrophages and monocytes. (Naive PBS n=3 (grey), Naive Romiplostim n=4 (light pink), *Sm* PBS n=4 (blue), *Sm* Romiplostim n=6 (pink)). Data representative of a single experiment. Statistical significance determined by one-way ANOVA with post-hoc Tukey's test on the mean of each group (A-D). Non-significance ($p>0.05$) not shown.

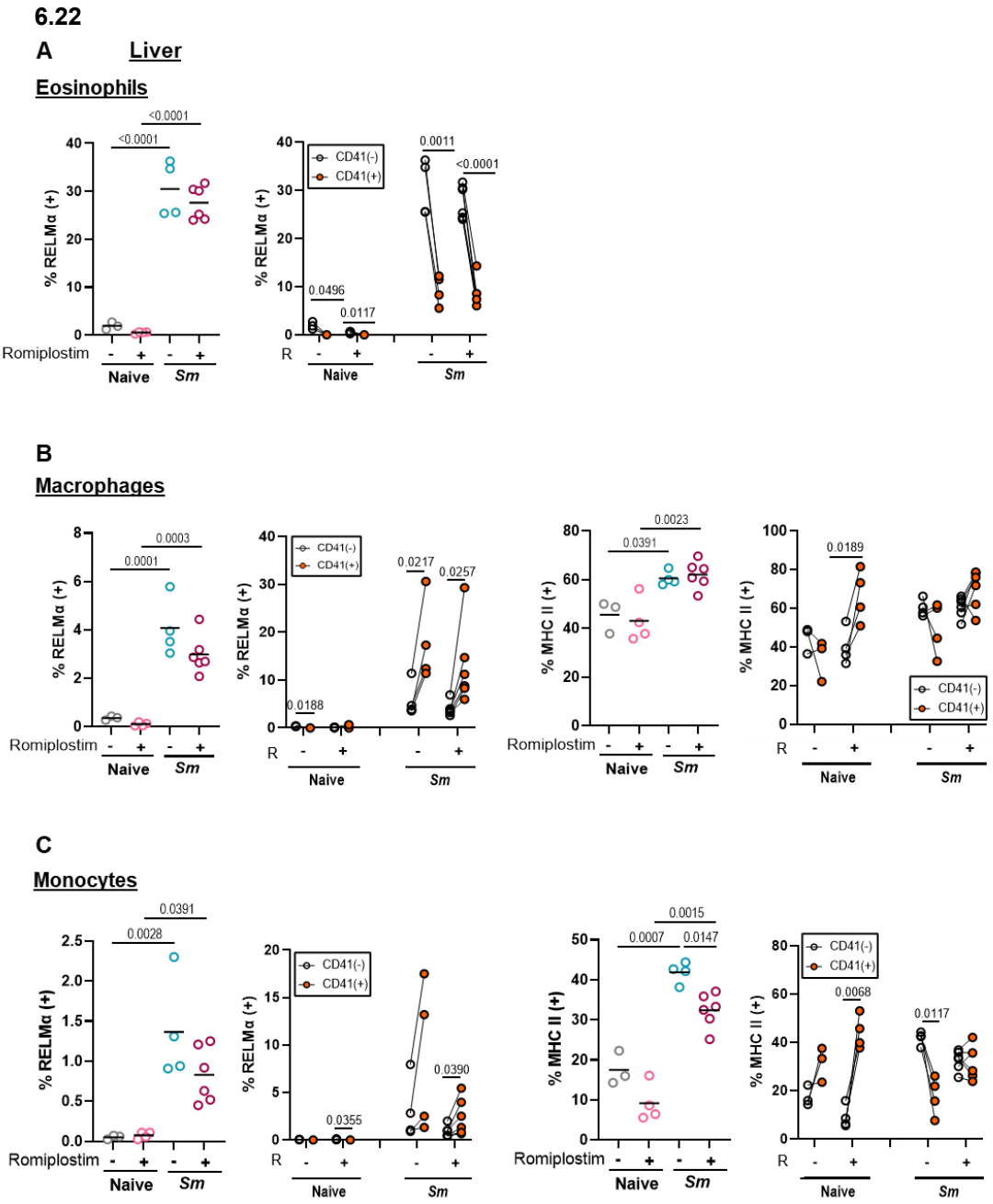

Figure 6.22 Significantly lower MHCII expression by hepatic monocytes after Romiplostim treatment

C57BL/6 mice were infected with ~35 *S. mansoni* cercariae (*Sm*), at 6 weeks mice were injected subcutaneously with 2.2µg/mouse Romiplostim or PBS once a week for 4 weeks, with weekly tail bleed monitoring. Mice were harvested at 10 weeks post-infection. A) Percentage of RELMα in hepatic eosinophils and pairwise analysis of $CD41^{+/-}$ subsets. Percentage of RELMα and MHCII by hepatic B) $Ly6C^{lo}$ macrophages and C) $Ly6C^{hi}$ monocytes and pairwise analysis of the $CD41^{+/-}$ subsets. (Naive PBS n=3, Naive Romiplostim n=4, *Sm* PBS n=4, *Sm* Romiplostim n=6). $CD41^{-}$-white, $CD41^{+}$-orange. Data representative of a single experiment. Statistical significance determined by one-way ANOVA with post-hoc Tukey's test on the mean of each group and paired t-test of the mean between $CD41^{+}$ and $CD41^{-}$ populations (A-C). Non-significance ($p>0.05$) not shown.

6.23

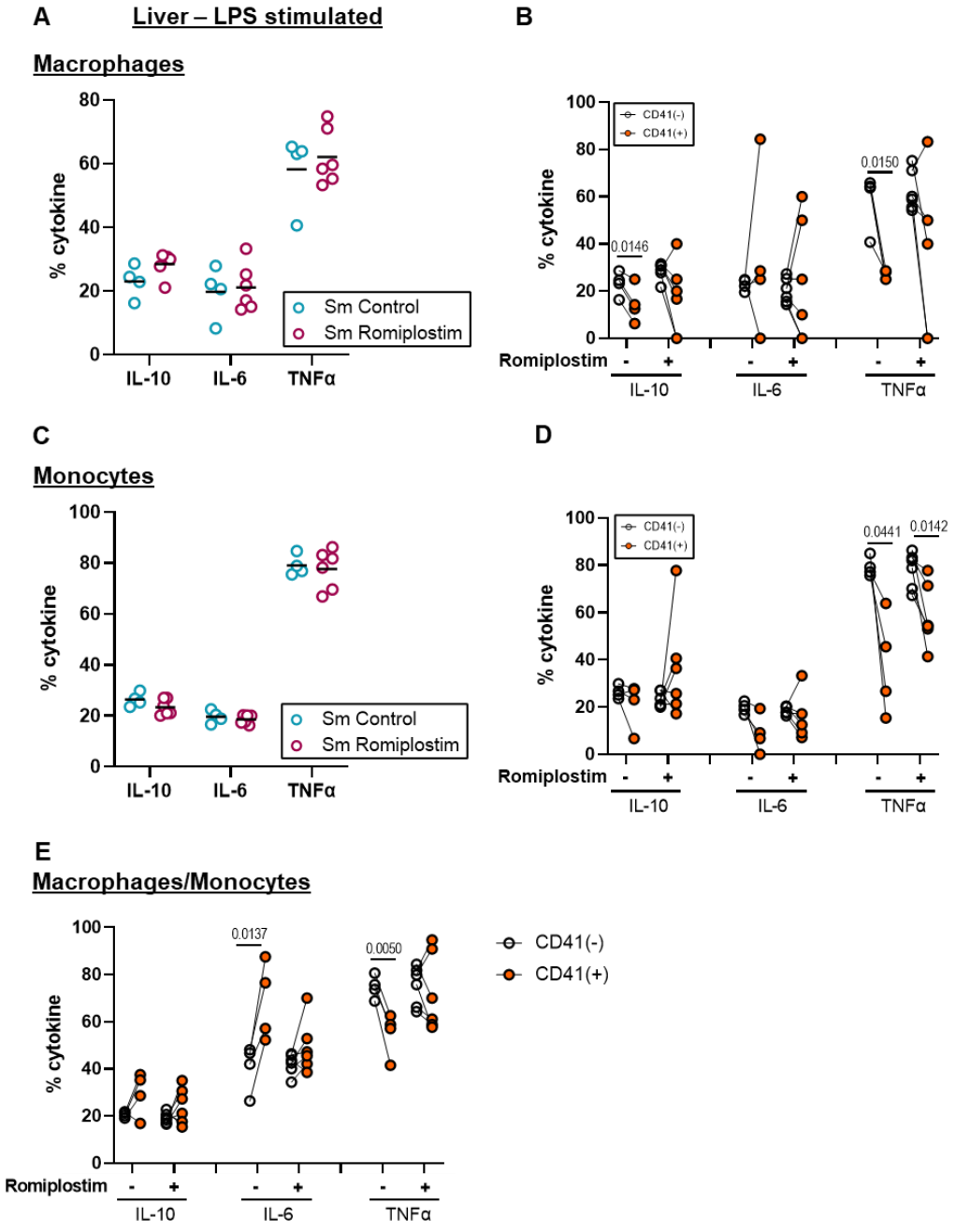

Figure 6.23 No difference in the response of macrophages and monocytes to LPS between Romiplostim and untreated mice

C57BL/6 mice were infected with ~35 *S. mansoni* cercariae (*Sm*), at 6 weeks mice were injected subcutaneously with 2.2µg/mouse Romiplostim or PBS once a week for 4 weeks, with weekly tail bleed monitoring. Mice were harvested at 10 weeks post-infection. Single cell suspensions (2-4x10^6 cells) from liver isolation processing were cultured for 3hr at 37°C with 1µg/ml LPS and 10µg/ml Brefeldin A. A) Percentage of IL-10, IL-6 and TNFα and B) pairwise analysis of CD41+/- subsets of Ly6C^{lo} macrophages. C) Percentage of IL-10, IL-6 and TNFα and D) pairwise analysis of CD41+/- subsets of Ly6C^{hi} monocytes. (*Sm* PBS n=4 (blue), *Sm* Romiplostim n=6 (pink)). CD41$^-$-white, CD41$^+$-orange. Data representative of a single experiment. Statistical significance determined by Student's unpaired t-test (A, C) and paired t-test of the mean between CD41$^+$ and CD41$^-$ populations (D, D-E). Non-significance (p>0.05) not shown.

6.24

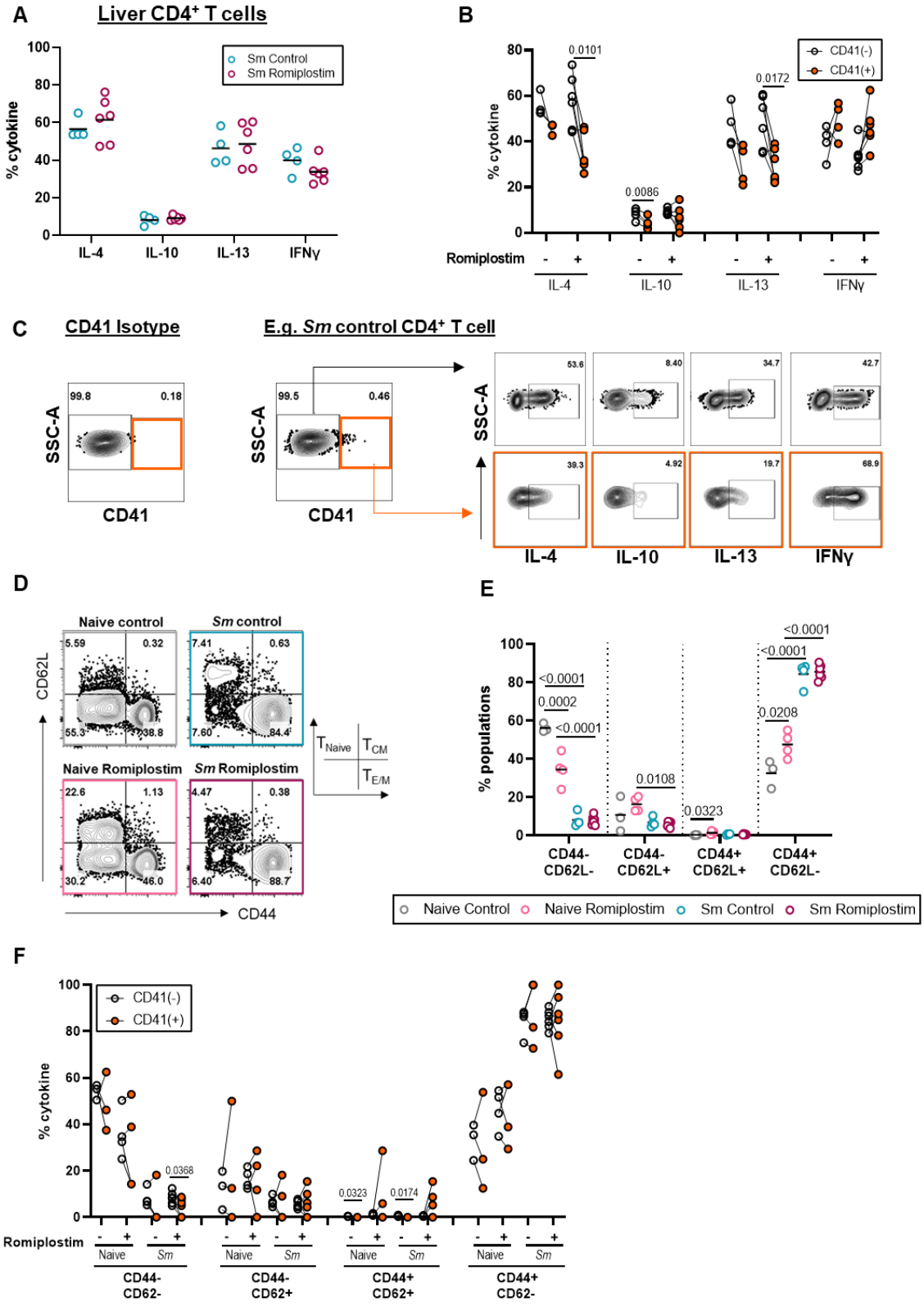

Figure 6.24 Romiplostim enhances hepatic CD44⁺CD62L⁻ T cells in naive mice but not in schistosome infection

C57BL/6 mice were infected with ~35 *S. mansoni* cercariae (*Sm*), at 6 weeks mice were injected subcutaneously with 2.2µg/mouse Romiplostim or PBS once a week for 4 weeks, with weekly tail bleed monitoring. Mice were harvested at 10 weeks post-infection. Single cell

suspensions (2-4x10^6 cells) from liver isolation processing were cultured for 4hr at 37^{o}C with 1µg/ml Ionomycin, 10µg/ml PMA and 10µg/ml Brefeldin A A) Percentage of cytokine production and B) pairwise analysis of CD41$^{+/-}$ subsets. C) Representative FACS plots and D) quantification of CD4$^+$ T cell activation markers CD44 and CD62L. E) Pairwise analysis of CD41$^{+/-}$ subsets with respect to CD44 and CD62L expression. (Naive PBS n=3 (grey), Naive Romiplostim n=4 (light pink), *Sm* PBS n=4 (blue), *Sm* Romiplostim n=6 (pink)). CD41$^+$-white, CD41$^+$-orange. Data representative of a single experiment. Statistical significance determined by Student's unpaired t-test (A), paired t-test between CD41$^{+/-}$ groups (B, E) and one-way ANOVA with post-hoc Tukey's test on the mean of each group. Non-significance ($p>0.05$) not shown.

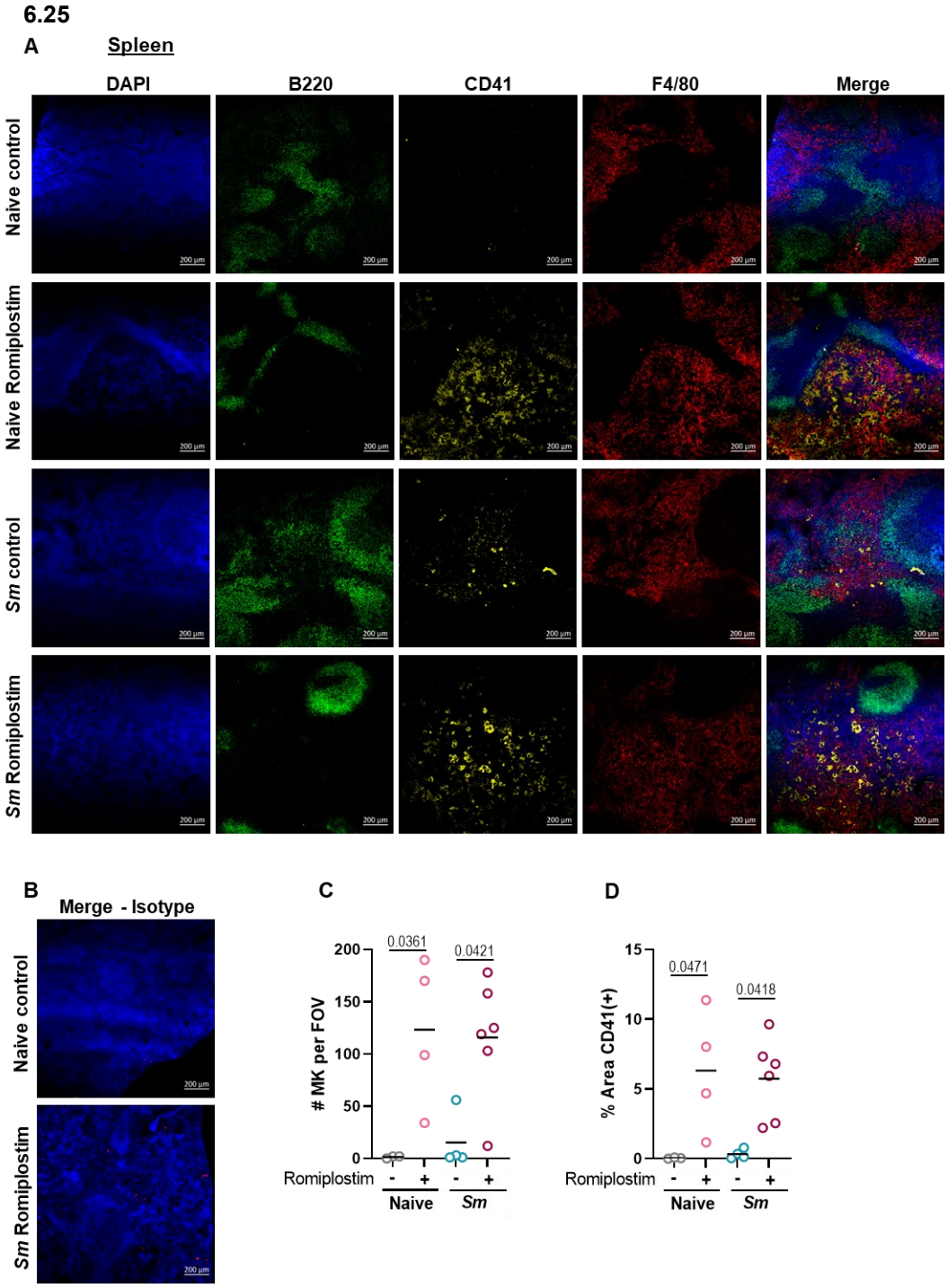

Figure 6.25 Significantly more MK in the spleen of both naive and infected mice with Romiplostim treatment

C57BL/6 mice were infected with ~35 *S. mansoni* cercariae (*Sm*), at 6 weeks mice were injected subcutaneously with 2.2µg/mouse Romiplostim or PBS once a week for 4 weeks, with weekly tail bleed monitoring. Mice were harvested at 10 weeks post-infection. A) Representative fluorescent staining of spleens with DAPI (blue), B220 (green), CD41 (yellow) and F4/80 (red) and B) isotype controls. Images taken using 10x objective and 0.6x zoom. Quantification of fluorescent images of C) the number of MK per field of view and D) percentage coverage of CD41 staining. (Naive PBS n=3, Naive Romiplostim n=4, *Sm* PBS n=4, *Sm* Romiplostim n=6). Data representative of a single experiment. Statistical significance determined by one-way ANOVA with post-hoc Tukey's test on the mean of each group (C-D). Non-significance (p>0.05) not shown.

6.26

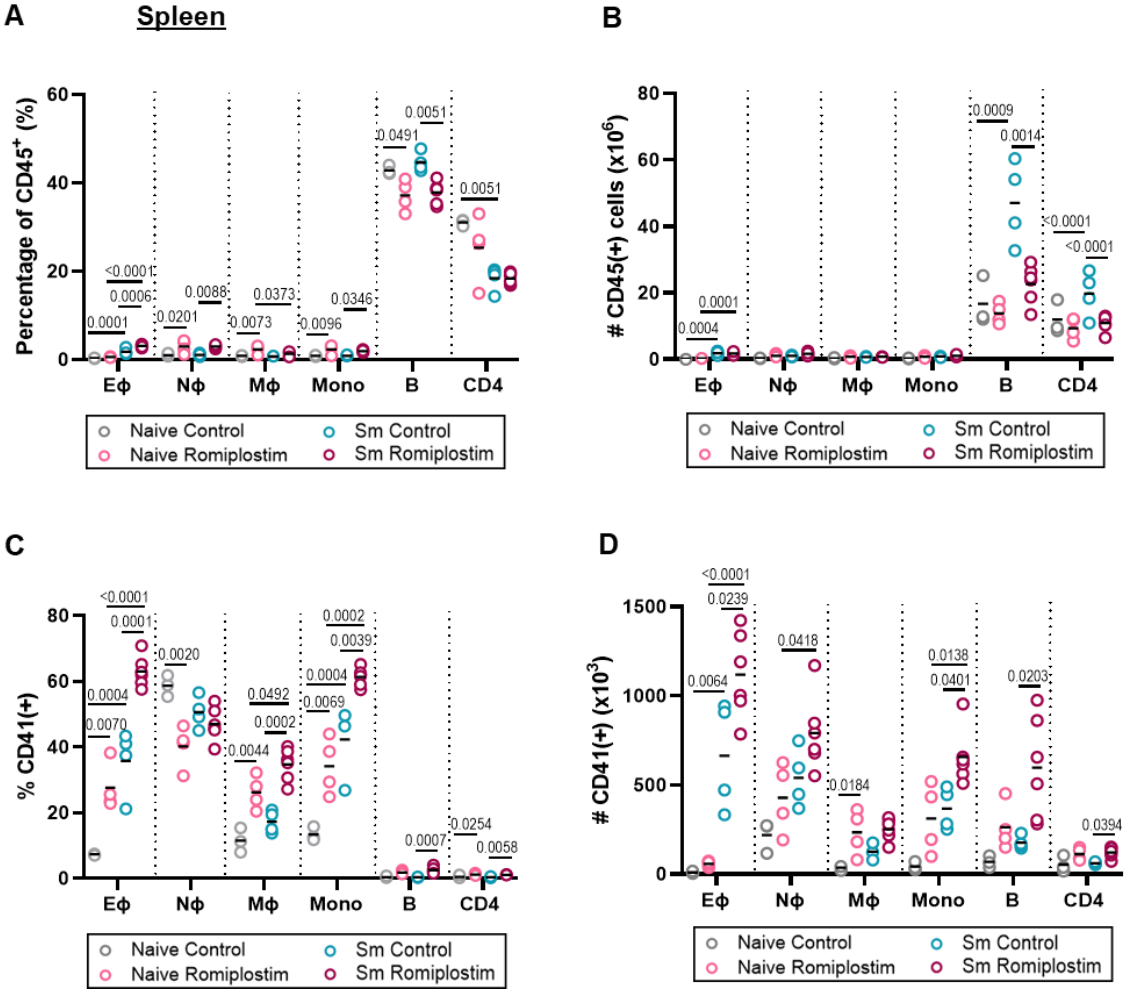

Figure 6.26 Romiplostim significantly increases the percentage and number of PLA in the spleen

C57BL/6 mice were infected with ~35 *S. mansoni* cercariae (*Sm*), at 6 weeks mice were injected subcutaneously with 2.2µg/mouse Romiplostim or PBS once a week for 4 weeks, with weekly tail bleed monitoring. Mice were harvested at 10 weeks post-infection. A) Percentage and B) number of leukocyte populations in the spleen and C) percentage and D) number of CD41⁺ leukocyte populations. (Naive PBS n=3 (grey), Naive Romiplostim n=4 (light pink), *Sm* PBS n=4 (blue), *Sm* Romiplostim n=6 (pink)). Data representative of a single experiment. Statistical significance determined by one-way ANOVA with post-hoc Tukey's test on the mean of each group (A-D). Non-significance (p>0.05) not shown.

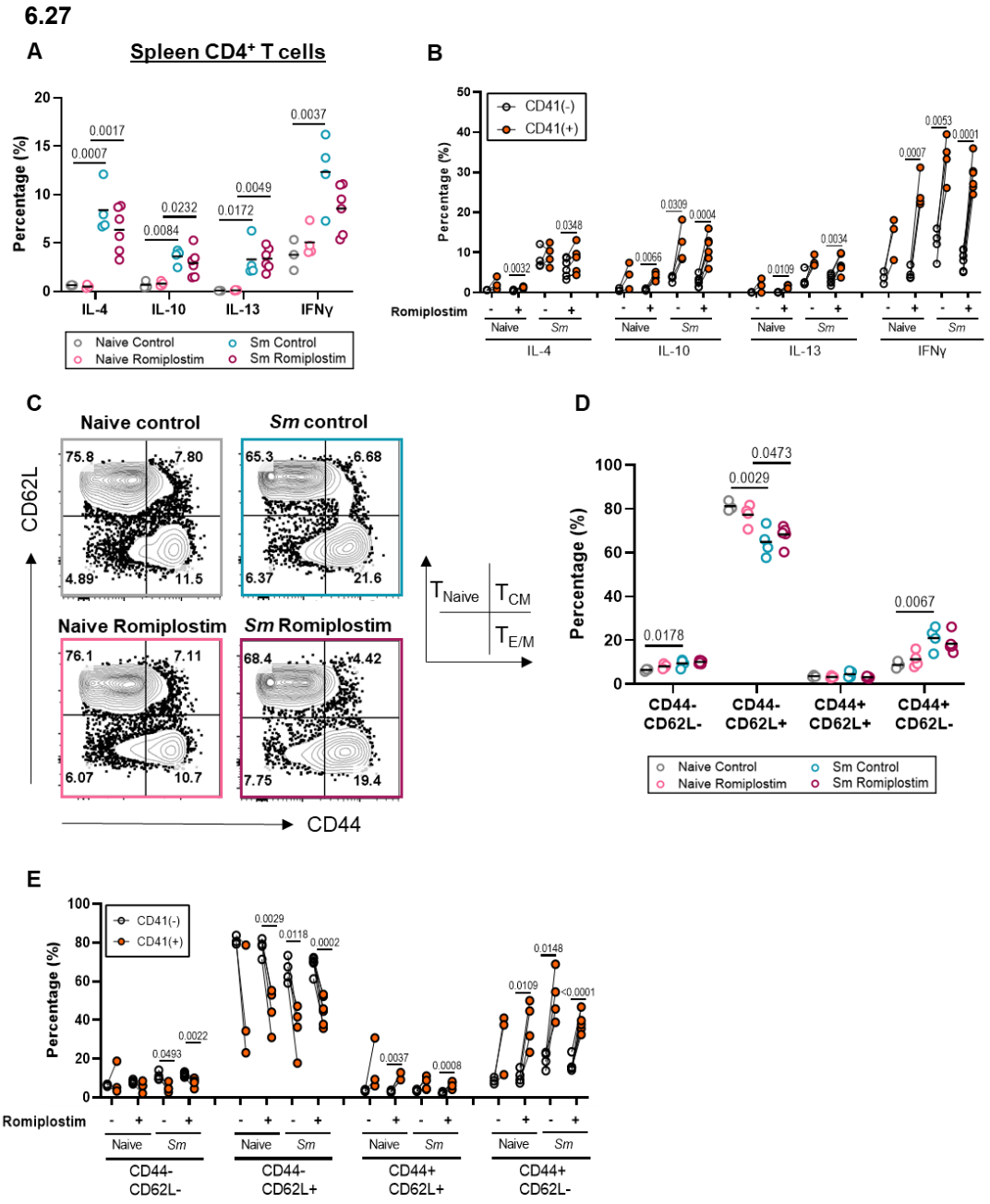

Figure 6.27 Romiplostim reduced IFNγ production by splenic CD4⁺ T cells in schistosome infection

C57BL/6 mice were infected with ~35 *S. mansoni* cercariae (*Sm*), at 6 weeks mice were injected subcutaneously with 2.2µg/mouse Romiplostim or PBS once a week for 4 weeks, with weekly tail bleed monitoring. Mice were harvested at 10 weeks post-infection. Single cell suspensions (2-4x10^6 cells) from spleen isolation processing were cultured for 4hr at 37°C with 1µg/ml Ionomycin, 10µg/ml PMA and 10µg/ml Brefeldin A A) Percentage of cytokine production and B) pairwise analysis of CD41$^{+/-}$ subsets. C) Representative FACS plots and D) quantification of activation markers CD44 and CD62L. E) Pairwise analysis of CD41$^{+/-}$ subsets with respect to CD44 and CD62L expression. (Naive PBS n=3 (grey), Naive Romiplostim n=4 (light pink), *Sm* PBS n=3 (blue), *Sm* Romiplostim n=6 (pink)). CD41^{+}-white, CD41^{+}-orange. Data representative of a single experiment. Statistical significance determined by Student's unpaired t-test (A), paired t-test between CD41$^{+/-}$ groups (B, E) and one-way ANOVA with post-hoc Tukey's test on the mean of each group. Non-significance ($p>0.05$) not shown.

6.4 Discussion

Schistosome infection induced enhanced PLA with specific subsets of hepatic macrophages and monocytes (RELMα^{hi} MHCII^{lo}). However, platelets did not modulate these molecules *in vitro* and instead platelets preferentially interacted with activated macrophages. Therefore, we were interested to test whether enhancing or decreasing these interactions *in vivo* would impact on the immunological response to schistosome infection. As we have not identified receptor-ligand pair(s) responsible for PLA formation, we chose to examine the impact of systemic platelet depletion and enhancement *in vivo*.

We first utilised the well-characterised model of monoclonal antibody-mediated platelet depletion. Here, we only observed a partial platelet reduction in schistosome infection which may reflect infection-induced impairments in phagocytic capacity of macrophages and monocytes that mediate ITP, as is the case in HIV (414). This is also consistent with our data in **Chapter 5** that showed M2-like macrophages in isolation were less able to phagocytose *E. coli* particles than M1-like macrophages. An alternative explanation for partial depletion may be due to poorer drainage and circulation of the IP-injected anti-CD41 antibody in infected mice with hepatosplenomegaly. However, platelet counts began to rise even in the naive anti-CD41 group by day 14, highlighting the challenges associated with repeated treatments of immunogenic rat antibodies. Host antibodies against the administered anti-CD41 mAb may be promoted by the relatively high dose of antibody (0.4mg/kg) given from day 9, however similar dosing regimens have been shown to sustain platelet depletion for up to 28 days (405). As anticipated, we observed an increase in MPV with anti-CD41 treatment and this was further enhanced in our schistosome-infected group. This contrasted with a similar study performed in mice infected with *L. donovani* where anti-CD41 treatment actually reduced the infection-induced high MPV, thus highlighting the context specificity of platelet responses (238). As schistosome infection has a greater bleeding phenotype compared with *L. donovani* infection, depleting platelets in schistosomiasis may cause more bleeding which causes greater BM stress and results in the higher MPV. Despite only partial platelet depletion, anti-CD41 treatment caused substantially reduced

survival in schistosome-infected mice, consistent with that observed by findings from Ngaiza *et al.* (1990) (269). Interestingly, we did not observe an increase in hepatic schistosome egg burden in platelet-depleted mice as shown by Ngaiza *et al.* but this may reflect the lower cercarial infection dose used in our study (~30 cercariae vs 150-200 cercariae), the difference in mouse strain (C57BL/6 vs CBA), and/or the mechanism of platelet depletion (anti-CD41 antibodies vs rabbit anti-mouse platelet serum). It is unclear what is driving platelet-depletion associated death in infected animals as there were no overt changes in multiple pathological parameters and immune cell responses including no difference in haematocrit, red blood cell number or size. One hypothesis is that as injection of anti-CD41 antibodies drives the immune recognition of Fc regions by immune cells such as macrophages and monocytes this binding and internalisation drives metabolic reprogramming or changes the cytokine milieu to that which is unfavourable for an anti-schistosome response (415).

In order to assess the effect of sustained low platelet count on schistosome infection through a different route we moved to using $MPL^{-/-}$ mice. Despite the absence of TPO signalling these mice had very low platelet counts ~$100x10^3/mm^3$ (normal ~$1000x10^3/mm^3$), the presence of this TPO-independent population highlights that other cytokines can promote some level of platelet production (121,319). Schistosome infection led to a further decrease in platelet counts, although this was not significant (p=0.053). If we were able to continue this experiment to a later time-point in schistosome infection or with a higher cercarial burden it would be interesting to see whether platelet counts continued to fall or whether they would plateau at a low level. As platelets were still detectable in circulation of these mice it suggests alternative, emergency platelet-producing mechanisms are occurring. The MPV in schistosome-infected $MPL^{-/-}$ mice was significantly higher than in WT mice which again may reflect the production of platelets by TPO-independent mechanisms such as IL-1α-stimulated thrombopoiesis which results in platelets with a greater MPV compared with those from TPO-stimulated MK (311). In this platelet depletion model, we saw severe sickness and were forced to harvest at the early 7.5 week time-point. This was most

likely because of BM failure, anaemia and intestinal haemorrhaging. Given the low infection dose and early time-point we were surprised to see signs of intestinal haemorrhaging which is normally associated with high infection burden during later stages of infection. This suggests there were insufficient platelets in these $MPL^{-/-}$ mice to stem bleeding in the vascular wall following schistosome egg transit across the gut. Moreover, we observed a complete failure of all the BM stem and progenitor cell populations to respond to infection. TPO has been shown as an important regulator of stem cell quiescence, it can activate HIF1α to drive a feedback loop to reduce oxidative stress and mediate glycolytic metabolism (416). Therefore, in $MPL^{-/-}$ mice, they are unable to receive TPO signals and self-renewal proliferation is impeded leading to BM exhaustion (409). In this regard, transplanted BM from $MPL^{-/-}$ mice failed to reconstitute in competition assays with WT cells even when given in 10-fold excess (409). Given these significant BM changes, it was surprising that infected $MPL^{-/-}$ animals still had the same number of leukocytes in the liver after schistosome infection. This may suggest that the extramedullary HSC found in the liver in schistosome infection are functional and sufficient to compensate for the BM failure (284). It would therefore be interesting to isolate the extramedullary stem and progenitor cells and perform colony formation or transplant experiments to characterise their functionality. When we performed a pilot experiment using Fgd5-reporter mice (*Fgd5*$^{ZsGreen•ZsGreen/+}$) to look for stem and progenitor cells in the liver in our model of chronic schistosome infection (417) we saw very few LT-HSC ($ESLAM^{+}$) but did observe LSK progenitor populations, predominantly $CD48^{+}CD150^{-}$ MPPs.

In the future it would be of great value to perform schistosome infection in platelet specific conditional depletion mouse models. For example the PF4-DTR mouse line would allow longer periods of platelet depletion compared with antibody-mediated depletion and it would be specific to platelets and megakaryocytes rather than HSC (418,419).

Given some of the challenges and caveats associated with platelet depletion we tried the complementary approach of enhancing platelet numbers using rTPO. Here we observed minimal platelet elevation despite following a

treatment regimen previously optimised by members of the Hitchcock lab (unpublished data). We also performed a repeat experiment using recombinant human TPO, instead of recombinant mouse TPO and this gave very similar results to those shown in **Figure 6.12 - Figure 6.16**. Despite only a subtle increase in circulating platelets, a significant increase in high ploidy (>32N) MK in the BM was observed which was consistent with that described in the literature (420). High-MK ploidy was also increased in schistosome infection with rTPO treatment, which along with the subtle enhancement of platelets, may suggest that MEP in schistosome infection are still capable of generating platelet-producing MK as TPO itself does not drive the proplatelet formation and release of platelets into circulation (420). This may also indicate that TPO-independent mechanisms of megakaryopoieis occur in schistosome infection due to depleted hepatic and circulating TPO, and these are less-able to support the generation of platelet-producing MK.

In contrast to rTPO, Romiplostim treatment induced a far more striking increase in total platelet count, MPV as well as MK number in the spleen and BM. Infected mice treated with Romiplostim responded less well having lower platelet counts than their naive counterparts, which is consistent with accelerated platelet clearance in schistosome infection, pseudo-thrombocytopenia due to more PLA and potentially MK that are less able to produce platelets in the BM.

In these Romiplostim experiments there was a significant increase in the percentage of LSK cells in the BM in both naive and schistosome-infected mice (421). This is consistent with the known stimulatory TPO signalling pathway and also with our results in $MPL^{-/-}$ mice that lack TPO signalling and had significantly reduced LSK levels.

In the future it would be logical to look in sites such as the liver and spleen for extramedullary stem and progenitor populations. This is of particular interest because in sepsis there are more MEP in the spleen that are capable of differentiating into MK whilst the total number of MK in the BM remained unchanged (164). Moreover, Valet *et al.* (2022) identified a range of chemoattractant molecules such as stem cell factor that are reduced in the BM

during infection but are enhanced in the circulation. This chemoattractant gradient then drives the egress of progenitor cells out of the BM to extramedullary sites (164). It would therefore be interesting to assess whether a similar situation is occurring in schistosome infection which is contributing to the extramedullary MK that we have observed in the liver and spleen in **Chapter 3**. A cytokine bead array assay performed by the Hewitson lab showed no change in stem cell factor in BM aspirates between naive and infected mice, suggesting stem cell factor might not be the cytokine involved here. However, further chemokine arrays have shown other molecules such as CCL5 were elevated in BM aspirates in schistosome infection. Consistent with previous reports, here we have shown that Romiplostim significantly increased the number of MK in the spleen as well as in the BM (422). We also noted an increase of MK in the liver after Romiplostim treatment. Surprisingly, there were actually fewer MK in the liver of schistosome-infected mice than in naive animals that had received Romiplostim. This may be due to the altered inflammatory environment within the liver following schistosome egg deposition. This could mean there was no longer such a favourable concentration gradient to drive the egress of MEP from the BM to the liver. However, due to the absence of schistosome eggs in the spleen the migration of stem and progenitor cells could still occur to the same extent as in the absence of schistosome infection.

Regular platelet transfusions could be performed from naive animals at different time-points during infection as an alternative approach to assess whether having more platelets in circulation is beneficial. This would minimise the modulation of other HSC through TPO-MPL signalling. However, ensuring platelets remained completely inactive during the isolation and purification process would be challenging. It would be of great interest to perform these infection studies and platelet transfusions in humanised mouse models given some of the differences in platelet surface receptors e.g. mice do not express FcγRIIA or the PAR1 receptor (423). Moreover, humanised mouse models (423,424) would enable the transfusion of human platelets which can be isolated from venepuncture rather than a terminal cardiac bleed on a mouse which makes this a more ethically appealing model.

When considering the platelet-leukocyte interactions, there were minimal differences in the presence or absence of anti-CD41 treatment. There were more platelet-neutrophil, and platelet-monocyte interactions in naive blood but this was not seen to the same extent in the liver or spleen. This may reflect the different method of detecting platelets required in this experiment. As shown in **Chapter 3**, *in vivo* X649 platelet labelling marks both platelets that have been internalised as well as those that are surface-bound. In these ITP experiments, we were unable to determine whether platelets were inside or outside cells which may be responsible for the differences seen. In a future experiment, isolated immune samples could be co-stained for anti-rat IgG to detect injected rat anti-CD41 antibody opsonised platelets which may also be adhering to leukocytes. This would enable the distinction between surface-bound and internalised platelets.

There was a significant reduction in both circulating platelets (7-fold) and PLA (e.g. ~4-fold reduction in platelet-macrophage aggregates) in $MPL^{-/-}$ mice compared with their WT counterparts. The formation of PLA potentially reduces the circulating pool of free platelets that can prevent bleeding, e.g. in the intestine. Alternatively, PLA may be beneficial in schistosome infection as they can promote the trafficking of immune cells or platelets themselves to the right place to aid the anti-schistosome response (226). Although rTPO treatment only caused a small increase (~1.3 fold) in circulating platelets, this was sufficient to induce a significant increase in PLA in the liver of schistosome-infected mice e.g. 3-fold more platelet-eosinophil aggregates than untreated controls. This suggests schistosome infection and the associated inflammatory environment intrinsically alters platelets to drive enhanced leukocyte adhesion and/or the phenotype of leukocytes in schistosome infection favours platelet adhesion e.g. activated eosinophils are more “sticky” for platelets. As anticipated given the significantly elevated platelet counts, there were significantly more PLA after Romiplostim treatment. As the percentage of $CD41^{+}$ cells was highest in the macrophage and monocyte populations in Romiplostim treated infected mice, this supports our findings in **Chapter 3** that platelets preferentially interact with hepatic monocytes and macrophages. Furthermore, eosinophils were the second

most abundant CD41^{+} cell type, reflecting the large total number of these cells. However, despite there being ~10-fold fewer total monocytes in the liver than eosinophils in schistosome infection, monocytes were still the cell population which contributed most to the PLA.

To explore these interactions further and better understand whether platelets were indeed preferentially interacting with particular subsets of immune cells i.e. RELMα^{lo} eosinophils and RELMα^{hi} MHCII^{lo} macrophages/monocytes, we analysed the expression of these molecules in both our platelet depletion and enhancement models.

In MPL$^{-/-}$ mice there was a general trend of higher RELMα expression in liver eosinophils, although this was non-significant. Increased RELMα in platelet-deficient mice would be consistent with CD41^{+} eosinophils being RELMα^{lo} as shown in **Chapter 3** and may suggest that platelets do in fact modulate eosinophil RELMα expression. This could be answered through *in vitro* experiments with BM-derived eosinophils (425). However, whilst both rTPO and Romiplostim enhanced platelet numbers there was no significant difference in eosinophil RELMα expression, which is instead consistent with platelets not modulating expression but rather preferentially interacting with the RELMα^{lo} subset of eosinophils.

RELMα expression by monocytes and macrophages in MPL$^{-/-}$ mice as well as after rTPO and Romiplostim treatment also showed no consistent differences compared with their respective controls, which is consistent with platelets not modulating the production of RELMα by macrophages as shown in **Chapter 5**. In **Chapter 3** we showed that CD41^{+} monocytes and macrophages were primarily MHCII^{lo}. As such, if platelets were responsible for this down-regulation we would have expected to see an overall increase in MHCII expression by monocytes and macrophages in the MPL$^{-/-}$ platelet depletion model and conversely decreased MHCII after rTPO and Romiplostim treatment. We were surprised then that both MPL$^{-/-}$ and Romiplostim treated infected mice showed reduced monocyte and/or macrophage MHCII expression compared with controls, whereas there was no difference in anti-CD41 or rTPO treated mice. This may suggest the differences in

monocyte/macrophage MHCII expression are driven by other confounding factors which themselves impact the activation of these cells in schistosome infection rather than any direct platelet effect. For example, the greatest HSC changes were seen in the $MPL^{-/-}$ and Romiplostim groups, so the changes in myeloid MHCII may reflect these earlier haematopoietic alterations, rather than differences in platelet number.

Although platelet-T cell aggregates contribute far less than myeloid cells towards the total PLA count, we were interested to assess whether T cell responses were altered by platelet interactions either directly or indirectly via APC. We focused primarily on the $CD4^+$ T cell response as Th2 and broader type 2 responses characterise the host response to schistosomes and other helminths (75,76). We found platelets preferentially interacted with cytokine-producing (IL-4, IL-10, IL-13 and IFNγ) splenic $CD4^+$ T cells. Consistent with this, platelet-interacting $CD4^+$ T cells were enriched for the activated $CD44^+CD62L^-$ subsets. Given $T_{E/M}$ $CD4^+$ T cells migrate to peripheral tissues it would be interesting to assess upon entry into peripheral tissues, such as the liver whether platelets switch to primarily interacting with hepatic macrophage and monocyte populations rather than the $T_{E/M}$ cells. This may also explain the low frequency of platelet-T cell interactions in the liver. Moreover, it would be interesting to investigate whether platelets facilitate the migration of $T_{E/M}$ cells to peripheral tissues or whether platelets utilise this T cell characteristic in order to reach a particular destination. Given platelet depletion or enhancement resulted in minimal changes to liver immune cells, it suggests platelets may be harnessing the migratory capacity of these T cells rather than directly driving $T_{E/M}$ migration.

Splenic $CD4^+$ T cells produced more IFNγ when platelets were low (i.e. $MPL^{-/-}$ mice) and less IFNγ when platelets were boosted with Romiplostim. This may indicate platelets directly regulate $CD4^+$ T cell IFNγ production. Alternatively, it may reflect the importance of platelets in plugging vascular damage in the intestines following schistosome egg transit across the intestinal wall. We hypothesise that egg-induced intestinal bleeding in platelet-depleted $MPL^{-/-}$ mice allowed pathogenic bacteria to translocate across the gut wall thereby enhancing the pro-inflammatory immune response and IFNγ

production by $CD4^+$ T cells. Consistent with this idea, in schistosome-infected mice treated with Romiplostim there were 3-fold more platelets, thereby reducing intestinal bacterial leakage, ultimately reducing IFNγ production by $CD4^+$ T cells in these mice. To test this hypothesis mice could be orally inoculated with fluorescently-labelled bacteria which could be tracked and imaged by fluorescence microscopy and flow cytometry along with the inflammatory response of immune cell populations (426). Unfortunately, since this experiment was performed we have discovered considerable immunological differences that have arisen in the CD45.1 line of this C57BL/6 mouse strain and therefore, these experiments need to be repeated in mice that have been fully screened.

Together our complimentary approaches of manipulating platelet numbers *in vivo* in schistosome infection have demonstrated that platelets are preferentially interacting with specific subsets of hepatic monocytes and macrophages in schistosome infection but do not appear to modulate the expression of RELMα and MHCII within the time frames studied. Depletion of platelets in schistosome infection, as a result of infection-induced thrombocytopenia (and exaggerated in platelet-deficient models), may result in intestinal bleeding due to an inability to plug vascular damage following the transiting of schistosome eggs. As a consequence, there is a stronger pro-inflammatory response which may result in the metabolic reprogramming of immune populations, impeding their function in the anti-schistosome response. Therefore, boosting platelet numbers might be able to reverse bacterial translocation and immune cell metabolic reprogramming. The immune consequences of egg-induced intestinal damage, bacterial translocation, and the role of platelets in stemming these processes must now be considered.

7. Discussion

7.1 Key findings

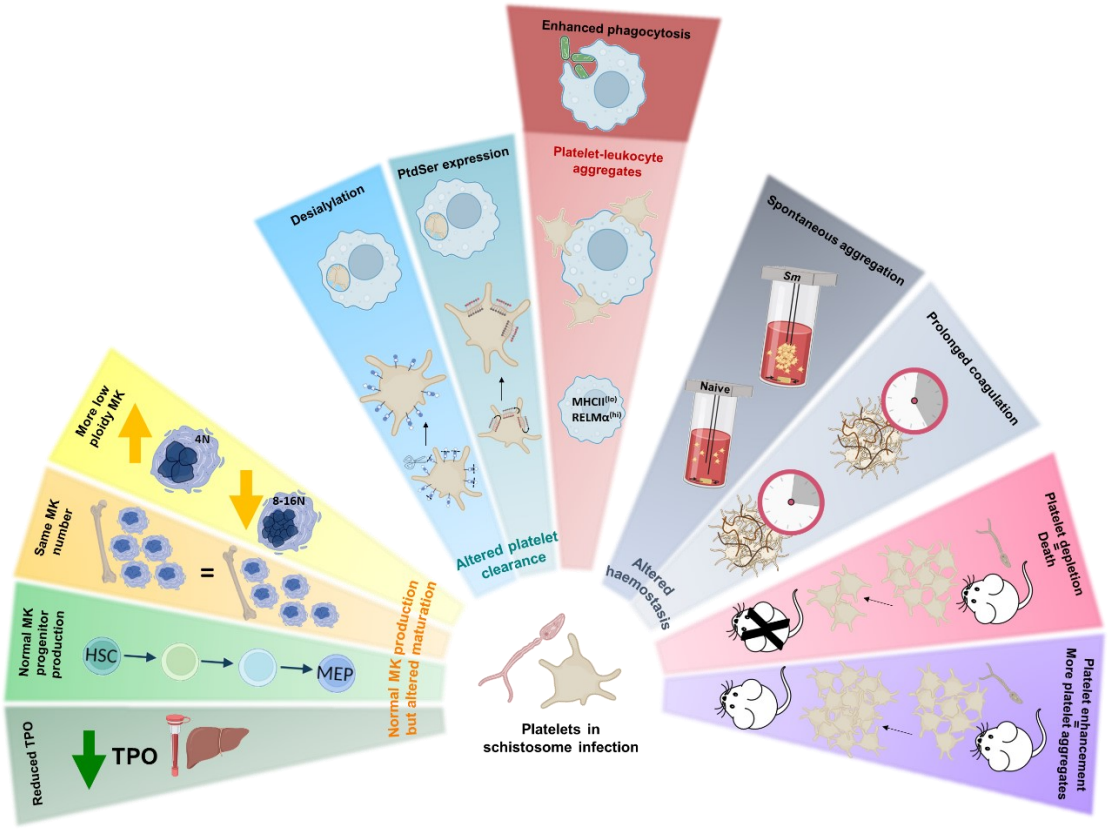

Figure 7.1 Graphical summary of the key results shown in this thesis
Thrombocytopenia observed in schistosome infection may be result of fewer platelet-producing MK in the BM, accelerated platelet clearance and PLA. There are multiple haemostatic changes in schistosome infection. Platelet depletion resulted in ill-health of schistosome-infected mice and enhanced platelet numbers increased the number of PLA.

7.1.1 Schistosome infection induces thrombocytopenia through multiple mechanisms

We have used a murine model of chronic schistosomiasis to assess the impact of schistosome-induced type 2 immune responses on platelet production and immune cell interactions. We have shown thrombocytopenia in schistosome infection to be multifaceted and partially sustained after elimination of adult worms. Despite significantly reduced hepatic and circulatory TPO, the number of BM MK remained unchanged. However, the reduction in high ploidy, platelet-producing MK would suggest there were fewer MK present that are able to produce platelets. In addition, there is a significant increase in PLA in

schistosome infection, with enhanced surface-bound platelets in the blood (pseudo-thrombocytopenia) and platelet internalisation in the liver (immune-mediated thrombocytopenia). Platelet clearance was accelerated in schistosome infection but occurred in an FcRγ-independent manner and was coincident with enhanced platelet membrane asymmetry and exposure of "eat-me" signals such as PS and platelet desialylation.

Hepatic monocytes and macrophages were the major populations interacting with platelets. Given that platelets are now known to be highly immunomodulatory, we dissected the consequences of these interactions. Platelet(+) monocytes/macrophages were primarily MHCII^{lo} RELMα^{hi} compared with their platelet(-) counterparts. Moreover, platelet(+) monocytes/ macrophages also expressed more *Il6, Cxcl12* and *Retlna* but less *Tnf* at the transcript level compared with platelet(-) cells. We have shown that this specific subset of monocyte/macrophages was found deeper within tissues and so likely do not represent a population of cells that has recently exited from the circulation.

7.1.2 Schistosome infection has broad haemostatic consequences

We are the first group to have explored the haemostatic changes in a murine model of schistosomiasis using whole blood aggregometry and longitudinal coagulometry. The development of these two assays revealed schistosome infection induces spontaneous platelet aggregation in the absence of exogenous agonists or an overtly active platelet phenotype. However, infected mice also have a prolonged clotting time with respect to both the intrinsic and extrinsic pathways as infection progressed to the chronic stages (10-12 weeks). This again highlights the idea that the intravascular adult worms, the highly immunogenic eggs and resultant systemic type 2 granulomatous response affects the complex haemostatic pathways at multiple levels.

7.1.3 Platelets both preferentially interact with polarised macrophages and drive changes in macrophage phagocytosis

Given the enhanced PLA with specific subsets of hepatic monocytes/macrophages, we used *in vitro* experiments with BM-Mϕ to reveal that rather than modulating macrophage polarisation, platelets instead

preferentially interact with polarised macrophages. However, platelets also enhance the ability of M2-like macrophages to phagocytose *E. coli* bioparticles, although this is reduced when platelets from infected mice are used. Furthermore, M2-like macrophages were the only population to show enhanced phagocytosis of platelets from infected mice compared with naive controls. Together these experiments demonstrated the functional changes of M2-like macrophages that occur as a result of interactions with platelets from naive and infected mice.

7.1.4 *In vivo* modulation of platelet levels reveals potential for their dual role in haemostasis and immune modulation

Using multiple *in vivo* models of platelet depletion and enhancement we have shown the interconnected role of platelets in both haemostasis and immune modulation. Platelet deficient mice, both $MPL^{-/-}$ and WT treated with anti-CD41 mAb failed to survive schistosome infection. Additional factors such as suspected BM failure and altered immune cell responses respectively make it difficult to definitively identify platelets as the drivers of the enhanced mortality. Therefore, an alternative approach of enhancing platelet counts was used to assess their importance in schistosome infection inflammatory environment. Recombinant mouse TPO treatment caused only subtle increases in circulating platelet numbers, although it did significantly increase PLA compared with infection alone. However, there were no overt changes in pathology or immune responses. To achieve a more robust increase in platelets, we treated mice with Romiplostim which caused a significant increase in circulating platelets, PLA and platelet-platelet aggregates in multiple tissues. Surprisingly, given the extensive literature showing platelets are immunomodulatory (**Chapter 1.3**), PLA caused relatively small changes in the immune response. Liver egg counts and granuloma diameter showed an upwards trend with Romiplostim treatment, however this was not significant. There was an enhanced pro-inflammatory $CD4^+$ T cell response in the spleen of schistosome-infected $MPL^{-/-}$ mice and Romiplostim treatment caused a moderate (non-significant) decrease in IFNγ-producing $CD4^+$ T cells. Together, this may indicate platelets stem intestinal bleeding after schistosome egg migration, and their absence causes greater commensal translocation.

Notably, this experiment also showed that schistosome-infected mice responded less well to Romiplostim treatment with lower platelet counts than their naive counterparts which is consistent with MK in schistosome infection being less able to produce platelets alongside infection-induced increases in platelets clearance.

7.2 Future work and applications

Global transcriptomic, proteomic and metabolomic analysis of isolated platelets from naive and schistosome-infected mice would provide great insight not only into the haemostatic pathways but also help to identify the surface molecules responsible for enhanced PLA. Moreover, sequencing FACS sorted hepatic $CD41^+$ and $CD41^-$ monocytes/macrophages would help elucidate some of the functional changes that occur as a result of these interactions. This would allow us to assess whether the changes we observed *in vitro* with BM-Mϕ (e.g. enhanced ability to phagocytose in the presence of platelets) can be mapped onto metabolomic changes like in the case of tumour associated macrophages following phagocytosis of neoplastic cells (322).

Identifying the receptor-ligand pair or pairs responsible for the PLA is crucial in dissecting the effects of these aggregates *in vivo* in schistosome infection. Once identified, antibodies can be used to block the respective candidates, potentially alongside platelet-specific receptor/ligand knock-out animals. This would allow for mechanistic examination of the effects of platelets on immune cell function in schistosome infection to assess whether they were beneficial or detrimental to pathology progression. For example, blocking P-selectin in allergic asthma significantly reduced eosinophil activation, recruitment and overall hyperactivation (314). As we have shown that P-selectin expression on platelets did not change with schistosome infection it is unlikely to be the receptor responsible for PLA. However, identification of the receptor-ligand pair would provide a novel therapeutic target for schistosomiasis. Although inhibiting or boosting PLA and platelet numbers is unlikely to prevent schistosome infection, if boosting platelet numbers reduces the pro-inflammatory response and re-programmes immune cells, this may offer an alternative therapeutic option to PZQ. We have shown that thrombocytopenia was sustained 4 weeks after PZQ treatment and adult worm clearance, and

this poses the interesting question as to how long infection-induced platelet changes are sustained. This extends to other work performed by the Hewitson lab which is exploring the extent to which BM HSC/progenitors are impacted by the systemic inflammatory response and how this affects the immune response to subsequent infections or other challenges. In a mouse model of chronic ITP, whilst stromal changes that occur in the BM revert back to normal after platelet counts recover, the vascular remodelling persists (405). Following PZQ treatment the number of PLA in the liver reduced, mirroring changes in total cell number. However, the percentage frequency of PLA did not change, suggesting schistosome infection has re-programmed platelets and/or immune cells, resulting in changes to cell surface and/or intracellular components e.g. as has been shown by platelets response to dengue virus (427).

Once it has been confirmed if there is an intrinsic change in platelets from schistosome-infected mice and that this is responsible for the spontaneous aggregation, it would be of great value to perform longitudinal aggregometry and coagulometry alongside PZQ treatment. This would provide crucial information as to whether liver hepatocytes repair and restore production of TPO and the multiple haemostatic and clotting factors as the inflammatory response wanes. It would be interesting to examine whether these changes are specific to schistosome infection or whether it is a more general feature of type 2 inflammation. As intestinal schistosomiasis causes severe liver pathology, analysis of other helminth infections such as hookworm or other intestinal nematodes would be interesting. These organisms induce strong type 2 inflammatory responses and may still cause BM changes but in the absence of liver pathology, therefore enabling the separation between pathology and the type 2 immune response. We performed preliminary experiments treating mice with IL4-complex intraperitoneally for 2 weeks prior to harvesting the tissue. We observed a similar increase in hepatic and splenic PLA, however the $CD41^{+}$ monocytes/macrophages were $RELM\alpha^{hi}$ and $MHCII^{hi}$, and therefore did not show the same platelet interactions with specific ($RELM\alpha^{hi}$ and $MHCII^{lo}$) hepatic monocyte/macrophage populations as in schistosome infection.

TPO production by hepatocytes is fine-tuned by platelets and MK, and it has been shown that as platelets age they become desialylated. Binding of exposed terminal galactose to the Ashwell-Morrel Receptor on hepatocytes subsequently drives TPO production (371). Recently as yet unpublished work suggests Kupffer cells are essential intermediaries that enable platelet communication with hepatocytes. Clodronate depletion of Kupffer cells in mice results in a significant reduction of TPO that could not be rescued even after transfusion of desialylated platelets (428). This provides a potential new explanation for reduced hepatic and circulating TPO in schistosome infection. Despite increased numbers of desialylated platelets in schistosome infection, there are low levels of liver-resident Kupffer cells due to recruitment of BM-derived monocytes and macrophages (116,115). This would mean hepatocytes are less able to detect the desialylated platelets so would not produce additional TPO. This hypothesis would depend on the BM-derived monocytes and macrophages in schistosome infection being unable to fulfil the role of Kupffer cells despite being educated in the liver environment. Similar chlodronate liposome experiments could be performed in schistosome infection to deplete BM-derived monocytes and macrophages, and TPO could be measured to see if it was further reduced. In addition, desialylated platelets could also be transfused both before and after chlodronate depletion to test whether these could stimulate hepatic TPO production.

Despite reduced TPO, there were still the same number of MK in the BM of naive and schistosome-infected mice which may be due to compensation by emergency megakaryopoiesis. IL-1α, IGF-1, LIF, IL-6, IL-11 and CCL-5 have all been shown to play a role in emergency megakaryopoiesis (429) and there is evidence to suggest that both IL-6 and CCL-5 are also upregulated in schistosome infection (430–432). Of note, IL-6 is thought to act by stimulating hepatic production of TPO and driving a positive feedback loop, whereas CCL-5 is thought to act in a TPO-independent manner and signals via CCR-5 to inhibit MK apoptosis via the Akt pathway, ultimately driving megakaryopoiesis and pro-platelet formation (433,434). Together, these data suggest the systemic inflammatory response present during schistosome infection is also having a significant impact on HSC development and differentiation in the BM.

Unpublished work in the Hewitson lab is continuing to dissect the long-term changes that are occurring in the BM using transplantation assays, *in vitro* single cell HSC cultures and transcriptomic approaches. As observed in a recent pre-print by Wijshake *et al*. (2023), we have demonstrated a variety of short- and long-term changes to the BM composition (including massive eosinophilia, reduction of $CD68^{+}$ macrophages, changes to stem and progenitor populations and alterations to the stem cell stromal niche) (284). The implications of an altered BM microenvironment are likely to have resulted in extramedullary MK in the liver and spleen in schistosome infection. Key questions that remain include whether extramedullary MK are functionally capable of producing platelets, but this remains challenging due to their small number, large size and fragility. Using the recently reported protocol of Sun *et al.* (2021), we could perform single-cell RNA sequencing on MK isolated from BM, as well as the extramedullary MK found in the liver and spleen in schistosome infection, to phenotype the sub-populations. With MK now shown to secrete CXCL4, TGF-β, fibroblasts growth factor 1 and IGF-1 in the BM, the potential immunomodulatory roles of MK in the liver and spleen is very likely (429). Moreover, assessing the lung MK population would be extremely valuable, given that it is now widely accepted that platelet production is at least in part carried out by lung MK (157–159). This would be of particular relevance in severe cases of schistosomiasis which cause portal shunting and leads to schistosome eggs becoming lodged within the lung (435). In some schistosome infections we isolated lung tissue as well as the spleen and liver. Preliminary findings suggest there is also enhanced PLA in this tissue, however further imaging and analysis would be required to identify MK and any changes that may be occurring. As it has been suggested that lung MK share features of macrophages (including pathogen internalisation and antigen presentation (159)), it would also be interesting to use intra-vital microscopy to assess interactions between MK and schistosome eggs to determine whether they are involved in granuloma formation in a similar manner to alternatively activated macrophages. An alternative approach for studying the lung would be to intravenously inject schistosome eggs into mice, this would enable us to dissect specific platelet interactions and MK changes

in the lung in a type 2 inflammatory environment in the absence of severe liver fibrosis (436–438).

We have concentrated exclusively on schistosome infection using a mouse model to better understand the specific mechanisms and interactions that are occurring. However, human infections are much more complicated due to both repeated exposure to schistosomes and the potential for co-infection with other pathogens. Many clinical studies have described the frequency and complexities of co-infection alongside schistosomiasis. Whilst prior schistosome infection reduces the severity of subsequent infections by *Helicobacter pylori* (*H. pylori*) (439), it can also worsen infections such as, *Plasmondium spp*, *Leishmania spp.* and *Salmonella spp.*(439,440).

Salmonella is a water borne bacterium that tends to reside within monocytes and macrophages in the liver and spleen of infected hosts (439). This induces a Th1, IFNγ-dominated immune response which contrasts with the strong Th2, IL-4 mediated response in a chronic schistosome infection. *Salmonella* induces severe thrombocytopenia and thrombus formation in the liver following platelet activation through the upregulation of podoplanin on macrophages which binds its cognate receptor CLEC-2 on platelets (441). Given the close association between platelets and macrophages in both infections it would be interesting to assess whether these interactions are altered in a co-infection and contributing to the increased severity of infection. *H. pylori* is another bacterium that induces a strong Th1 inflammatory response. Bhattacharjee *et al*. (2019) identified T cell misdirection as one mechanism for the protective effect on both infections in a murine model (442). As we have shown that platelets enhance the ability of M2-like BM-Mϕ to phagocytose *E. coli* bioparticles *in vitro*, a co-infection model would be a good way to assess whether this is a similar case *in vivo* and whether this was also contributing to the improved bacteraemia.

Currently schistosomiasis is diagnosed through the direct detection of schistosome eggs in the stool or urine or through immunological assays for antibodies against egg or adult worm antigens (443). The limitation of egg detection is that adult worms have fully matured and the eggs being produced

will already be driving an inflammatory response. All these assays fail to reliably detect low-level infection resulting in false negative test results. Moreover, the immunological assays are unable to distinguish between past and current infections. We have shown platelet count decreases, MPV increases and platelets spontaneously aggregate in murine schistosome infection. If this also reflects human infection, all of these could be used in combination for the diagnosis and prediction of schistosomiasis instead of just using one parameter alone which has shown variable success as a predictor (444).

In recent years due to the abundance of platelets in the blood and their accessibility they have become an appealing bio-source for liquid biopsies. In the context of cancer, platelets have been identified as a novel repository of multiple RNA biomarkers (mRNA, long noncoding RNA and mitochondrial RNA) (445). Platelets acquire this material through their direct interaction with tumour cells and/or from their ability to scavenge tumour derived EV and releasates from circulation (446). Platelets are anucleate cells but do possess functional translational machinery enabling them to process the acquired transcripts. Isolated platelets can be analysed not only to assess their number, size and activation but also their tumour genetic material content. This can be identified through a range of omics approaches using next generation sequencing, mass spectrometry, qPCR and microarrays (445). This type of analysis has potential implications for infectious diseases such as schistosomiasis. We have shown increased PLA in circulation and therefore it would be interesting to assess whether platelets in schistosome infection acquire genetic material from the monocytes/macrophages or eosinophils they interact with and whether this could be used for diagnosis at earlier stages of infection, prior to egg laying. Furthermore, as schistosomes release a plethora of different excretory/secretory products at different lifecycle stages it would be of great interest to find out whether platelets scavenge any of this material (447) (**Figure 7.2**). This could facilitate early detection prior to worm maturation and egg laying from a single blood test. Moreover, as platelets have a relatively short half-life it may mean only current infections are

detected. As schistosomiasis is endemic in many low-income countries the development of fast and easy, low-cost tests is essential.

We have shown in this thesis that separating the haemostatic and immunological roles of platelets in schistosome infection is challenging given that a lack of platelets drives a bleeding phenotype, ill health, potential bacterial translocation, BM stress which together result in indirect effects on the immune response. Therefore, directly targeting specific platelet-immune cell interactions would be the logical alternative option. However, targeting specific genes or blocking specific immune receptors on platelets may result in impeded aggregation and impact on the haemostatic cascade. These interdependencies make it difficult to determine whether platelets are specifically modulating immune cell responses in schistosome infection. However, we have clearly identified accelerated immune-mediated platelet clearance alongside a pseudo-thrombocytopenia. We have also identified schistosome-specific platelet interactions with hepatic macrophages and monocytes which provides an exciting focus for future work.

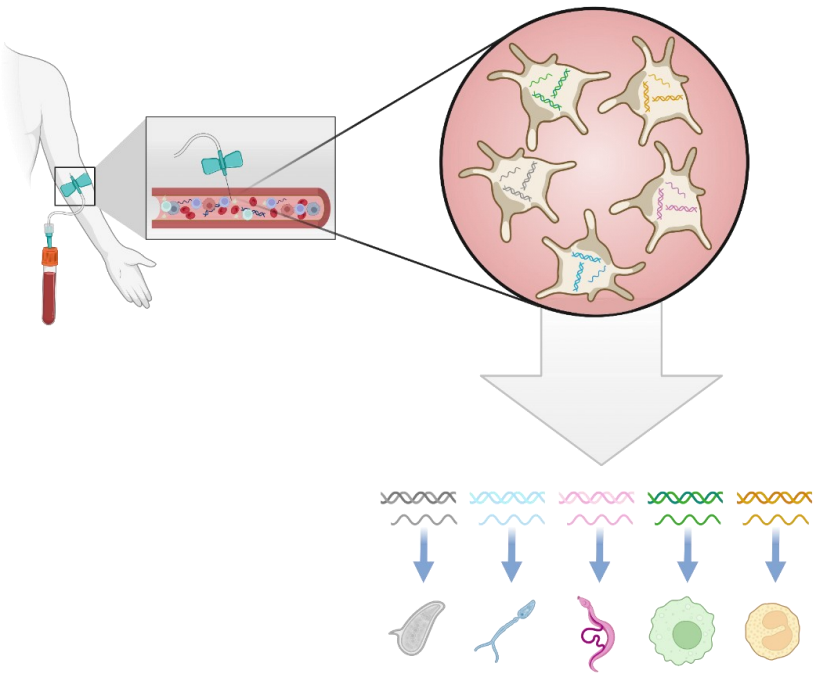

Figure 7.2 Potential use of platelets for liquid biopsy detection of schistosome infection
Blood samples taken from a peripheral vein of patients who potentially have schistosomiasis. Platelets can be isolated and nucleic acid extracted from the cells. Isolated nucleic acid could then be used to identify a range of cells and schistosome lifecycle stages that platelets have scavenged from circulation or acquired through their aggregation.

Abbreviations

ACD	Acid-citrate-dextrose
ACE	Angiotensin-converting enzyme
ACK	Ammonium-Chloride-Potassium
ADP	Adenosine diphosphate
AMP	Adenosine monophosphate
AMR	Ashwell-Morrell Receptor
ANOVA	Analysis of Variance
AP	Alkaline phosphatase
aPTT	Activated partial thromboplastin time
BM	Bone marrow
BM-Mϕ	Bone marrow-derived macrophages
C57BL/6	Common laboratory-bred strain of mice, often referred to as C57 black 6, C57, black 6 or B6
CCL	Chemokine ligand
CCR	Chemokine receptor
CD	Cluster of Differentiation
CD62P	P-selectin
Cercs	Cercariae
CLD	Chronic liver disease
CLEC	C-type lectin-like immune receptor
CMP	Common myeloid progenitor
CNRIP	Cannabinoid receptor interacting protein
CXCR	C-X-C motif chemokine receptor
DAPI	4′,6-diamidino-2-phenylindole
DC	Dendritic cell
DC-SIGN	Dendritic cell-specific intercellular adhesion molecule-3-grabbing nonintegrin
DIC	Disseminated intravascular coagulation
DMEM	Dulbecco's Modified Eagle Medium
EBV	Epstein-Barr virus
E. coli	*Escherichia coli*
ELISA	Enzyme linked immunosorbent assay
EPCR	Endothelial Protein C Receptor
ES	Excretory/Secretory
EtOH	Ethanol
EV	Extracellular vesicle
FACS	Fluorescence-activated cell sorter
FCS	Foetal Calf Serum
FOV	Field of View
GMP	Granulocyte/monocyte progenitor

GP	Glycoprotein
HBSS	Hank's balanced salt solution
HCMV	Human cytomegalovirus
HIV	Human immunodeficiency virus
HMGB1	High-mobility group box 1
H. pylori	*Helicobacter pylori*
HSC	Haematopoietic stem cell
ICAM	Intracellular adhesion molecule
IFN	Interferon
Ig	Immunoglobulin
IL	Interleukin
ILC	Innate lymphoid cell
iNOS	Inducible nitric oxide synthase
INR	International normalised ratio
IP	Intraperitoneally
IPSE	IL-4 inducing principle of *S. mansoni* eggs
ITP	Immune thrombocytopenia
IV	Intravenously
JAK	Janus kinase
KLF	Krüppel-like factor
kDa	Kilo Dalton
Ld	*Leishmania donovani* (*L. donovani*)
LDL	Low-density lipoproteins
LEF1	Lymphoid enhancer-binding factor 1
LPS	Lipopolysaccharide
LSK	Lineage(-) Sca-1(+) c-Kit(+)
mAb	Monoclonal antibody
MEP	Megakaryocyte/erythroid progenitor
MHC	Major histocompatibility complex
MK	Megakaryocytes
MPP	Multipotent progenitor
MPV	Mean platelet volume
NET	Neutrophil extracellular traps
NFB	Nuclear factor B
NK	Natural killer cell
NO	Nitric oxide
NPP	Ectonucleotide pyrophosphatase-phosphodiesterase
OCT	Optimal cutting temperature compound
oxPL	Oxidised phospholipids
PAMP	Pattern associated molecular patterns

PAR	Protease-activated receptors
PBS	Phosphate Buffered Saline
PDGF	Platelet-derived growth factor
PD-L1	Programmed Cell Death Ligand 1
PE	Phycoerythrin
PF4	Platelet-factor 4
PFA	Paraformaldehyde
pHrodo	pH sensitive rhodamine
PLA	Platelet-leukocyte aggregates
PMA	Phorbol 12-myristate 13-acetate
PolyP	Polyphosphate
PRP	Platelet Rich Plasma
PSGL-1	P-selectin glycoprotein ligand 1
PT	Pro-thrombin time
PTT	Partial thromboplastin time
PZQ	Praziquantel
qRT-PCR	Quantitative Reverse Transcription- Polymerase Chain Reaction
RANTES	Regulated upon activation normal T cell expressed and presumably secreted
RCA-1	Ricinus Communis Agglutinin-1
RELMα	Resistin-like molecule α
RNA	Ribonucleic acid
S. haematobium	*Schistosoma haematobium*
S. japonicum	*Schistosoma japonicum*
S. mansoni	*Schistosoma mansoni*
SARS-CoV2	Severe acute respiratory syndrome coronavirus 2
SEA	Schistosome/soluble egg antigen
SOCS	Suppressor of cytokine signalling
STAT	Signal transducer and activator of transcription
TCR	T cell receptor
$T_{E/M}$	T effector/memory
TF	Tissue factor
TGF	Transforming growth factor
Th	T helper
Thio-Mφ	Thioglycollate-elicited macrophages
TLR	Toll-like receptor
TNF	Tumour Necrosis Factor
TPO	Thrombopoietin
Tregs	Regulatory T cells
TSLP	Thymic stromal lymphopoietin

TSP	Thrombospondin 1
VEGF	Vascular endothelial growth factor
VCAM	Vascular cell adhesion molecule 1
VL	Visceral leishmaniasis
vWF	Von Willebrand Factor
WHO	World Health Organisation
WT	Wild Type

References

1. McManus DP, Dunne DW, Sacko M, Utzinger J, Vennervald BJ, Zhou X-N. Schistosomiasis. Nat Rev Dis Primers. 2018 Aug 9;4(1):1–19.

2. Schistosomiasis [Internet]. WHO. [cited 2023 May 1]. Available from: https://www.who.int/news-room/fact-sheets/detail/schistosomiasis

3. LoVerde PT. Schistosomiasis. In: Toledo R, Fried B, editors. Digenetic Trematodes [Internet]. Cham: Springer International Publishing; 2019 [cited 2022 Jul 17]. p. 45–70. (Advances in Experimental Medicine and Biology). Available from: https://doi.org/10.1007/978-3-030-18616-6_3

4. Bocanegra C, Gallego S, Mendioroz J, Moreno M, Sulleiro E, Salvador F, et al. Epidemiology of Schistosomiasis and Usefulness of Indirect Diagnostic Tests in School-Age Children in Cubal, Central Angola. PLoS Negl Trop Dis [Internet]. 2015 Oct 16 [cited 2019 Nov 27];9(10). Available from: https://www.ncbi.nlm.nih.gov/pmc/articles/PMC4608768/

5. Colley DG, Bustinduy AL, Secor WE, King CH. Human schistosomiasis. The Lancet. 2014 Jun 28;383(9936):2253–64.

6. Skelly PJ, Da'dara AA, Li X-H, Castro-Borges W, Wilson RA. Schistosome Feeding and Regurgitation. PLoS Pathog. 2014 Aug 14;10(8):e1004246.

7. Lu Z, Sessler F, Holroyd N, Hahnel S, Quack T, Berriman M, et al. Schistosome sex matters: a deep view into gonad-specific and pairing-dependent transcriptomes reveals a complex gender interplay. Scientific Reports. 2016 Aug 8;6(1):1–14.

8. Cheever AW, Macedonia JG, Mosimann JE, Cheever EA. Kinetics of egg production and egg excretion by Schistosoma mansoni and S. japonicum in mice infected with a single pair of worms. Am J Trop Med Hyg. 1994 Mar;50(3):281–95.

9. Colley DG, Secor WE. Immunology of human schistosomiasis. Parasite Immunol. 2014 Aug;36(8):347–57.

10. What is schistosomiasis? [Internet]. @yourgenome · Science website. [cited 2023 Jul 24]. Available from: https://www.yourgenome.org/facts/what-is-schistosomiasis/

11. Pearce EJ, MacDonald AS. The immunobiology of schistosomiasis. Nature Reviews Immunology. 2002 Jul;2(7):499–511.

12. King CL, Malhotra I, Mungai P, Wamachi A, Kioko J, Ouma JH, et al. B cell sensitization to helminthic infection develops in utero in humans. J Immunol. 1998 Apr 1;160(7):3578–84.

13. Dunne DW, Jones FM, Doenhoff MJ. The purification, characterization, serological activity and hepatotoxic properties of two cationic glycoproteins (alpha 1 and omega 1) from Schistosoma mansoni eggs. Parasitology. 1991 Oct;103 Pt 2:225–36.

14. Schramm G, Mohrs K, Wodrich M, Doenhoff MJ, Pearce EJ, Haas H, et al. Cutting edge: IPSE/alpha-1, a glycoprotein from Schistosoma mansoni eggs, induces IgE-dependent, antigen-independent IL-4 production by murine basophils in vivo. J Immunol. 2007 May 15;178(10):6023–7.

15. Klion AD, Nutman TB. The role of eosinophils in host defense against helminth parasites. Journal of Allergy and Clinical Immunology. 2004 Jan 1;113(1):30–7.

16. Brunet LR, Finkelman FD, Cheever AW, Kopf MA, Pearce EJ. IL-4 protects against TNF-alpha-mediated cachexia and death during acute schistosomiasis. J Immunol. 1997 Jul 15;159(2):777–85.

17. Fallon PG, Richardson EJ, McKenzie GJ, McKenzie AN. Schistosome infection of transgenic mice defines distinct and contrasting pathogenic roles for IL-4 and IL-13: IL-13 is a profibrotic agent. J Immunol. 2000 Mar 1;164(5):2585–91.

18. Hoffmann KF, Cheever AW, Wynn TA. IL-10 and the dangers of immune polarization: excessive type 1 and type 2 cytokine responses induce distinct forms of lethal immunopathology in murine schistosomiasis. J Immunol. 2000 Jun 15;164(12):6406–16.

19. Williams GT, Williams WJ. Granulomatous inflammation--a review. J Clin Pathol. 1983 Jul;36(7):723–33.

20. Wilson MS, Mentink-Kane MM, Pesce JT, Ramalingam TR, Thompson R, Wynn TA. Immunopathology of schistosomiasis. Immunol Cell Biol. 2007;85(2):148–54.

21. Olveda DU, Li Y, Olveda RM, Lam AK, Chau TNP, Harn DA, et al. Bilharzia: Pathology, Diagnosis, Management and Control. Trop Med Surg [Internet]. 2013 Aug 20 [cited 2019 Nov 27];1(4). Available from: https://www.ncbi.nlm.nih.gov/pmc/articles/PMC4208666/

22. Hams E, Aviello G, Fallon PG. The Schistosoma Granuloma: Friend or Foe? Front Immunol [Internet]. 2013 [cited 2020 Nov 23];4. Available from: https://www.frontiersin.org/articles/10.3389/fimmu.2013.00089/full

23. Schwartz C, Fallon PG. Schistosoma “Eggs-Iting” the Host: Granuloma Formation and Egg Excretion. Front Immunol [Internet]. 2018 Oct 29 [cited 2020 Apr 16];9. Available from: https://www.ncbi.nlm.nih.gov/pmc/articles/PMC6232930/

24. Onguru D, Liang Y, Griffith Q, Nikolajczyk B, Mwinzi P, Ganley-Leal L. Human Schistosomiasis Is Associated with Endotoxemia and Toll-Like

Receptor 2- and 4-Bearing B Cells. Am J Trop Med Hyg. 2011 Feb 4;84(2):321–4.

25. Lima K de M, Negro-Dellacqua M, Dos Santos VEFA, de Castro CMMB. Post-splenectomy infections in chronic schistosomiasis as a consequence of bacterial translocation. Rev Soc Bras Med Trop. 2015;48(3):314–20.

26. Kaonga P, Kaimoyo E, Besa E, Zyambo K, Sinkala E, Kelly P. Direct Biomarkers of Microbial Translocation Correlate with Immune Activation in Adult Zambians with Environmental Enteropathy and Hepatosplenic Schistosomiasis. Am J Trop Med Hyg. 2017 Nov 8;97(5):1603–10.

27. Klemperer KM, Reust MJ, Lee MH, Corstjens PLAM, van Dam GJ, Mazigo HD, et al. Plasma Endotoxin Levels Are Not Increased in Schistosoma mansoni–Infected Women without Signs or Symptoms of Hepatosplenic Disease. Am J Trop Med Hyg. 2020 Jun;102(6):1382–5.

28. Andrews P. Praziquantel: mechanisms of anti-schistosomal activity. Pharmacol Ther. 1985;29(1):129–56.

29. Vale N, Gouveia MJ, Rinaldi G, Brindley PJ, Gärtner F, Costa JMC da. Praziquantel for Schistosomiasis: Single-Drug Metabolism Revisited, Mode of Action, and Resistance. Antimicrobial Agents and Chemotherapy [Internet]. 2017 May 1 [cited 2019 Nov 29];61(5). Available from: https://aac.asm.org/content/61/5/e02582-16

30. Cotton JA, Doyle SR. A genetic TRP down the channel to praziquantel resistance. Trends in Parasitology. 2022 May 1;38(5):351–2.

31. Le Clec'h W, Chevalier FD, Mattos ACA, Strickland A, Diaz R, McDew-White M, et al. Genetic analysis of praziquantel response in schistosome parasites implicates a Transient Receptor Potential channel. Sci Transl Med. 2021 Dec 22;13(625):eabj9114.

32. Pax R, Bennett JL, Fetterer R. A benzodiazepine derivative and praziquantel: effects on musculature of Schistosoma mansoni and Schistosoma japonicum. Naunyn Schmiedebergs Arch Pharmacol. 1978 Oct;304(3):309–15.

33. Harnett W, Kusel JR. Increased exposure of parasite antigens at the surface of adult male Schistosoma mansoni exposed to praziquantel in vitro. Parasitology. 1986 Oct;93 (Pt 2):401–5.

34. Kohn AB, Anderson PA, Roberts-Misterly JM, Greenberg RM. Schistosome calcium channel beta subunits. Unusual modulatory effects and potential role in the action of the antischistosomal drug praziquantel. J Biol Chem. 2001 Oct 5;276(40):36873–6.

35. Pica-Mattoccia L, Valle C, Basso A, Troiani AR, Vigorosi F, Liberti P, et al. Cytochalasin D abolishes the schistosomicidal activity of praziquantel. Exp Parasitol. 2007 Apr;115(4):344–51.

36. Pica-Mattoccia L, Orsini T, Basso A, Festucci A, Liberti P, Guidi A, et al. Schistosoma mansoni: lack of correlation between praziquantel-induced intra-worm calcium influx and parasite death. Exp Parasitol. 2008 Jul;119(3):332–5.

37. Nogi T, Zhang D, Chan JD, Marchant JS. A novel biological activity of praziquantel requiring voltage-operated Ca2+ channel beta subunits: subversion of flatworm regenerative polarity. PLoS Negl Trop Dis. 2009 Jun 23;3(6):e464.

38. Aragon AD, Imani RA, Blackburn VR, Cupit PM, Melman SD, Goronga T, et al. Towards an understanding of the mechanism of action of praziquantel. Mol Biochem Parasitol. 2009 Mar;164(1):57–65.

39. Hines-Kay J, Cupit PM, Sanchez MC, Rosenberg GH, Hanelt B, Cunningham C. Transcriptional analysis of Schistosoma mansoni treated with praziquantel in vitro. Mol Biochem Parasitol. 2012 Dec;186(2):87–94.

40. You H, McManus DP, Hu W, Smout MJ, Brindley PJ, Gobert GN. Transcriptional responses of in vivo praziquantel exposure in schistosomes identifies a functional role for calcium signalling pathway member CamKII. PLoS Pathog. 2013 Mar;9(3):e1003254.

41. Chan JD, Agbedanu PN, Zamanian M, Gruba SM, Haynes CL, Day TA, et al. 'Death and axes': unexpected Ca^{2+} entry phenologs predict new anti-schistosomal agents. PLoS Pathog. 2014 Feb;10(2):e1003942.

42. Siddiqui AA, Siddiqui BA, Ganley-Leal L. Schistosomiasis vaccines. Hum Vaccin. 2011 Nov 1;7(11):1192–7.

43. Aruleba RT, Adekiya TA, Oyinloye BE, Masamba P, Mbatha LS, Pretorius A, et al. PZQ Therapy: How Close are we in the Development of Effective Alternative Anti-schistosomal Drugs? Infect Disord Drug Targets. 2019 Dec;19(4):337–49.

44. Mutapi F, Ndhlovu PD, Hagan P, Spicer JT, Mduluza T, Turner CM, et al. Chemotherapy accelerates the development of acquired immune responses to Schistosoma haematobium infection. J Infect Dis. 1998 Jul;178(1):289–93.

45. Woolhouse ME, Hagan P. Seeking the ghost of worms past. Nat Med. 1999 Nov;5(11):1225–7.

46. Wiegand RE, Mwinzi PNM, Montgomery SP, Chan YL, Andiego K, Omedo M, et al. A Persistent Hotspot of Schistosoma mansoni Infection in a Five-Year Randomized Trial of Praziquantel Preventative Chemotherapy Strategies. J Infect Dis. 2017 Dec 12;216(11):1425–33.

47. Vianney TJ, Berger DJ, Doyle SR, Sankaranarayanan G, Serubanja J, Nakawungu PK, et al. Genome-wide analysis of Schistosoma mansoni reveals limited population structure and possible praziquantel drug

selection pressure within Ugandan hot-spot communities. PLoS Negl Trop Dis. 2022 Aug;16(8):e0010188.

48. Assaré RK, N'Tamon RN, Bellai LG, Koffi JA, Mathieu T-BI, Ouattara M, et al. Characteristics of persistent hotspots of Schistosoma mansoni in western Côte d'Ivoire. Parasit Vectors. 2020 Jul 2;13(1):337.

49. Summers S, Bhattacharyya T, Allan F, Stothard JR, Edielu A, Webster BL, et al. A review of the genetic determinants of praziquantel resistance in Schistosoma mansoni: Is praziquantel and intestinal schistosomiasis a perfect match? Frontiers in Tropical Diseases [Internet]. 2022 [cited 2023 Apr 11];3. Available from: https://www.frontiersin.org/articles/10.3389/fitd.2022.933097

50. Bergquist R, Elmorshedy H. Artemether and Praziquantel: Origin, Mode of Action, Impact, and Suggested Application for Effective Control of Human Schistosomiasis. Trop Med Infect Dis. 2018 Dec 19;3(4):125.

51. Rugel AR, Guzman MA, Taylor AB, Chevalier FD, Tarpley RS, McHardy SF, et al. Why does oxamniquine kill Schistosoma mansoni and not S. haematobium and S. japonicum? Int J Parasitol Drugs Drug Resist. 2020 Apr 10;13:8–15.

52. Mazigo HD, Dunne DW, Kinung'hi SM, Nuwaha F. Praziquantel efficacy against Schistosoma mansoni among HIV-1 infected and uninfected adults living in fishing villages along Lake Victoria, Northwest Tanzania. Infectious Diseases of Poverty. 2014 Dec 15;3(1):47.

53. Modha J, Lambertucci J r., Doenhoff M j., McLAREN DJ. Immune dependence of schistosomicidal chemotherapy: an ultrastructural study of Schistosoma mansoni adult worms exposed to praziquantel and immune serum in vivo. Parasite Immunology. 1990;12(3):321–34.

54. Doenhoff MJ, Bain J. The immune-dependence of schistosomicidal chemotherapy: relative lack of efficacy of an antimonial in Schistosoma mansoni-infected mice deprived of their T-cells and the demonstration of drug-antiserum synergy. Clin Exp Immunol. 1978 Aug;33(2):232–8.

55. Molehin AJ, McManus DP, You H. Vaccines for Human Schistosomiasis: Recent Progress, New Developments and Future Prospects. Int J Mol Sci. 2022 Feb 18;23(4):2255.

56. Hewitson JP, Maizels RM. Vaccination against helminth parasite infections. Expert Review of Vaccines. 2014 Apr 1;13(4):473–87.

57. Molehin AJ, Rojo JU, Siddiqui SZ, Gray SA, Carter D, Siddiqui AA. Development of a Schistosomiasis Vaccine. Expert Rev Vaccines. 2016 May;15(5):619–27.

58. Maizels RM. Identifying novel candidates and configurations for human helminth vaccines. Expert Review of Vaccines. 2021 Nov 2;20(11):1389–93.

59. Ridi RE, Tallima H. Vaccine-Induced Protection Against Murine Schistosomiasis Mansoni with Larval Excretory–Secretory Antigens and Papain or Type-2 Cytokines. para. 2013 Apr;99(2):194–202.

60. Drurey C, Coakley G, Maizels RM. Extracellular vesicles: new targets for vaccines against helminth parasites. Int J Parasitol. 2020 Aug;50(9):623–33.

61. Molehin AJ. Schistosomiasis vaccine development: update on human clinical trials. Journal of Biomedical Science. 2020 Jan 22;27(1):28.

62. Winkelmann F, Gesell Salazar M, Hentschker C, Michalik S, Macháček T, Scharf C, et al. Comparative proteome analysis of the tegument of male and female adult Schistosoma mansoni. Sci Rep. 2022 May 9;12:7569.

63. Zhang W, Le L, Ahmad G, Molehin AJ, Siddiqui AJ, Torben W, et al. Fifteen Years of Sm-p80-Based Vaccine Trials in Nonhuman Primates: Antibodies From Vaccinated Baboons Confer Protection in vivo and in vitro From Schistosoma mansoni and Identification of Putative Correlative Markers of Protection. Frontiers in Immunology [Internet]. 2020 [cited 2023 Apr 11];11. Available from: https://www.frontiersin.org/articles/10.3389/fimmu.2020.01246

64. Marichal T, Mesnil C, Bureau F. Homeostatic Eosinophils: Characteristics and Functions. Frontiers in Medicine [Internet]. 2017 [cited 2023 Apr 11];4. Available from: https://www.frontiersin.org/articles/10.3389/fmed.2017.00101

65. Kanda A, Yun Y, Bui DV, Nguyen LM, Kobayashi Y, Suzuki K, et al. The multiple functions and subpopulations of eosinophils in tissues under steady-state and pathological conditions. Allergology International. 2021 Jan 1;70(1):9–18.

66. Huang L, Appleton JA. Eosinophils in helminth infection: defenders and dupes. Trends Parasitol. 2016 Oct;32(10):798–807.

67. Rosenberg HF, Dyer KD, Foster PS. Eosinophils: changing perspectives in health and disease. Nat Rev Immunol. 2013;13(1):9–22.

68. Fettrelet T, Gigon L, Karaulov A, Yousefi S, Simon H-U. The Enigma of Eosinophil Degranulation. Int J Mol Sci. 2021 Jun 30;22(13):7091.

69. Wu D, Molofsky AB, Liang H-E, Ricardo-Gonzalez RR, Jouihan HA, Bando JK, et al. Eosinophils sustain adipose alternatively activated macrophages associated with glucose homeostasis. Science. 2011 Apr 8;332(6026):243–7.

70. Dasgupta P, Keegan AD. Contribution of alternatively activated macrophages to allergic lung inflammation: a tale of mice and men. J Innate Immun. 2012;4(5–6):478–88.

71. Moore DL, Grove DI, Warren KS. The Schistosoma mansoni egg granuloma: quantitation of cell populations. J Pathol. 1977 Jan;121(1):41–50.

72. Swartz JM, Dyer KD, Cheever AW, Ramalingam T, Pesnicak L, Domachowske JB, et al. Schistosoma mansoni infection in eosinophil lineage–ablated mice. Blood. 2006 Oct 1;108(7):2420–7.

73. Sher A, Coffman RL, Hieny S, Cheever AW. Ablation of eosinophil and IgE responses with anti-IL-5 or anti-IL-4 antibodies fails to affect immunity against Schistosoma mansoni in the mouse. J Immunol. 1990 Dec 1;145(11):3911–6.

74. Jackson DJ, Korn S, Mathur SK, Barker P, Meka VG, Martin UJ, et al. Safety of Eosinophil-Depleting Therapy for Severe, Eosinophilic Asthma: Focus on Benralizumab. Drug Saf. 2020;43(5):409–25.

75. Williams DL, Asahi H, Botkin DJ, Stadecker MJ. Schistosome Infection Stimulates Host CD4+ T Helper Cell and B-Cell Responses against a Novel Egg Antigen, Thioredoxin Peroxidase. Infect Immun. 2001 Feb;69(2):1134–41.

76. Kaplan MH, Whitfield JR, Boros DL, Grusby MJ. Th2 cells are required for the Schistosoma mansoni egg-induced granulomatous response. J Immunol. 1998 Feb 15;160(4):1850–6.

77. Karanja DMS, Colley DG, Nahlen BL, Ouma JH, Secor WE. Studies on Schistosomiasis in Western Kenya: I. Evidence for Immune-Facilitated Excretion of Schistosome Eggs from Patients with Schistosoma mansoni and Human Immunodeficiency Virus Coinfections. The American Journal of Tropical Medicine and Hygiene. 1997 May 1;56(5):515–21.

78. Zheng B, Zhang J, Chen H, Nie H, Miller H, Gong Q, et al. T Lymphocyte-Mediated Liver Immunopathology of Schistosomiasis. Front Immunol. 2020 Feb 18;11:61.

79. Ondigo BN, Ndombi EM, Nicholson SC, Oguso JK, Carter JM, Kittur N, et al. Functional Studies of T Regulatory Lymphocytes in Human Schistosomiasis in Western Kenya. The American Journal of Tropical Medicine and Hygiene. 2018 Apr 23;98(6):1770–81.

80. Turner JD, Jenkins GR, Hogg KG, Aynsley SA, Paveley RA, Cook PC, et al. CD4+CD25+ Regulatory Cells Contribute to the Regulation of Colonic Th2 Granulomatous Pathology Caused by Schistosome Infection. PLOS Neglected Tropical Diseases. 2011 Aug 9;5(8):e1269.

81. Layland LE, Mages J, Loddenkemper C, Hoerauf A, Wagner H, Lang R, et al. Pronounced Phenotype in Activated Regulatory T Cells during a Chronic Helminth Infection. The Journal of Immunology. 2010 Jan 15;184(2):713–24.

82. Walsh CM, Smith P, Fallon PG. Role for CTLA-4 but not CD25+ T cells during Schistosoma mansoni infection of mice. Parasite Immunology. 2007;29(6):293–308.

83. Baumgart M, Tompkins F, Leng J, Hesse M. Naturally Occurring CD4+Foxp3+ Regulatory T Cells Are an Essential, IL-10-Independent Part of the Immunoregulatory Network in Schistosoma mansoni Egg-Induced Inflammation. The Journal of Immunology. 2006 May 1;176(9):5374–87.

84. Hori S, Nomura T, Sakaguchi S. Control of Regulatory T Cell Development by the Transcription Factor Foxp3. Science. 2003 Feb 14;299(5609):1057–61.

85. Gerdes N, Zhu L, Ersoy M, Hermansson A, Hjemdahl P, Hu H, et al. Platelets regulate $CD4^+$ T-cell differentiation via multiple chemokines in humans. Thromb Haemost. 2011 Aug;106(2):353–62.

86. Polasky C, Wendt F, Pries R, Wollenberg B. Platelet Induced Functional Alteration of CD4+ and CD8+ T Cells in HNSCC. Int J Mol Sci. 2020 Oct 12;21(20):7507.

87. Zamora C, Cantó E, Nieto JC, Bardina J, Diaz-Torné C, Moya P, et al. Binding of Platelets to Lymphocytes: A Potential Anti-Inflammatory Therapy in Rheumatoid Arthritis. The Journal of Immunology. 2017 Apr 15;198(8):3099–108.

88. Semple JW, Freedman J. Increased antiplatelet T helper lymphocyte reactivity in patients with autoimmune thrombocytopenia. Blood. 1991 Nov 15;78(10):2619–25.

89. Seifert U, Greinacher A. Platelets modulate T-cell activity. Blood. 2021 Aug 5;138(5):358–60.

90. Jankovic D, Kullberg MC, Dombrowicz D, Barbieri S, Caspar P, Wynn TA, et al. Fc epsilonRI-deficient mice infected with Schistosoma mansoni mount normal Th2-type responses while displaying enhanced liver pathology. J Immunol. 1997 Aug 15;159(4):1868–75.

91. Hernandez HJ, Wang Y, Stadecker MJ. In infection with Schistosoma mansoni, B cells are required for T helper type 2 cell responses but not for granuloma formation. The Journal of Immunology. 1997 May 15;158(10):4832–7.

92. Fairfax KC, Everts B, Smith AM, Pearce EJ. Regulation of the Development of the Hepatic B Cell Compartment During Schistosoma mansoni Infection. J Immunol. 2013 Oct 15;191(8):10.4049/jimmunol.1301357.

93. Lopes LM, Pereira MA, Gerken SE, Vaz N. Polyclonal activation of B lymphocytes during experimental infection with Schistosoma mansoni. Parasitology. 1990 Feb;100 Pt 1:83–91.

94. Fischer E, Camus D, Santoro F, Capron A. Schistosoma mansoni: autoantibodies and polyclonal B cell activation in infected mice. Clin Exp Immunol. 1981 Oct;46(1):89–97.

95. Boros DL, Amsden AF, Hood AT. Modulation of granulomatous hypersensitivity. IV. Immunoglobulin and antibody production by vigorous and immunomodulated liver granulomas of Schistosoma mansoni-infected mice. J Immunol. 1982 Mar;128(3):1050–3.

96. Goes AM, Gazzinelli G, Rocha R, Katz N, Doughty BL. Granulomatous Hypersensitivity to Schistosoma Mansoni Egg Antigens in Human Schistosomiasis. III. in Vitro Granuloma Modulation Induced by Immune Complexes. The American Journal of Tropical Medicine and Hygiene. 1991 Apr 1;44(4):434–43.

97. Mills CD, Kincaid K, Alt JM, Heilman MJ, Hill AM. M-1/M-2 Macrophages and the Th1/Th2 Paradigm. The Journal of Immunology. 2000 Jun 15;164(12):6166–73.

98. Ley K. M1 Means Kill; M2 Means Heal. The Journal of Immunology. 2017 Oct 1;199(7):2191–3.

99. Murray PJ, Allen JE, Biswas SK, Fisher EA, Gilroy DW, Goerdt S, et al. Macrophage activation and polarization: nomenclature and experimental guidelines. Immunity. 2014 Jul 17;41(1):14–20.

100. Mosser DM, Zhang X. Activation of Murine Macrophages. Curr Protoc Immunol. 2008 Nov;CHAPTER:Unit.

101. Wynn TA, Chawla A, Pollard JW. Macrophage biology in development, homeostasis and disease. Nature. 2013 Apr;496(7446):445–55.

102. Ginhoux F, Schultze JL, Murray PJ, Ochando J, Biswas SK. New insights into the multidimensional concept of macrophage ontogeny, activation and function. Nature Immunology. 2016 Jan;17(1):34–40.

103. Gundra UM, Girgis NM, Ruckerl D, Jenkins S, Ward LN, Kurtz ZD, et al. Alternatively activated macrophages derived from monocytes and tissue macrophages are phenotypically and functionally distinct. Blood. 2014 May 15;123(20):e110–22.

104. Jablonski KA, Amici SA, Webb LM, Ruiz-Rosado J de D, Popovich PG, Partida-Sanchez S, et al. Novel Markers to Delineate Murine M1 and M2 Macrophages. PLOS ONE. 2015 Dec 23;10(12):e0145342.

105. Yu T, Gan S, Zhu Q, Dai D, Li N, Wang H, et al. Modulation of M2 macrophage polarization by the crosstalk between Stat6 and Trim24. Nature Communications. 2019 Sep 25;10(1):4353.

106. Martinez FO, Helming L, Milde R, Varin A, Melgert BN, Draijer C, et al. Genetic programs expressed in resting and IL-4 alternatively activated

mouse and human macrophages: similarities and differences. Blood. 2013 Feb 28;121(9):e57–69.

107. Sieweke MH, Allen JE. Beyond Stem Cells: Self-Renewal of Differentiated Macrophages. Science. 2013 Nov 22;342(6161):1242974.

108. Schulz C, Perdiguero EG, Chorro L, Szabo-Rogers H, Cagnard N, Kierdorf K, et al. A Lineage of Myeloid Cells Independent of Myb and Hematopoietic Stem Cells. Science. 2012 Apr 6;336(6077):86–90.

109. Wen Y, Lambrecht J, Ju C, Tacke F. Hepatic macrophages in liver homeostasis and diseases-diversity, plasticity and therapeutic opportunities. Cell Mol Immunol. 2021 Jan;18(1):45–56.

110. Deppermann C, Kratofil RM, Peiseler M, David BA, Zindel J, Castanheira FVES, et al. Macrophage galactose lectin is critical for Kupffer cells to clear aged platelets. J Exp Med. 2020 Apr 6;217(4):e20190723.

111. Guilliams M, Bonnardel J, Haest B, Vanderborght B, Wagner C, Remmerie A, et al. Spatial proteogenomics reveals distinct and evolutionarily conserved hepatic macrophage niches. Cell. 2022 Jan 20;185(2):379-396.e38.

112. Askenase MH, Han S-J, Byrd AL, Morais da Fonseca D, Bouladoux N, Wilhelm C, et al. Bone-Marrow-Resident NK Cells Prime Monocytes for Regulatory Function during Infection. Immunity. 2015 Jun 16;42(6):1130–42.

113. Shi C, Pamer EG. Monocyte recruitment during infection and inflammation. Nat Rev Immunol. 2011 Nov;11(11):762–74.

114. Souza COS, Gardinassi LG, Rodrigues V, Faccioli LH. Monocyte and Macrophage-Mediated Pathology and Protective Immunity During Schistosomiasis. Frontiers in Microbiology [Internet]. 2020 [cited 2022 May 3];11. Available from: https://www.frontiersin.org/article/10.3389/fmicb.2020.01973

115. Girgis NM, Gundra UM, Ward LN, Cabrera M, Frevert U, Loke P. Ly6Chigh Monocytes Become Alternatively Activated Macrophages in Schistosome Granulomas with Help from CD4+ Cells. PLOS Pathogens. 2014 Jun 26;10(6):e1004080.

116. Rolot M, M Dougall A, Javaux J, Lallemand F, Machiels B, Martinive P, et al. Recruitment of hepatic macrophages from monocytes is independent of IL-4Rα but is associated with ablation of resident macrophages in schistosomiasis. Eur J Immunol. 2019 Jul;49(7):1067–81.

117. Hou Y, Carrim N, Wang Y, Gallant RC, Marshall A, Ni H. Platelets in hemostasis and thrombosis: Novel mechanisms of fibrinogen-

independent platelet aggregation and fibronectin-mediated protein wave of hemostasis. J Biomed Res. 2015 Nov;29(6):437–44.

118. Howell WH. Observations upon the occurrence, structure, and function of the giant cells of the marrow. Journal of Morphology. 1890;4(1):117–30.

119. WRIGHT JH. The Origin and Nature of the Blood Plates. The Boston Medical and Surgical Journal. 1906 Jun 7;154(23):643–5.

120. Li M, Li X, Fan K, Yu Y, Gong J, Geng S, et al. Platelet desialylation is a novel mechanism and a therapeutic target in thrombocytopenia during sepsis: an open-label, multicenter, randomized controlled trial. J Hematol Oncol. 2017 May 11;10:104.

121. Noetzli Leila J., French Shauna L., Machlus Kellie R. New Insights Into the Differentiation of Megakaryocytes From Hematopoietic Progenitors. Arteriosclerosis, Thrombosis, and Vascular Biology. 2019 Jul 1;39(7):1288–300.

122. Sola-Visner MC, Christensen RD, Hutson AD, Rimsza LM. Megakaryocyte Size and Concentration in the Bone Marrow of Thrombocytopenic and Nonthrombocytopenic Neonates. Pediatric Research. 2007 Apr;61(4):479–84.

123. Schmitt A, Guichard J, Massé J-M, Debili N, Cramer EM. Of mice and men: Comparison of the ultrastructure of megakaryocytes and platelets. Experimental Hematology. 2001 Nov 1;29(11):1295–302.

124. Nutt SL, Metcalf D, D'Amico A, Polli M, Wu L. Dynamic regulation of PU.1 expression in multipotent hematopoietic progenitors. J Exp Med. 2005 Jan 17;201(2):221–31.

125. Akashi K, Traver D, Miyamoto T, Weissman IL. A clonogenic common myeloid progenitor that gives rise to all myeloid lineages. Nature. 2000 Mar;404(6774):193–7.

126. Deutsch VR, Tomer A. Advances in megakaryocytopoiesis and thrombopoiesis: from bench to bedside. British Journal of Haematology. 2013;161(6):778–93.

127. Psaila B, Barkas N, Iskander D, Roy A, Anderson S, Ashley N, et al. Single-cell profiling of human megakaryocyte-erythroid progenitors identifies distinct megakaryocyte and erythroid differentiation pathways. Genome Biology. 2016 May 3;17(1):83.

128. Rodriguez-Fraticelli AE, Wolock SL, Weinreb CS, Panero R, Patel SH, Jankovic M, et al. Clonal analysis of lineage fate in native haematopoiesis. Nature. 2018 Jan;553(7687):212–6.

129. Sanjuan-Pla A, Macaulay IC, Jensen CT, Woll PS, Luis TC, Mead A, et al. Platelet-biased stem cells reside at the apex of the haematopoietic stem-cell hierarchy. Nature. 2013 Oct;502(7470):232–6.

130. Yamamoto R, Morita Y, Ooehara J, Hamanaka S, Onodera M, Rudolph KL, et al. Clonal Analysis Unveils Self-Renewing Lineage-Restricted Progenitors Generated Directly from Hematopoietic Stem Cells. Cell. 2013 Aug 29;154(5):1112–26.

131. Vitrat N, Cohen-Solal K, Pique C, LeCouedic JP, Norol F, Larsen AK, et al. Endomitosis of Human Megakaryocytes Are Due to Abortive Mitosis. Blood. 1998 May 15;91(10):3711–23.

132. Nagata Y, Muro Y, Todokoro K. Thrombopoietin-induced Polyploidization of Bone Marrow Megakaryocytes Is Due to a Unique Regulatory Mechanism in Late Mitosis. J Cell Biol. 1997 Oct 20;139(2):449–57.

133. Lordier L, Jalil A, Aurade F, Larbret F, Larghero J, Debili N, et al. Megakaryocyte endomitosis is a failure of late cytokinesis related to defects in the contractile ring and Rho/Rock signaling. Blood. 2008 Oct 15;112(8):3164–74.

134. Sim X, Poncz M, Gadue P, French DL. Understanding platelet generation from megakaryocytes: implications for in vitro–derived platelets. Blood. 2016 Mar 10;127(10):1227–33.

135. Thon JN, Montalvo A, Patel-Hett S, Devine MT, Richardson JL, Ehrlicher A, et al. Cytoskeletal mechanics of proplatelet maturation and platelet release. J Cell Biol. 2010 Nov 15;191(4):861–74.

136. Junt T, Schulze H, Chen Z, Massberg S, Goerge T, Krueger A, et al. Dynamic visualization of thrombopoiesis within bone marrow. Science. 2007 Sep 21;317(5845):1767–70.

137. Machlus KR, Italiano JE. The incredible journey: From megakaryocyte development to platelet formation. J Cell Biol. 2013 Jun 10;201(6):785–96.

138. Richardson JL, Shivdasani RA, Boers C, Hartwig JH, Italiano JE. Mechanisms of organelle transport and capture along proplatelets during platelet production. Blood. 2005 Dec 15;106(13):4066–75.

139. Battinelli EM, Thon JN, Okazaki R, Peters CG, Vijey P, Wilkie AR, et al. Megakaryocytes package contents into separate α-granules that are differentially distributed in platelets. Blood Adv. 2019 Oct 22;3(20):3092–8.

140. Gurney A, Carvermoore K, Desauvage F, Moore M. Thrombocytopenia in C-Mpl-Deficient Mice. Science. 1994 Sep 2;265(5177):1445–7.

141. Hammond W, Kaplan A, Kaplan S, Kaushansky K. Thrombopoietin (tpo) Activates Platelets in-Vitro. Blood. 1994 Nov 15;84(10):A534–A534.

142. Kaushansky K. Historical review: megakaryopoiesis and thrombopoiesis. Blood. 2008 Feb 1;111(3):981–6.

143. Kaushansky K, Lok S, Holly RD, Broudy VC, Lin N, Bailey MC, et al. Promotion of megakaryocyte progenitor expansion and differentiation by the c-Mpl ligand thrombopoietin. Nature. 1994 Jun;369(6481):568–71.

144. de Sauvage FJ, Hass PE, Spencer SD, Malloy BE, Gurney AL, Spencer SA, et al. Stimulation of megakaryocytopoiesis and thrombopoiesis by the c-Mpl ligand. Nature. 1994 Jun;369(6481):533–8.

145. Shimada Y, Kato T, Ogami K, Horie K, Kokubo A, Kudo Y, et al. Thrombopoietin (tpo) Is Produced by Liver. Blood. 1994 Nov 15;84(10):A326–A326.

146. Zeigler FC, de Sauvage F, Widmer HR, Keller GA, Donahue C, Schreiber RD, et al. In vitro megakaryocytopoietic and thrombopoietic activity of c-mpl ligand (TPO) on purified murine hematopoietic stem cells. Blood. 1994 Dec 15;84(12):4045–52.

147. Kuter DJ. The biology of thrombopoietin and thrombopoietin receptor agonists. Int J Hematol. 2013 Jul 1;98(1):10–23.

148. Nagasawa T, Hasegawa Y, Shimizu S, Kawashima Y, Nishimura S, Suzukawa K, et al. Serum thrombopoietin level is mainly regulated by megakaryocyte mass rather than platelet mass in human subjects. Br J Haematol. 1998 May;101(2):242–4.

149. Lebois M, Dowling MR, Gangatirkar P, Hodgkin PD, Kile BT, Alexander WS, et al. Regulation of platelet lifespan in the presence and absence of thrombopoietin signaling. Journal of Thrombosis and Haemostasis. 2016;14(9):1882–7.

150. Kuter DJ, Gernsheimer TB. Thrombopoietin and Platelet Production in Chronic Immune Thrombocytopenia. Hematol Oncol Clin North Am. 2009 Dec;23(6):1193–211.

151. Varghese LN, Defour J-P, Pecquet C, Constantinescu SN. The Thrombopoietin Receptor: Structural Basis of Traffic and Activation by Ligand, Mutations, Agonists, and Mutated Calreticulin. Front Endocrinol (Lausanne) [Internet]. 2017 Mar 31 [cited 2020 Jun 9];8. Available from: https://www.ncbi.nlm.nih.gov/pmc/articles/PMC5374145/

152. Grozovsky R, Giannini S, Falet H, Hoffmeister KM. Novel mechanisms of platelet clearance and thrombopoietin regulation. Curr Opin Hematol. 2015 Sep;22(5):445–51.

153. Zucker-Franklin D, Philipp CS. Platelet production in the pulmonary capillary bed: new ultrastructural evidence for an old concept. Am J Pathol. 2000 Jul;157(1):69–74.

154. Howell WH, Donahue DD. THE PRODUCTION OF BLOOD PLATELETS IN THE LUNGS. J Exp Med. 1937 Jan 31;65(2):177–203.

155. Levine RF, Eldor A, Shoff PK, Kirwin S, Tenza D, Cramer EM. Circulating megakaryocytes: Delivery of large numbers of intact, mature megakaryocytes to the lungs. European Journal of Haematology. 1993;51(4):233–46.

156. Aschoff L. Ueber capilläre Embolie von riesenkernhaltigen Zellen. Archiv f pathol Anat. 1893 Oct 1;134(1):11–25.

157. Weyrich AS, Zimmerman GA. Platelets in lung biology. Annu Rev Physiol. 2013;75:569–91.

158. Lefrançais E, Ortiz-Muñoz G, Caudrillier A, Mallavia B, Liu F, Sayah DM, et al. The lung is a site of platelet biogenesis and a reservoir for haematopoietic progenitors. Nature. 2017 Apr 6;544(7648):105–9.

159. Pariser DN, Hilt ZT, Ture SK, Blick-Nitko SK, Looney MR, Cleary SJ, et al. Lung megakaryocytes are immune modulatory cells. J Clin Invest. 2021;131(1):e137377.

160. Cenariu D, Iluta S, Zimta A-A, Petrushev B, Qian L, Dirzu N, et al. Extramedullary Hematopoiesis of the Liver and Spleen. J Clin Med. 2021 Dec 13;10(24):5831.

161. Francisco JS, Terra MABL, Klein GCT, Dias de Oliveira BCEP, Pelajo-Machado M. The hepatic extramedullary hematopoiesis during experimental murine Schistosomiasis mansoni. Front Immunol. 2022 Aug 25;13:955034.

162. Glatman Zaretsky A, Silver JS, Siwicki M, Durham A, Ware CF, Hunter CA. Infection with Toxoplasma gondii Alters Lymphotoxin Expression Associated with Changes in Splenic Architecture. Infection and Immunity. 2012 Oct;80(10):3602–10.

163. Rossi MID, Dutra HS, El-Cheikh MC, Bonomo A, Borojevic R. Extramedullar B lymphopoiesis in liver schistosomal granulomas: presence of the early stages and inhibition of the full B cell differentiation. International Immunology. 1999 Apr 1;11(4):509–18.

164. Valet C, Magnen M, Qiu L, Cleary SJ, Wang KM, Ranucci S, et al. Sepsis promotes splenic production of a protective platelet pool with high CD40 ligand expression. J Clin Invest [Internet]. 2022 Apr 1 [cited 2023 Apr 12];132(7). Available from: https://www.jci.org/articles/view/153920

165. Davenport P, Liu Z-J, Sola-Visner M. Fetal vs adult megakaryopoiesis. Blood. 2022 Jun 2;139(22):3233–44.

166. Ghoshal K, Bhattacharyya M. Overview of Platelet Physiology: Its Hemostatic and Nonhemostatic Role in Disease Pathogenesis. ScientificWorldJournal [Internet]. 2014 Mar 3 [cited 2020 Apr 22];2014. Available from: https://www.ncbi.nlm.nih.gov/pmc/articles/PMC3960550/

167. Gale AJ. Current Understanding of Hemostasis. Toxicol Pathol. 2011;39(1):273–80.

168. Grover Steven P., Mackman Nigel. Intrinsic Pathway of Coagulation and Thrombosis. Arteriosclerosis, Thrombosis, and Vascular Biology. 2019 Mar 1;39(3):331–8.

169. Wheeler AP, Gailani D. The Intrinsic Pathway of Coagulation as a Target for Antithrombotic Therapy. Hematol Oncol Clin North Am. 2016 Oct;30(5):1099–114.

170. Mackman Nigel, Tilley Rachel E., Key Nigel S. Role of the Extrinsic Pathway of Blood Coagulation in Hemostasis and Thrombosis. Arteriosclerosis, Thrombosis, and Vascular Biology. 2007 Aug 1;27(8):1687–93.

171. Sangkuhl K, Shuldiner AR, Klein TE, Altman RB. Platelet aggregation pathway. Pharmacogenet Genomics. 2011 Aug;21(8):516–21.

172. Semple JW, Italiano JE, Freedman J. Platelets and the immune continuum. Nature Reviews Immunology. 2011 Apr;11(4):264–74.

173. Jackson SP. The growing complexity of platelet aggregation. Blood. 2007 Jun 15;109(12):5087–95.

174. Coughlin SR. Thrombin signalling and protease-activated receptors. Nature. 2000 Sep;407(6801):258–64.

175. Cines DB, Bussel JB, Liebman HA, Luning Prak ET. The ITP syndrome: pathogenic and clinical diversity. Blood. 2009 Jun 25;113(26):6511–21.

176. Neunert CE, Buchanan GR, Blanchette V, Barnard D, Young NL, Curtis C, et al. Relationships among bleeding severity, health-related quality of life, and platelet count in children with immune thrombocytopenic purpura. Pediatr Blood Cancer. 2009 Oct;53(4):652–4.

177. Harrington WJ, Minnich V, Hollingsworth JW, Moore CV. Demonstration of a thrombocytopenic factor in the blood of patients with thrombocytopenic purpura. J Lab Clin Med. 1951 Jul;38(1):1–10.

178. Nishioka T, Yamane T, Takubo T, Ohta K, Park K, Hino M. Detection of various platelet-associated immunoglobulins by flow cytometry in idiopathic thrombocytopenic purpura. Cytometry Part B: Clinical Cytometry. 2005;68B(1):37–42.

179. Cines DB, Wilson SB, Tomaski A, Schreiber AD. Platelet antibodies of the IgM class in immune thrombocytopenic purpura. J Clin Invest. 1985 Apr 1;75(4):1183–90.

180. Provan D, Semple JW. Recent advances in the mechanisms and treatment of immune thrombocytopenia. eBioMedicine. 2022 Feb 1;76:103820.

181. Swinkels M, Rijkers M, Voorberg J, Vidarsson G, Leebeek FWG, Jansen AJG. Emerging Concepts in Immune Thrombocytopenia. Frontiers in Immunology [Internet]. 2018 [cited 2023 Jan 16];9. Available from: https://www.frontiersin.org/articles/10.3389/fimmu.2018.00880

182. Al-Samkari H, Rosovsky RP, Karp Leaf RS, Smith DB, Goodarzi K, Fogerty AE, et al. A modern reassessment of glycoprotein-specific direct platelet autoantibody testing in immune thrombocytopenia. Blood Advances. 2019 Dec 31;4(1):9–18.

183. McMillan R. The Pathogenesis of Chronic Immune Thrombocytopenic Purpura. Seminars in Hematology. 2007 Oct 1;44:S3–11.

184. Psaila B, Bussel JB. Fc receptors in immune thrombocytopenias: a target for immunomodulation? J Clin Invest. 2008 Aug 1;118(8):2677–81.

185. Norris PAA, Segel GB, Sachs UJ, Bayat B, Vidarsson G, Kapur R, et al. Fcγ Receptors I and III on Splenic Macrophages Mediate GPIIb/IIIa Autoantibody-Dependent Phagocytosis of Platelets in Human Immune Thrombocytopenia. Blood. 2018 Nov 29;132(Supplement 1):129.

186. McMillan R, Wang L, Tomer A, Nichol J, Pistillo J. Suppression of in vitro megakaryocyte production by antiplatelet autoantibodies from adult patients with chronic ITP. Blood. 2004 Feb 15;103(4):1364–9.

187. Cooper N, Ghanima W. Immune Thrombocytopenia. N Engl J Med. 2019 Sep 5;381(10):945–55.

188. Witkowski M, Witkowska M, Robak T. Autoimmune thrombocytopenia: Current treatment options in adults with a focus on novel drugs. Eur J Haematol. 2019 Dec;103(6):531–41.

189. Cao Y, Cai J, Zhang S, Yuan N, Li X, Fang Y, et al. Loss of autophagy leads to failure in megakaryopoiesis, megakaryocyte differentiation, and thrombopoiesis in mice. Experimental Hematology. 2015 Jun 1;43(6):488–94.

190. Li S, Wang L, Zhao C, Li L, Peng J, Hou M. CD8+ T cells suppress autologous megakaryocyte apoptosis in idiopathic thrombocytopenic purpura. British Journal of Haematology. 2007;139(4):605–11.

191. Zhang F, Chu X, Wang L, Zhu Y, Li L, Ma D, et al. Cell-mediated lysis of autologous platelets in chronic idiopathic thrombocytopenic purpura. European Journal of Haematology. 2006;76(5):427–31.

192. Qiu J, Liu X, Li X, Zhang X, Han P, Zhou H, et al. CD8+ T cells induce platelet clearance in the liver via platelet desialylation in immune thrombocytopenia. Sci Rep. 2016 Jun 20;6(1):27445.

193. Qamar AA, Grace ND, Groszmann RJ, Garcia–Tsao G, Bosch J, Burroughs AK, et al. Incidence, Prevalence, and Clinical Significance of Abnormal Hematologic Indices in Compensated Cirrhosis. Clinical Gastroenterology and Hepatology. 2009 Jun 1;7(6):689–95.

194. Mitchell O, Feldman DM, Diakow M, Sigal SH. The pathophysiology of thrombocytopenia in chronic liver disease. Hepat Med. 2016 Apr 15;8:39–50.

195. Aster RH. Pooling of platelets in the spleen: role in the pathogenesis of 'hypersplenic' thrombocytopenia. J Clin Invest. 1966 May;45(5):645–57.

196. Tsai H-M. Shear stress and von Willebrand factor in health and disease. Semin Thromb Hemost. 2003 Oct;29(5):479–88.

197. Pereira J, Accatino L, Alfaro J, Brahm J, Hidalgo P, Mezzano D. Platelet autoantibodies in patients with chronic liver disease. American Journal of Hematology. 1995;50(3):173–8.

198. Flores B, Trivedi HD, Robson SC, Bonder A. Hemostasis, bleeding and thrombosis in liver disease. J Transl Sci. 2017 May;3(3):10.15761/JTS.1000182.

199. Battina HL, Alentado VJ, Srour EF, Moliterno AR, Kacena MA. Interaction of the inflammatory response and megakaryocytes in COVID-19 infection. Exp Hematol. 2021 Dec;104:32–9.

200. Dib PRB, Quirino-Teixeira AC, Merij LB, Pinheiro MBM, Rozini SV, Andrade FB, et al. Innate immune receptors in platelets and platelet-leukocyte interactions. Journal of Leukocyte Biology. 2020;108(4):1157–82.

201. Fukui H. Gut-liver axis in liver cirrhosis: How to manage leaky gut and endotoxemia. World J Hepatol. 2015 Mar 27;7(3):425–42.

202. Kalambokis G, Tsianos EV. Endotoxaemia in the pathogenesis of cytopenias in liver cirrhosis. Could oral antibiotics raise blood counts? Medical Hypotheses. 2011 Jan 1;76(1):105–9.

203. von Hundelshausen P, Weber C. Platelets as immune cells: bridging inflammation and cardiovascular disease. Circ Res. 2007 Jan 5;100(1):27–40.

204. Morrell CN, Aggrey AA, Chapman LM, Modjeski KL. Emerging roles for platelets as immune and inflammatory cells. Blood. 2014 May 1;123(18):2759–67.

205. Eriksson O, Mohlin C, Nilsson B, Ekdahl KN. The Human Platelet as an Innate Immune Cell: Interactions Between Activated Platelets and the Complement System. Front Immunol. 2019 Jul 10;10:1590.

206. Shah SA, Page CP, Pitchford SC. Platelet–Eosinophil Interactions As a Potential Therapeutic Target in Allergic Inflammation and Asthma. Front Med [Internet]. 2017 [cited 2020 Apr 8];4. Available from: https://www.frontiersin.org/articles/10.3389/fmed.2017.00129/full

207. Page MJ, Pretorius E. A Champion of Host Defense: A Generic Large-Scale Cause for Platelet Dysfunction and Depletion in Infection. Semin Thromb Hemost. 2020 Apr;46(3):302–19.

208. Stoiber D, Assinger A. Platelet-Leukocyte Interplay in Cancer Development and Progression. Cells. 2020 Apr 1;9(4):855.

209. Strasenburg W, Jóźwicki J, Durślewicz J, Kuffel B, Kulczyk MP, Kowalewski A, et al. Tumor Cell-Induced Platelet Aggregation as an Emerging Therapeutic Target for Cancer Therapy. Frontiers in Oncology [Internet]. 2022 [cited 2022 Sep 19];12. Available from: https://www.frontiersin.org/articles/10.3389/fonc.2022.909767

210. Palacios-Acedo AL, Mège D, Crescence L, Dignat-George F, Dubois C, Panicot-Dubois L. Platelets, Thrombo-Inflammation, and Cancer: Collaborating With the Enemy. Front Immunol. 2019 Jul 31;10:1805.

211. Zhang X, Wang J, Chen Z, Hu Q, Wang C, Yan J, et al. Engineering PD-1-Presenting Platelets for Cancer Immunotherapy. Nano Lett. 2018 Sep 12;18(9):5716–25.

212. Alique M, Luna C, Carracedo J, Ramírez R. LDL biochemical modifications: a link between atherosclerosis and aging. Food Nutr Res. 2015 Dec 3;59:10.3402/fnr.v59.29240.

213. Badimon L, Padró T, Vilahur G. Atherosclerosis, platelets and thrombosis in acute ischaemic heart disease. Eur Heart J Acute Cardiovasc Care. 2012 Apr;1(1):60–74.

214. Dann R, Hadi T, Montenont E, Boytard L, Alebrahim D, Feinstein J, et al. Platelet-Derived MRP-14 Induces Monocyte Activation in Patients With Symptomatic Peripheral Artery Disease. Journal of the American College of Cardiology. 2018 Jan 2;71(1):53–65.

215. Schrottmaier WC, Schmuckenschlager A, Pirabe A, Assinger A. Platelets in Viral Infections – Brave Soldiers or Trojan Horses. Front Immunol. 2022 Mar 28;13:856713.

216. Barrett TJ, Bilaloglu S, Cornwell M, Burgess HM, Virginio VW, Drenkova K, et al. Platelets contribute to disease severity in COVID-19. J Thromb Haemost. 2021 Dec;19(12):3139–53.

217. Barrett TJ, Schlegel M, Zhou F, Gorenchtein M, Bolstorff J, Moore KJ, et al. Platelet regulation of myeloid suppressor of cytokine signaling 3 accelerates atherosclerosis. Science Translational Medicine [Internet]. 2019 Nov 6 [cited 2020 Apr 8];11(517). Available from: https://stm.sciencemag.org/content/11/517/eaax0481

218. Gomez-Casado C, Villaseñor A, Rodriguez-Nogales A, Bueno JL, Barber D, Escribese MM. Understanding Platelets in Infectious and Allergic Lung Diseases. Int J Mol Sci [Internet]. 2019 Apr 8 [cited 2020 May 4];20(7). Available from: https://www.ncbi.nlm.nih.gov/pmc/articles/PMC6480134/

219. Page C, Pitchford S. Platelets and allergic inflammation. Clinical & Experimental Allergy. 2014;44(7):901–13.

220. Yue M, Hu M, Fu F, Ruan H, Wu C. Emerging Roles of Platelets in Allergic Asthma. Front Immunol. 2022 Apr 1;13:846055.

221. Benton AS, Kumar N, Lerner J, Wiles A, Foerster M, Teach SJ, et al. Airway Platelet Activation is Associated with Airway Eosinophilic Inflammation in Asthma. J Investig Med. 2010 Dec;58(8):987–90.

222. Pitchford SC, Yano H, Lever R, Riffo-Vasquez Y, Ciferri S, Rose MJ, et al. Platelets are essential for leukocyte recruitment in allergic inflammation. Journal of Allergy and Clinical Immunology. 2003 Jul 1;112(1):109–18.

223. Amison RT, Momi S, Morris A, Manni G, Keir S, Gresele P, et al. RhoA signaling through platelet $P2Y_1$ receptor controls leukocyte recruitment in allergic mice. J Allergy Clin Immunol. 2015 Feb;135(2):528–38.

224. Hamzeh-Cognasse H, Damien P, Chabert A, Pozzetto B, Cognasse F, Garraud O. Platelets and Infections – Complex Interactions with Bacteria. Front Immunol. 2015 Feb 26;6:82.

225. Kerrigan SW, Cox D. Platelet–bacterial interactions. Cell Mol Life Sci. 2010 Feb 1;67(4):513–23.

226. Rossaint J, Thomas K, Mersmann S, Skupski J, Margraf A, Tekath T, et al. Platelets orchestrate the resolution of pulmonary inflammation in mice by T reg cell repositioning and macrophage education. J Exp Med. 2021 Jul 5;218(7).

227. Carestia A, Mena HA, Olexen CM, Ortiz Wilczyñski JM, Negrotto S, Errasti AE, et al. Platelets Promote Macrophage Polarization toward Pro-inflammatory Phenotype and Increase Survival of Septic Mice. Cell Reports. 2019 Jul 23;28(4):896-908.e5.

228. Ruf W, Riewald M. Regulation of Tissue Factor Expression [Internet]. Madame Curie Bioscience Database [Internet]. Landes Bioscience; 2013 [cited 2023 Jan 20]. Available from: https://www.ncbi.nlm.nih.gov/books/NBK6620/

229. Shannon O. The role of platelets in sepsis. Research and Practice in Thrombosis and Haemostasis. 2021;5(1):27–37.

230. Antoniak S, Mackman N. Platelets and viruses. Platelets. 2021 Apr 3;32(3):325–30.

231. Simon AY, Sutherland MR, Pryzdial ELG. Dengue virus binding and replication by platelets. Blood. 2015 Jul 16;126(3):378–85.

232. Chaipan C, Soilleux EJ, Simpson P, Hofmann H, Gramberg T, Marzi A, et al. DC-SIGN and CLEC-2 mediate human immunodeficiency virus type 1 capture by platelets. J Virol. 2006 Sep;80(18):8951–60.

233. Ghasemzadeh M, Ahmadi J, Hosseini E. Platelet-leukocyte crosstalk in COVID-19: How might the reciprocal links between thrombotic events and inflammatory state affect treatment strategies and disease prognosis? Thromb Res. 2022 May;213:179–94.

234. Jevtic SD, Nazy I. The COVID Complex: A Review of Platelet Activation and Immune Complexes in COVID-19. Frontiers in Immunology [Internet]. 2022 [cited 2022 Sep 19];13. Available from: https://www.frontiersin.org/articles/10.3389/fimmu.2022.807934

235. McMorran BJ. Immune role of platelets in malaria. ISBT Science Series. 2019;14(1):67–76.

236. O'Sullivan JM, O'Donnell JS. Platelets in malaria pathogenesis. Blood. 2018 Sep 20;132(12):1222–4.

237. Kreil A, Wenisch C, Brittenham G, Looareesuwan S, Peck-Radosavljevic M. Thrombopoietin in Plasmodium falciparum malaria. British Journal of Haematology. 2000;109(3):534–6.

238. Rani GF, Preham O, Ashwin H, Brown N, Hitchcock IS, Kaye PM. Dissecting pathways to thrombocytopenia in a mouse model of visceral leishmaniasis. Blood Advances. 2021 Mar 12;5(6):1627–37.

239. Gramaglia I, Velez J, Combes V, Grau GER, Wree M, van der Heyde HC. Platelets activate a pathogenic response to blood-stage Plasmodium infection but not a protective immune response. Blood. 2017 Mar 23;129(12):1669–79.

240. Eyayu T, Zeleke AJ, Seyoum M, Worku L. Basic Coagulation Profiles and Platelet Count Among Schistosoma mansoni-Infected Adults Attending Sanja Primary Hospital, Northwest Ethiopia. Res Rep Trop Med. 2020;11:27–36.

241. Vasconcellos L de S, Petroianu A, Romeiro JR, Tavares Junior WC, Resende V, Vasconcellos L de S, et al. Correlation between the values of circulating blood elements with the size of spleen in the presence of schistosomal splenomegaly. Acta Cirurgica Brasileira. 2018 Dec;33(12):1103–9.

242. Leite LAC, Filho AAP, Fonseca CSM da, Santos BS dos, Ferreira R de C dos S, Montenegro SML, et al. Hemostatic Dysfunction Is Increased in Patients with Hepatosplenic Schistosomiasis Mansoni and Advanced Periportal Fibrosis. PLOS Neglected Tropical Diseases. 2013 Jul 18;7(7):e2314.

243. Correia MCB, Domingues ALC, Lacerda HR, Santos EM, Machado CGF, Hora V, et al. Platelet function and the von Willebrand factor antigen in the hepatosplenic form of schistosomiasis mansoni. Trans R Soc Trop Med Hyg. 2009 Oct;103(10):1053–8.

244. Köpke-Aguiar LA, de Leon CP, Shigueoka DC, Lourenço DM, Kouyomdjian M, Borges DR. Reticulated platelets and thrombopoietin in schistosomiasis patients. Int J Lab Hematol. 2009 Feb;31(1):69–73.

245. Souza MRA, Aguiar LAK, Goto JM, Carvente CT, Toledo CF, Borges DR. Thrombopoietin serum levels do not correlate with thrombocytopenia in hepatic schistosomiasis. Liver. 2002 Apr;22(2):127–9.

246. Omran SA, El-Bassiouni NE, Hussein NA, Akl MM, Hussein AT, Mohamed AA. Disseminated Intravascular Coagulation in Endemic Hepatosplenic Schistosomiasis. PHT. 1995;25(5):218–28.

247. Omran SA, Elashmawi S, Hassanein AA, Elroby A. Effect of schistosomal infection on some functional activities of blood platelets. Egypt J Bilharz. 1978;5(1–2):41–8.

248. Bisetegn H, Feleke DG, Ebrahim H, Tesfaye M, Gedefie A, Erkihun Y. A Comparative Cross-Sectional Study of Coagulation Profiles and Platelet Parameters of *Schistosoma mansoni*-Infected Adults at Haik Primary Hospital, Northeast Ethiopia. Interdisciplinary Perspectives on Infectious Diseases. 2022 Jun 27;2022:e5954536.

249. Drummond SC, Pereira PN, Otoni A, Chaves BA, Antunes CM, Lambertucci JR. Thrombocytopenia as a surrogate marker of hepatosplenic schistosomiasis in endemic areas for Schistosomiasis mansoni. Rev Soc Bras Med Trop. 2014 Apr;47(2):218–22.

250. Sorgho H, Da O, Rouamba T, Savadogo B, Tinto H, Ouedraogo J-B. Schistosoma mansoni infection and hematological profile in an endemic foci in Western Burkina Faso. Afr J Parasitol Res. 2017 Dec;

251. Noha MA, Enas AE, Aly E, Mohamed AE. Multidisciplinary biomarkers aggrieve morbidity in schistosomiasis. Trop Biomed. 2019 Dec 1;36(4):833–44.

252. Eissa LA, Gad LS, Rabie AM, El-Gayar AM. Thrombopoietin level in patients with chronic liver diseases. Ann Hepatol. 2008 Jul 1;7(3):235–44.

253. Aref S, Mabed M, Selim T, Goda T, Khafagy N. Thrombopoietin (TPO) Levels in Hepatic Patients with Thrombocytopenia. Hematology. 2004 Oct 1;9(5–6):351–6.

254. Medeiros TB, Domingues ALC, Luna CF, Lopes EP. Correlation between platelet count and both liver fibrosis and spleen diameter in patients with schistosomiasis mansoni. Arq Gastroenterol. 2014;51(1):34–8.

255. Agha A, Abdulhadi MM, Marenco S, Bella A, AlSaudi D, El-Haddad A, et al. Use of the Platelet Count/Spleen Diameter Ratio for the Noninvasive Diagnosis of Esophageal Varices in Patients with Schistosomiasis. Saudi J Gastroenterol. 2011;17(5):307–11.

256. Stanley RG, Ngaiza JR, Atieno E, Jell G, Francklow K, Jackson CL, et al. Immune-dependent thrombocytopaenia in mice infected with Schistosoma mansoni. Parasitology. 2003 Mar;126(Pt 3):225–9.

257. Kamel MM, Romeyia SA, Ali MM, Aziz HA, Abdel-Moneim AS. P selectin and T cell profiles provide verification to understand the pathogenesis of liver cirrhosis in HCV and Schistosoma mansoni infections. Microbial Pathogenesis. 2014 Aug 1;73:19–24.

258. Maugeri N, Malato S, Femia EA, Pugliano M, Campana L, Lunghi F, et al. Clearance of circulating activated platelets in polycythemia vera and essential thrombocythemia. Blood. 2011 Sep 22;118(12):3359–66.

259. Mebius MM, Genderen PJJ van, Urbanus RT, Tielens AGM, Groot PG de, Hellemond JJ van. Interference with the Host Haemostatic System by Schistosomes. PLOS Pathogens. 2013 Dec 26;9(12):e1003781.

260. Bhardwaj R, Krautz-Peterson G, Da'dara A, Tzipori S, Skelly PJ. Tegumental Phosphodiesterase SmNPP-5 Is a Virulence Factor for Schistosomes ▿. Infect Immun. 2011 Oct;79(10):4276–84.

261. Elzoheiry M, Da'dara AA, deLaforcade AM, El-Beshbishi SN, Skelly PJ. The Essential Ectoenzyme SmNPP5 from the Human Intravascular Parasite Schistosoma mansoni is an ADPase and a Potent Inhibitor of Platelet Aggregation. Thromb Haemost. 2018;118(6):979–89.

262. Elzoheiry M, Da'dara AA, Nation CS, El-Beshbishi SN, Skelly PJ. Schistosomes can hydrolyze proinflammatory and prothrombotic

polyphosphate (polyP) via tegumental alkaline phosphatase, SmAP. Mol Biochem Parasitol. 2019;232:111190.

263. Bhardwaj R, Skelly PJ. Characterization of Schistosome Tegumental Alkaline Phosphatase (SmAP). PLoS Negl Trop Dis [Internet]. 2011 Apr 5 [cited 2020 Jun 16];5(4). Available from: https://www.ncbi.nlm.nih.gov/pmc/articles/PMC3071363/

264. Travers RJ, Smith SA, Morrissey JH. Polyphosphate, Platelets, and Coagulation. Int J Lab Hematol. 2015 May;37(0 1):31–5.

265. Da'dara AA, Skelly PJ. Schistosomes versus platelets. Thrombosis Research. 2014 Dec 1;134(6):1176–81.

266. DeMarco R, Kowaltowski AT, Mortara RA, Verjovski-Almeida S. Molecular characterization and immunolocalization of Schistosoma mansoni ATP-diphosphohydrolase. Biochemical and Biophysical Research Communications. 2003 Aug 8;307(4):831–8.

267. deWalick S, Hensbergen PJ, Bexkens ML, Grosserichter-Wagener C, Hokke CH, Deelder AM, et al. Binding of von Willebrand factor and plasma proteins to the eggshell of Schistosoma mansoni. International Journal for Parasitology. 2014 Apr 1;44(5):263–8.

268. Wu YP, Lenting PJ, Tielens AGM, Groot PGD, Hellemond JJV. Differential platelet adhesion to distinct life-cycle stages of the parasitic helminth Schistosoma mansoni. Journal of Thrombosis and Haemostasis. 2007;5(10):2146–8.

269. Ngaiza JR, Doenhoff MJ. Blood platelets and schistosome egg excretion. Proc Soc Exp Biol Med. 1990 Jan;193(1):73–9.

270. Ngaiza JR, Doenhoff MJ, Jaffe EA. Schistosoma mansoni egg attachment to cultured human umbilical vein endothelial cells: an in vitro model of an early step of parasite egg excretion. J Infect Dis. 1993 Dec;168(6):1576–80.

271. Doenhoff MJ, Stanley RG, Pryce D, Curtis RCH, Parry H, Griffiths K, et al. Identification of a fibrinolytic enzyme in Schistosoma mansoni eggs and modulated blood fibrinogen metabolism in S. mansoni-infected mice. Parasitology. 2003 Mar;126(Pt 3):231–4.

272. Stanley RG, Ngaiza JR, Wambayi E, Lewis J, Doenhoff MJ. Platelets as an innate defence mechanism against Schistosoma mansoni infections in mice. Parasite Immunology. 2003;25(10):467–73.

273. Damonneville M, Pancré V, Capron A, Auriault C. Protection of rats against Schistosoma mansoni infection induced by platelets stimulated with the murine recombinant tumor necrosis factor alpha. Int Arch Allergy Appl Immunol. 1990;92(4):361–3.

274. Bout D, Joseph M, Pontet M, Vorng H, Deslee D, Capron A. Rat resistance to schistosomiasis: platelet-mediated cytotoxicity induced by C-reactive protein. Science. 1986 Jan 10;231(4734):153–6.

275. Joseph M, Auriault C, Capron A, Vorng H, Viens P. A new function for platelets: IgE-dependent killing of schistosomes. Nature. 1983 Jun;303(5920):810–2.

276. Schmittgen TD, Livak KJ. Analyzing real-time PCR data by the comparative C T method. Nature Protocols. 2008 Jun;3(6):1101–8.

277. Costain AH, Phythian-Adams AT, Colombo SAP, Marley AK, Owusu C, Cook PC, et al. Dynamics of Host Immune Response Development During Schistosoma mansoni Infection. Frontiers in Immunology [Internet]. 2022 [cited 2023 May 15];13. Available from: https://www.frontiersin.org/articles/10.3389/fimmu.2022.906338

278. Stanley RG, Ngaiza JR, Atieno E, Jell G, Francklow K, Jackson CL, et al. Immune-dependent thrombocytopaenia in mice infected with Schistosoma mansoni. Parasitology. 2003 Mar;126(Pt 3):225–9.

279. Grodzielski M, Goette NP, Glembotsky AC, Constanza Baroni Pietto M, Méndez-Huergo SP, Pierdominici MS, et al. Multiple concomitant mechanisms contribute to low platelet count in patients with immune thrombocytopenia. Scientific Reports. 2019 Feb 18;9(1):1–10.

280. Morrell CN. Platelets: killers of parasites or patients? Blood. 2017 Mar 23;129(12):1571–2.

281. Golebiewska EM, Poole AW. Platelet secretion: From haemostasis to wound healing and beyond. Blood Rev. 2015 May;29(3):153–62.

282. Duerschmied D, Suidan GL, Demers M, Herr N, Carbo C, Brill A, et al. Platelet serotonin promotes the recruitment of neutrophils to sites of acute inflammation in mice. Blood. 2013 Feb 7;121(6):1008–15.

283. Xiang B, Zhang G, Guo L, Li X-A, Morris AJ, Daugherty A, et al. Platelets protect from septic shock by inhibiting macrophage-dependent inflammation via the cyclooxygenase 1 signalling pathway. Nat Commun. 2013;4:2657.

284. Wijshake T, Wang J, Rose J, Marlar-Pavey M, Collins JJ, Agathocleous M. Helminth infection impacts hematopoiesis. bioRxiv. 2023 Feb 10;2023.02.10.528073.

285. Ngaiza JR, Doenhoff MJ. Schistosoma mansoni-induced thrombocytopenia in mice. Transactions of The Royal Society of Tropical Medicine and Hygiene. 1987 Jul 1;81(4):655–6.

286. Amison RT, Cleary SJ, Riffo-Vasquez Y, Bajwa M, Page CP, Pitchford SC. Platelets Play a Central Role in Sensitization to Allergen. Am J Respir Cell Mol Biol. 2018 Jan 24;59(1):96–103.

287. Bhattacharjee S, Banerjee M. Immune Thrombocytopenia Secondary to COVID-19: a Systematic Review. SN Compr Clin Med. 2020;2(11):2048–58.

288. Costain AH, MacDonald AS, Smits HH. Schistosome Egg Migration: Mechanisms, Pathogenesis and Host Immune Responses. Front Immunol. 2018;9:3042.

289. El-Faham MH, Eissa MM, Igetei JE, Amer EI, Liddell S, El-Azzouni MZ, et al. Treatment of Schistosoma mansoni with miltefosine in vitro enhances serological recognition of defined worm surface antigens. PLOS Neglected Tropical Diseases. 2017 Aug 25;11(8):e0005853.

290. Pinto-Almeida A, Mendes T, de Oliveira RN, Corrêa S de AP, Allegretti SM, Belo S, et al. Morphological Characteristics of Schistosoma mansoni PZQ-Resistant and -Susceptible Strains Are Different in Presence of Praziquantel. Front Microbiol [Internet]. 2016 [cited 2020 Apr 9];7. Available from: https://www.frontiersin.org/articles/10.3389/fmicb.2016.00594/full

291. Jatsa H, Sock EN, Tchuente LT, Kamtchouing P. Evaluation of the In Vivo Activity of Different Concentrations of Clerodendrum Umbellatum Poir Against Schistosoma Mansoni Infection in Mice. Afr J Tradit Complement Altern Med. 2009 May 7;6(3):216–21.

292. Park MK, Hoffmann KF, Cheever AW, Amichay D, Wynn TA, Farber JM. Patterns of Chemokine Expression in Models of Schistosoma mansoni Inflammation and Infection Reveal Relationships between Type 1 and Type 2 Responses and Chemokines In Vivo. Infection and Immunity. 2001 Nov 1;69(11):6755–68.

293. Bagamery K, Kvell K, Landau R, Graham J. Flow cytometric analysis of CD41-labeled platelets isolated by the rapid, one-step OptiPrep method from human blood. Cytometry Part A. 2005;65A(1):84–7.

294. Butterworth A, Vadas M, Wassom D, Dessein A, Hogan M, Sherry B, et al. Interactions between human eosinophils and schistosomula of schistosoma mansoni. II. The mechanism of irreversible eosinophil adherence. J Exp Med. 1979 Dec 1;150(6):1456–71.

295. Cooper PJ, Awadzi K, Ottesen EA, Remick D, Nutman TB. Eosinophil Sequestration and Activation Are Associated with the Onset and Severity of Systemic Adverse Reactions following the Treatment of Onchocerciasis with Ivermectin. J Infect Dis. 1999 Mar 1;179(3):738–42.

296. Sun S, Jin C, Si J, Lei Y, Chen K, Cui Y, et al. Single-cell analysis of ploidy and the transcriptome reveals functional and spatial divergency in murine megakaryopoiesis. Blood. 2021 Oct 7;138(14):1211–24.

297. Gao A, Gong Y, Zhu C, Yang W, Li Q, Zhao M, et al. Bone marrow endothelial cell-derived interleukin-4 contributes to thrombocytopenia in acute myeloid leukemia. Haematologica. 2019 Oct 1;104(10):1950–61.

298. Sonoda Y, Kuzuyama Y, Tanaka S, Yokota S, Maekawa T, Clark SC, et al. Human interleukin-4 inhibits proliferation of megakaryocyte progenitor cells in culture. Blood. 1993 Feb 1;81(3):624–30.

299. Grosse J, Braun A, Varga-Szabo D, Beyersdorf N, Schneider B, Zeitlmann L, et al. An EF hand mutation in Stim1 causes premature platelet activation and bleeding in mice. J Clin Invest. 2007 Nov 1;117(11):3540–50.

300. Sun S, Urbanus RT, Ten Cate H, de Groot PG, de Laat B, Heemskerk JWM, et al. Platelet Activation Mechanisms and Consequences of Immune Thrombocytopenia. Cells. 2021 Dec 1;10(12):3386.

301. Ali RA, Wuescher LM, Worth RG. Platelets: essential components of the immune system. Curr Trends Immunol. 2015;16:65–78.

302. Chaturvedi S, Arnold DM, McCrae KR. Splenectomy for immune thrombocytopenia: down but not out. Blood. 2018 Mar 15;131(11):1172–82.

303. Sánchez-Martín L, Estecha A, Samaniego R, Sánchez-Ramón S, Vega MÁ, Sánchez-Mateos P. The chemokine CXCL12 regulates monocyte-macrophage differentiation and RUNX3 expression. Blood. 2011 Jan 6;117(1):88–97.

304. Sanin DE, Ge Y, Marinkovic E, Kabat AM, Castoldi A, Caputa G, et al. A common framework of monocyte-derived macrophage activation. Science Immunology. 2022 Apr 15;7(70):eabl7482.

305. Belton M, Brilha S, Manavaki R, Mauri F, Nijran K, Hong YT, et al. Hypoxia and tissue destruction in pulmonary TB. Thorax. 2016 Dec;71(12):1145–53.

306. Via LE, Lin PL, Ray SM, Carrillo J, Allen SS, Eum SY, et al. Tuberculous Granulomas Are Hypoxic in Guinea Pigs, Rabbits, and Nonhuman Primates. Infection and Immunity. 2008 Jun;76(6):2333–40.

307. Anderson KG, Mayer-Barber K, Sung H, Beura L, James BR, Taylor JJ, et al. Intravascular staining for discrimination of vascular and tissue leukocytes. Nat Protoc. 2014 Jan;9(1):209–22.

308. Lloyd CM, Snelgrove RJ. Type 2 immunity: Expanding our view. Sci Immunol. 2018 06;3(25).

309. Pitchford SC, Yano H, Lever R, Riffo-Vasquez Y, Ciferri S, Rose MJ, et al. Platelets are essential for leukocyte recruitment in allergic inflammation. J Allergy Clin Immunol. 2003 Jul;112(1):109–18.

310. Patko Z, Csaszar A, Acsady G, Peter K, Schwarz M. Roles of Mac-1 and glycoprotein IIb/IIIa integrins in leukocyte-platelet aggregate formation: stabilization by Mac-1 and inhibition by GpIIb/IIIa blockers. Platelets. 2012;23(5):368–75.

311. Handtke S, Thiele T. Large and small platelets—(When) do they differ? Journal of Thrombosis and Haemostasis. 2020;18(6):1256–67.

312. Assinger A. Platelets and Infection – An Emerging Role of Platelets in Viral Infection. Front Immunol [Internet]. 2014 Dec 18 [cited 2021 Jun 4];5. Available from: https://www.ncbi.nlm.nih.gov/pmc/articles/PMC4270245/

313. de Bruijne-Admiraal LG, Modderman PW, Von dem Borne AE, Sonnenberg A. P-selectin mediates Ca(2+)-dependent adhesion of activated platelets to many different types of leukocytes: detection by flow cytometry. Blood. 1992 Jul 1;80(1):134–42.

314. Pitchford SC, Momi S, Giannini S, Casali L, Spina D, Page CP, et al. Platelet P-selectin is required for pulmonary eosinophil and lymphocyte recruitment in a murine model of allergic inflammation. Blood. 2005 Mar 1;105(5):2074–81.

315. Gaertner F, Massberg S. Patrolling the vascular borders: platelets in immunity to infection and cancer. Nature Reviews Immunology. 2019 Dec;19(12):747–60.

316. Goncalves R, Zhang X, Cohen H, Debrabant A, Mosser DM. Platelet activation attracts a subpopulation of effector monocytes to sites of Leishmania major infection. J Exp Med. 2011 Jun 6;208(6):1253–65.

317. Membe Femoe U, Boukeng Jatsa H, Greigert V, Brunet J, Cannet C, Kenfack MC, et al. Pathological and immunological evaluation of different regimens of praziquantel treatment in a mouse model of Schistosoma mansoni infection. PLoS Negl Trop Dis. 2022 Apr 21;16(4):e0010382.

318. Nakamura-Ishizu A, Matsumura T, Stumpf PS, Umemoto T, Takizawa H, Takihara Y, et al. Thrombopoietin Metabolically Primes Hematopoietic Stem Cells to Megakaryocyte-Lineage Differentiation. Cell Rep. 2018 Nov 13;25(7):1772-1785.e6.

319. Zheng C, Yang R, Han Z, Zhou B, Liang L, Lu M. TPO-independent megakaryocytopoiesis. Critical Reviews in Oncology/Hematology. 2008 Mar 1;65(3):212–22.

320. Tomer A, Friese P, Conklin R, Bales W, Archer L, Harker LA, et al. Flow cytometric analysis of megakaryocytes from patients with abnormal platelet counts. Blood. 1989 Aug 1;74(2):594–601.

321. Fairfax KC, Amiel E, King IL, Freitas TC, Mohrs M, Pearce EJ. IL-10R Blockade during Chronic Schistosomiasis Mansoni Results in the Loss

of B Cells from the Liver and the Development of Severe Pulmonary Disease. PLOS Pathogens. 2012 Jan 26;8(1):e1002490.

322. Gonzalez MA, Lu DR, Yousefi M, Kroll A, Lo CH, Briseño CG, et al. Phagocytosis increases an oxidative metabolic and immune suppressive signature in tumor macrophages. Journal of Experimental Medicine. 2023 Mar 30;220(6):e20221472.

323. Gordon S. Alternative activation of macrophages. Nat Rev Immunol. 2003 Jan;3(1):23–35.

324. Nascimento M, Huang SC, Smith A, Everts B, Lam W, Bassity E, et al. Ly6Chi Monocyte Recruitment Is Responsible for Th2 Associated Host-Protective Macrophage Accumulation in Liver Inflammation due to Schistosomiasis. PLoS Pathog. 2014 Aug 21;10(8):e1004282.

325. de Souza R da P, Araújo MI, Lopes DM, de Almeida TVVS, Page B, Oliveira RR, et al. Characterization of memory T cells in individuals resistant to Schistosoma mansoni infection. Parasite Immunology. 2019;41(12):e12671.

326. Tan S, Li S, Min Y, Gisterå A, Moruzzi N, Zhang J, et al. Platelet factor 4 enhances CD4+ T effector memory cell responses via Akt-PGC1α-TFAM signaling-mediated mitochondrial biogenesis. J Thromb Haemost. 2020 Oct;18(10):2685–700.

327. Koch CJ. Measurement of absolute oxygen levels in cells and tissues using oxygen sensors and 2-nitroimidazole EF5. Methods Enzymol. 2002;352:3–31.

328. Delaney C, Davizon-Castillo P, Allawzi A, Posey J, Gandjeva A, Neeves K, et al. Platelet activation contributes to hypoxia-induced inflammation. Am J Physiol Lung Cell Mol Physiol. 2021 Mar 1;320(3):L413–21.

329. Li Q-R, Xu H-Z, Xiao R-C, Liu Y, Tang J-M, Li J, et al. Platelets are highly efficient and efficacious carriers for tumor-targeted nano-drug delivery. Drug Deliv. 2022 Dec;29(1):937–49.

330. Ho-Tin-Noé B, Boulaftali Y, Camerer E. Platelets and vascular integrity: how platelets prevent bleeding in inflammation. Blood. 2018 Jan 18;131(3):277–88.

331. Iannacone M, Sitia G, Isogawa M, Whitmire JK, Marchese P, Chisari FV, et al. Platelets prevent IFN-α/β-induced lethal hemorrhage promoting CTL-dependent clearance of lymphocytic choriomeningitis virus. Proceedings of the National Academy of Sciences. 2008 Jan 15;105(2):629–34.

332. Boulaftali Y, Hess PR, Getz TM, Cholka A, Stolla M, Mackman N, et al. Platelet ITAM signaling is critical for vascular integrity in inflammation. J Clin Invest. 2013 Feb 1;123(2):908–16.

333. Stark K, Massberg S. Interplay between inflammation and thrombosis in cardiovascular pathology. Nat Rev Cardiol. 2021 Sep;18(9):666–82.

334. Gaertner F, Ahmad Z, Rosenberger G, Fan S, Nicolai L, Busch B, et al. Migrating Platelets Are Mechano-scavengers that Collect and Bundle Bacteria. Cell. 2017 Nov 30;171(6):1368-1382.e23.

335. Schultz BM, Acevedo OA, Kalergis AM, Bueno SM. Role of Extracellular Trap Release During Bacterial and Viral Infection. Frontiers in Microbiology [Internet]. 2022 [cited 2023 May 5];13. Available from: https://www.frontiersin.org/articles/10.3389/fmicb.2022.798853

336. Jackson SP, Darbousset R, Schoenwaelder SM. Thromboinflammation: challenges of therapeutically targeting coagulation and other host defense mechanisms. Blood. 2019 Feb 28;133(9):906–18.

337. Gaertner F, Massberg S. Blood coagulation in immunothrombosis—At the frontline of intravascular immunity. Seminars in Immunology. 2016 Dec 1;28(6):561–9.

338. Darlington DN, Wu X, Chang KL, Bynum J, Cap AP. Regulation of Platelet Function By Adenosine Receptors. Blood. 2019 Nov 13;134(Supplement_1):2348.

339. Iba T, Levy JH. Inflammation and thrombosis: roles of neutrophils, platelets and endothelial cells and their interactions in thrombus formation during sepsis. J Thromb Haemost. 2018 Feb;16(2):231–41.

340. Burzynski LC, Humphry M, Pyrillou K, Wiggins KA, Chan JNE, Figg N, et al. The Coagulation and Immune Systems Are Directly Linked through the Activation of Interleukin-1α by Thrombin. Immunity. 2019 Apr 16;50(4):1033-1042.e6.

341. Da'dara AA, de Laforcade AM, Skelly PJ. The impact of schistosomes and schistosomiasis on murine blood coagulation and fibrinolysis as determined by thromboelastography (TEG). J Thromb Thrombolysis. 2016 May;41(4):671–7.

342. Maurya P, Ture SK, Li C, Scheible KM, McGrath KE, Palis J, et al. Transfusion of Adult, but Not Neonatal, Platelets Promotes Monocyte Trafficking in Neonatal Mice. Arteriosclerosis, Thrombosis, and Vascular Biology. 2023 Jun;43(6):873–85.

343. Jirouskova M, Shet AS, Johnson GJ. A guide to murine platelet structure, function, assays, and genetic alterations. Journal of Thrombosis and Haemostasis. 2007;5(4):661–9.

344. Michelson AD, Furman MI. Laboratory markers of platelet activation and their clinical significance. Current Opinion in Hematology. 1999 Sep;6(5):342.

345. Bergmeier W, Schulte V, Brockhoff G, Bier U, Zirngibl H, Nieswandt B. Flow cytometric detection of activated mouse integrin αIIbβ3 with a novel monoclonal antibody. Cytometry. 2002;48(2):80–6.

346. van Geffen JP, Brouns SLN, Batista J, McKinney H, Kempster C, Nagy M, et al. High-throughput elucidation of thrombus formation reveals sources of platelet function variability. Haematologica. 2019 Jun;104(6):1256–67.

347. Cognasse F, Duchez AC, Audoux E, Ebermeyer T, Arthaud CA, Prier A, et al. Platelets as Key Factors in Inflammation: Focus on CD40L/CD40. Front Immunol. 2022 Feb 3;13:825892.

348. Kim H, Conway EM. Platelets and Complement Cross-Talk in Early Atherogenesis. Frontiers in Cardiovascular Medicine [Internet]. 2019 [cited 2023 Jul 5];6. Available from: https://www.frontiersin.org/articles/10.3389/fcvm.2019.00131

349. Allan HE, Vadgama A, Armstrong PC, Warner TD. Platelet ageing: A review. Thrombosis Research [Internet]. 2022 Dec 16 [cited 2023 Jul 5]; Available from: https://www.sciencedirect.com/science/article/pii/S0049384822004819

350. Naeini MB, Bianconi V, Pirro M, Sahebkar A. The role of phosphatidylserine recognition receptors in multiple biological functions. Cellular & Molecular Biology Letters. 2020 Mar 26;25(1):23.

351. Lentz BR. Exposure of platelet membrane phosphatidylserine regulates blood coagulation. Progress in Lipid Research. 2003 Sep 1;42(5):423–38.

352. Reddy EC, Rand ML. Procoagulant Phosphatidylserine-Exposing Platelets in vitro and in vivo. Frontiers in Cardiovascular Medicine [Internet]. 2020 [cited 2022 Dec 1];7. Available from: https://www.frontiersin.org/articles/10.3389/fcvm.2020.00015

353. van Gorp ECM, Suharti C, ten Cate H, Dolmans WMV, van der Meer JWM, ten Cate JW, et al. Review: Infectious Diseases and Coagulation Disorders. The Journal of Infectious Diseases. 1999 Jul 1;180(1):176–86.

354. Krause S, May J, Koslowski H, Heptinstall S, Lösche W. Enhanced Spontaneous Platelet Aggregation and red Blood Cell Fragility in Whole Blood Obtained from Patients with Diabetes. Platelets. 1991;2(4):203–6.

355. Duan R, Goldmann L, Li Y, Weber C, Siess W, von Hundelshausen P. Spontaneous Platelet Aggregation in Blood Is Mediated by FcγRIIA Stimulation of Bruton's Tyrosine Kinase. Int J Mol Sci. 2021 Dec 22;23(1):76.

356. Bigalke B, Stellos K, Geisler T, Kremmer E, Seizer P, May AE, et al. Expression of platelet glycoprotein VI is associated with transient ischemic attack and stroke. Eur J Neurol. 2010 Jan;17(1):111–7.

357. Jin J, Quinton TM, Zhang J, Rittenhouse SE, Kunapuli SP. Adenosine diphosphate (ADP)–induced thromboxane A2generation in human platelets requires coordinated signaling through integrin αIIbβ3 and ADP receptors. Blood. 2002 Jan 1;99(1):193–8.

358. Bourne JH, Colicchia M, Di Y, Martin E, Slater A, Roumenina LT, et al. Heme induces human and mouse platelet activation through C-type-lectin-like receptor-2. Haematologica. 2020 Apr 30;106(2):626–9.

359. Truscott M, Evans DA, Gunn M, Hoffmann KF. Schistosoma mansoni Hemozoin Modulates Alternative Activation of Macrophages via Specific Suppression of Retnla Expression and Secretion. Infect Immun. 2013 Jan;81(1):133–42.

360. Jaramillo M, Plante I, Ouellet N, Vandal K, Tessier PA, Olivier M. Hemozoin-Inducible Proinflammatory Events In Vivo: Potential Role in Malaria Infection 1. The Journal of Immunology. 2004 Mar 1;172(5):3101–10.

361. Lautenschlager S de OS, Kim T, Bidóia DL, Nakamura CV, Anders H-J, Steiger S. Plasma Proteins and Platelets Modulate Neutrophil Clearance of Malaria-Related Hemozoin Crystals. Cells. 2019 Dec 30;9(1):93.

362. Kujovich JL. Coagulopathy in liver disease: a balancing act. Hematology. 2015 Dec 5;2015(1):243–9.

363. Peck-Radosavljevic M. Review article: coagulation disorders in chronic liver disease. Alimentary Pharmacology & Therapeutics. 2007;26(s1):21–8.

364. Papageorgiou C, Jourdi G, Adjambri E, Walborn A, Patel P, Fareed J, et al. Disseminated Intravascular Coagulation: An Update on Pathogenesis, Diagnosis, and Therapeutic Strategies. Clin Appl Thromb Hemost. 2018 Dec;24(9 Suppl):8S-28S.

365. Szmitko PE, Wang C-H, Weisel RD, de Almeida JR, Anderson TJ, Verma S. New Markers of Inflammation and Endothelial Cell Activation. Circulation. 2003 Oct 21;108(16):1917–23.

366. Ritter DM, McKerrow JH. Intercellular adhesion molecule 1 is the major adhesion molecule expressed during schistosome granuloma formation. Infect Immun. 1996 Nov;64(11):4706–13.

367. Figliuolo da Paz VR, Figueiredo-Vanzan D, dos Santos Pyrrho A. Interaction and involvement of cellular adhesion molecules in the pathogenesis of Schistosomiasis mansoni. Immunology Letters. 2019 Feb 1;206:11–8.

368. Hassanein H, Hanallah S, El-Ahwany E, Doughty B, El-Ghorab N, Badir B, et al. Immunolocalization of intercellular adhesion molecule-1 and leukocyte functional associated antigen-1 in schistosomal soluble egg antigen-induced granulomatous hyporesponsiveness. APMIS. 2001 May;109(5):376–82.

369. Li J, Tong D, Chen F, Song B, Wang Y, Liu Y, et al. Inflammatory cytokines enhance procoagulant activity of platelets and endothelial cells through phosphatidylserine exposure in patients with essential hypertension. J Thromb Thrombolysis. 2021 May 1;51(4):933–40.

370. Heemskerk JWM, Mattheij NJA, Cosemans JMEM. Platelet-based coagulation: different populations, different functions. Journal of Thrombosis and Haemostasis. 2013 Jan 1;11(1):2–16.

371. Li J, van der Wal DE, Zhu G, Xu M, Yougbare I, Ma L, et al. Desialylation is a mechanism of Fc-independent platelet clearance and a therapeutic target in immune thrombocytopenia. Nat Commun. 2015 Jul 17;6:7737.

372. Morrell CN, Pariser DN, Hilt ZT, Vega Ocasio D. The Platelet Napoleon Complex-Small Cells, but Big Immune Regulatory Functions. Annu Rev Immunol. 2019 Apr 26;37:125–44.

373. Kral JB, Schrottmaier WC, Salzmann M, Assinger A. Platelet Interaction with Innate Immune Cells. Transfus Med Hemother. 2016 Mar;43(2):78–88.

374. Phillips JH, Chang CW, Lanier LL. Platelet-induced expression of Fc gamma RIII (CD16) on human monocytes. Eur J Immunol. 1991 Apr;21(4):895–9.

375. Lee SJ, Yoon BR, Kim HY, Yoo S-J, Kang SW, Lee W-W. Activated Platelets Convert CD14+CD16- Into CD14+CD16+ Monocytes With Enhanced FcγR-Mediated Phagocytosis and Skewed M2 Polarization. Front Immunol [Internet]. 2021 [cited 2021 May 27];11. Available from: https://www.frontiersin.org/articles/10.3389/fimmu.2020.611133/full

376. Zajd CM, Ziemba AM, Miralles GM, Nguyen T, Feustel PJ, Dunn SM, et al. Bone Marrow-Derived and Elicited Peritoneal Macrophages Are Not Created Equal: The Questions Asked Dictate the Cell Type Used. Frontiers in Immunology. 2020;11:269.

377. Uchiyama R, Toyoda E, Maehara M, Wasai S, Omura H, Watanabe M, et al. Effect of Platelet-Rich Plasma on M1/M2 Macrophage Polarization. Int J Mol Sci. 2021 Feb 26;22(5):2336.

378. Zhang X, Goncalves R, Mosser DM. The Isolation and Characterization of Murine Macrophages. Curr Protoc Immunol. 2008 Nov;CHAPTER:Unit-14.1.

379. O'Connell KE, Mikkola AM, Stepanek AM, Vernet A, Hall CD, Sun CC, et al. Practical Murine Hematopathology: A Comparative Review and Implications for Research. Comp Med. 2015 Apr;65(2):96–113.

380. Rigg RA, Healy LD, Chu TT, Ngo ATP, Mitrugno A, Zilberman-Rudenko J, et al. Protease-activated receptor 4 (PAR4) activity promotes platelet granule release and platelet-leukocyte interactions. Platelets. 2019;30(1):126–35.

381. Barra A, Freitas KM, Marconato DG, Faria-Pinto P, Lopes MTP, Klein A. Protease-activated receptor 4 plays a role in lipopolysaccharide-induced inflammatory mechanisms in murine macrophages. Naunyn-Schmiedeberg's Arch Pharmacol. 2021 May 1;394(5):853–62.

382. Asfaha S, Cenac N, Houle S, Altier C, Papez MD, Nguyen C, et al. Protease-activated receptor-4: a novel mechanism of inflammatory pain modulation. Br J Pharmacol. 2007 Jan;150(2):176–85.

383. Kapellos TS, Taylor L, Lee H, Cowley SA, James WS, Iqbal AJ, et al. A novel real time imaging platform to quantify macrophage phagocytosis. Biochem Pharmacol. 2016 Sep 15;116:107–19.

384. Miksa M, Komura H, Wu R, Shah KG, Wang P. A novel method to determine the engulfment of apoptotic cells by macrophages using pHrodo succinimidyl ester. Journal of Immunological Methods. 2009 Mar 15;342(1):71–7.

385. Segawa K, Nagata S. An Apoptotic 'Eat Me' Signal: Phosphatidylserine Exposure. Trends Cell Biol. 2015 Nov;25(11):639–50.

386. Ma R, Xie R, Yu C, Si Y, Wu X, Zhao L, et al. Phosphatidylserine-mediated platelet clearance by endothelium decreases platelet aggregates and procoagulant activity in sepsis. Scientific Reports. 2017 Jul 10;7(1):4978.

387. Guilliams M, Mildner A, Yona S. Developmental and Functional Heterogeneity of Monocytes. Immunity. 2018 16;49(4):595–613.

388. de Sousa JR, Da Costa Vasconcelos PF, Quaresma JAS. Functional aspects, phenotypic heterogeneity, and tissue immune response of macrophages in infectious diseases. Infect Drug Resist. 2019 Aug 22;12:2589–611.

389. Murray PJ. Macrophage Polarization. Annu Rev Physiol. 2017 10;79:541–66.

390. Gleissner CA. Macrophage Phenotype Modulation by CXCL4 in Atherosclerosis. Front Physiol. 2012 Jan 13;3:1.

391. Rückerl D, Cook PC. Macrophages assemble! But do they need IL-4R during schistosomiasis? Eur J Immunol. 2019 Jul;49(7):996–1000.

392. Misharin AV, Saber R, Perlman H. Eosinophil contamination of thioglycollate-elicited peritoneal macrophage cultures skews the functional readouts of in vitro assays. J Leukoc Biol. 2012 Aug;92(2):325–31.

393. Minutti CM, Jackson-Jones LH, García-Fojeda B, Knipper JA, Sutherland TE, Logan N, et al. Local enhancers of Type 2-mediated macrophage activation and proliferation promote tissue repair. Science. 2017 Jun 9;356(6342):1076–80.

394. Rychter JW, Van Nassauw L, Brown JK, Van Marck E, Knight PA, Miller HRP, et al. Impairment of intestinal barrier and secretory function as well as egg excretion during intestinal schistosomiasis occur independently of mouse mast cell protease-1. Parasite Immunol. 2010 Apr;32(4):221–31.

395. Muniz-Junqueira MI, Prata A, Tosta CE. Phagocytic and Bactericidal Function of Mouse Macrophages to Salmonella Typhimurium in Schistosomiasis Mansoni. The American Journal of Tropical Medicine and Hygiene. 1992 Feb 1;46(2):132–6.

396. English K, Tan SY, Kwan R, Holz LE, Sierro F, McGuffog C, et al. The liver contains distinct interconnected networks of CX3CR1+ macrophages, XCR1+ type 1 and CD301a+ type 2 conventional dendritic cells embedded within portal tracts. Immunology & Cell Biology. 2022;100(6):394–408.

397. Iqbal AJ, McNeill E, Kapellos TS, Regan-Komito D, Norman S, Burd S, et al. Human CD68 promoter GFP transgenic mice allow analysis of monocyte to macrophage differentiation in vivo. Blood. 2014 Oct 9;124(15):e33–44.

398. Coyle AJ, Page CP, Atkinson L, Flanagan R, Metzger WJ. The Requirement for Platelets in Allergen-induced Late Asthmatic Airway Obstruction: Eosinophil Infiltration and Heightened Airway Responsiveness in Allergic Rabbits. Am Rev Respir Dis. 1990 Sep;142(3):587–93.

399. Rumi E, Cazzola M. How I treat essential thrombocythemia. Blood. 2016 Nov 17;128(20):2403–14.

400. Kuter DJ, Tarantino MD, Lawrence T. Clinical overview and practical considerations for optimizing romiplostim therapy in patients with immune thrombocytopenia. Blood Reviews. 2021 Sep 1;49:100811.

401. Kuter DJ. Thrombopoietin and Thrombopoietin Mimetics in the Treatment of Thrombocytopenia. Annual Review of Medicine. 2009;60(1):193–206.

402. Beutier H, Hechler B, Godon O, Wang Y, Gillis CM, de Chaisemartin L, et al. Platelets expressing IgG receptor FcγRIIA/CD32A determine the

severity of experimental anaphylaxis. Science Immunology. 2018 Apr 13;3(22):eaan5997.

403. Zhou Z, Feng T, Xie Y, Huang P, Xie H, Tian R, et al. The effect of recombinant human thrombopoietin (rhTPO) on sepsis patients with acute severe thrombocytopenia: a study protocol for a multicentre randomised controlled trial (RESCUE trial). BMC Infectious Diseases. 2019 Sep 6;19(1):780.

404. Bussel JB, Soff G, Balduzzi A, Cooper N, Lawrence T, Semple JW. A Review of Romiplostim Mechanism of Action and Clinical Applicability. Drug Design, Development and Therapy. 2021 Dec 31;15:2243–68.

405. Herd OJ, Rani GF, Hewitson JP, Hogg K, Stone AP, Cooper N, et al. Bone marrow remodeling supports hematopoiesis in response to immune thrombocytopenia progression in mice. Blood Adv. 2021 Dec 14;5(23):4877–89.

406. Kuwana M, Okazaki Y, Ikeda Y. Splenic macrophages maintain the anti-platelet autoimmune response via uptake of opsonized platelets in patients with immune thrombocytopenic purpura. Journal of Thrombosis and Haemostasis. 2009;7(2):322–9.

407. Descotes J. Immunotoxicity of monoclonal antibodies. MAbs. 2009;1(2):104–11.

408. Lannutti BJ, Epp A, Roy J, Chen J, Josephson NC. Incomplete restoration of Mpl expression in the mpl−/− mouse produces partial correction of the stem cell–repopulating defect and paradoxical thrombocytosis. Blood. 2009 Feb 19;113(8):1778–85.

409. de Graaf CA, Metcalf D. Thrombopoietin and hematopoietic stem cells. Cell Cycle. 2011 May 15;10(10):1582–9.

410. Kimura S, Roberts AW, Metcalf D, Alexander WS. Hematopoietic stem cell deficiencies in mice lacking c-Mpl, the receptor for thrombopoietin. Proceedings of the National Academy of Sciences. 1998 Feb 3;95(3):1195–200.

411. Kuter DJ. Biology and Chemistry of Thrombopoietic Agents. Semin Hematol. 2010 Jul;47(3):243–8.

412. Kühne T, Imbach P. Eltrombopag: an update on the novel, non-peptide thrombopoietin receptor agonist for the treatment of immune thrombocytopenia. Ann Hematol. 2010 Jul 1;89(1):67–74.

413. Boshkov LK, Kelton JG, Halloran PF. HLA-DR expression by platelets in acute idiopathic thrombocytopenic purpura. British Journal of Haematology. 1992;81(4):552–7.

414. Debaisieux S, Lachambre S, Gross A, Mettling C, Besteiro S, Yezid H, et al. HIV-1 Tat inhibits phagocytosis by preventing the recruitment of Cdc42 to the phagocytic cup. Nat Commun. 2015 Feb 4;6:6211.

415. Liu Y, Xu R, Gu H, Zhang E, Qu J, Cao W, et al. Metabolic reprogramming in macrophage responses. Biomarker Research. 2021 Jan 6;9(1):1.

416. Hirao A. TPO signal for stem cell genomic integrity. Blood. 2014 Jan 23;123(4):459–60.

417. Gazit R, Mandal PK, Ebina W, Ben-Zvi A, Nombela-Arrieta C, Silberstein LE, et al. Fgd5 identifies hematopoietic stem cells in the murine bone marrow. J Exp Med. 2014 Jun 30;211(7):1315–31.

418. Wuescher LM, Nishat S, Worth RG. Characterization of a transgenic mouse model of chronic conditional platelet depletion. Research and Practice in Thrombosis and Haemostasis. 2019;3(4):704–12.

419. Saito M, Iwawaki T, Taya C, Yonekawa H, Noda M, Inui Y, et al. Diphtheria toxin receptor–mediated conditional and targeted cell ablation in transgenic mice. Nat Biotechnol. 2001 Aug;19(8):746–50.

420. Kuter DJ, Begley CG. Recombinant human thrombopoietin: basic biology and evaluation of clinical studies. Blood. 2002 Nov 15;100(10):3457–69.

421. Wilk CM, Kovtonyuk LV, Manz MG. Addition of romiplostim to conditioning prior to HSCT allows chemotherapy reduction while maintaining engraftment levels. Blood Adv. 2022 Jun 24;6(15):4485–9.

422. Léon C, Evert K, Dombrowski F, Pertuy F, Eckly A, Laeuffer P, et al. Romiplostim administration shows reduced megakaryocyte response-capacity and increased myelofibrosis in a mouse model of MYH9-RD. Blood. 2012 Apr 5;119(14):3333–41.

423. Paul DS, Bergmeier W. Novel Mouse Model for Studying Hemostatic Function of Human Platelets. Arteriosclerosis, Thrombosis, and Vascular Biology. 2020 Aug;40(8):1891–904.

424. Hu Z, Yang Y-G. Full reconstitution of human platelets in humanized mice after macrophage depletion. Blood. 2012 Aug 23;120(8):1713–6.

425. Lu TX, Rothenberg ME. Bone Marrow Derived Eosinophil Cultures. Bio Protoc. 2014 Jun 20;4(12):e1161.

426. Jarchum I. Keeping track of gut bacteria. Nat Methods. 2015 Oct;12(10):908–908.

427. Hottz ED, Lopes JF, Freitas C, Valls-de-Souza R, Oliveira MF, Bozza MT, et al. Platelets mediate increased endothelium permeability in

dengue through NLRP3-inflammasome activation. Blood. 2013 Nov 14;122(20):3405–14.

428. Karakas, D N H. The emerging role of Kupffer cells in thrombopoietin generation [Internet]. ISTH Congress Abstracts. 2023 [cited 2023 Jul 6]. Available from: https://abstracts.isth.org/abstract/the-emerging-role-of-kupffer-cells-in-thrombopoietin-generation/

429. Khatib-Massalha E, Méndez-Ferrer S. Megakaryocyte Diversity in Ontogeny, Functions and Cell-Cell Interactions. Front Oncol. 2022 Feb 4;12:840044.

430. Castro VN, Rodrigues JL, Cardoso DT, Resende SD, Magalhães FC, Souza DC, et al. Systemic Cytokine and Chemokine Profiles in Individuals With Schistosoma mansoni Infection and Low Parasite Burden. Frontiers in Immunology [Internet]. 2018 [cited 2023 Jul 6];9. Available from: https://www.frontiersin.org/articles/10.3389/fimmu.2018.02975

431. Khalil RMA, Hültner L, Mailhammer R, Luz A, Moeller J, Mohamed AA, et al. Kinetics of interleukin-6 production after experimental infection of mice with Schistosoma mansoni. Immunology. 1996;89(2):256–61.

432. Souza ALS, Souza PRS, Pereira CA, Fernandes A, Guabiraba R, Russo RC, et al. Experimental Infection with Schistosoma mansoni in CCR5-Deficient Mice Is Associated with Increased Disease Severity, as CCR5 Plays a Role in Controlling Granulomatous Inflammation. Infect Immun. 2011 Apr;79(4):1741–9.

433. Couldwell G, Machlus KR. Modulation of megakaryopoiesis and platelet production during inflammation. Thrombosis Research. 2019 Jul 1;179:114–20.

434. Machlus KR, Johnson KE, Kulenthirarajan R, Forward JA, Tippy MD, Soussou TS, et al. CCL5 derived from platelets increases megakaryocyte proplatelet formation. Blood. 2016 Feb 18;127(7):921–6.

435. Houlder EL, Costain AH, Cook PC, MacDonald AS. Schistosomes in the Lung: Immunobiology and Opportunity. Frontiers in Immunology [Internet]. 2021 [cited 2022 Jun 2];12. Available from: https://www.frontiersin.org/article/10.3389/fimmu.2021.635513

436. Pearce EJ. Priming of the immune response by schistosome eggs. Parasite Immunology. 2005;27(7–8):265–70.

437. Costain AH, MacDonald AS, Smits HH. Schistosome Egg Migration: Mechanisms, Pathogenesis and Host Immune Responses. Front Immunol [Internet]. 2018 Dec 20 [cited 2020 Apr 22];9. Available from: https://www.ncbi.nlm.nih.gov/pmc/articles/PMC6306409/

438. Joyce KL, Morgan W, Greenberg R, Nair MG. Using Eggs from Schistosoma mansoni as an In vivo Model of Helminth-induced Lung Inflammation. J Vis Exp. 2012 Jun 5;(64):3905.

439. Bajinka O, Qi M, Barrow A, Touray AO, Yang L, Tan Y. Pathogenicity of Salmonella During Schistosoma-Salmonella Co-infections and the Importance of the Gut Microbiota. Curr Microbiol. 2022;79(1):26.

440. Getie S, Wondimeneh Y, Getnet G, Workineh M, Worku L, Kassu A, et al. Prevalence and clinical correlates of Schistosoma mansoni co-infection among malaria infected patients, Northwest Ethiopia. BMC Res Notes. 2015 Sep 28;8(1):480.

441. Hitchcock JR, Cook CN, Bobat S, Ross EA, Flores-Langarica A, Lowe KL, et al. Inflammation drives thrombosis after Salmonella infection via CLEC-2 on platelets. J Clin Invest. 125(12):4429–46.

442. Bhattacharjee S, Mejías-Luque R, Loffredo-Verde E, Toska A, Flossdorf M, Gerhard M, et al. Concomitant Infection of S. mansoni and H. pylori Promotes Promiscuity of Antigen-Experienced Cells and Primes the Liver for a Lower Fibrotic Response. Cell Reports. 2019 Jul 2;28(1):231-244.e5.

443. Chala B. Advances in Diagnosis of Schistosomiasis: Focus on Challenges and Future Approaches. Int J Gen Med. 2023 Mar 18;16:983–95.

444. Schnyder JL, Gobbi F, Schunk M, Lindner A, Salvador F, Duvignaud A, et al. Can haematological changes constitute a surrogate diagnostic parameter to detect schistosomiasis in migrants and travellers? - A retrospective analysis. New Microbes and New Infections. 2023 Jun 1;53:101136.

445. Antunes-Ferreira M, Koppers-Lalic D, Würdinger T. Circulating platelets as liquid biopsy sources for cancer detection. Mol Oncol. 2021 Jun;15(6):1727–43.

446. Ding S, Dong X, Song X. Tumor educated platelet: the novel BioSource for cancer detection. Cancer Cell International. 2023 May 11;23(1):91.

447. Dvořák J, Fajtová P, Ulrychová L, Leontovyč A, Rojo-Arreola L, Suzuki BM, et al. Excretion/secretion products from Schistosoma mansoni adults, eggs and schistosomula have unique peptidase specificity profiles. Biochimie. 2016 Mar;122:99–109.

Appendix

Appendix 1

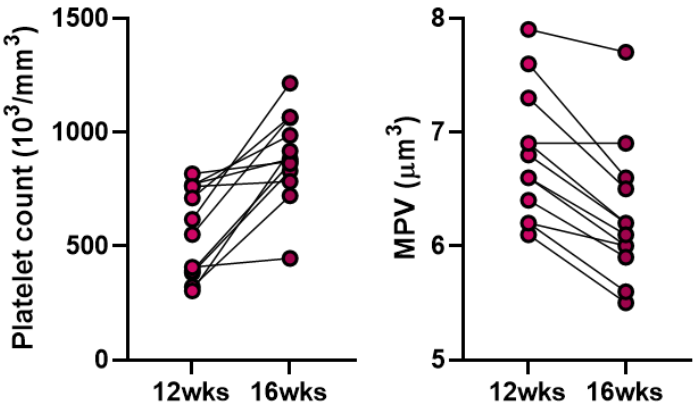

C57BL/6 mice were percutaneously infected with 35 cercariae. 12 weeks post infection infected mice were tail bled and platelet count and MPV measured. Mice were subsequently treated with 250mg/kg praziquantel (PZQ) in 10% kolliphor® EL by oral gavage for 3 consecutive days and harvested 4 weeks later (16 weeks total post-infection). Tail blood was collected at the harvest end point of the PZQ-treated mice.

Appendix 2

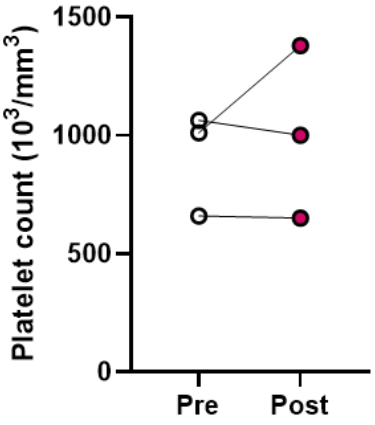

Tail bleeds were taken prior to IV injection (0.05µg/gram of body weight) of anti-GPIb-V-IX conjugated DyLight 649 (X649) and then 24hr post injection and platelet count was measured. (n=3) Significance determined by paired t-test. Non-significance (p>0.05) not shown.

Appendix 3

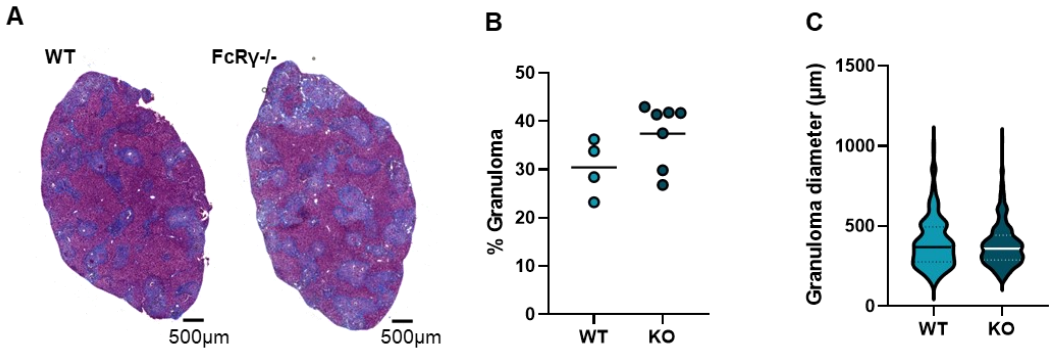

WT and FcRγ$^{-/-}$ mice were infected with 40 *S. mansoni* cercariae and harvested 11 weeks later. Post-mortem liver tissue was stained with Masson's Trichrome, and granulomas manually quantified. A) Representative liver sections of schistosome infected WT and FcRγ$^{-/-}$ livers. Quantification of B) the percentage coverage of granulomas and B) granuloma diameter. Solid line represents media and dotted lines represent inter-quartile range. Data from a single experiment, representative of 2 independent experiments (WT N n=3, WT *Sm* n=5, FcRγ$^{-/-}$ N n=3, FcRγ$^{-/-}$ *Sm* n=7). Statistical significance was determined by Student's t-test (B-C) on the mean of each treatment group. Non-significance (p >0.05) not shown.

Appendix 4

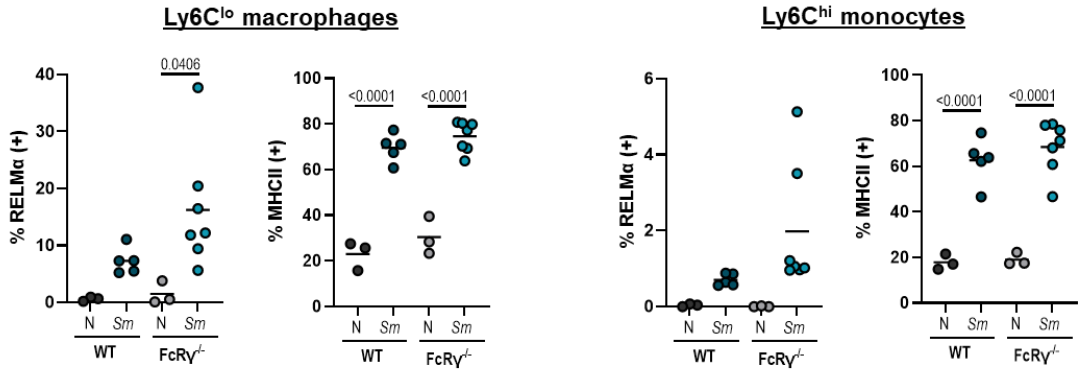

WT and FcRγ$^{-/-}$ mice were infected with 40 *S. mansoni* cercariae and harvested 11 weeks later. Quantification of the percentage of RELMα and MHCII expression in hepatic macrophages and monocytes. Data from a single experiment, representative of 2 independent experiments (WT N n=3, WT *Sm* n=5, FcRγ$^{-/-}$ N n=3, FcRγ$^{-/-}$ *Sm* n=7). Statistical significance was determined by one way ANOVA and post-hoc Tukey test on the mean of each treatment group. Non-significance (p >0.05) not shown.

Appendix 5

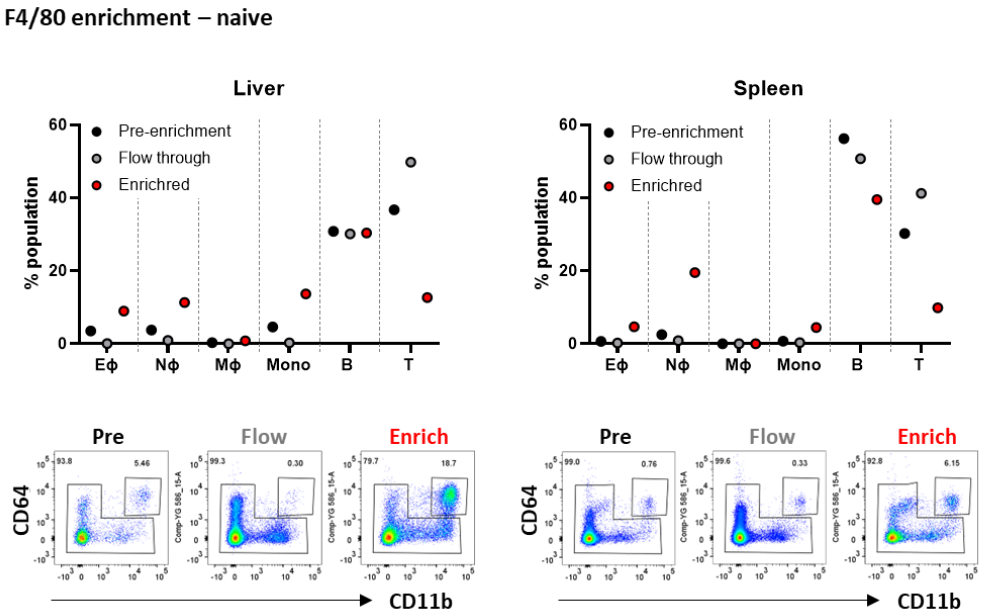

A liver and spleen were isolated from a C57BL/6 mouse and processed to generate single cell suspensions. Samples were enriched using LS-columns F4/80-biotin positive selection. Samples were stained for flow cytometry analysis. Quantification of flow cytometry staining and representative FACS plots of the macrophage/monocyte population in the liver and the spleen. Black – samples removed pre-F4/80 enrichment, grey – samples obtained in the negative column fraction, red – samples positively enriched for F4/80 expressing cells. Representative of 3 independent experiments.

Appendix 6

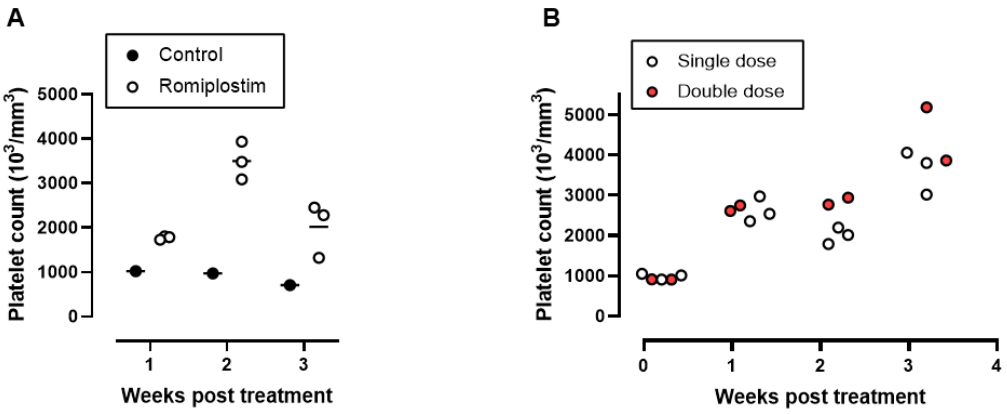

A) C57BL/6 mice were injected subcutaneously with 2.2µg/mouse Romiplostim or PBS once a week for 3 weeks, with weekly tail bleed monitoring. B) C57BL/6 mice were injected subcutaneously with 2.2µg/mouse Romiplostim once (white) or twice (red) a week for 4 weeks, with weekly tail bleed monitoring.

Appendix 7

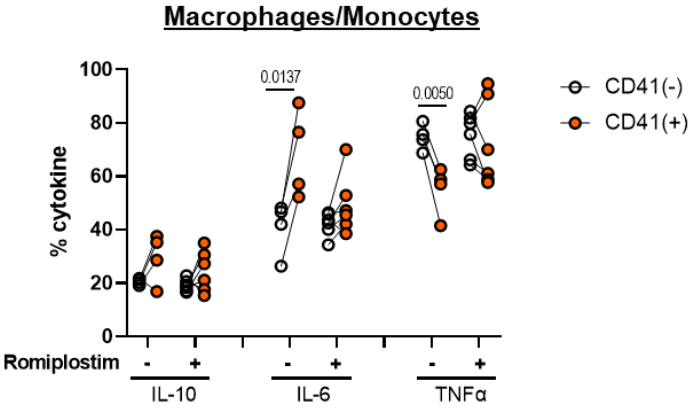

C57BL/6 mice were infected with ~35 *S. mansoni* cercariae (*Sm*), at 6 weeks mice were injected subcutaneously with 2.2µg/mouse Romiplostim or PBS once a week for 4 weeks, with weekly tail bleed monitoring. Mice were harvested at 10 weeks post-infection. Single cell suspensions (2-4x10^6cells) from liver isolation processing were cultured for 3hr at 37^{o}C with 1µg/ml LPS and 10µg/ml Brefeldin A. Pairwise analysis of CD41$^{+/-}$ subsets of monocytes/macrophages (CD11b$^+$CD64$^+$). (N PBS n=3, N Romiplostim n=4, *Sm* PBS n=4, *Sm* Romiplostim n=6). Data representative of a single experiment. Statistical significance determined by Student's paired t-test of the mean between CD41$^+$ and CD41$^-$ populations. Non-significance (p>0.05) not shown.